

## **A Primate View on Multiple Sclerosis**

Visies van een primate op multiple sclerose

ISBN: 978-90-73436-92-3

No parts of this thesis may be reproduced or transmitted in any form by any means, electronic or mechanical, including photocopying, recording or any information storage and retrieval system, without permission in writing from the publisher (Y.S. Kap, Department of Immunology, Erasmus MC, P.O. Box 2040, 3000 CA Rotterdam, The Netherlands).

# **A Primate View on Multiple Sclerosis**

Visies van een primate op multiple sclerose

## **PROEFSCHRIFT**

ter verkrijging van de graad van doctor  
aan de Erasmus Universiteit Rotterdam  
op gezag van de rector magnificus  
prof.dr. H.G. Schmidt  
en volgens besluit van het College voor Promoties.

De openbare verdediging zal plaatsvinden op  
woensdag 6 oktober 2010 om 09.30 uur

door

**Yolanda Susanna Kap**

geboren te Amstelveen



## PROMOTIECOMMISSIE

**Promotoren:** prof. dr. J.D. Laman  
prof. dr. R. Benner

**Overige leden:** prof. dr. H.W.G.M. Boddeke  
prof. dr. R.E. Bontrop  
prof. dr. R.Q. Hintzen

**Copromotor:** dr. B.A. 't Hart



The studies described in this thesis were performed at the Department of Immunobiology, Biomedical Primate Research Centre, Rijswijk, The Netherlands and at the Department of Immunology, Erasmus MC, University Medical Centre, Rotterdam, The Netherlands.

Printing of this thesis was financially supported by the Biomedical Primate Research Centre, the Erasmus University Rotterdam, the J.E. Jurriaanse Stichting, the Remmert Adriaan Laan Fonds, and U-CyTech Biosciences.

Illustrations: Henk van Westbroek

Lay-out : Wendy Schoneveld-Tijsterman

Cover : Ridderprint Offsetdrukkerij B.V., Ridderkerk

Printing : Ridderprint Offsetdrukkerij B.V., Ridderkerk



# A Primate View on Multiple Sclerosis

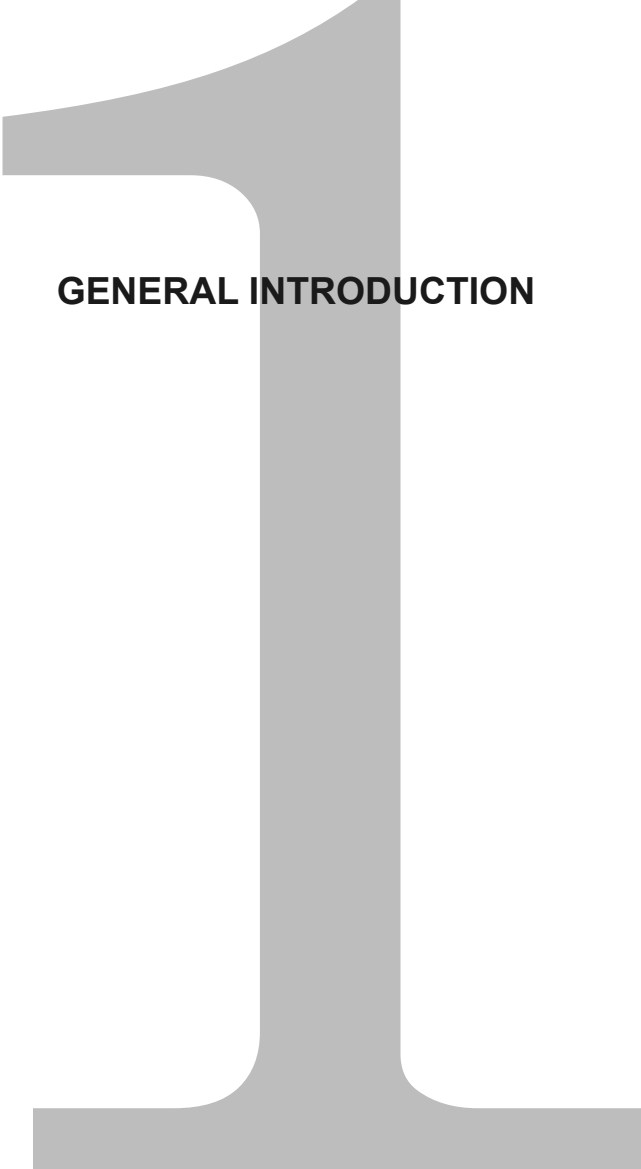
## Visies van een primate op multiple sclerose

### CONTENTS

<b>Chapter 1 General introduction</b>	<b>9</b>
<i>Parts of this chapter are published in J Neuroimmune Pharmacol 2010, 5: 220-230</i>	
<b>Chapter 2 Method development</b>	<b>47</b>
2.1 A monoclonal antibody selection for immunohistochemical examination of lymphoid tissues from non-human primates	49
<i>J Histochem Cytochem 2009, 57: 1159-1167</i>	
<b>Chapter 3 Exploration of critical pathogenic mechanisms</b>	<b>67</b>
3.1 Fast progression of rhMOG-induced experimental autoimmune encephalomyelitis in marmosets is associated with the activation of MOG34-56-specific cytotoxic T-cells	69
<i>J Immunol 2008, 180: 1326-1337</i>	
3.2 Induction of progressive demyelinating autoimmune encephalomyelitis in common marmoset monkeys using MOG34-56 peptide in incomplete Freund adjuvant	101
<i>J Neuropathol Exp Neurol 2010, 69: 372-385</i>	
<b>Chapter 4 Validation of pathogenic mechanisms using novel therapeutics</b>	<b>127</b>
4.1 Effects of early IL-17A neutralization on disease induction in a primate model of experimental autoimmune encephalomyelitis	129
<i>J Neuroimmune Pharmacol (in press)</i>	

4.2	Late B-cell depletion with a human anti-human CD20 IgGκ mAb halts the development of experimental autoimmune encephalomyelitis in marmosets <i>J Immunol (in press)</i>	151
4.3	Late CD20 <sup>+</sup> B-cell depletion attenuates demyelination in the CNS white and grey matter of EAE-affected marmoset monkeys <i>Manuscript in preparation</i>	183
4.4	Role of amino-Nogo-A antagonism in oligodendrocyte differentiation and myelination in experimental demyelinating diseases <i>Submitted for publication</i>	209
4.5	Early treatment with the synthetic hCG-related tetrapeptide LQGV does not modulate experimental autoimmune encephalomyelitis in marmosets	233
<b>Chapter 5 General discussion</b>		<b>255</b>
<b>Chapter 6 Summary/Samenvatting</b>		<b>287</b>
	Summary	288
	Samenvatting	291
<b>Chapter 7 Appendices</b>		<b>297</b>
	Abbreviations	298
	Dankwoord	300
	Curriculum vitae	302
	PhD Portfolio	303
	List of publications	306
	Color figures	309



A large, stylized grey number '1' that serves as a background for the chapter title. The number has a curved top and a wide base.

# **GENERAL INTRODUCTION**

*Parts of this chapter are published in J Neuroimmune Pharmacol 2010, 5: 220-230*

## PREFACE

The current success rate of new drugs for central nervous system (CNS) disorders, including multiple sclerosis (MS), is very low, i.e. between 5 and 8%. The main cause of this low success rate is a lack of efficacy of new drugs in humans<sup>1</sup>. A widely recognized bottleneck in the selection of promising CNS drug candidates from the development pipeline is the lack of sufficiently predictive animal models. The choice of the animal model(s) to be used for the selection of the most promising agents from the development pipeline is a strategically important decision.

While selecting an animal model for preclinical safety and efficacy evaluation of a new drug the following selection criteria should be considered:

1. The biodistribution and pharmacological properties of the target molecule should be comparable between humans and the chosen animal model.
2. The binding kinetics of the therapeutic agent to the target molecule should be comparable between humans and the chosen animal model.
3. The model should preferably reveal unwanted side-effects of the treatment that could also occur in humans, such as cytokine release syndrome, complement activation, immune deficiency, and the exacerbation of latent infections.
4. The animal model should be ethically acceptable.
5. The model should resemble the disease in the clinical manifestation, the pathology of the target organ, and the (immuno)pathogenesis.

When selecting an animal model for MS, the first three considerations plead for the development of relevant preclinical animal models that are pathogenetically more closely related to MS than the classical rodent models. Furthermore, new therapeutic agents, especially monoclonal antibodies (mAb), often have high species specificity and are therefore not cross-reactive with the target in rodents. A preclinical animal model that satisfies the first two criteria is experimental autoimmune encephalomyelitis (EAE) in the common marmoset. In principle, unwanted side-effects may occur in the marmoset EAE model, although these have not been seen in the therapies tested thus far<sup>2-5</sup> (**Chapter 4**). The marmoset EAE model also satisfies the last two criteria, but these will be refined in this thesis, e.g. by replacing the adjuvant that is used to induce the disease.

The research strategy of this thesis integrates exploratory and applied research, which are closely linked. In the exploratory research, pathogenic mechanisms are investigated, which may lead to the identification of new therapy targets. Applied research focuses on the development of new therapies. This will validate known pathogenic mechanisms and reveal new pathogenic mechanisms if the intervention is successful (Figure 1).

## MULTIPLE SCLEROSIS

### Clinical

MS is a chronic disease affecting the CNS with an average disease onset in the third or fourth decade of life. Clinical symptoms are caused by changes in the motor, sensory, visual, and autonomic systems. Most common symptoms include visual and balance disturbances, spasticity, bladder dysfunction, pain, and fatigue. At a later disease stage, paralysis may occur. Other symptoms are Lhermitte's symptom, an electrical sensation running down the spine or limbs when the neck bends, and Uhthoff phenomenon, worsening of symptoms when the core body temperature increases<sup>6-9</sup>.

At least five clinical variants of MS are recognized, i.e. benign, relapsing-remitting (RRMS), secondary progressive (SPMS), primary progressive (PPMS), and progressive relapsing (PRMS) (Figure 2). In about 80% of the patients, the disease starts as RRMS. After 10-15 years, most of these patients develop SPMS, a stage with irreversible neurological decline. In about 20% of the patients the disease is progressive from onset, with (PRMS) or without relapses (PPMS)<sup>6-10</sup>.

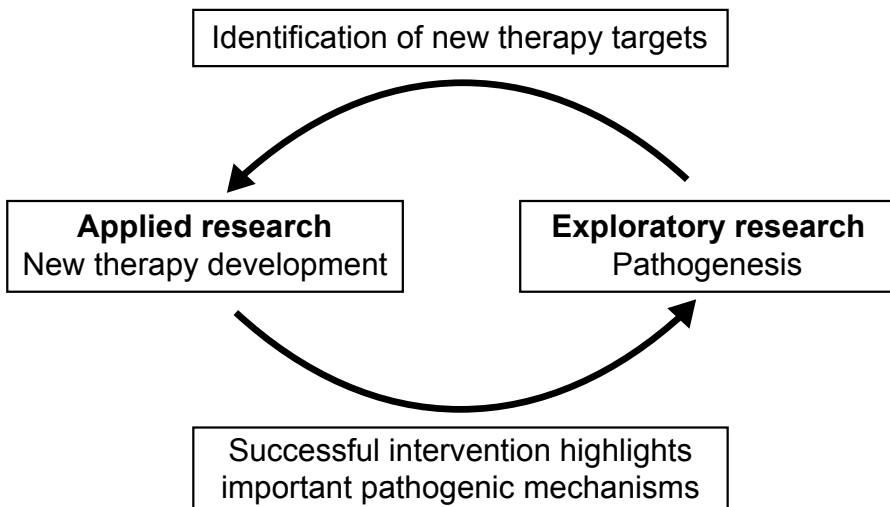


**Figure 1. Research strategy.**

Pathogenic mechanisms are investigated by exploratory research, which can lead to the identification of new therapy targets. Applied research focuses on the development of new therapies, which validates known pathogenic mechanisms and reveals new pathogenic mechanisms when the intervention is successful.

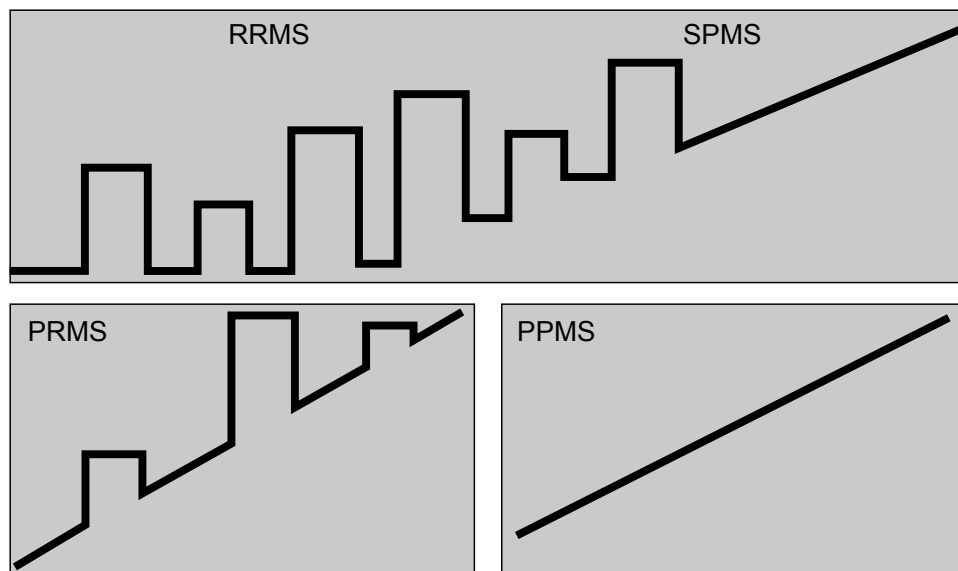


**Figure 2. Clinical course of MS.**

About 80% of the MS patients start with relapsing-remitting MS (RRMS), which is characterized by relapses and remissions. Most RRMS patients develop secondary progressive MS (SPMS) after 10-15 years. About 20% of the patients have progressive MS from onset, with (progressive relapsing, PRMS) or without relapses (primary progressive, PPMS). Based on<sup>10</sup>.

## Etiology

The cause of MS is still unknown, but it is highly likely that MS is a complex disease involving the interaction of genetic and environmental factors. The concordance rate between monozygotic twins is about 6 times higher than among dizygotic twins (respectively 31% and 5%) suggesting contribution of genetic factors<sup>11</sup>. The risk for MS is increased by normally occurring polymorphisms in the human leukocyte antigen (HLA) gene complex, such as *DQA1\*0102*, *DQB2\*0602*, *DRB1\*1501*, and *DRB4\*0101*<sup>12</sup>. In contrast, other HLA alleles may cause resistance, such as *DRB1\*14* and *DRB1\*11*<sup>13</sup>. *DRB1\*1501* not only increases the risk for MS, but also increases disease severity compared to *DRB1\*1501*-negative patients<sup>14</sup>. Genome-wide association studies and meta-analyses identified other risk genes, such as interleukin (IL)-2 receptor  $\alpha$  chain, IL-7 receptor  $\alpha$  chain, CLEC16A, CD6, CD58, tumor necrosis factor receptor superfamily member 1A, interferon response factor 8, and STAT3<sup>15-17</sup>. Another genome wide association study revealed a polymorphism in the *KIF1B* locus<sup>18</sup>, although this could not be confirmed by others<sup>19</sup>. *KIF1B* encodes a kinesin that is important for axonal transport and which is the first genetic association without an apparent prominent role

in the immune system. Integration of these genetic risk factors may lead to a predictive algorithm in the future<sup>20</sup>.

Environmental factors that may influence the risk for MS include sunlight exposure and infections. The risk for MS increases when moving away from the equator and is especially higher in the northern regions of the United States and Europe. This may be explained by a higher prevalence of HLA risk alleles in these regions, but also by the low UV-B exposure<sup>21,22</sup>, which may lead to low vitamin D levels<sup>8</sup>. High vitamin D levels in serum are associated with a lower risk for MS and a lower relapse rate<sup>23-25</sup>. In addition, vitamin D may change the T-cell activation and the cytokine profile<sup>25</sup>, but also *HLA-DRB1\*1501* expression<sup>26</sup>.

The risk of developing a relapse increases around the time of an infection, especially during upper respiratory tract infections. A relapse associated with an infection induces more sustained neurological deficit than a non-infectious relapse<sup>24,27</sup>. Human herpesviruses (HHV) are suggested to increase the risk for MS<sup>28</sup>. One of the most frequently studied HHV in MS is Epstein-Barr virus (EBV), albeit with contradictory results. Infection with EBV increases the risk for MS, which is even higher when the infection occurs after the age of 17 years<sup>29</sup>. All MS patients have serum immunoglobulin (Ig) G antibodies (Ab) against EBV, whereas anti-EBV IgG are detected in 80-90% of healthy individuals<sup>30</sup>. In contrast, anti-EBV IgG levels in cerebrospinal fluid (CSF) did not differ between MS patients and non-MS inflammatory CNS disease control patients<sup>31</sup>. Furthermore, EBV RNA could not be detected in CSF of MS patients<sup>31</sup>. It has been suggested that EBV-infected B-cells migrate to the target organ where they become a source of autoantibodies and provide co-stimulatory signals to T-cells<sup>32</sup>. Indeed, EBV-positive B-cells were found in the meninges of MS brains<sup>33</sup>. However, others could not confirm this<sup>31,34</sup>.

How pathogens modulate the immune response in MS is currently unknown. It has been suggested that the gut flora is involved in the expansion of T-cells<sup>35</sup>. A change in the gut flora composition by a pathogen may alter the immune response. EBV modulates the immune response by infecting and activating B-cells<sup>32</sup>, which play an important role in MS<sup>36,37</sup>. To investigate the role of a human pathogen in MS it is essential that the animal, in which the disease is modeled, is susceptible to infection with that pathogen or closely related counterparts. As for HHV, higher non-human primate (NHP) species are naturally infected with viruses that are closely related to their human counterpart. Thus, in contrast to rodents, conventionally held colonies of NHP have experienced the immune shaping effect by similar environmental pathogens throughout their development and may therefore be a good representative for the situation in humans.

## Pathology

One of the criteria for the diagnosis of MS is the detection of white matter (WM) lesions in the brain with magnetic resonance imaging (MRI)<sup>38</sup>. WM lesions are the major pathological hallmark of MS and disseminate in time and space. They are characterized by inflammation, demyelination, axonal injury, edema, and blood-brain barrier (BBB) dysfunction<sup>7,9</sup>.

WM lesions develop through several stages, i.e. pre-active, active, chronic active, and chronic inactive. Pre-active, or early active, lesions are characterized by focal

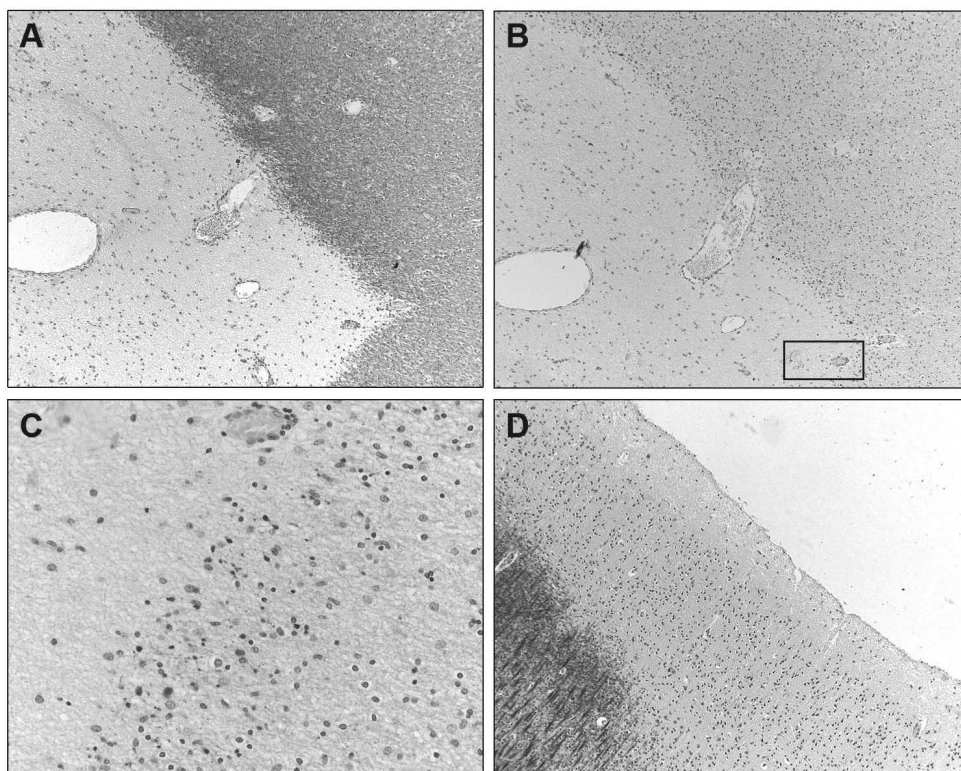


**Figure 3. Pathology of MS.**

A, A staining for proteolipid protein (PLP) shows the demyelinated hypocellular center of a chronic active lesion in the white matter of a MS brain (original magnification x50). B, At the rim of the lesion, where myelin is phagocytosed by macrophages, axonal transections are visualized by a staining for the amyloid precursor protein (original magnification x50). Axonal transections at the rim of the lesion in the square are enlarged in C (original magnification x100). D, A PLP staining of the grey matter shows a subpial lesion (original magnification x50). Photographs are kindly provided by E.-J. Kooi and Dr. J. Geurts (Department of Pathology, VU University Medical Center, Amsterdam, The Netherlands). See page 309 for a full-color representation of this figure.

abnormalities in the WM, such as clusters of major histocompatibility complex (MHC) class II positive cells and perivascular infiltration. The MHC class II positive cells are mainly activated microglia or infiltrated macrophages. No demyelination is present in this lesion stage. In active lesions, MHC class II positive cells that have phagocytosed myelin are present in the center of the demyelinated area. Several other immune cells are also present, such as T-cells, B-cells, and plasma cells. In chronic active lesions the center of the lesion is hypocellular, whereas the rim is hypercellular with myelin positive phagocytic cells indicating ongoing demyelination (Figure 3). Chronic inactive lesions are hypocellular with astrogliosis and widened extracellular spaces<sup>39-41</sup>. Axonal transection is observed in active and chronic active lesions<sup>42,43</sup> (Figure 3).

Four patterns of demyelination have been described, based on the target of injury and the mechanism of demyelination. Myelin is the target in patterns I and II, whereas the oligodendrocyte is the target in patterns III and IV. Patterns I and II are both characterized by the presence of T-cells, macrophages, and activated microglia. Deposition of Ig and complement occurs in pattern II lesions. Pattern III lesions also contain T-cells and activated microglia/macrophages, but these lesions are especially characterized by apoptotic oligodendrocytes and the specific loss of myelin associated glycoprotein (MAG). Pattern IV lesions were only detected in a subgroup of PPMS patients. Pattern IV lesions are characterized by infiltrated T-cells and macrophages and oligodendrocyte death. Deposition of Ig and complement, apoptosis, and specific loss of MAG are absent in this pattern<sup>44</sup>. Lucchinetti et al. described that the demyelination pattern was heterogeneous between patients, but homogeneous within a patient<sup>44</sup>. However, others could not detect lesion heterogeneity between patients<sup>45</sup> or suggested that pattern III lesions may represent an early stage of lesion formation instead of a different pattern<sup>46,47</sup>. The different patterns may also represent different immunological effector mechanisms in response to a core process of T-cell mediated inflammation rather than disease heterogeneity<sup>9</sup>.

Brain WM lesions detected by MRI do not always correlate well with clinical signs and disease progression. This is known as the clinico-radiological paradox<sup>48,49</sup>. Factors that contribute to clinical deterioration include axonal injury and grey matter (GM) lesions. Axonal injury is present in active and chronic active lesions<sup>42,43,50</sup>. Progressive degeneration of axons, which is difficult to visualize with classical MRI techniques, contributes to brain atrophy, especially of the cortex, which may be a better correlate of clinical deterioration<sup>51,52</sup>. It has been proposed that when axonal injury reaches a certain threshold the disease transits from RRMS to SPMS<sup>50</sup>.

GM lesions can be observed in the neocortex, but also in other GM areas, such as in the hippocampus and the cerebellum. GM lesions are classified into four types. Leukocortical (type I) lesions extend in both the white and GM. Type II and type IV lesions are intracortical lesions with type IV lesions extending through the full width

of the cortex. Type III lesions are subpial lesions and are the most common cortical lesions, which can extend several gyri<sup>53-56</sup> (Figure 3). The pathology of GM lesions differs from WM lesions in the low number of lymphocytes, low level of complement deposition, and the absence of BBB disruption<sup>54,57,58</sup>. However, profound activation of microglia is observed at the border of GM lesions<sup>53,54</sup>. It is suggested that changes in the GM correlate well with clinical disability in MS, probably more than WM lesions<sup>51,56,59</sup>. Therefore, a better understanding of GM lesions is needed as well as a therapy that reduces the GM lesion load.

### **Immunopathogenesis**

The exact pathogenesis of MS is still unknown, but it is well accepted that once the disease has been initiated the immune system plays a major pathogenic role. The classical and general view on MS pathogenesis is that autoreactive T-cells are activated in the periphery by antigen presenting cells (APC) that present CNS or CNS cross-reactive antigens (Ag). These activated T-cells may enter the CNS via the BBB or the choroid plexus<sup>60</sup>. Within the CNS, they encounter CNS Ag presented by local APC. This leads to T-cell reactivation and a cascade of events that induce demyelination, axonal injury, and gliosis. Autoantibodies directed against myelin or neuronal proteins enhance the immune response, for instance by activating the complement system. Infiltrated macrophages or resident microglia phagocytose myelin and produce inflammatory mediators<sup>6,9,61,62</sup> (Figure 4).

Demyelination is the pathological hallmark of MS and is caused by a combined cellular and humoral autoimmune attack on myelin. The myelin sheath is produced by oligodendrocytes and is wrapped around axons to increase the conductivity. Myelin is composed of 80% lipids and 20% proteins, such as myelin basic protein (MBP), proteolipid protein (PLP), MAG, and myelin oligodendrocyte glycoprotein (MOG) (Figure 5). MOG is a type I membrane glycoprotein and a member of the Ig superfamily produced by oligodendrocytes. MOG is located on the outer myelin sheath with the N-terminal amino acids 1 to 125 exposed to the extracellular environment where it is accessible for immune cells<sup>63,64</sup> (Figure 5). MOG probably forms homodimers<sup>65</sup> and is highly conserved among species, but has a still unknown function<sup>66,67</sup>. The MOG gene is located on chromosome 6 within the distal region of the MHC gene complex and therefore closely linked to gene loci associated with MS<sup>68</sup>.

A significant increase of the number of MOG-specific T-cells was reported in peripheral blood mononuclear cells (PBMC) and CSF of MS patients<sup>69</sup>. Half of the 24 MS patients that were tested for proliferation against myelin epitopes showed proliferation against MOG, but only five MS patients showed proliferation against MBP and only two against PLP<sup>70</sup>. MOG-reactive T-cells are also present in the natural T-cell repertoire of healthy individuals<sup>71,72</sup>. The fact that these autoreactive T-cells are not depleted

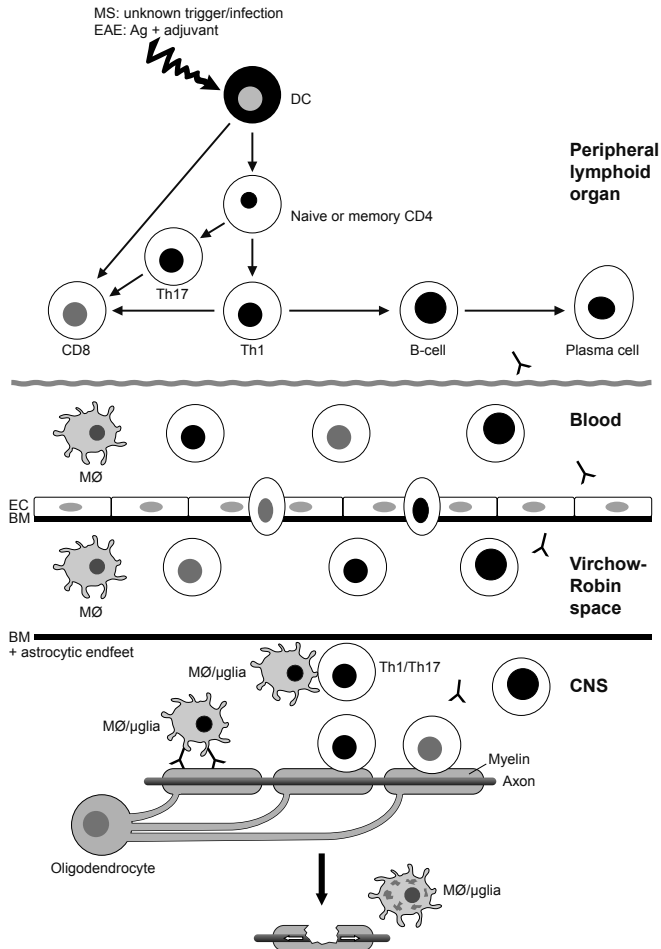


**Figure 4. Overview of the hypothetical pathogenesis of MS.**

The triggers that cause MS are unknown, in contrast to the trigger in EAE, which is immunization with a myelin protein or peptide emulsified in an adjuvant. The classical and general view on MS pathogenesis is that autoreactive T-cells are activated in the periphery by antigen presenting cells (APC) that present CNS or CNS cross-reactive antigens (Ag). Both Th1 and Th17 cells may play a role in the pathogenesis. Also B-cells are activated via T-cell help leading to plasma cells and the production of autoantibodies. Activated lymphocytes, antibodies, and macrophages migrate via blood to the CNS, across the blood-brain barrier, enter the Virchow-Robin space, and migrate into the parenchyma when the appropriate signals are provided. T-cells are then reactivated by local antigen presenting cells, such as activated microglia. This leads to a cascade of events that induce demyelination, axonal injury, and gliosis. Autoantibodies directed against myelin or neuronal proteins enhance the immune response, for instance by activating the complement system. Infiltrated macrophages or resident microglia phagocytose myelin and produce inflammatory mediators. Ag, antigen; BM, basement membrane; DC, dendritic cell; EC, endothelial cells; (MØ), macrophages; µglia, microglia. Based on<sup>6,9,61,62</sup>.

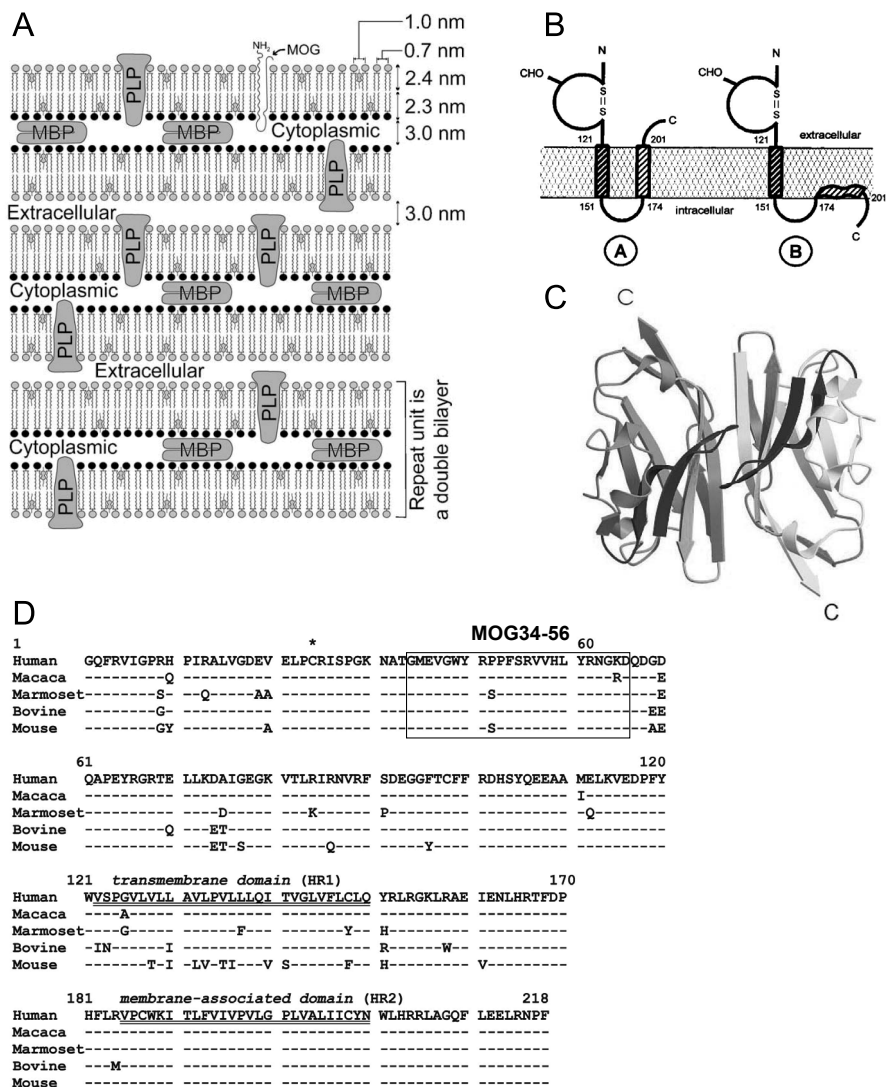


**Figure 5. Structure of myelin oligodendrocyte glycoprotein (MOG).**

A, MOG is present on the outer surface of myelin. B, Proposed models for the membrane topology of MOG. The N-terminus is localized on the extracellular side. The C-terminus is localized on the extracellular side (model A) or the C-terminal is associated with the lipid bilayer (model B). In both models, MOG34-56 is localized on the extracellular side. C, Schematic representation of the three-dimensional structure of MOG that forms a dimer. MOG35-55 maps to the dark grey residues. D, Amino acid sequence of MOG of human, cynomolgus macaque, common marmoset, bovine, and mouse. MOG34-56 is indicated by the square. Based on<sup>63-65,67</sup>.

during development of the immune system has been explained by the absence of MOG expression in the thymus<sup>73</sup>. It is suggested that these MOG-reactive T-cells are Th0 cells in healthy individuals and Th1 cells in MS patients<sup>72,74</sup>. The T-cell response is mainly directed against three domains in the extracellular part of MOG, i.e. 1-22, 34-56, and 64-96<sup>74-76</sup>. The phenotype of these T-cells is CD4<sup>+</sup>CD8<sup>-</sup> and they use the  $\alpha\beta$  T-cell receptor (TCR) for Ag recognition. MOG-reactive T-cells can induce cytolysis of MOG-pulsed PBMC<sup>72,74</sup>. It has long been thought that Th1 cells were the main pathogenic T-cells in MS, but more recent literature highlights an important pathogenic contribution of Th17 cells and CD8<sup>+</sup> T-cells as well. Blood, CSF, and CNS lesions of MS patients contain IL-17A, Th17 cells<sup>77-82</sup>, and clonally expanded CD8<sup>+</sup> T-cells<sup>33,83,84</sup>. However, the exact role of Th17 and CD8<sup>+</sup> cells is still under investigation.

B-cells have long been thought to function in MS only as Ab-producing plasma cells. Indeed, intrathecal Ab production can be detected as oligoclonal bands in the CSF<sup>85</sup>. In addition, autoantibodies are present in serum and CNS lesions<sup>44,86</sup>. MS patients have increased IgG titers to native MOG<sup>87,88</sup>. There is some indirect evidence that B-cells also have other roles in MS, since treatment with the anti-CD20 Ab rituximab improved clinical symptoms and CNS pathology without changing total IgM and IgG levels. One suggested role for B-cells in MS, i.e. Ag presentation to T-cells<sup>36,37</sup>, is addressed in this thesis.

## Therapy

Acute MS relapses are often treated with high doses of corticosteroids, such as methyl prednisolone, which inhibit the pro-inflammatory immune response and decrease the extravasation of immune cells into the CNS<sup>89-91</sup>. Generally used drugs suppress some of the chronic symptoms, such as bladder dysfunction and spasticity<sup>9</sup>. However, to date there is no treatment that effectively prevents all symptoms and pathology of MS.

The availability of new therapeutic agents for RRMS has tremendously improved in the past decade<sup>92</sup> (Table 1). Approved drugs include mitoxantrone, interferon (IFN)  $\beta$ , glatiramer acetate, and natalizumab. Mitoxantrone is a synthetic antineoplastic cytotoxic drug that inhibits DNA and RNA synthesis. Because of its toxic effects mitoxantrone has only been approved for short treatment periods of aggressive MS relapses<sup>93</sup>. Mitoxantrone enhances the production of Th2 cytokines, but does not alter the production of Th1 and Th17 cytokines<sup>94</sup>. IFN- $\beta$  reduces clinical signs and MRI detectable lesions in RRMS, especially when the treatment is started in the early phase of the disease<sup>95-97</sup>. IFN- $\beta$  promotes the production of Th2 cytokines and reduces IL-17A production *in vitro*<sup>98,99</sup>. Furthermore, IFN- $\beta$  may reduce the migration of immune cells into the CNS by altering the BBB or by increasing the expression of chemokines or chemokine receptors by leukocytes<sup>100,101</sup>. Unfortunately, treatment with IFN- $\beta$  is not effective in all patients, which could be due to the development of neutralizing Ab<sup>102</sup>.

Another explanation, based on findings in the animal model for MS, may be that IFN- $\beta$  inhibits Th1-mediated pathology, but exacerbates symptoms mediated by Th17 cells<sup>103</sup>. This suggests that IFN- $\beta$  is effective in patients with Th1-mediated disease,

**Table 1. A selection of therapies for MS.**

Generic name	Drug name	Main target	Anticipated mechanism of action
<b>Approved</b>			
Mitoxantrone	Novantrone® Ralenova®	T-cells, B-cells, and macrophages	<ul style="list-style-type: none"> <li>• Inhibits DNA and RNA synthesis</li> <li>• Enhances production of Th2 cytokines, but without changing IFN-<math>\gamma</math> and IL-17A levels</li> </ul>
$\beta$ Interferons	Rebif® Avonex® Betaseron®	Leukocytes	<ul style="list-style-type: none"> <li>• Promotes Th2 cytokines</li> <li>• Inhibits Th1-mediated pathology, but exacerbates Th17-mediated pathology</li> <li>• Inhibits leukocyte migration into CNS</li> </ul>
Glatiramer acetate	Copaxone®	MHC class II molecules	<ul style="list-style-type: none"> <li>• Replacement of MBP in MHC II complex</li> <li>• Promotes Th2 skewing</li> </ul>
Natalizumab <sup>a</sup>	Tysabri®	$\alpha$ 4 $\beta$ 1/VLA-4 on lymphocytes and monocytes	<ul style="list-style-type: none"> <li>• Inhibits leukocyte migration into CNS</li> </ul>
<b>Under development</b>			
Statins			<ul style="list-style-type: none"> <li>• Lowers cholesterol</li> <li>• Promotes Th2 skewing</li> <li>• Inhibits lymphocyte migration into CNS</li> <li>• Inhibits IFN-<math>\gamma</math> induced MHC class II expression</li> </ul>
FTY720	Fingolimod®	S1P receptor on e.g. lymphocytes and CNS cells	<ul style="list-style-type: none"> <li>• Prevents egress of lymphocytes from lymph nodes</li> <li>• May promote CNS repair mechanisms</li> </ul>
Alemtuzumab <sup>a</sup>	Campath®	CD52 on lymphocytes and monocytes	<ul style="list-style-type: none"> <li>• Depletes lymphocytes and monocytes</li> </ul>
Daclizumab <sup>a</sup>	Zenapax®	CD25/IL-2R $\alpha$ on activated T-cells	<ul style="list-style-type: none"> <li>• Inhibits T-cell proliferation</li> </ul>
Rituximab <sup>a</sup>	Rituxan®	CD20 on B-cells	<ul style="list-style-type: none"> <li>• Reversible depletion of B-cells, but not plasma cells</li> </ul>

<sup>a</sup> mAb monoclonal antibody

BBB, blood-brain barrier; S1P, sphingosine-1-phosphate; VLA-4, very late antigen-4

but not in patients with a Th17 dominant phenotype. Glatiramer acetate is a synthetic mixture of polypeptides composed of four amino acids and is used as a therapy for RRMS<sup>104</sup>. The immunological effects of glatiramer acetate are widespread and include replacement of MBP epitopes on MHC class II complexes and Th2 skewing<sup>105,106</sup>. Natalizumab is a mAb that binds to  $\alpha 4\beta 1$  integrin (VLA-4), which is expressed by lymphocytes and monocytes. Natalizumab prevents the interaction of immune cells with vascular cell adhesion molecule 1 expressed by endothelial cells of the BBB and thereby reduces leukocyte infiltration into the CNS. Natalizumab profoundly reduces disease progression in RRMS patients<sup>107</sup>. Natalizumab was voluntarily withdrawn from the market for a while, because a few patients developed progressive multifocal leukoencephalopathy (PML), which is caused by the JC polyomavirus<sup>108-110</sup>. The drug was reintroduced on the market with several restrictions<sup>111</sup>. It is currently under investigation whether monitoring JC virus reactivation can be used to diagnose the risk for PML development<sup>112,113</sup>.

Drugs that are currently in clinical trials include statins, FTY720, and mAb targeting CD52 (Alemtuzumab), CD20 (Rituximab), or the  $\alpha$  chain of the IL-2 receptor/CD25 (Daclizumab). Statins are cholesterol-lowering drugs that are extensively used for cardiovascular diseases. In addition, statins skew the T-cell response towards Th2 and inhibit lymphocyte migration across the BBB<sup>114-116</sup>. Statins have been tested in clinical trials for RRMS with promising results<sup>117</sup>. However, *in vitro* statins hamper myelin formation by oligodendrocytes indicating that they may inhibit remyelination *in vivo*<sup>118</sup>. FTY720, also known as fingolimod, is a small molecule that targets sphingosine-1-phosphate receptors expressed by many cell types including lymphocytes and CNS cells. FTY720 prevents the egress of lymphocytes from lymph nodes and may promote repair in the CNS<sup>119</sup>. FTY720 reduces MRI detectable lesions and clinical symptoms of RRMS<sup>120,121</sup>. Alemtuzumab targets CD52 that is widely expressed by T-cells and B-cells as well as by a subpopulation of granulocytes<sup>122</sup>. Alemtuzumab reduces the relapse rate and lesion load<sup>123</sup>. Daclizumab prevents T-cell expansion by blocking the IL-2 receptor  $\alpha$  chain expressed by activated T-cells<sup>124</sup>. However, daclizumab also reduces the frequency of systemic regulatory T-cells of which the effect is currently unknown<sup>125</sup>. RRMS patients with an incomplete response to IFN- $\beta$  responded very well to daclizumab<sup>126</sup>. Rituximab targets CD20/B-1 antigen expressed by B-cells, but not by plasma cells. Rituximab profoundly reduces the relapse rate and lesion formation in RRMS<sup>36,37</sup>. B-cell depletion by rituximab resulted in PML in a few non-MS patients<sup>110</sup>. Second-generation B-cell depleting Ab directed against CD20, such as ofatumumab and ocrelizumab, are now also under development for clinical trials in MS<sup>127,128</sup>.

The therapies described above are immunomodulatory treatments and most appropriate for RRMS. When these treatments were tested in PPMS they were less effective<sup>129,130</sup>. Inflammation may play a less dominant role in the progressive phase

of MS and in GM lesions. Therefore, therapies are required that interfere with axonal injury, that prevent GM lesions, or that stimulate remyelination<sup>131</sup>. Suggested targets are myelin-associated inhibitory factors, such as Nogo-A, which inhibit neurite outgrowth<sup>132</sup>.

## EXPERIMENTAL AUTOIMMUNE ENCEPHALOMYELITIS

For both exploratory and applied research into MS the use of a valid animal model is indispensable. The history of the animal model for MS starts in 1885 when humans were found to develop paralytic diseases after injection with rabies vaccine, which was isolated from the spinal cord of rabies infected rabbits<sup>133</sup>. Rivers started to investigate the cause of this paralysis by repeated intramuscular injection of rhesus macaques with rabbit brain homogenate. Only two of the eight monkeys developed symptoms and pathology after more than 50 injections<sup>134</sup>. However, when aqueous solutions and alcohol-ether extracts of rabbit brains were intramuscularly injected, six of the eight monkeys developed clinical signs and pathology<sup>135</sup>. Next, the procedure was refined to a single injection with brain homogenate in complete Freund's adjuvant (CFA) or vaseline oil containing killed *Mycobacterium bovis*. This led to an acute neuroinflammatory disease with paralytic symptoms resembling acute disseminated encephalomyelitis rather than MS<sup>136,137</sup>.

Nowadays, there are several animal models for MS that spontaneously develop in transgenic mice<sup>138-142</sup>, or that are induced by viruses<sup>143-145</sup>, toxins<sup>146,147</sup>, adoptive transfer, or immunization<sup>148-160</sup> (Table 2). The most widely used animal model is EAE, which is induced by active immunization with myelin derivatives and an adjuvant. EAE can be induced in several species, such as rabbits, guinea pigs, rats, mice, and NHP. Most commonly used are inbred mouse and rat strains and outbred common marmosets in which different immunization protocols lead to different disease variants (Table 2).

### The marmoset EAE model

The EAE model in the marmoset has first been developed fifteen years ago<sup>157</sup>. Since then, the model has been continuously refined. To induce EAE, marmosets were initially immunized with whole human myelin emulsified in CFA containing *Mycobacterium tuberculosis* in combination with two intravenous doses of heat-inactivated *Bordetella pertussis* organisms or particles<sup>157,161</sup>. This led to an experimental model with an acute onset of a relapsing-remitting disease course in which the animals were sacrificed with neurological symptoms as paresis and paralysis within 13 weeks. The CNS pathology was characterized by active lesions and disrupted axons. Furthermore, a destructive

**Table 2. Selection of commonly used animal models for multiple sclerosis.**

Type	Species/strain	Induction	Features	Reference
<b>Transgenic</b>				
TCR for MBP1-11	Mouse: B10.PL		Spontaneous EAE when housed in a non-sterile facility	138
TCR for PLP139-151	Mouse: SJL		Spontaneous EAE	139
TCR for MOG35-55	Mouse: C57BL/6		Spontaneous optic neuritis	140
TCR for MOG92-106	Mouse: SJL		Spontaneous RR-EAE	141
Humanized with HLA-DR15 and TCR for MBP85-99	Mouse: C57BL/6		Spontaneous EAE	142
<b>Viral</b>				
SFV	Mouse: Biozzi ABH	Intraperitoneal injection of SFV	CNS infection, inflammation, and demyelination	143
TMEV	Mouse: SJL	Intracranial injection of TMEV	Chronic progressive demyelination and grey matter pathology	144,145
<b>Toxic</b>				
Cuprizone	Mouse and rat	Oral administration of cuprizone	A non-inflammatory model to study demyelination and remyelination	146
LPC	Mouse and rat	intracranial injection of LPC	A non-inflammatory model to study demyelination and remyelination	147
<b>Autoimmune (passive)</b>				
Adoptive transfer	Mouse, rat, non-human primate	Transfer of myelin-specific T-cells isolated from immunized donors	Especially useful in determining pathogenicity of a specific T-cell subset	Reviewed in <sup>159</sup>
<b>Autoimmune (active)</b>				
EAE	Mouse: C57BL/6	<b>Antigen</b> MOG34-55	<b>Adjuvant</b> CFA	Chronic monophasic/chronic
	Mouse: SJL	PLP139-151	CFA	Acute monophasic
	Mouse: Biozzi ABH	MOG, MOG8-21	CFA	Chronic relapsing-remitting
	Mouse: Biozzi ABH	MOG35-55	CFA	Chronic acute
	Rat: Lewis	MBP88-86	CFA	Monophasic
	Rat: Dark agouti	SCH, MBP63-81	IFA	Protracted relapsing
	Rhesus macaque	RhMOG, MOG34-56	CFA	Acute progressive, visual impairment
	Common marmoset	Myelin, rhMOG MOG34-56	CFA CFA/IFA	Chronic monophasic or RR, visual impairment
				148,149
				150
				151
				151
				152
				153,154
				155
				156-158,161
				This thesis

CFA, complete Freund's adjuvant; IFA, incomplete Freund's adjuvant; LPC, lysophosphatidyl choline; MOG, myelin oligodendrocyte glycoprotein; PLP, proteolipid protein; RR, relapsing-remitting; SCH, spinal cord homogenate; SFV, Semliki forest virus; TCR, T-cell receptor; TMEV, Theiler's murine encephalomyelitis virus

inflammatory process was observed rather than selective demyelination as seen in MS. Cellular infiltrates consisted of lymphocytes, macrophages, and neutrophils<sup>161</sup>.

To create a model with a milder clinical course and pathology, five marmosets were immunized with human myelin in CFA that contained a lower dose of *M. tuberculosis*. *Bordetella pertussis* was omitted from the EAE induction protocol. The average day of sacrifice was delayed to almost 37 weeks after immunization. Inactive lesions dominated over active lesions and the cellular infiltrates contained lymphocytes and macrophages<sup>161</sup>.

The next step was to determine the contribution of specific immune reactions against the myelin proteins MBP and MOG to the development of EAE. Immunization with MBP in CFA, containing *M. butyricum*, without *Bordetella pertussis* induced only mild symptoms, such as loss of appetite and altered walking pattern, and small CNS lesions in two of the three marmosets. In contrast, immunization with recombinant human (rh) MOG, which represents the N-terminal domain of MOG from amino acid 1 to 125 and is produced as non-glycosylated protein in *E. coli*, formulated with CFA, containing *M. butyricum*, induced neurological symptoms as paresis and paralysis. As in the previous models with human myelin, a single immunization with rhMOG in CFA led to a 100% disease incidence with a variable disease onset<sup>158</sup>. The heterogeneous disease onset is caused by the outbred nature of the marmosets. The analysis of the immune process underlying this heterogeneous disease course is one of the subjects of this thesis.

The first lesions in the rhMOG/CFA model are detected by MRI between 5 and 39 (mean 14) weeks after immunization. Lesions disseminate in time and space as is also seen in MS. The majority of the animals showed an increase in lesion load before neurological symptoms were detectable<sup>162</sup>. Active and inactive lesions were detected side-by-side, but most lesions were in the active phase and resembled the MS pattern II lesions with complement/Ab-mediated damage<sup>162-165</sup>. Histological signs of axonal injury, assessed by immunoreactivity for accumulated  $\beta$ -amyloid precursor protein and non-phosphorylated neurofilaments (SMI-32), was confined to inflammatory active lesions<sup>163</sup>.

Three types of GM lesions are present in this EAE model, which are comparable with GM lesions observed in MS<sup>55,166,167</sup>. Leukocortical lesions were found in all six examined marmoset brains and accounted for 57% of the total number of cortical lesions. Intracortical lesions were found in two of the six marmoset brains, whereas subpial lesions were found in five of the six marmosets and accounted for 88% of the total demyelinated cortical area. Activated macrophages and microglia were found in leukocortical and intracortical lesions, but the density was lower than in WM lesions, as has also been described for MS. Subpial lesions expressed only little signs of inflammation<sup>166</sup>. Furthermore, the cortical thickness was reduced in marmosets with

EAE compared to controls, but no differences were observed between demyelinated and myelinated areas<sup>168</sup>. Intracortical, but not subpial, lesions displayed Ig leakage and complement deposition<sup>167</sup>.

### **Myelin oligodendrocyte glycoprotein**

The function of MOG in the CNS is unknown as MOG-deficient mice do not present clinical or histological abnormalities<sup>169</sup>. However, MOG is an important target of the autoimmune attack in EAE. Autoimmunity against MOG is crucial for the progression of EAE in Biozzi ABH mice<sup>170</sup> and marmosets<sup>171</sup>. Immunization with rhMOG protein or MOG peptides induces Ab and T-cell responses<sup>172,173</sup>. Ab against MOG facilitate demyelination and phagocytosis *in vitro*<sup>174,175</sup> and enhance demyelination *in vivo* in mice<sup>176</sup>, rats<sup>177,178</sup>, and marmosets<sup>156,179</sup>. T-cell responses against MOG are found in EAE models in mice<sup>148</sup>, rats<sup>180</sup>, marmosets<sup>158</sup>, and rhesus macaques<sup>155</sup>. Rearrangement of the TCR of MOG-specific T-cells is essential for the development of a relapse in mouse EAE models<sup>181</sup>. EAE can be induced by adoptive transfer of MOG-specific T-cells, demonstrating their pathogenic capacity<sup>182</sup>. Anti-MOG T-cells are present in the normal repertoire of marmosets, as was also observed in healthy human donors<sup>182</sup>. Both Th1 and Th17 cells play a role in EAE, but the exact contribution of each cell type is still under debate<sup>183-190</sup>.

An interesting feature of MOG is that the sequence of MOG39-46 (WYRPPFSR) is almost identical to amino acid 986 to 993 (WLRSPFSR) from the major capsid protein UL86 of cytomegalovirus (CMV) and to amino acid 963 to 970 (WQRTPFSV) from the major capsid protein of HHV-6. MOG34-56-specific T-cell lines (TCL) obtained from MOG34-56/CFA-immunized rhesus macaques proliferated *in vitro* in response to the peptide from CMV, but not to the peptide from HHV-6. Immunization of rhesus macaques with UL86 peptide 981-1003, which includes the cross-reactive T-cell epitope 986-993, induced the activation of MOG34-56-specific T-cells *in vivo*, but neurological deficit was not observed<sup>191</sup>. This suggests that CMV-induced memory T-cells can be activated by APC that present MOG39-46.

### **Adjuvants**

The best-known and most widely used adjuvant for EAE induction is CFA, which is composed of paraffin oil containing the surfactant mannide mono-oleate (incomplete Freund's adjuvant (IFA)) and heat-killed *M. tuberculosis* or *M. butyricum*. When IFA or CFA is mixed with the Ag in an aqueous solution, a viscous water-in-oil emulsion is formed.

The exact mechanism of action of IFA and CFA is unknown, but several mechanisms are suggested. First, IFA and CFA form an Ag-depot prolonging the presence of the Ag at the injection site. Second, IFA and CFA enhance the uptake of Ag by local dendritic

cells (DC) that migrate to the draining lymphoid organs. Third, CFA, and to a lesser extent IFA, provide several signals to the (innate) immune system<sup>192</sup>. IFA and CFA can enhance the production of Ab. CFA skews the T-cell response towards Th1, but recently it was suggested that also Th17 cells can be activated by CFA<sup>192,193</sup>. IFA may favor Th2 skewing<sup>194,195</sup>. Furthermore, CFA enhances the permeability of the BBB<sup>196</sup>. CFA and IFA do not activate the inflammasome via Nalp3<sup>197</sup>.

Both IFA and CFA cause inflammation and granuloma formation at the injection sites and in organs, such as lung and liver, although this is more severe with CFA<sup>192</sup>. Furthermore, CFA also induces enlargement of lymphoid organs, haematopoietic dysfunction, and disruption of lymph node architecture<sup>192</sup>.

The addition of bacterial components, such as Toll-like receptor ligands or bacterial cell wall components, to IFA may also be sufficient to induce EAE<sup>198</sup>. Indeed, EAE in C57BL/6 mice can be induced by immunization with MOG35-55 in IFA with the addition of peptidoglycan derived from *Staphylococcus aureus*<sup>199</sup>. In contrast, EAE cannot be induced in SJL mice with PLP139-151 in IFA when CpG dinucleotides are added to activate TLR9<sup>193</sup>.

In addition to CFA, EAE induction in several mouse strains requires injection with inactivated *Bordetella pertussis* or pertussis toxin. Both adjuvants enhance the Th1 skewing effect of CFA and increase the expression of inducible nitric oxide synthase and TNF- $\alpha$ <sup>200,201</sup>. Moreover, they facilitate EAE development by inducing permeabilization of the BBB<sup>202</sup>. In addition, pertussis toxin induces clinical disease and peripheral proliferation of Th17 cells when co-injected with PLP and IFA in SJL mice<sup>203</sup>.

## THE MARMOSSET

### General features

The common marmoset, also called cotton-eared monkey or white-tufted ear monkey, is a New World monkey that belongs to the family of Callitrichidae, the genus *Callithrix*, and the species *jacchus* (*Callithrix jacchus*). The marmoset is a non-endangered species and has an evolutionary distance from humans of 35 million years<sup>204</sup>. The marmoset has its natural habitat in the Amazon forest in Brasil, has an average length of 20 cm with a 30 cm tail, an average weight of 300-350 gram, and an average life span of 10 years. Marmosets reach sexual maturation between 10 and 15 months and have an average gestational period of 143 days. Once or twice a year, marmosets give birth to a twin or triplet<sup>205</sup>. Marmosets are social animals living in groups of about eight individuals usually comprising adults and their offspring<sup>206</sup>.

Marmosets are used in several disciplines of biomedical research, e.g. infectious

**Table 3. Advantages and limitations of the marmoset.**

<b>Advantage</b>
<ul style="list-style-type: none"> <li>• (Neuro)anatomical, immunological, physiological and microbiological <b>proximity to humans</b>.</li> <li>• <b>Outbred nature</b> of the marmoset more closely reflects the genetic heterogeneity of the human population than inbred animal strains.</li> <li>• EAE or other diseases are induced <b>at adult age</b> when the immune system is fully matured.</li> <li>• The <b>conventional housing</b> implies free exposure to immune shaping pathogens both from the 'milieu exterieur' (environment, gut flora) and the 'milieu interieur' (e.g. latent infection with herpesviruses such as CMV, EBV).</li> <li>• Biological therapeutics developed for human diseases, such as monoclonal antibodies or cytokines, often <b>cross-react</b> with marmosets. These can thus be tested in marmosets as a preclinical evaluation of efficacy and safety.</li> <li>• <b>Easy housing and handling</b> due to its small size.</li> <li>• Therapeutic experiments require 10- to 20-fold <b>less compound</b> than in the larger macaques.</li> <li>• Twins are born as <b>bone-marrow chimeras</b> caused by the shared placental blood stream. Therefore, twins can be used as pairs in adoptive transfer studies or in the validation of new therapeutics.</li> </ul>
<b>Limitation</b>
<ul style="list-style-type: none"> <li>• <b>Ethical</b>: When the same information can be obtained in lower species, marmosets cannot be used. Also experimental manipulations are limited.</li> <li>• <b>Outbred nature</b>: the genetic heterogeneity creates clinical and pathological heterogeneity, which may affect the interpretation of data. This feature can be compensated in part by using twins, which due to the bone marrow chimerism are immunologically more comparable than unrelated monkeys.</li> <li>• <b>High costs</b> not only of the monkeys themselves, but also of the housing and care.</li> <li>• <b>Cross-reactivity</b> of diagnostic reagents, such as FACS antibodies is more limited than for rhesus macaques.</li> <li>• <b>Blood volume</b> that can be withdrawn is limited.</li> <li>• <b>Adoptive transfer</b> studies are technically difficult.</li> </ul>

diseases, neuroscience, and drug development<sup>207,208</sup>. The use of marmosets in biomedical research has several advantages, but also limitations (Table 3). A particularly interesting aspect of marmosets is the stable bone marrow chimerism between twin siblings that is caused by the sharing of the placental blood stream. Consequently, the immune systems of twins are educated in the same thymic environment, making fraternal siblings immunologically more similar than siblings from different births<sup>209</sup>. This principle can be used in therapy trials where one twin sibling is treated with an experimental agent and the other sibling with placebo.

### **Immunogenetics and immunology**

The *Mhc* is a dense genomic region, mainly comprising immune genes involved in Ag presentation. Two main regions are discerned within the *Mhc*, i.e. class I and II. *Mhc* class I contains the classical *A*, *B*, and *C* and the nonclassical *E*, *F*, *G*, *H*, and *J* genes. The classical class I molecules are heterodimers of a heavy  $\alpha$  chain with  $\beta$ 2-microglobulin

and are expressed by all nucleated cell types where they present intracellular Ag to cytotoxic (CD8<sup>+</sup>) T-cells. The nonclassical molecules have more diverse functions and are often cell type specific. *Mhc* class II is arranged in *DP*, *DQ*, and *DR* regions, each containing at least one pair of A and B genes encoding the  $\alpha$  and  $\beta$  polypeptide chains of the MHC molecule. Class II molecules are only expressed by APC and present Ag to CD4<sup>+</sup> T-cells. The *Mhc* region is characterized by genetic diversity as shown by the high number of genes and loci, which are acquired by duplication during evolution, and the presence of allelic polymorphisms. There is a lot of diversity between species through gain and loss of loci<sup>210</sup>.

In the marmoset, *Mhc* class I diversity is very limited. *Caja-A*, *-B*, and *-C* could not be identified and only 2 *Caja-E* and 5 *Caja-G* alleles have been described until now<sup>211,212</sup> (Table 4). It has been suggested that *Caja-E* is orthologous to *HLA-E*, whereas a relationship between *Caja-G* and *HLA-G* is doubtful<sup>213</sup>. It is highly likely that *Caja-G* contains more alleles and that *Caja-G* functions as classical HLA molecule.

**Table 4. MHC alleles described for the marmoset.**

Class I <sup>b</sup>		
Locus	Lineage	
E	*01	
E	*02	
G	*01	
G	*02	
G	*03	
G	*04	
G	*05	
Class II <sup>c</sup>		
Locus	Lineage	Alleles
DQA1	*01	01
	*27 <sup>a</sup>	01
DQB1	*2201	01, 02
	*23	01, 02
DQB2	*01	01, 02
DRB1	*03	01, 02, 03, 04, 05, 06, 07, 08, 09, 10, 11, 12, 14
DRB	*W12	01, 02
DRB	*W16	01, 04, 05, 06, 07, 08, 09, 10, 11, 12, 13, 14, 15, 16, 17, 18, 20, 22, 23, 24

<sup>a</sup> previously described as \*25

<sup>b</sup> Class I is based on <sup>211,212</sup>

<sup>c</sup> Class II is based on <sup>214-217</sup>

The marmoset *Mhc* class II contains *DQA1*, *DQB1*, and *DQB2*, but *Caja-DQA2* and *Caja-DP* could not be identified (Table 4). The *Caja-DQA1\*0101* allele clusters together with humans, apes, Old World monkeys, and New World monkeys. In contrast, *Caja-DQA1\*2701* (previously called \*2501) is restricted to New World monkeys. Although *DQA2* and *DQB2* are considered to be pseudogenes, *Caja-DQB2* is highly similar to *HLA-DQB2*<sup>214</sup>. Marmosets contain one *DRB* region configuration, containing the three lineages *DRB1\*03*, *DRB\*W12*, and *DRB\*W16*. *Caja-DRB1\*03* and *-DRB\*W16* are polymorphic with 13 and 20 alleles, respectively (Table 4). *Caja-DRB\*W12* appears to be monomorphic with two alleles, which differ only two codons from each other. All marmosets express *Caja-DRB\*W1201* or *-DRB\*W1202*<sup>214-217</sup>. The expression of *Caja-DRB1\*03* is very low, if detectable at all. Exceptional alleles are *DRB1\*0307* and *DRB1\*0312* that are highly expressed. Interestingly, exon 2 of *DRB1\*0307* and *DRB1\*0312* is similar to *HLA-DRB1\*03* and matches all features of the *Caja-DRB1\*03* locus, whereas the other exons align with *Caja-DRB\*W16*<sup>217</sup>. The exact nucleotide sequence of the alleles of the marmoset *Mhc* region has been published in an online database<sup>218</sup>. The low variability in MHC class II in marmosets may explain the increased susceptibility to fatal infections with certain bacteria, such as *Klebsiella*, *Bordetella*, *Clostridium*, and *Shigella*<sup>208,219</sup>.

Despite the limited polymorphism of the *Mhc*, marmosets have a diverse and evolutionary stable TCR  $\alpha$ - and  $\beta$ -chain repertoire. The constant region of the  $\alpha$ -chain gene of marmosets has an 89% nucleotide and 80% amino acid similarity with humans. Furthermore, 46 joining genes and 35 genes for the variable region were identified. The similarity with humans at the nucleotide and amino acid level was higher than 80% and 69%, respectively<sup>220</sup>. Analysis of the variable (V), diversity (D), and joining (J) genes of the  $\beta$ -chain identified 15 V, 2 D, and 13 J genes. These genes are highly similar to the human genes. For example, the 15 V genes of the marmoset TCR had an average similarity of 88.5% to human V genes. Two constant (C) genes were identified in the marmoset TCR, named CjCB1 and CjCB2, which were similar to two constant genes in humans, BC1 and BC2. In addition, the complementarity-determining region 3 (CDR3) of the TCR in marmosets has an average length of 10 amino acids, which is similar to the length in mice and humans<sup>221</sup>.

Six Ig heavy chain variable subgroups were detected, which show a high degree of sequence similarity to the heavy chain variable regions in humans. The major difference with humans is the absence of the second subgroup in the marmoset<sup>222</sup>. The IgE system is similar to humans, but IgE plasma levels were much lower in marmosets than in humans<sup>223</sup>. Further knowledge about the Ig genes in marmosets is still very limited, although this will likely improve in the near future since the marmoset genome has been sequenced recently.

A large panel of mAb against human cluster of differentiation (CD) markers, which are developed to detect human leukocyte subsets, is cross-reactive with marmoset leukocytes<sup>224,225</sup>. This suggests a high level of conservation of CD markers in New World monkeys.

## Neuroanatomy

The marmoset brain has an average weight of 7.9 gram, which represents about 2.7% of its body weight. This is equivalent to the 2% brain mass in humans, whereas a rat brain only weights 0.5% of its total body weight<sup>207</sup>. The index of cranial capacity assesses the relationship between the observed cranial capacity and the expected cranial capacity. Marmosets have a cranial capacity index of 6.0, which is comparable to 8.2 of the rhesus macaque. Humans have a cranial capacity index of 23<sup>226</sup>.

The neuroanatomy and the ratio between WM and GM in the marmoset brain are comparable to humans<sup>227</sup>. Several neurotransmitter receptors, such as the NMDA receptors, show a similar distribution pattern in the striate cortex of marmosets and humans<sup>228</sup>. The optic chiasm in marmosets has the same segregation hemispheric pathway as in humans, in contrast to rodents in which crossed and non-crossed fibers mix<sup>229</sup>.

To model MS in marmosets, it is important that the anatomy and function of the cortex is comparable between humans and marmosets as GM changes may play a role in the clinical deterioration of MS patients<sup>51,56,59</sup>. The marmoset cortex has indeed similarities with Old World monkeys and humans, but also several differences. The orbital and medial frontal cortices are highly conserved, whereas the granular frontal cortex has changed during evolution. For example, the histological subdivision of the granular frontal cortex is less obvious in marmosets than in humans<sup>230,231</sup>.

Marmosets are extremely useful for application of imaging techniques *in vivo* and post mortem (Figure 6). The preferred imaging tool for the visualization and characterization of lesions in the brain is MRI, which can be performed *in vivo* or post mortem. In MRI the magnetic properties of protons, which occur at different concentrations in different regions of a tissue or organ, are used to generate contrast. The most frequently monitored MRI parameters in MS diagnosis are T2-weighted (T2W) and contrast-enhanced T1-weighted (T1W) images (Table 5). GM lesions can be analysed by post mortem MRI using inversion images in which the GM signal is suppressed (Table 5, Figure 6) and small lesions may be visualized by fluid-attenuated inversion recovery imaging.

Taken together, the multidisciplinary research conducted over the past decade has transformed the EAE model in marmosets into a preclinical model for translational research into the pathogenesis of MS and for the development of novel treatments, which are described in the following chapters.

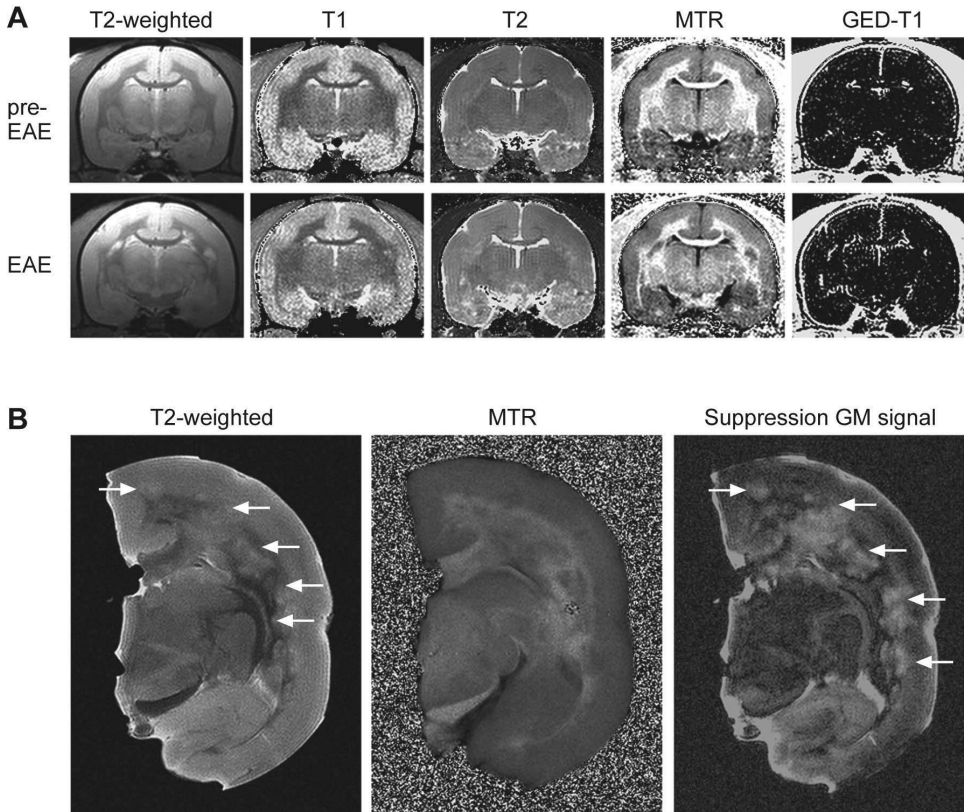


**Figure 6. MRI sequences used for visualization of brain lesions.**

A, A marmoset monkey in which EAE was induced by immunization with rhMOG/CFA was subjected at 14 days interval to brain MRI at 4.7 Tesla. Scans of the same monkey before brain lesions were detected (pre-EAE) and during clinical EAE (EAE) are shown. The first picture is a high contrast T2-weighted scan visualizing the spatial distribution and shape of lesions. The next three pictures are semi-quantitative scans in which the T1 and T2 relaxation times and the MTR ratios are plotted. The last picture shows a differential scan created by subtracting T1-weighted images recorded before and after intravenous injection of the paramagnetic contrast probe gadolinium-DTPA. B, High-contrast post mortem MRI shows white and grey matter lesions (arrows) on a T2-weighted scan, on a scan with the MTR ratios, and on a scan in which the grey matter (GM) signal was suppressed leading to a better visualization of GM lesions.

**Table 5. MRI parameters.**

T1-weighted	Detects disappearance of tissue, e.g. due to demyelination or axonal injury. T1W images are sensitized for the T1 relaxation time, a time constant that describes the rate in which the longitudinal component of the magnetization vector recovers.
T1-weighted + contrast agent	Visualization of the permeability of the BBB. Data is shown as percentage increase in signal intensity due to presence of the leaking MR contrast agent in the brain parenchyma.
T2-weighted	Used to determine lesion volume (voxel or mm <sup>3</sup> ). T2W images are sensitized for the T2 values.
T2 relaxation time images	T2 values are sensitive to changes in water content (edema) and demyelination. T2 image displays T2 relaxation time values, a time constant (~ milliseconds) describing the decay of the magnetization vector in the transversal plane.
Magnetization Transfer Ratio	The MTR is reduced by demyelination and edema. Measures the ratio of protons of macromolecule-bound water and freely moving water. The macromolecule-bound protons of water are saturated by a magnetization transfer pulse and this saturation is transferred to the protons of freely moving water. The latter is, together with the T1 and T2 relaxation time, the main contributor to the MR signal. Data is shown as percentage decrease in signal intensity due to the saturation pulse.
Inversion recovery image	Images in which the signal arising from a specific fluid or tissue, such as CSF, white matter, or grey matter, is suppressed. Suppression of the grey matter signal facilitates the detection of grey matter lesions.
Diffusion tensor imaging	Diffusion MRI measures the diffusion of freely moving water molecules in tissue. The presence of cell boundaries may restrict this diffusion. In diffusion tensor imaging (DTI) the preferred direction of the water diffusion is calculated. For an intact axon this will be mainly along the direction of the myelinated axons as the myelin sheaths will limit the diffusion of water perpendicular to this direction. In an injured axon water will also diffuse perpendicular to the direction of the axon.

## AIM AND OUTLINE OF THIS THESIS

Despite many years of research, the (immuno)pathogenic mechanisms causing MS are still unknown and a therapy to arrest the disease is still lacking. For both exploratory and applied research (Figure 1) the marmoset EAE model can be used, because this model closely resembles MS in an immunological, clinical, and pathological manner. The aim of the research described in this thesis has been to investigate pathogenic mechanisms underlying EAE and MS and to identify new targets for MS therapy.

To study immunopathogenic mechanisms in experimental models, flow cytometry and immunohistochemistry are indispensable techniques. A large panel of anti-human Ab that can be used for flow cytometry analysis of marmoset cells has already been described<sup>225</sup>. In **chapter 2**, we have investigated the cross-reactivity of a selection of anti-human Ab with lymphoid tissue from six NHP species, including the marmoset.

Immunization of marmosets with rhMOG induces a 100% EAE incidence, but with a heterogeneous disease onset<sup>158</sup>. In **chapter 3.1**, we have investigated the autoimmune mechanisms underlying this heterogeneous disease course. In addition, we describe a new marmoset EAE model induced with MOG34-56 and the phenotype and function of T-cells associated with this disease.

In **chapter 3.1**, we demonstrate that MOG34-56 in IFA induces EAE in MOG74-96/CFA sensitized animals. This led to the hypothesis that EAE in marmosets can be induced without CFA. Indeed, in **chapter 3.2** we show that immunization with MOG34-56 in IFA induced a disease with clinical symptoms and pathology similar to rhMOG/CFA- and MOG34-56/CFA-induced marmoset EAE models.

The pathogenic role of IL-17A in rodent EAE models and in MS is still under debate. In marmosets, MOG34-56-specific T-cells produce IL-17A. Therefore, we have investigated the role of IL-17A in the marmoset EAE model. In **chapter 4.1**, EAE was induced by rhMOG in CFA and IL-17A was neutralized by two doses of a mAb.

The B-cell depleting Ab rituximab is a promising treatment for MS, since clinical deterioration is prevented and the brain WM lesion load is reduced<sup>36,37</sup>. In **chapters 4.2 and 4.3**, EAE was induced by rhMOG in CFA and B-cells were depleted by a mAb (HuMab 7D8) 21 days after immunization to avoid interference of the B-cell depletion with the induction of the immunopathogenic process. The pathogenic mechanisms underlying the effect of B-cell depletion in MS is unknown since total Ig levels were not changed. In **chapter 4.2**, we have investigated the effect of late B-cell depletion on the immune system. Here, evidence is shown that it is likely that B-cells act as APC in EAE. In **chapter 4.3**, we have investigated the effect of B-cell depletion on CNS pathology. The development of WM and GM lesions were analysed by *in vivo* and post mortem MRI. In addition, demyelination and inflammation were assessed in the WM and GM of the brain as well as in spinal cord and optic nerve by histology.

Instead of interfering with the immune response, promotion of (re)myelination and neuronal outgrowth may be a promising aim of therapy. To investigate this, MOG34-56/CFA-immunized marmosets were treated with a mAb against the neurite outgrowth inhibitor Nogo-A in **chapter 4.4**. In addition, we demonstrate the role of Nogo-A in differentiation and myelination of oligodendrocyte precursor cells (OPC).

MS relapse rate decreases during pregnancy, especially during the third trimester. In this phase, fragments derived from the  $\beta$ -subunit of the pregnancy hormone human chorionic gonadotropin (hCG) are present in serum and urine. Previous studies showed that synthetic  $\beta$ -hCG-related peptides have modulatory effects in acute immune responses. Therefore, we have investigated whether the  $\beta$ -hCG-related tetrapeptide LQGV can modulate EAE in **chapter 4.5**.

In this thesis, EAE is induced in marmosets by three different induction protocols. In **chapter 5**, we discuss similarities and differences between these models. The experimental data presented in this thesis are discussed in relation to the pathogenic mechanisms of EAE and MS in the periphery and in the CNS. Furthermore, the mechanisms underlying the IFA model are discussed.

## REFERENCES

1. Kola I. The state of innovation in drug development. *Clin Pharmacol Ther* 83:227-230 (2008)
2. 't Hart BA et al. Treatment with chimeric anti-human CD40 antibody suppresses MRI-detectable inflammation and enlargement of pre-existing brain lesions in common marmosets affected by MOG-induced EAE. *J Neuroimmunol* 163:31-39 (2005)
3. Boon L et al. Prevention of experimental autoimmune encephalomyelitis in the common marmoset (*Callithrix jacchus*) using a chimeric antagonist monoclonal antibody against human CD40 is associated with altered B cell responses. *J Immunol* 167:2942-2949 (2001)
4. Brok HP et al. Prevention of experimental autoimmune encephalomyelitis in common marmosets using an anti-IL-12p40 monoclonal antibody. *J Immunol* 169:6554-6563 (2002)
5. Laman JD et al. Protection of marmoset monkeys against EAE by treatment with a murine antibody blocking CD40 ( $\mu$ 5D12). *Eur J Immunol* 32:2218-2228 (2002)
6. Noseworthy JH et al. Multiple sclerosis. *N Engl J Med* 343:938-952 (2000)
7. Compston A et al. Multiple sclerosis. *Lancet* 359:1221-1231 (2002)
8. Sospedra M et al. Immunology of multiple sclerosis. *Annu Rev Immunol* 23:683-747 (2005)
9. Compston A et al. Multiple sclerosis. *Lancet* 372:1502-1517 (2008)
10. Lublin FD et al. Defining the clinical course of multiple sclerosis: results of an international survey. National Multiple Sclerosis Society (USA) Advisory Committee on Clinical Trials of New Agents in Multiple Sclerosis. *Neurology* 46:907-911 (1996)
11. Willer CJ et al. Twin concordance and sibling recurrence rates in multiple sclerosis. *Proc Natl Acad Sci USA* 100:12877-12882 (2003)
12. Barcellos LF et al. Heterogeneity at the HLA-DRB1 locus and risk for multiple sclerosis. *Hum Mol Genet* 15:2813-2824 (2006)
13. Ramagopalan SV et al. The inheritance of resistance alleles in multiple sclerosis. *PLoS Genet* 3:1607-1613 (2007)
14. Okuda DT et al. Genotype-Phenotype correlations in multiple sclerosis: HLA genes influence disease severity inferred by 1HMR spectroscopy and MRI measures. *Brain* 132:250-259 (2009)
15. Hafler DA et al. Risk alleles for multiple sclerosis identified by a genome-wide study. *N Engl J Med* 357:851-862 (2007)
16. De Jager PL et al. Meta-analysis of genome scans and replication identify CD6, IRF8 and TNFRSF1A as new multiple sclerosis susceptibility loci. *Nat Genet* 41:776-782 (2009)
17. Jakkula E et al. Genome-wide association study in a high-risk isolate for multiple sclerosis reveals associated variants in STAT3 gene. *Am J Hum Genet* 86:285-291 (2010)
18. Aulchenko YS et al. Genetic variation in the KIF1B locus influences susceptibility to multiple sclerosis. *Nat Genet* 40:1402-1403 (2008)
19. Booth DR et al. Lack of support for association between the KIF1B rs10492972[C] variant and multiple sclerosis. *Nat Genet* 42:469-470 (2010)
20. De Jager PL et al. Integration of genetic risk factors into a clinical algorithm for multiple sclerosis susceptibility: a weighted genetic risk score. *Lancet Neurol* 8:1111-1119 (2009)
21. Pugliatti M et al. The epidemiology of multiple sclerosis in Europe. *Eur J Neurol* 13:700-722 (2006)
22. Beretich BD et al. Explaining multiple sclerosis prevalence by ultraviolet exposure: a geospatial analysis. *Mult Scler* 15:891-898 (2009)
23. Munger KL et al. Serum 25-hydroxyvitamin D levels and risk of multiple sclerosis. *Jama* 296:2832-2838 (2006)
24. Tremlett H et al. Monthly ambient sunlight, infections and relapse rates in multiple sclerosis. *Neuroepidemiology* 31:271-279 (2008)
25. Correale J et al. Immunomodulatory effects of vitamin D in multiple sclerosis. *Brain* 132:1146-1160 (2009)

26. Ramagopalan SV et al. Expression of the multiple sclerosis-associated MHC class II Allele HLA-DRB1\*1501 is regulated by vitamin D. *PLoS Genet* 5:e1000369 (2009)
27. Buljevac D et al. Prospective study on the relationship between infections and multiple sclerosis exacerbations. *Brain* 125:952-960 (2002)
28. Christensen T. Human herpesviruses in MS. *Int MS J* 14:41-47 (2007)
29. Martyn CN et al. Symptomatic Epstein-Barr virus infection and multiple sclerosis. *J Neurol Neurosurg Psychiatry* 56:167-168 (1993)
30. Buljevac D et al. Epstein-Barr virus and disease activity in multiple sclerosis. *J Neurol Neurosurg Psychiatry* 76:1377-1381 (2005)
31. Sargsyan SA et al. Absence of Epstein-Barr virus in the brain and CSF of patients with multiple sclerosis. *Neurology* 74:1127-1135 (2010)
32. Pender MP. Infection of autoreactive B lymphocytes with EBV, causing chronic autoimmune diseases. *Trends Immunol* 24:584-588 (2003)
33. Serafini B et al. Dysregulated Epstein-Barr virus infection in the multiple sclerosis brain. *J Exp Med* 204:2899-2912 (2007)
34. Willis SN et al. Epstein-Barr virus infection is not a characteristic feature of multiple sclerosis brain. *Brain* 132:3318-3328 (2009)
35. Niess JH et al. Commensal gut flora drives the expansion of proinflammatory CD4 T cells in the colonic lamina propria under normal and inflammatory conditions. *J Immunol* 180:559-568 (2008)
36. Bar-Or A et al. Rituximab in relapsing-remitting multiple sclerosis: a 72-week, open-label, phase I trial. *Ann Neurol* 63:395-400 (2008)
37. Hauser SL et al. B-cell depletion with rituximab in relapsing-remitting multiple sclerosis. *N Engl J Med* 358:676-688 (2008)
38. McDonald WI et al. Recommended diagnostic criteria for multiple sclerosis: guidelines from the International Panel on the diagnosis of multiple sclerosis. *Ann Neurol* 50:121-127 (2001)
39. Bo L et al. Detection of MHC class II-antigens on macrophages and microglia, but not on astrocytes and endothelia in active multiple sclerosis lesions. *J Neuroimmunol* 51:135-146 (1994)
40. Lassmann H et al. Immunopathology of multiple sclerosis: report on an international meeting held at the Institute of Neurology of the University of Vienna. *J Neuroimmunol* 86:213-217 (1998)
41. van der Valk P et al. Staging of multiple sclerosis (MS) lesions: pathology of the time frame of MS. *Neuropathol Appl Neurobiol* 26:2-10 (2000)
42. Ferguson B et al. Axonal damage in acute multiple sclerosis lesions. *Brain* 120:393-399 (1997)
43. Trapp BD et al. Axonal transection in the lesions of multiple sclerosis. *N Engl J Med* 338:278-285 (1998)
44. Lucchinetti C et al. Heterogeneity of multiple sclerosis lesions: implications for the pathogenesis of demyelination. *Ann Neurol* 47:707-717 (2000)
45. Breij EC et al. Homogeneity of active demyelinating lesions in established multiple sclerosis. *Ann Neurol* 63:16-25 (2008)
46. Barnett MH et al. Relapsing and remitting multiple sclerosis: pathology of the newly forming lesion. *Ann Neurol* 55:458-468 (2004)
47. Barnett MH et al. The pathology of multiple sclerosis: a paradigm shift. *Curr Opin Neurol* 19:242-247 (2006)
48. Barkhof F. MRI in multiple sclerosis: correlation with expanded disability status scale (EDSS). *Mult Scler* 5:283-286 (1999)
49. Barkhof F. The clinico-radiological paradox in multiple sclerosis revisited. *Curr Opin Neurol* 15:239-245 (2002)
50. Trapp BD et al. Axonal pathology in multiple sclerosis: relationship to neurologic disability. *Curr Opin Neurol* 12:295-302 (1999)
51. Kutzelnigg A et al. Cortical lesions and brain atrophy in MS. *J Neurol Sci* 233:55-59 (2005)
52. Lazeron RH et al. Brain atrophy and lesion load as explaining parameters for cognitive impairment in multiple sclerosis. *Mult Scler* 11:524-531 (2005)

53. Bo L et al. Subpial demyelination in the cerebral cortex of multiple sclerosis patients. *J Neuropathol Exp Neurol* 62:723-732 (2003)
54. Bo L et al. Intracortical multiple sclerosis lesions are not associated with increased lymphocyte infiltration. *Mult Scler* 9:323-331 (2003)
55. Bo L et al. Grey matter pathology in multiple sclerosis. *Acta Neurol Scand Suppl* 183:48-50 (2006)
56. Geurts JJ et al. Grey matter pathology in multiple sclerosis. *Lancet Neurol* 7:841-851 (2008)
57. Brink BP et al. The pathology of multiple sclerosis is location-dependent: no significant complement activation is detected in purely cortical lesions. *J Neuropathol Exp Neurol* 64:147-155 (2005)
58. van Horssen J et al. The blood-brain barrier in cortical multiple sclerosis lesions. *J Neuropathol Exp Neurol* 66:321-328 (2007)
59. Vrenken H et al. Altered diffusion tensor in multiple sclerosis normal-appearing brain tissue: cortical diffusion changes seem related to clinical deterioration. *J Magn Reson Imaging* 23:628-636 (2006)
60. Reboldi A et al. C-C chemokine receptor 6-regulated entry of TH-17 cells into the CNS through the choroid plexus is required for the initiation of EAE. *Nat Immunol* 10:514-523 (2009)
61. Hauser SL et al. The neurobiology of multiple sclerosis: genes, inflammation, and neurodegeneration. *Neuron* 52:61-76 (2006)
62. Goverman J. Autoimmune T cell responses in the central nervous system. *Nat Rev Immunol* 9:393-407 (2009)
63. Kroepfl JF et al. Investigation of myelin/oligodendrocyte glycoprotein membrane topology. *J Neurochem* 67:2219-2222 (1996)
64. Ohler B et al. Role of lipid interactions in autoimmune demyelination. *Biochim Biophys Acta* 1688:10-17 (2004)
65. Clements CS et al. The crystal structure of myelin oligodendrocyte glycoprotein, a key autoantigen in multiple sclerosis. *Proc Natl Acad Sci USA* 100:11059-11064 (2003)
66. Meslele MF et al. Marmoset fine B cell and T cell epitope specificities mapped onto a homology model of the extracellular domain of human myelin oligodendrocyte glycoprotein. *Neurobiol Dis* 9:160-172 (2002)
67. Delarasse C et al. Complex alternative splicing of the myelin oligodendrocyte glycoprotein gene is unique to human and non-human primates. *J Neurochem* 98:1707-1717 (2006)
68. Pham-Dinh D et al. Myelin/oligodendrocyte glycoprotein is a member of a subset of the immunoglobulin superfamily encoded within the major histocompatibility complex. *Proc Natl Acad Sci USA* 90:7990-7994 (1993)
69. Sun J et al. T and B cell responses to myelin-oligodendrocyte glycoprotein in multiple sclerosis. *J Immunol* 146:1490-1495 (1991)
70. Kerlero de Rosbo N et al. Reactivity to myelin antigens in multiple sclerosis. Peripheral blood lymphocytes respond predominantly to myelin oligodendrocyte glycoprotein. *J Clin Invest* 92:2602-2608 (1993)
71. Diaz-Villoslada P et al. Autoreactivity to myelin antigens: myelin/oligodendrocyte glycoprotein is a prevalent autoantigen. *J Neuroimmunol* 99:36-43 (1999)
72. Koehler NK et al. The human T cell response to myelin oligodendrocyte glycoprotein: a multiple sclerosis family-based study. *J Immunol* 168:5920-5927 (2002)
73. Bruno R et al. Multiple sclerosis candidate autoantigens except myelin oligodendrocyte glycoprotein are transcribed in human thymus. *Eur J Immunol* 32:2737-2747 (2002)
74. Van der Aa A et al. Functional properties of myelin oligodendrocyte glycoprotein-reactive T cells in multiple sclerosis patients and controls. *J Neuroimmunol* 137:164-176 (2003)
75. Kerlero de Rosbo N et al. Predominance of the autoimmune response to myelin oligodendrocyte glycoprotein (MOG) in multiple sclerosis: reactivity to the extracellular domain of MOG is directed against three main regions. *Eur J Immunol* 27:3059-3069 (1997)
76. Bielekova B et al. Expansion and functional relevance of high-avidity myelin-specific CD4+ T cells in multiple sclerosis. *J Immunol* 172:3893-3904 (2004)

77. Matusevicius D et al. Interleukin-17 mRNA expression in blood and CSF mononuclear cells is augmented in multiple sclerosis. *Mult Scler* 5:101-104 (1999)
78. Lock C et al. Gene-microarray analysis of multiple sclerosis lesions yields new targets validated in autoimmune encephalomyelitis. *Nat Med* 8:500-508 (2002)
79. Kebir H et al. Human TH17 lymphocytes promote blood-brain barrier disruption and central nervous system inflammation. *Nat Med* 13:1173-1175 (2007)
80. Ifergan I et al. The blood-brain barrier induces differentiation of migrating monocytes into Th17-polarizing dendritic cells. *Brain* 131:785-799 (2008)
81. Tzartos JS et al. Interleukin-17 production in central nervous system-infiltrating T cells and glial cells is associated with active disease in multiple sclerosis. *Am J Pathol* 172:146-155 (2008)
82. Brucklacher-Waldert V et al. Phenotypical and functional characterization of T helper 17 cells in multiple sclerosis. *Brain* 132:3329-3341 (2009)
83. Babbe H et al. Clonal expansions of CD8(+) T cells dominate the T cell infiltrate in active multiple sclerosis lesions as shown by micromanipulation and single cell polymerase chain reaction. *J Exp Med* 192:393-404 (2000)
84. Skulina C et al. Multiple sclerosis: brain-infiltrating CD8+ T cells persist as clonal expansions in the cerebrospinal fluid and blood. *Proc Natl Acad Sci USA* 101:2428-2433 (2004)
85. Holmoy T. The discovery of oligoclonal bands: a 50-year anniversary. *Eur Neurol* 62:311-315 (2009)
86. Genain CP et al. Identification of autoantibodies associated with myelin damage in multiple sclerosis. *Nat Med* 5:170-175 (1999)
87. Zhou D et al. Identification of a pathogenic antibody response to native myelin oligodendrocyte glycoprotein in multiple sclerosis. *Proc Natl Acad Sci USA* 103:19057-19062 (2006)
88. Lalive PH et al. Antibodies to native myelin oligodendrocyte glycoprotein are serologic markers of early inflammation in multiple sclerosis. *Proc Natl Acad Sci USA* 103:2280-2285 (2006)
89. Sellebjerg F et al. Double-blind, randomized, placebo-controlled study of oral, high-dose methylprednisolone in attacks of MS. *Neurology* 51:529-534 (1998)
90. Miller DM et al. A meta-analysis of methylprednisolone in recovery from multiple sclerosis exacerbations. *Mult Scler* 6:267-273 (2000)
91. Sloka JS et al. The mechanism of action of methylprednisolone in the treatment of multiple sclerosis. *Mult Scler* 11:425-432 (2005)
92. Lopez-Diego RS et al. Novel therapeutic strategies for multiple sclerosis-a multifaceted adversary. *Nat Rev Drug Discov* 7:909-925 (2008)
93. Martinelli V et al. Mitoxantrone: benefits and risks in multiple sclerosis patients. *Neurol Sci* 30 Suppl 2:S167-170 (2009)
94. Vogelgesang A et al. Mitoxantrone treatment in multiple sclerosis induces TH2-type cytokines. *Acta Neurol Scand*, in press (2009)
95. Ebers GCea. Randomised double-blind placebo-controlled study of interferon beta-1a in relapsing/remitting multiple sclerosis. PRISMS (Prevention of Relapses and Disability by Interferon beta-1a Subcutaneously in Multiple Sclerosis) Study Group. *Lancet* 352:1498-1504 (1998)
96. Jacobs LD et al. Intramuscular interferon beta-1a therapy initiated during a first demyelinating event in multiple sclerosis. CHAMPS Study Group. *N Engl J Med* 343:898-904 (2000)
97. Kappos L et al. Effect of early versus delayed interferon beta-1b treatment on disability after a first clinical event suggestive of multiple sclerosis: a 3-year follow-up analysis of the BENEFIT study. *Lancet* 370:389-397 (2007)
98. Wiesemann E et al. Interferon-beta increases the stimulatory capacity of monocyte-derived dendritic cells to induce IL-13, IL-5 and IL-10 in autologous T-cells. *J Neuroimmunol* 123:160-169 (2002)
99. Chen M et al. Regulatory effects of IFN-beta on production of osteopontin and IL-17 by CD4+ T Cells in MS. *Eur J Immunol* 39:2525-2536 (2009)
100. Niemela J et al. IFN-beta regulates CD73 and adenosine expression at the blood-brain barrier. *Eur J Immunol* 38:2718-2726 (2008)

101. Cepok S et al. Enhancement of chemokine expression by interferon beta therapy in patients with multiple sclerosis. *Arch Neurol* 66:1216-1223 (2009)
102. Petkau AJ et al. Longitudinal analyses of the effects of neutralizing antibodies on interferon beta-1b in relapsing-remitting multiple sclerosis. *Mult Scler* 10:126-138 (2004)
103. Axtell RC et al. T helper type 1 and 17 cells determine efficacy of interferon-beta in multiple sclerosis and experimental encephalomyelitis. *Nat Med* 16:406-412 (2010)
104. Johnson KP et al. Copolymer 1 reduces relapse rate and improves disability in relapsing-remitting multiple sclerosis: results of a phase III multicenter, double-blind placebo-controlled trial. The Copolymer 1 Multiple Sclerosis Study Group. *Neurology* 45:1268-1276 (1995)
105. Duda PW et al. Glatiramer acetate (Copaxone) induces degenerate, Th2-polarized immune responses in patients with multiple sclerosis. *J Clin Invest* 105:967-976 (2000)
106. Schrempf W et al. Glatiramer acetate: mechanisms of action in multiple sclerosis. *Autoimmun Rev* 6:469-475 (2007)
107. Polman CH et al. A randomized, placebo-controlled trial of natalizumab for relapsing multiple sclerosis. *N Engl J Med* 354:899-910 (2006)
108. Kleinschmidt-DeMasters BK et al. Progressive multifocal leukoencephalopathy complicating treatment with natalizumab and interferon beta-1a for multiple sclerosis. *N Engl J Med* 353:369-374 (2005)
109. Linda H et al. Progressive multifocal leukoencephalopathy after natalizumab monotherapy. *N Engl J Med* 361:1081-1087 (2009)
110. Carson KR et al. Monoclonal antibody-associated progressive multifocal leukoencephalopathy in patients treated with rituximab, natalizumab, and efalizumab: a Review from the Research on Adverse Drug Events and Reports (RADAR) Project. *Lancet Oncol* 10:816-824 (2009)
111. Johnson KP. Natalizumab (Tysabri) treatment for relapsing multiple sclerosis. *Neurologist* 13:182-187 (2007)
112. Chen Y et al. Asymptomatic reactivation of JC virus in patients treated with natalizumab. *N Engl J Med* 361:1067-1074 (2009)
113. Sadiq SA et al. JCV detection in multiple sclerosis patients treated with natalizumab. *J Neurol* 257:954-958 (2010)
114. Youssef S et al. The HMG-CoA reductase inhibitor, atorvastatin, promotes a Th2 bias and reverses paralysis in central nervous system autoimmune disease. *Nature* 420:78-84 (2002)
115. Greenwood J et al. Lovastatin inhibits brain endothelial cell Rho-mediated lymphocyte migration and attenuates experimental autoimmune encephalomyelitis. *Faseb J* 17:905-907 (2003)
116. Ifergan I et al. Statins reduce human blood-brain barrier permeability and restrict leukocyte migration: relevance to multiple sclerosis. *Ann Neurol* 60:45-55 (2006)
117. Vollmer T et al. Oral simvastatin treatment in relapsing-remitting multiple sclerosis. *Lancet* 363:1607-1608 (2004)
118. Klopffleisch S et al. Negative impact of statins on oligodendrocytes and myelin formation in vitro and in vivo. *J Neurosci* 28:13609-13614 (2008)
119. Chun J et al. Mechanism of action of oral fingolimod (FTY720) in multiple sclerosis. *Clin Neuropharmacol* 33:91-101 (2010)
120. Kappos L et al. Oral fingolimod (FTY720) for relapsing multiple sclerosis. *N Engl J Med* 355:1124-1140 (2006)
121. Kappos L et al. A placebo-controlled trial of oral fingolimod in relapsing multiple sclerosis. *N Engl J Med* 362:387-401 (2010)
122. Gilleece MH et al. Effect of Campath-1H antibody on human hematopoietic progenitors in vitro. *Blood* 82:807-812 (1993)
123. Coles AJ et al. Alemtuzumab vs. interferon beta-1a in early multiple sclerosis. *N Engl J Med* 359:1786-1801 (2008)
124. Ali EN et al. Daclizumab in treatment of multiple sclerosis patients. *Mult Scler* 15:272-274 (2009)

125. Oh U et al. Regulatory T cells are reduced during anti-CD25 antibody treatment of multiple sclerosis. *Arch Neurol* 66:471-479 (2009)
126. Bielekova B et al. Humanized anti-CD25 (daclizumab) inhibits disease activity in multiple sclerosis patients failing to respond to interferon beta. *Proc Natl Acad Sci USA* 101:8705-8708 (2004)
127. Castillo J et al. Ofatumumab, a second-generation anti-CD20 monoclonal antibody, for the treatment of lymphoproliferative and autoimmune disorders. *Expert Opin Investig Drugs* 18:491-500 (2009)
128. Kausar F et al. Ocrelizumab: a step forward in the evolution of B-cell therapy. *Expert Opin Biol Ther* 9:889-895 (2009)
129. Leary SM et al. Interferon beta-1a in primary progressive multiple sclerosis. *J Neurol Sci* 206:215-216 (2003)
130. Hawker K et al. Rituximab in patients with primary progressive multiple sclerosis: Results of a randomized double-blind placebo-controlled multicenter trial. *Ann Neurol* 66:460-471 (2009)
131. Miller DH et al. Primary-progressive multiple sclerosis. *Lancet Neurol* 6:903-912 (2007)
132. Petratos S et al. Novel therapeutics for axonal degeneration in multiple sclerosis. *J Neuropathol Exp Neurol* 69:323-334 (2010)
133. Baxter AG. The origin and application of experimental autoimmune encephalomyelitis. *Nat Rev Immunol* 7:904-912 (2007)
134. Rivers TM et al. Observations on Attempts to Produce Acute Disseminated Encephalomyelitis in Monkeys. *J Exp Med* 58:39-53 (1933)
135. Rivers TM et al. Encephalomyelitis Accompanied by Myelin Destruction Experimentally Produced in Monkeys. *J Exp Med* 61:689-702 (1935)
136. Kabat EA et al. Studies on acute disseminated encephalomyelitis produced experimentally in rhesus monkeys. *J Exp Med* 93:615-633 (1951)
137. Ravkina L et al. Hyperacute experimental allergic encephalomyelitis in rhesus monkeys as a model of acute necrotizing hemorrhagic encephalomyelitis. *J Neurol* 221:113-125 (1979)
138. Goverman J et al. Transgenic mice that express a myelin basic protein-specific T cell receptor develop spontaneous autoimmunity. *Cell* 72:551-560 (1993)
139. Waldner H et al. Fulminant spontaneous autoimmunity of the central nervous system in mice transgenic for the myelin proteolipid protein-specific T cell receptor. *Proc Natl Acad Sci USA* 97:3412-3417 (2000)
140. Bettelli E et al. Myelin oligodendrocyte glycoprotein-specific T cell receptor transgenic mice develop spontaneous autoimmune optic neuritis. *J Exp Med* 197:1073-1081 (2003)
141. Pollinger B et al. Spontaneous relapsing-remitting EAE in the SJL/J mouse: MOG-reactive transgenic T cells recruit endogenous MOG-specific B cells. *J Exp Med* 206:1303-1316 (2009)
142. Ellmerich S et al. High incidence of spontaneous disease in an HLA-DR15 and TCR transgenic multiple sclerosis model. *J Immunol* 174:1938-1946 (2005)
143. Smith JP et al. A role for alpha4-integrin in the pathology following Semliki Forest virus infection. *J Neuroimmunol* 106:60-68 (2000)
144. Oleszak EL et al. Theiler's virus infection: a model for multiple sclerosis. *Clin Microbiol Rev* 17:174-207 (2004)
145. Tsunoda I et al. Inside-Out versus Outside-In models for virus induced demyelination: axonal damage triggering demyelination. *Springer Semin Immunopathol* 24:105-125 (2002)
146. Lindner M et al. Chronic toxic demyelination in the central nervous system leads to axonal damage despite remyelination. *Neurosci Lett* 453:120-125 (2009)
147. Degaonkar MN et al. Determination of relaxation characteristics during preacute stage of lysophosphatidyl choline-induced demyelinating lesion in rat brain: an animal model of multiple sclerosis. *Magn Reson Imaging* 23:69-73 (2005)
148. Mendel I et al. A myelin oligodendrocyte glycoprotein peptide induces typical chronic experimental autoimmune encephalomyelitis in H-2b mice: fine specificity and T cell receptor V beta expression of encephalitogenic T cells. *Eur J Immunol* 25:1951-1959 (1995)

149. Slavin A et al. Induction of a multiple sclerosis-like disease in mice with an immunodominant epitope of myelin oligodendrocyte glycoprotein. *Autoimmunity* 28:109-120 (1998)
150. Sobel RA et al. The immunopathology of acute experimental allergic encephalomyelitis induced with myelin proteolipid protein. T cell receptors in inflammatory lesions. *J Immunol* 149:1444-1451 (1992)
151. Amor S et al. Biozzi mice: of mice and human neurological diseases. *J Neuroimmunol* 165:1-10 (2005)
152. Swanborg RH. Experimental autoimmune encephalomyelitis in the rat: lessons in T-cell immunology and autoreactivity. *Immunol Rev* 184:129-135 (2001)
153. Lenz DC et al. Strain variation in autoimmunity: attempted tolerization of DA rats results in the induction of experimental autoimmune encephalomyelitis. *J Immunol* 163:1763-1768 (1999)
154. Lorentzen JC et al. Protracted, relapsing and demyelinating experimental autoimmune encephalomyelitis in DA rats immunized with syngeneic spinal cord and incomplete Freund's adjuvant. *J Neuroimmunol* 63:193-205 (1995)
155. Kerlero de Rosbo N et al. Rhesus monkeys are highly susceptible to experimental autoimmune encephalomyelitis induced by myelin oligodendrocyte glycoprotein: characterisation of immunodominant T- and B-cell epitopes. *J Neuroimmunol* 110:83-96 (2000)
156. Genain CP et al. Antibody facilitation of multiple sclerosis-like lesions in a nonhuman primate. *J Clin Invest* 96:2966-2974 (1995)
157. Massaccesi L et al. Active and passively induced experimental autoimmune encephalomyelitis in common marmosets: a new model for multiple sclerosis. *Ann Neurol* 37:519-530 (1995)
158. Brok HP et al. Myelin/oligodendrocyte glycoprotein-induced autoimmune encephalomyelitis in common marmosets: the encephalitogenic T cell epitope pMOG24-36 is presented by a monomorphic MHC class II molecule. *J Immunol* 165:1093-1101 (2000)
159. Gold R et al. Understanding pathogenesis and therapy of multiple sclerosis via animal models: 70 years of merits and culprits in experimental autoimmune encephalomyelitis research. *Brain* 129:1953-1971 (2006)
160. Wekerle H et al. Animal models of multiple sclerosis. *Drug Discov Today: Disease models* 3:359-367 (2006)
161. 't Hart BA et al. Histopathological characterization of magnetic resonance imaging-detectable brain white matter lesions in a primate model of multiple sclerosis: a correlative study in the experimental autoimmune encephalomyelitis model in common marmosets (*Callithrix jacchus*). *Am J Pathol* 153:649-663 (1998)
162. Blezer EL et al. Quantitative MRI-pathology correlations of brain white matter lesions developing in a non-human primate model of multiple sclerosis. *NMR Biomed* 20:90-103 (2007)
163. Mancardi G et al. Demyelination and axonal damage in a non-human primate model of multiple sclerosis. *J Neurol Sci* 184:41-49 (2001)
164. 't Hart BA et al. Modelling of multiple sclerosis: lessons learned in a non-human primate. *Lancet Neurol* 3:588-597 (2004)
165. Merkler D et al. Myelin oligodendrocyte glycoprotein-induced experimental autoimmune encephalomyelitis in the common marmoset reflects the immunopathology of pattern II multiple sclerosis lesions. *Mult Scler* 12:369-374 (2006)
166. Pomeroy IM et al. Demyelinated neocortical lesions in marmoset autoimmune encephalomyelitis mimic those in multiple sclerosis. *Brain* 128:2713-2721 (2005)
167. Merkler D et al. Differential macrophage/microglia activation in neocortical EAE Lesions in the marmoset monkey. *Brain Pathol* 16:117-123 (2006)
168. Pomeroy IM et al. Diffuse cortical atrophy in a marmoset model of multiple sclerosis. *Neurosci Lett* 437:121-124 (2008)
169. Delarasse C et al. Myelin/oligodendrocyte glycoprotein-deficient (MOG-deficient) mice reveal lack of immune tolerance to MOG in wild-type mice. *J Clin Invest* 112:544-553 (2003)
170. Smith PA et al. Native myelin oligodendrocyte glycoprotein promotes severe chronic neurological disease and demyelination in Biozzi ABH mice. *Eur J Immunol* 35:1311-1319 (2005)

171. Jagessar SA et al. Autoimmunity against myelin oligodendrocyte glycoprotein is dispensable for the initiation although essential for the progression of chronic encephalomyelitis in common marmosets. *J Neuropathol Exp Neurol* 67:326-340 (2008)
172. von Büdingen HC et al. Immune responses against the myelin/oligodendrocyte glycoprotein in experimental autoimmune demyelination. *J Clin Immunol* 21:155-170 (2001)
173. Iglesias A et al. T- and B-cell responses to myelin oligodendrocyte glycoprotein in experimental autoimmune encephalomyelitis and multiple sclerosis. *Glia* 36:220-234 (2001)
174. Kerlero de Rosbo N et al. Demyelination induced in aggregating brain cell cultures by a monoclonal antibody against myelin/oligodendrocyte glycoprotein. *J Neurochem* 55:583-587 (1990)
175. Van der Goes A et al. The role of anti-myelin (auto)-antibodies in the phagocytosis of myelin by macrophages. *J Neuroimmunol* 101:61-67 (1999)
176. Morris-Downes MM et al. Pathological and regulatory effects of anti-myelin antibodies in experimental allergic encephalomyelitis in mice. *J Neuroimmunol* 125:114-124 (2002)
177. Schliesener HJ et al. A monoclonal antibody against a myelin oligodendrocyte glycoprotein induces relapses and demyelination in central nervous system autoimmune disease. *J Immunol* 139:4016-4021 (1987)
178. Linington C et al. Augmentation of demyelination in rat acute allergic encephalomyelitis by circulating mouse monoclonal antibodies directed against a myelin/oligodendrocyte glycoprotein. *Am J Pathol* 130:443-454 (1988)
179. McFarland HI et al. Determinant spreading associated with demyelination in a nonhuman primate model of multiple sclerosis. *J Immunol* 162:2384-2390 (1999)
180. Stefferl A et al. Butyrophilin, a milk protein, modulates the encephalitogenic T cell response to myelin oligodendrocyte glycoprotein in experimental autoimmune encephalomyelitis. *J Immunol* 165:2859-2865 (2000)
181. Fazilleau N et al. T cell repertoire diversity is required for relapses in myelin oligodendrocyte glycoprotein-induced experimental autoimmune encephalomyelitis. *J Immunol* 178:4865-4875 (2007)
182. Villoslada P et al. Frequency, heterogeneity and encephalitogenicity of T cells specific for myelin oligodendrocyte glycoprotein in naive outbred primates. *Eur J Immunol* 31:2942-2950 (2001)
183. Komiyama Y et al. IL-17 plays an important role in the development of experimental autoimmune encephalomyelitis. *J Immunol* 177:566-573 (2006)
184. Langrish CL et al. IL-23 drives a pathogenic T cell population that induces autoimmune inflammation. *J Exp Med* 201:233-240 (2005)
185. Hofstetter HH et al. Therapeutic efficacy of IL-17 neutralization in murine experimental autoimmune encephalomyelitis. *Cell Immunol* 237:123-130 (2005)
186. Rohn TA et al. Vaccination against IL-17 suppresses autoimmune arthritis and encephalomyelitis. *Eur J Immunol* 36:2857-2867 (2006)
187. Uyttenhove C et al. Anti-IL-17A autovaccination prevents clinical and histological manifestations of experimental autoimmune encephalomyelitis. *Ann N Y Acad Sci* 1110:330-336 (2007)
188. Kroenke MA et al. IL-12- and IL-23-modulated T cells induce distinct types of EAE based on histology, CNS chemokine profile, and response to cytokine inhibition. *J Exp Med* 205:1535-1541 (2008)
189. O'Connor RA et al. Cutting edge: Th1 cells facilitate the entry of Th17 cells to the central nervous system during experimental autoimmune encephalomyelitis. *J Immunol* 181:3750-3754 (2008)
190. Haak S et al. IL-17A and IL-17F do not contribute vitally to autoimmune neuro-inflammation in mice. *J Clin Invest* 119:61-69 (2009)
191. Brok HP et al. The human CMV-UL86 peptide 981-1003 shares a crossreactive T-cell epitope with the encephalitogenic MOG peptide 34-56, but lacks the capacity to induce EAE in rhesus monkeys. *J Neuroimmunol* 182:135-152 (2007)
192. Billiau A et al. Modes of action of Freund's adjuvants in experimental models of autoimmune diseases. *J Leukoc Biol* 70:849-860 (2001)

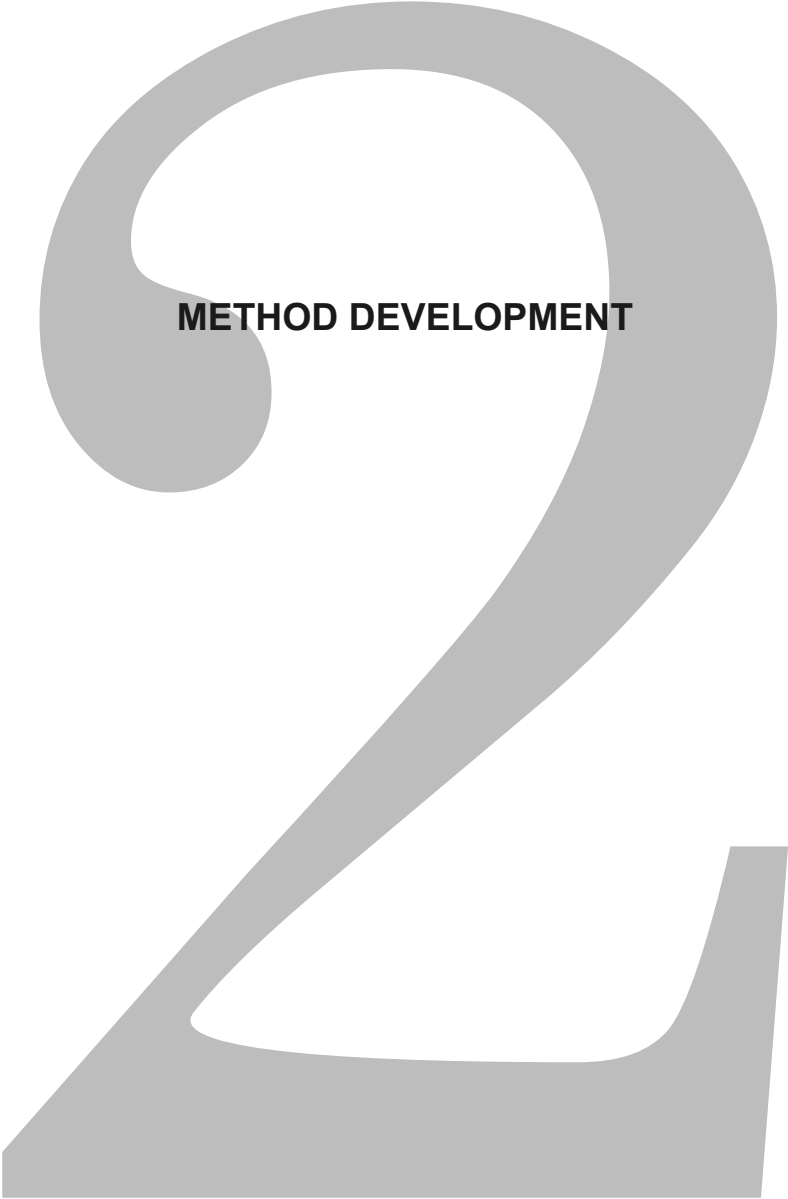
193. Tigno-Aranjuez JT et al. Encephalitogenicity of complete Freund's adjuvant relative to CpG is linked to induction of Th17 Cells. *J Immunol* 183:5654-5661 (2009)
194. Yip HC et al. Adjuvant-guided type-1 and type-2 immunity: infectious/noninfectious dichotomy defines the class of response. *J Immunol* 162:3942-3949 (1999)
195. Heeger PS et al. Revisiting tolerance induced by autoantigen in incomplete Freund's adjuvant. *J Immunol* 164:5771-5781 (2000)
196. Rabchevsky AG et al. Peripheral injections of Freund's adjuvant in mice provoke leakage of serum proteins through the blood-brain barrier without inducing reactive gliosis. *Brain Res* 832:84-96 (1999)
197. Eisenbarth SC et al. Crucial role for the Nalp3 inflammasome in the immunostimulatory properties of aluminium adjuvants. *Nature* 453:1122-1126 (2008)
198. Seya T et al. Role of Toll-like receptors in adjuvant-augmented immune therapies. *Evid Based Complement Alternat Med* 3:31-38 (2006)
199. Visser L et al. Proinflammatory bacterial peptidoglycan as a cofactor for the development of central nervous system autoimmune disease. *J Immunol* 174:808-816 (2005)
200. Ahn M et al. Pertussis toxin-induced hyperacute autoimmune encephalomyelitis in Lewis rats is correlated with increased expression of inducible nitric oxide synthase and tumor necrosis factor alpha. *Neurosci Lett* 308:41-44 (2001)
201. Hofstetter HH et al. Pertussis toxin modulates the immune response to neuroantigens injected in incomplete Freund's adjuvant: induction of Th1 cells and experimental autoimmune encephalomyelitis in the presence of high frequencies of Th2 cells. *J Immunol* 169:117-125 (2002)
202. Bruckener KE et al. Permeabilization in a cerebral endothelial barrier model by pertussis toxin involves the PKC effector pathway and is abolished by elevated levels of cAMP. *J Cell Sci* 116:1837-1846 (2003)
203. Hofstetter HH et al. The PLPp-specific T-cell population promoted by pertussis toxin is characterized by high frequencies of IL-17-producing cells. *Cytokine* 40:35-43 (2007)
204. Enard W et al. Comparative primate genomics. *Annu Rev Genomics Hum Genet* 5:351-378 (2004)
205. Tardif SD et al. Reproduction in captive common marmosets (*Callithrix jacchus*). *Comp Med* 53:364-368 (2003)
206. Layne DG et al. Husbandry, handling, and nutrition for marmosets. *Comp Med* 53:351-359 (2003)
207. Abbott DH et al. Aspects of common marmoset basic biology and life history important for biomedical research. *Comp Med* 53:339-350 (2003)
208. Mansfield K. Marmoset models commonly used in biomedical research. *Comp Med* 53:383-392 (2003)
209. Niblack GD et al. T- and B-lymphocyte chimerism in the marmoset. *Immunology* 32:257-263 (1977)
210. Kelley J et al. Comparative genomics of major histocompatibility complexes. *Immunogenetics* 56:683-695 (2005)
211. Cadavid LF et al. Evolutionary instability of the major histocompatibility complex class I loci in New World primates. *Proc Natl Acad Sci USA* 94:14536-14541 (1997)
212. Knapp LA et al. The MHC-E locus is the most well conserved of all known primate class I histocompatibility genes. *J Immunol* 160:189-196 (1998)
213. Adams EJ et al. Species-specific evolution of MHC class I genes in the higher primates. *Immunol Rev* 183:41-64 (2001)
214. Antunes SG et al. The common marmoset: a new world primate species with limited Mhc class II variability. *Proc Natl Acad Sci USA* 95:11745-11750 (1998)
215. Wu MS et al. MHC (major histocompatibility complex)-DRB genes and polymorphisms in common marmoset. *J Mol Evol* 51:214-222 (2000)

## Chapter 1

216. Prasad S et al. MHC Class II DRB genotyping is highly predictive of in-vitro alloreactivity in the common marmoset. *J Immunol Methods* 314:153-163 (2006)
217. Doxiadis GG et al. Reactivation by exon shuffling of a conserved HLA-DR3-like pseudogene segment in a New World primate species. *Proc Natl Acad Sci USA* 103:5864-5868 (2006)
218. Robinson J et al. IMGT/HLA and IMGT/MHC: sequence databases for the study of the major histocompatibility complex. *Nucleic Acids Res* 31:311-314 (2003)
219. Ludlage E et al. Clinical care and diseases of the common marmoset (*Callithrix jacchus*). *Comp Med* 53:369-382 (2003)
220. Fujii Y et al. Comprehensive analysis and characterization of the TCR alpha chain sequences in the common marmoset. *Immunogenetics* 62:383-395 (2010)
221. Uccelli A et al. Characterization of the TCRB chain repertoire in the New World monkey *Callithrix jacchus*. *J Immunol* 158:1201-1207 (1997)
222. von Büdingen HC et al. Characterization of the expressed immunoglobulin IGHV repertoire in the New World marmoset *Callithrix jacchus*. *Immunogenetics* 53:557-563 (2001)
223. Schmidt S et al. Studies on the immunoglobulin-E system of the common marmoset in comparison with human data. *Life Sci* 59:719-730 (1996)
224. Neubert R et al. Cross-reactivity of antihuman monoclonal antibodies with cell surface receptors in the common marmoset. *Life Sci* 58:317-324 (1996)
225. Brok HP et al. An extensive monoclonal antibody panel for the phenotyping of leukocyte subsets in the common marmoset and the cotton-top tamarin. *Cytometry* 45:294-303 (2001)
226. Godfrey LR. *General anatomy*. Elsevier, 2005.
227. Tokuno H et al. Web-accessible digital brain atlas of the common marmoset (*Callithrix jacchus*). *Neurosci Res* 64:128-131 (2009)
228. Gebhard R et al. Distribution of seven major neurotransmitter receptors in the striate cortex of the New World monkey *Callithrix jacchus*. *Neuroscience* 56:877-885 (1993)
229. Jeffery G et al. Segregated hemispheric pathways through the optic chiasm distinguish primates from rodents. *Neuroscience* 157:637-643 (2008)
230. Burman KJ et al. Anatomical and physiological definition of the motor cortex of the marmoset monkey. *J Comp Neurol* 506:860-876 (2008)
231. Burman KJ et al. Architectural subdivisions of medial and orbital frontal cortices in the marmoset monkey (*Callithrix jacchus*). *J Comp Neurol* 514:11-29 (2009)







**METHOD DEVELOPMENT**



# 2.1

## **A monoclonal antibody selection for immunohistochemical examination of lymphoid tissues from non-human primates**

Yolanda S. Kap<sup>1,2,3</sup>, Marjan van Meurs<sup>2,3</sup>, Nikki van Driel<sup>1</sup>, Gerrit Koopman<sup>4</sup>, Marie-Jose Melief<sup>2,3</sup>, Herbert P.M. Brok<sup>5</sup>, Jon D. Laman<sup>2,3</sup>, and Bert A. 't Hart<sup>1,2,3</sup>

<sup>1</sup>Department of Immunobiology, Biomedical Primate Research Centre, Rijswijk, The Netherlands; <sup>2</sup>Department of Immunology, Erasmus Medical Centre, Rotterdam, The Netherlands; <sup>3</sup>MS Centre ErasMS, Rotterdam, The Netherlands; <sup>4</sup>Department of Virology, Biomedical Primate Research Centre, Rijswijk, The Netherlands; <sup>5</sup>Department of Animal Science, Biomedical Primate Research Centre, Rijswijk, The Netherlands



## ABSTRACT

Non-human primates (NHP) offer valuable animal models for basic research into human diseases and for the preclinical validation of new therapeutics. Detailed *in situ* examination of the involved cell types using immunohistochemistry is often hampered by the lack of cross-reactive antibodies (Ab). In the current study, we have tested a large panel of monoclonal Ab raised against human leukocyte differentiation and activation markers for cross-reactivity on cryosections of lymphoid tissue from six NHP species. In total, we have tested 130 Ab against 69 antigens expressed in tissues from one great ape species (chimpanzee/*Pan troglodytes*), two Old World species (rhesus macaque/*Macaca mulatta* and cynomolgus macaque/*Macaca fascicularis*), and three New World species (common marmoset/*Callithrix jacchus*, cotton-top tamarin/*Saguinus oedipus*, and owl monkey/*Aotus trivogatus*). We have found a large panel of cross-reactive Ab: 93 of 102 (91%) in chimpanzee, 97 of 125 (78%) in rhesus macaque, 70 of 109 (64%) in cynomolgus macaque, 69 of 116 (60%) in common marmoset, 40 of 81 (49%) in cotton-top tamarin, and 35 of 80 (44%) in owl monkey. Availability of a reliable panel of cross-reactive markers is important to gain further insight into immunological processes in disease-affected tissues from NHP species.

## INTRODUCTION

Non-human primates (NHP) provide important experimental models of immune-mediated inflammatory disorders in biomedical research, because of the outbred nature and the phylogenetic proximity with humans. Recent milestones in biotechnology have resulted in the development of species-specific therapeutics, such as humanized antibodies (Ab) or fully human Ab<sup>1</sup>, which need to be evaluated in relevant disease models before they can be tested in patients. In cases in which rodent models are precluded by the lack of sufficient cross-reactivity, NHP models provide a useful alternative<sup>2</sup>.

A variety of NHP species is used in biomedicine. Although biomedical research in great apes has been banned from Europe for a few years, chimpanzees have been and still are productively used as models for human immunodeficiency virus (HIV) infection<sup>3,4</sup> and for the development of certain vaccines, e.g. against hepatitis<sup>5</sup>. Old World monkeys, such as rhesus macaques and cynomolgus macaques, are frequently used as experimental models in transplantation<sup>6,7</sup>, tuberculosis<sup>8</sup>, malaria<sup>9</sup>, rheumatoid arthritis<sup>10</sup>, and HIV infection<sup>11</sup>. New World monkeys serve as important tools for e.g. Parkinson's disease<sup>12</sup>, idiopathic colitis<sup>13</sup>, malaria vaccine research<sup>14</sup>, and for modeling multiple sclerosis (MS) in experimental autoimmune encephalomyelitis (EAE)<sup>15</sup>.

Studies of immunopathogenic mechanisms in each of these experimental models rely on the availability of reagents and techniques for *ex vivo* immunodiagnosis, such as flow cytometry analysis or immunohistochemistry. Previously, the cross-reactivity in flow cytometry of anti-human monoclonal antibodies (mAb) with NHP has been reported<sup>16,17</sup>. However, little is known about the cross-reactivity of mAb on NHP tissue for usage in immunohistochemistry. In this study, we have investigated a set of 130 human-specific mAb against 69 molecules used in immunohistochemistry for cross-reactivity with lymphoid tissue of six NHP species. The mAb in this set were reactive against cluster of differentiation (CD) markers, cytokines, and other immunological markers, such as human leukocyte antigen (HLA) and immunoglobulins. The selection of CD markers included critical costimulatory molecules against which novel immunotherapeutics, such as CD40<sup>18,19</sup>, are under development. Furthermore, the selection included markers distinguishing leukocyte cell types as T-cells, B-cells, natural killer cells, and macrophages. The selected cytokines, such as interferon-gamma (IFN- $\gamma$ ), interleukin (IL)-12, and IL-17A, play a central role in inflammatory responses. The latter is produced by the newly identified Th17 functional T-cell subset, which is presumed to be critical in several autoimmune diseases, including rheumatoid arthritis and MS<sup>20</sup>. Furthermore, IL-17A may be involved in neutrophil recruitment<sup>21,22</sup>.

## MATERIALS AND METHODS

### Tissues

For the detection of cross-reactivity, lymph node and/or spleen samples were used. Material from the African chimpanzee (*Pan troglodytes*), as a representative species of the great apes, was used. The selected Old World species were the rhesus macaque (*Macaca mulatta*) and the cynomolgus macaque (*Macaca fascicularis*). As representatives of New World species the common marmoset (*Callithrix jacchus*), the cotton-top tamarin (*Saguinus oedipus*), and the owl monkey (*Aotus trivivatus*) were chosen. All animals, except the cynomolgus macaques, were obtained from the outbred, genetically typed, breeding colonies at the Biomedical Primate Research Centre (BPRC), Rijswijk, The Netherlands. The breeding policy is aimed at prevention of inbreeding using genetic typing and the regular introduction of new animals. Cynomolgus macaques were obtained from licensed breeders. Tissue samples were collected at necropsy and were snap frozen in liquid nitrogen and stored at  $-80^{\circ}\text{C}$  until use. Human tonsil served as positive control tissue.

### Monoclonal antibodies

All mAb described in this study are commercially available unless stated otherwise. Samples were kindly donated by the participating companies: Becton Dickinson (BD) bioscience (San Jose, CA), Dako (Glostrup, Denmark), Sanquin (Amsterdam, The Netherlands), Diaclone (Fleming, France), Serotec (Düsseldorf, Germany), Abcam (Cambridge, MA), Cymbus Biotech (Hampshire, UK), Beckman Coulter (Fullerton, CA), Bender MedSystems (Vienna, Austria), Genzyme (Framingham, MA), Sanbio (Uden, The Netherlands), Innogenetics (Gent, Belgium), Santa Cruz biotechnology (Santa Cruz, CA), U-Cytech (Utrecht, The Netherlands), Ebioscience (San Diego, CA), Nordic Labs (Tilburg, The Netherlands), Biosource (Nivelles, Belgium), and BMA Biomedicals (Augst, Switzerland). Other mAb were kindly provided by Dr. D. Boraschi (Centro Ricerche Sclavo, Sienna, Italy), Dr. R. Noelle (Dartmouth, Lebanon, NH), and Prof. Dr. G. Opdenakker (Rega Institute, Leuven, Belgium). BD bioscience and Cymbus biotech provided isotype-matched Ab as controls. All specificities and clone names are listed in Table 1.

### Immunohistochemistry

Immunohistochemistry was performed as described in detail previously<sup>23</sup>. Briefly, 6 µm frozen spleen and lymph node sections were cut and thawed and mounted on glass slides. Slides were kept overnight at room temperature (RT), which is below the optimum temperature for most proteolytic enzymes, in a humidified atmosphere to allow controlled drying of the tissue. After the slides were air dried for 1 h, they were fixed either in fresh acetone or 4% paraformaldehyde in PBS (pH 7.4), both containing 0.02% (v/v) H<sub>2</sub>O<sub>2</sub>. Acetone-fixed slides were air dried for 10 min and subsequently washed in PBS, whereas paraformaldehyde-fixed slides were immediately washed in PBS. Tissue sections were incubated with primary Ab overnight at 4°C in a humidified atmosphere. Ab were tested in a dose titration that was based on the recommended dilution for human tissue and included a 10x dilution of the provided Ab. The same dose titration was used for all species. If the staining in a given case was doubtful, a higher concentration was tested if sufficient Ab was available. Incubations with secondary and tertiary reagents were performed for 1 h at RT. Between incubation steps the slides were washed twice with PBS. Detection of primary unlabeled mouse anti-human Ab was followed by incubation with rabbit anti-mouse-Ig-horseradish peroxidase (HRP) (Dako, Glostrup, Denmark), or in a three step staining with anti-mouse-Ig-biotin (Dako) and HRP-labeled avidin-biotin-complex (Dako). HRP activity was revealed by incubation for 10 min at RT with 3-amino-9-ethyl-carbozole (Sigma, Zwijndrecht, The Netherlands), leading to a bright-red precipitate. Some positive stainings, i.e. IL-17A, IFN-γ, and CD40, were enhanced with the tyramide signal amplification kit (Invitrogen, Carlsbad, CA). Human tonsil was used as positive control tissue. Incubation with isotype-matched primary Ab of irrelevant specificity and omission of the primary Ab served as negative controls.

**Table 1. Cross-reaction of anti-human antibodies on cryosections of non-human primate lymphoid tissue.**

Clone	Provider <sup>a</sup>	Great ape	Old World monkey		New World monkey			
		Chimpanzee	Rhesus macaque	Cynomolgus macaque	Common marmoset	Cotton-top tamarin	Owl monkey	
<b>CD markers</b>								
CD2	CLB-T11/1 (6G4)	3	+	+	+	-	-	-
	RPA-2.10	1	+	+	+	-/+	-	-/+
	S5.2	1	+	+	+	+	+	-
	B-E2	4	+	+	+	+	+	-
	LT2	5	+	+	+	-	-	-
CD3	SK7	1	+					
	FN-18	6	+	+				
	CLB-T3/2 (16A9)	3	+	+	-	-/+	+	-
	SP34	1	+	+	-/+	-	-	-
CD4	SK3	1		-	-	-		
	MT477	1		-	-	-		
	CLB-T4/2 (6D10)	3	+	-	-	-	-	+
	SK3, SK4	1	+	-	-	-	-	+
	MT310	2	+	-	-	-	-	+
CD5	UCHT2	7	+	+	+	+	-/+	+
CD7	B-F12	4	+	+	-/+	-	+	+
CD8	DK25	2	+	+				
	SK1	1			-	-		
	LT8	5	+	+	+	-/+	-	+
	CLB-T8/4 (4H8)	3	+	+	+	+	-	+
	UCHT4	7	+	+	+	-	+	-
CD10	ALB1	8	+	-	-	+	+	+
CD11a	HI111	1	+	+	+	+	+	+
	G-25.2	1	+	+	+	+	+	+
	25.3	8	+	+	+	+	+	+
	B-B15	4	+	-/+	+	+	+	+
	R7.1	9	+	+	+	+	+	-
CD11b	D12	1	+	+	+	+		

Antibody selection for IHC in non-human primates

	Clone	Provider <sup>a</sup>	Chimpanzee	Rhesus macaque	Cynomolgus macaque	Common marmoset	Cotton-top tamarin	Owl monkey
CD13	B-F10	4	+	+	-/+	-/+	+	+
CD14	322A-1 (MY4)	8	+	+	-/+	+		
	B-A8	4	+	-/+	-/+	-	-/+	-
CD16	NKP15	1	-	+	+	-	-/+	-
	3G8	1	+	+	+	+	-	+
	B-E16	4	+	+	-	-	+	-
CD18	L130	1	+	+	+	+	+	-
	CLB-LFA-1/1 (54)	3	+	+	+	+	+	+
	6.7	1	+	+	+	+	+	+
CD19	SJ25C1 (FITC)	1	+	-	-	-	-	-
	4G7	1	+	-	-	-	+	-
CD20	L26	2	+	+	+	+		
	H299 (B1)	8	+	+	+	+	-	-
	B-H20	4	+	-/+	-	-	+	-
CD21	BL13	8	+	+	+	+	+	+
	B-LY4	1	+	+	+	+	+	+
	B-E5	4	+	+	+	+	+	+
CD24	SN3	5	+	-/+	-/+	-	-	-
CD25	B-B10	4	+	+	-	-	-	-
	Tu69	7	-	-	-	-	-	-
	CLB-IL2R/1 (TB30)	3	+	+	-	-	-	-
	2A3	1		+				
CD26	BA5	2	-/+	+	+	-	-	+
	L272	1	+	-	-	-	-	-
CD27	L128	1	+	-	-/+	-	-	-
CD28	CLB-CD28/1 (15E8)	3	+	+				
	L293	1	+	+	+	-	-	-
	B-T3	4	+	+	+	+	+	-/+

Chapter 2.1

	Clone	Provider <sup>a</sup>	Chimpanzee	Rhesus macaque	Cynomolgus macaque	Common marmoset	Cotton-top tamarin	Owl monkey
CD29	TDM29	7	+	+	+	+	+	+
	B-D15	4	+	+	+	+	-/+	+
CD30L	M81	10		+				
CD31	5.6E	8	+	+	+	-	+	-
CD33	D3HL60.251	8		+				
CD34	QBEnd 10	3	+	-				
CD35	E-11	1	+	+	+	+	+	+
CD38	T16	8	+	-	-/+	-	+	-
	HB7	1	+	-	-	-	-	-
CD40	5C3	1	+	+	-	-	-	
	CLB-14G7	3	+	+				
	B-B20	7	+	+	+	+	+	+
CD44	B-F24	4	+	+	-	-/+	+	+
	NKI-P2	3	+	+	+	+	+	+
	F10-44-2	5	+	-	-	+	+	+
CD45	B-A11	4	+	+	-/+	+	+	-
CD45RA	B-C15	4	+	+	+	+	-	+
CD45RO	UCHL-1	1	+	-				
CD49d	HP2/1	8	+	+	+	-	-/+	-
CD49e	SAM1	8	+	+	+	+	-	-
CD55	CLB-CD97L/1	3		-	-	+		
CD56	123C3	11	+	+				
	B-A19	4	+	-/+	-	-	-	-
	N901 (NKH-1)	8	-	-	+	+	+	-
	MEM188	7	-	+	+	-	+	-
	NCAM16.2	1	+	-	+	+	-	-
CD58	L306.4	1	-/+	-	-	-	-	-
	1C3	1	+	+	+	+	+	+
CD62L	FMC46	7	+	-	-	-	-	-
	DREG.55	9	+	+	+	+	-	+
CD64	10.1	1	+	+				
CD68	KP1	2	+	+	+	+		
CD70	CLB-2F2	3	+	+	-/+	-/+		

## Antibody selection for IHC in non-human primates

	Clone	Provider <sup>a</sup>	Chimpanzee	Rhesus macaque	Cynomolgus macaque	Common marmoset	Cotton-top tamarin	Owl monkey
CD80	M24	12		+	+	+		
CD83	HB15A	8	+	+	+	+		
CD86	1G10	12	+	+	+	+		
	B-T7	4	+	+	-/+	-	+	-
	IT2.2	1	-	+	+	+	-	-
CD95	UB2	8		+		+		
	FAS6	3		+	+	+		
	APO1-1	9	-/+	-/+	+	-	-	-
	DX2	1	+	+	+	-	-	-
	BMS-140	9	+	+	+	-/+	-	-
CD97	CLB-CD97/1	3		+		+		
CD138	BB4	8	+	+	+	-	-	-
	CLB-1D4	3	+	-	-	-	-	-
CD154/CD40L	TRAP1	1	+	+	+	+ <sup>b</sup>		
	24-31	13		+	+	+		
CD169	HSN1 (7D2)	5		+	+	+		
<b>Cytokines</b>								
IFN- $\alpha$	MC-16	14		+	+	+		
IFN- $\gamma$	MD-1	14	+					
	MD-2	14		+	+	+		
TNF- $\alpha$	61E71	14	-	+	-/+	+		
IL-1 $\alpha$	Vmp18	15		+		+		
IL-1 $\beta$	Vmp20	15		+		+		
IL-2	80-3418-01	10					+ <sup>b</sup>	
IL-4	QS-4	14		+	+	+		
	1842-01	10		+	-/+	+		
IL-6	BE-8	15		+	+	+		
IL-10	B-S10	16	+	+	+	+		
IL-12p40/p70	C8.6	1		+	-/+	+		
IL-17A	eBio64CAP17	17		+		+		
<b>Miscellaneous</b>								
HLA-ABC	G46-2.6	1	+	+	+	-	-	-
	W6/32	7	+	+	+	+	+	+

	Clone	Provider <sup>a</sup>	Chimpanzee	Rhesus macaque	Cynomolgus macaque	Common marmoset	Cotton-top tamarin	Owl monkey
HLA-DP, DQ, DR	CR3/43	2		+	+	+		
	TAL-1B5	2	+	+				
HLA-DR	B-F1	4	+	+	+	+	+	+
	CLB-HLA-DR (1E5)	3	+	+	+	+	+	+
	L243	1	+	+	+	+	+	+
HLA-DQ	SPV-L3	7	+	+	+	+	+	+
IgM	NI179	18			+	+		
IgG	-	19		+	+	+		
MMP-9	2D9	20		+		+		
MRP 14	27E10 (early)	21		+	+	+		

<sup>a</sup> Providers: 1, Becton Dickinson Bioscience; 2, Dako; 3, Sanquin; 4, Diaclone; 5, Serotec; 6, Abcam; 7, Cymbus biotech; 8, Beckman Coulter; 9, Bender MedSystems; 10, Genzyme; 11, Sanbio; 12, Innogenetics; 13, gift from Dr. R. Noelle; 14, U-Cytech; 15, gift from Dr. D. Boraschi; 16, Santa Cruz; 17, Ebioscience; 18, Nordic Labs; 19, Bioscience; 20, gift from Prof. Dr. G. Opendakker; 21, BMA Biomedicals.

<sup>b</sup> Only cross-reactive when paraformaldehyde is used as fixative

<sup>c</sup> +, cross-reactive; -, no specific staining; -/+, needs more investigation; blank boxes, not tested. CD, cluster of differentiation; HLA, human leukocyte antigen; IFN- $\gamma$ , interferon-gamma; IL, interleukin.

### Immunohistochemistry analysis

Cross-reactivity is expressed as follows: - = no specific staining; -/+ = doubtful and needs more investigation; + = specific staining.

### Ethics

All NHP tissues that were used for this study were obtained from purpose-bred animals at the BPRC or purchased from licensed breeders. All tissues were from animals from other experimental studies; no monkeys were sacrificed solely for the purpose of this study. All study protocols were reviewed and approved according to Dutch law on animal experimentation.

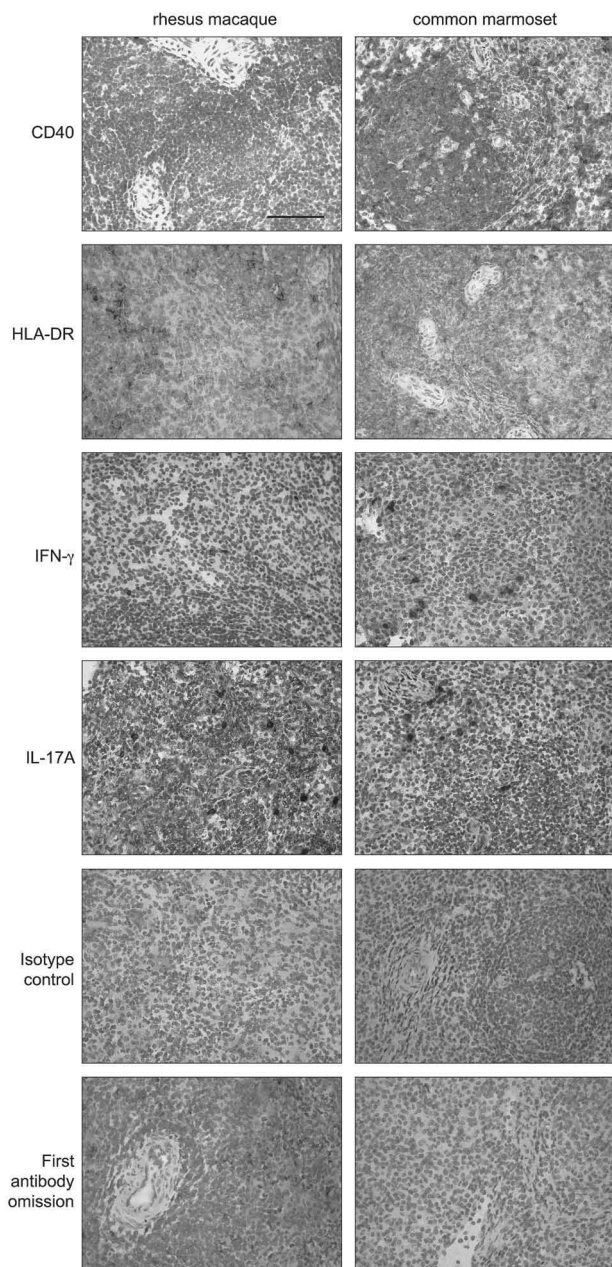


**Figure 1. Representative selection of cross-reactive monoclonal antibodies on spleen cryosections of rhesus macaque and common marmoset.**

Spleen sections were stained for CD40, HLA-DR, IFN- $\gamma$ , and IL-17A. Controls included isotype control and first antibody omission. Bar = 100  $\mu$ m. See page 310 for a full-color representation of this figure.

## RESULTS

Table 1 shows the Ab clustered according to their reactivity with CD markers, cytokines, and miscellaneous markers, such as HLA and immunoglobulins. For most markers, we have tested Ab clones obtained from several companies. Cross-reactivity was scored as: no specific staining (-), doubtful (-/+), or specific staining (+). Doubtful means that some staining is observed, but the specificity is unclear. To further investigate the cross-reactivity of these Ab, the titration of the mAb should be extended or another staining method will be necessary, but this was outside the scope of the current study.

In total, we have tested 130 mAb against 69 markers: 105 clones against 50 CD

**Table 2. Number and percentage of cross-reactive monoclonal antibodies.**

	Great ape	Old World monkey			New World monkey	
	Chimpanzee	Rhesus macaque	Cynomolgus macaque	Common marmoset	Cotton-top tamarin	Owl monkey
<b>CD markers</b>						
Tested ( <i>n</i> )	92	103	91	93	75	74
+	84	75	55	47	35	30
+ (%)	91	73	60	51	47	41
<b>Cytokines</b>						
Tested ( <i>n</i> )	3	11	8	12		
+	2	11	5	12		
+ (%)	67	100	63	100		
<b>Miscellaneous</b>						
Tested ( <i>n</i> )	7	11	10	11	6	6
+	7	11	10	10	5	5
+ (%)	100	100	100	91	83	83
<b>Total</b>						
Tested ( <i>n</i> )	102	125	109	116	81	80
+	93	97	70	69	40	35
+ (%)	91	78	64	60	49	44

markers, 13 clones against 11 cytokines, and 12 clones against 8 miscellaneous markers. The isotype controls and primary Ab omission were negative on all tissues tested (Figure 1). All Ab were directed against human antigens, and, as expected, were positive on human control tissue (data not shown). All mAb were first tested on acetone-fixed tissue. In addition, mAb of particular interest that failed to stain cryosections were next tested on paraformaldehyde-fixed tissue. For example, a mAb against IL-2 that showed no cross-reactivity on acetone-fixed tissue did display cross-reactivity on paraformaldehyde-fixed common marmoset tissue.

Table 2 summarizes the number and percentages of cross-reactive mAb tested per specificity per species. Predictably, the highest cross-reactivity was found in chimpanzees: 93 of 102 tested mAb showed cross-reactivity (91%). A somewhat lower percentage of cross-reactive mAb was found with the Old World species, i.e. 78% in rhesus macaques and 64% in cynomolgus macaques. An again lower, but still high, percentage of mAb were found to cross-react with New World species. In the common marmoset, cotton-top tamarin, and owl monkey the cross-reactivity was, respectively, 60%, 49%, and 44%.

Figure 1 shows a selection of cross-reactive mAb on the spleen of a rhesus macaque and a common marmoset, i.e. mAb directed against CD40, HLA-DR, IFN- $\gamma$ , and IL-17A.

## DISCUSSION

NHP models are invaluable models for research in biomedicine. For the study of immunopathological mechanisms in these models, mAb for flow cytometry and immunohistochemistry are indispensable. A selection of mAb directed against human antigens for flow cytometry analysis of NHP cells has previously been reported<sup>16,17</sup>. The purpose of the current study was to compose a panel of cross-reactive mAb that could be used for immunohistochemical analysis of lymphoid tissues from six NHP species. Cross-reactive mAb can be used for immunopathological examination of NHP disease models, which subsequently will increase our knowledge about NHP models and human diseases.

We have found a large panel of cross-reactive Ab for each species, with the highest level of cross-reactivity in chimpanzee, followed by monkeys of Old World origin and of New World origin. The decreasing level of cross-reactivity reflects the evolutionary distance, which has been estimated at 5 million years for chimpanzees, 25 million years for macaques, and 35 million years for marmosets<sup>24</sup>. We assessed the cross-reactivity in three categories, but not the intensity of the staining, although we did observe that some clones had more-intense staining than did other clones. We did not include this

observation in the results, because a subjective scoring of intensity grades may be confusing. Furthermore, the intensity of a staining can be enhanced today by several techniques, and the intensity may vary between batches.

The markers shown in figure 1 were chosen because CD40, HLA-DR, IFN- $\gamma$  and IL-17A are important in immune-mediated diseases. CD40 is a member of the tumor necrosis factor receptor family and is expressed on antigen presenting cells, such as B-cells, macrophages, and dendritic cells, and also on endothelial cells and fibroblasts. CD40 is a co-stimulatory molecule that binds to CD154 (CD40L) expressed on T-cells. Binding of CD40L to CD40 on B-cells induces B-cell proliferation and isotype switching. Interaction of CD40L with CD40 on monocytes induces the production of cytokines and nitric oxide. Furthermore, CD40 activation can prevent apoptosis of B-cells and monocytes. CD40 is involved in several immune-mediated diseases<sup>18,25,26</sup>. Blocking of CD40 prevents EAE in common marmosets<sup>19,27</sup> and kidney allograft rejection in rhesus macaques<sup>28</sup>. HLA-DR is associated with several disease susceptibilities, such as rheumatoid arthritis and MS<sup>29</sup>. In the common marmoset, in which HLA-DR is called Caja-DR, Caja-DRB\*W1201 is essential for the activation of Th1 cells that induce EAE<sup>30</sup>. IL-17A and IFN- $\gamma$  are both pro-inflammatory cytokines produced by T-cells. IFN- $\gamma$  is also produced by natural killer cells, and IL-17A may also be produced by non-T-cells, such as microglia<sup>31</sup> and lymphoid tissue inducer-like cells<sup>32</sup>. IL-17A is suggested to be involved in several immune-mediated inflammatory diseases, such as rheumatoid arthritis, psoriasis, and MS<sup>20</sup>. The IL-17-producing T-cells, called Th17, are now being recognized as a functional CD4<sup>+</sup> T-cell subset in addition to Th1 and Th2, as critically reviewed recently<sup>33</sup>. In MS, IL-17A may play a role in blood-brain barrier transmigration of inflammatory cells<sup>34</sup>.

Some mAb clones cannot be used for immunohistochemistry, but can be used for flow cytometry analysis<sup>17</sup> or vice versa. For example, the anti-CD4 clones MT310 and SK3, as well as the anti-CD3 clone SP34, can be used for flow cytometry analysis of common marmoset mononuclear cells, but cannot be used for immunohistochemistry on common marmoset tissue. Vice versa, clone B-B15 against CD11a can be used for immunohistochemistry of common marmoset tissue, but not for flow cytometry analysis of common marmoset cells. Representation and accessibility of Ab epitopes on live cells in cell suspensions can be quite different from that in frozen sections of solid tissue subjected to fixation, even with relatively mild fixatives such as acetone<sup>35</sup>. Another explanation is that the activation and differentiation status of leukocytes might differ between blood and lymphoid tissue.

Although rhesus macaques and cynomolgus macaques are closely related Old World species, differences in cross-reactivity can be found. For example, the anti-CD3 clone CLB-T3/2 showed cross-reactivity in rhesus macaque tissue, but not in cynomolgus macaque tissue. Differences between New World species were also observed. As an

example, clone CLB-T8/4 against CD8 showed cross-reactivity in common marmoset and owl monkey tissue, but not in cotton-top tamarin tissue. In contrast, clone UCHT4 directed against CD8 showed cross-reactivity in cotton-top tamarin tissue, but not in common marmoset and owl monkey tissue. This demonstrates that although species are closely related, differences in epitope conservation do occur.

Seven of the 69 markers seem to be highly conserved between human and NHP. Ab directed against CD11a, CD18, CD21, CD29, CD35, HLA-DR, and HLA-DQ were cross-reactive with tissue of all six NHP. CD21 is the complement receptor 2 and CD35 is the complement receptor 1, suggesting a conservation of complement receptors between humans and NHP. CD21 is expressed on B-cells and is the receptor for Epstein-Barr virus (EBV). Conservation of CD21 suggests that these NHP are susceptible to infection with EBV-related herpesviruses, which is indeed compatible with the literature<sup>36</sup>. CD11a and CD18, which together form lymphocyte function-associated antigen-1, as well as the very late antigen-4 component, CD29, are expressed on leukocytes and are involved in adhesion. This may suggest conservation in the adhesion system between humans and NHP.

For some markers, no cross-reactive mAb were found for a species. For example, no cross-reactive anti-CD3 or anti-CD4 mAb could be found for the common marmoset. This was expected because in earlier studies it was observed that Ab against human CD3 did not cross-react with rhesus monkeys, necessitating the generation of a specific Ab, known as FN18<sup>37</sup>. A polyclonal Ab that recognizes multiple epitopes may overcome the problem of no cross-reactivity with mAb. For example, a polyclonal Ab against CD3 (Dako) can be used to stain common marmoset tissue. To obtain Ab that recognize these species-specific epitopes, new Ab are being developed. For instance, Ito and colleagues recently generated mAb recognizing common marmoset lymphocytes<sup>38</sup>.

In summary, we have identified a large panel of cross-reactive mAb for *in situ* analysis of NHP lymphoid tissues and organs affected by inflammation, infection, or tumors. These mAb will serve as important tools in future investigations of leukocyte differentiation and activation status in NHP and will aid in dissecting the mechanisms underlying the efficacy of novel vaccination and immunotherapeutic regimens.

## ACKNOWLEDGEMENTS

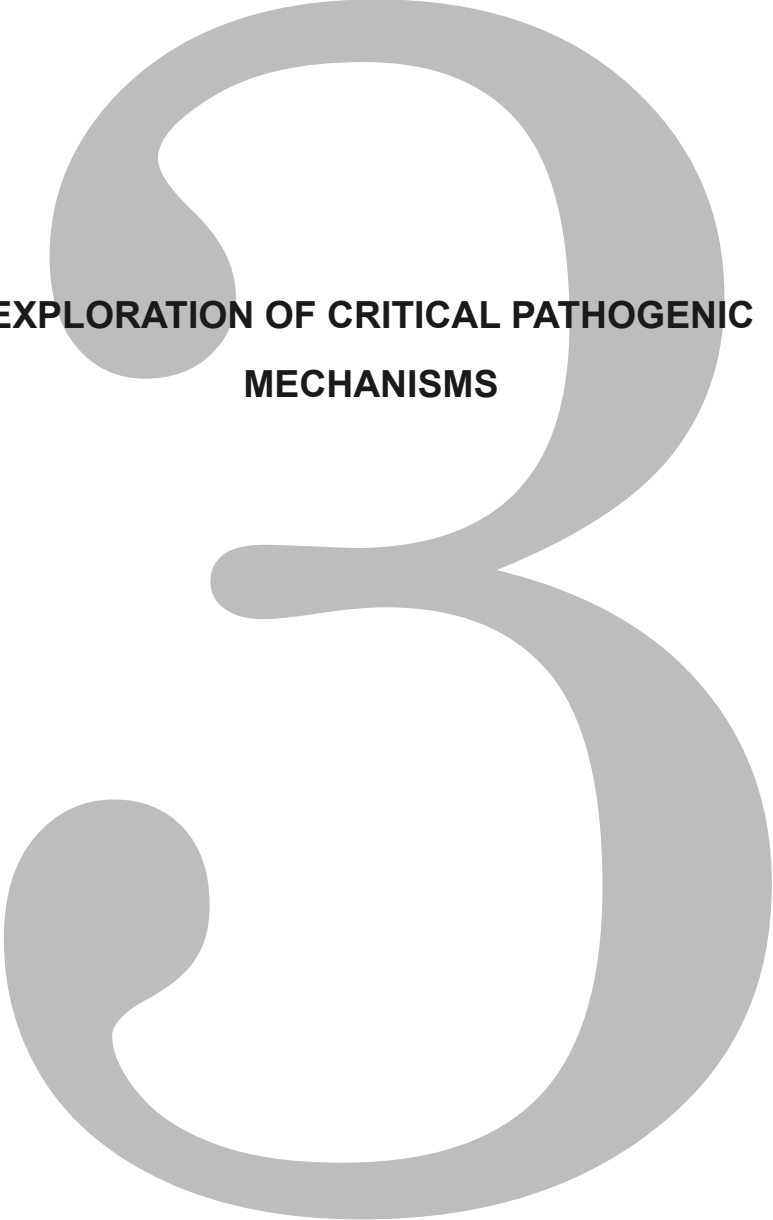
The authors thank the companies for donating the antibodies and Mr. Henk van Westbroek for the artwork.

## REFERENCES

1. Lutterotti A et al. Getting specific: monoclonal antibodies in multiple sclerosis. *Lancet Neurol* 7:538-547 (2008)
2. 't Hart BA et al. Evaluating the validity of animal models for research into therapies for immune-based disorders. *Drug Discov Today* 9:517-524 (2004)
3. Rutjens E et al. Lentivirus infections and mechanisms of disease resistance in chimpanzees. *Front Biosci* 8:d1134-1145 (2003)
4. Heeney JL et al. Origins of HIV and the evolution of resistance to AIDS. *Science* 313:462-466 (2006)
5. Bukh J. A critical role for the chimpanzee model in the study of hepatitis C. *Hepatology* 39:1469-1475 (2004)
6. Kean LS et al. Transplant tolerance in non-human primates: progress, current challenges and unmet needs. *Am J Transplant* 6:884-893 (2006)
7. Haanstra KG et al. Expression patterns of regulatory T-cell markers in accepted and rejected nonhuman primate kidney allografts. *Am J Transplant* 7:2236-2246 (2007)
8. Capuano SVr et al. Experimental Mycobacterium tuberculosis infection of cynomolgus macaques closely resembles the various manifestations of human M. tuberculosis infection. *Infect Immun* 71:5831-5844 (2003)
9. Moreno A et al. Preclinical assessment of the receptor-binding domain of Plasmodium vivax Duffy-binding protein as a vaccine candidate in rhesus macaques. *Vaccine* 26:4338-4344 (2008)
10. Vierboom MP et al. Preclinical models of arthritic disease in non-human primates. *Drug Discov Today* 12:327-335 (2007)
11. Ambrose Z et al. HIV/AIDS: in search of an animal model. *Trends Biotechnol* 25:333-337 (2007)
12. Eslamboli A. Marmoset monkey models of Parkinson's disease: which model, when and why? *Brain Res Bull* 68:140-149 (2005)
13. Warren BF et al. Animal models of inflammatory bowel disease. *J Pathol* 172:313-316 (1994)
14. Herrera S et al. Aotus monkeys: their great value for anti-malaria vaccines and drug testing. *Int J Parasitol* 32:1625-1635 (2002)
15. 't Hart BA et al. A new primate model for multiple sclerosis in the common marmoset. *Immunol Today* 21:290-297 (2000)
16. Neubert R et al. Cross-reactivity of antihuman monoclonal antibodies with cell surface receptors in the common marmoset. *Life Sci* 58:317-324 (1996)
17. Brok HP et al. An extensive monoclonal antibody panel for the phenotyping of leukocyte subsets in the common marmoset and the cotton-top tamarin. *Cytometry* 45:294-303 (2001)
18. Laman JD et al. Functions of CD40 and its ligand, gp39 (CD40L). *Crit Rev Immunol* 16:59-108 (1996)
19. Laman JD et al. Protection of marmoset monkeys against EAE by treatment with a murine antibody blocking CD40 (mu5D12). *Eur J Immunol* 32:2218-2228 (2002)
20. Ivanov S et al. Interleukin-17 as a drug target in human disease. *Trends Pharmacol Sci* 30:95-103 (2009)
21. Witowski J et al. IL-17 stimulates intraperitoneal neutrophil infiltration through the release of GRO alpha chemokine from mesothelial cells. *J Immunol* 165:5814-5821 (2000)
22. Yu JJ et al. An essential role for IL-17 in preventing pathogen-initiated bone destruction: recruitment of neutrophils to inflamed bone requires IL-17 receptor-dependent signals. *Blood* 109:3794-3802 (2007)
23. Laman JD et al. Expression of accessory molecules and cytokines in acute EAE in marmoset monkeys (*Callithrix jacchus*). *J Neuroimmunol* 86:30-45 (1998)
24. Enard W et al. Comparative primate genomics. *Annu Rev Genomics Hum Genet* 5:351-378 (2004)
25. Grewal IS et al. CD40 and CD154 in cell-mediated immunity. *Annu Rev Immunol* 16:111-135 (1998)

26. Vogel LA et al. CD40 and its crucial role as a member of the TNFR family. *Semin Immunol* 10:435-442 (1998)
27. Boon L et al. Prevention of experimental autoimmune encephalomyelitis in the common marmoset (*Callithrix jacchus*) using a chimeric antagonist monoclonal antibody against human CD40 is associated with altered B cell responses. *J Immunol* 167:2942-2949 (2001)
28. Haanstra KG et al. Prevention of kidney allograft rejection using anti-CD40 and anti-CD86 in primates. *Transplantation* 75:637-643 (2003)
29. Fernando MM et al. Defining the role of the MHC in autoimmunity: a review and pooled analysis. *PLoS Genet* 4:e1000024 (2008)
30. Brok HP et al. Myelin/oligodendrocyte glycoprotein-induced autoimmune encephalomyelitis in common marmosets: the encephalitogenic T cell epitope pMOG24-36 is presented by a monomorphic MHC class II molecule. *J Immunol* 165:1093-1101 (2000)
31. Kawanokuchi J et al. Production and functions of IL-17 in microglia. *J Neuroimmunol* 194:54-61 (2008)
32. Takatori H et al. Lymphoid tissue inducer-like cells are an innate source of IL-17 and IL-22. *J Exp Med* 206:35-41 (2009)
33. Steinman L. A brief history of T(H)17, the first major revision in the T(H)1/T(H)2 hypothesis of T cell-mediated tissue damage. *Nat Med* 13:139-145 (2007)
34. Kebir H et al. Human TH17 lymphocytes promote blood-brain barrier disruption and central nervous system inflammation. *Nat Med* 13:1173-1175 (2007)
35. Laman JD et al. Fixation of cryo-sections under HIV-1 inactivating conditions: integrity of antigen binding sites and cell surface antigens. *Histochemistry* 96:177-183 (1991)
36. Johannessen I et al. In vivo models for Epstein-Barr virus (EBV)-associated B cell lymphoproliferative disease (BLPD). *Rev Med Virol* 9:263-277 (1999)
37. Nooij FJ et al. Differentiation antigens on rhesus monkey lymphocytes. II. Characterization of RhT3, a CD3-like antigen on T cells. *Eur J Immunol* 16:981-984 (1986)
38. Ito R et al. Novel monoclonal antibodies recognizing different subsets of lymphocytes from the common marmoset (*Callithrix jacchus*). *Immunol Lett* 121:116-122 (2008)



A large, light gray, stylized number '3' is centered on the page. The number has a thick, rounded stroke and a decorative, swirling top loop. The text is centered within the upper loop of the '3'.

**EXPLORATION OF CRITICAL PATHOGENIC  
MECHANISMS**



# 3.1

## **Fast progression of recombinant human myelin/oligodendrocyte glycoprotein (MOG)-induced experimental autoimmune encephalomyelitis in marmosets is associated with the activation of MOG34-56-specific cytotoxic T-cells**

Yolanda S. Kap<sup>1,2,3</sup>, Paul Smith<sup>1,3</sup>, S. Anwar Jagessar<sup>1,3</sup>,  
Ed Remarque<sup>4</sup>, Erwin Blezer<sup>5</sup>, Gustav J. Strijkers<sup>6</sup>, Jon D. Laman<sup>2,3</sup>,  
Rogier Q. Hintzen<sup>3,7</sup>, Jan Bauer<sup>8</sup>, Herbert P.M. Brok<sup>9</sup>,  
and Bert A. 't Hart<sup>1,2,3</sup>

<sup>1</sup>Department of Immunobiology, Biomedical Primate Research Centre, Rijswijk, The Netherlands; <sup>2</sup>Department of Immunology, Erasmus Medical Centre, Rotterdam, The Netherlands; <sup>3</sup>MS Centre ErasMS, Rotterdam, The Netherlands; <sup>4</sup>Department of Parasitology, Biomedical Primate Research Centre, Rijswijk, The Netherlands; <sup>5</sup>Image Sciences Institute, University Medical Center Utrecht, Utrecht, The Netherlands; <sup>6</sup>Biomedical Nuclear Magnetic Resonance Group, Department of Medical Engineering, Eindhoven University of Technology, The Netherlands; <sup>7</sup>Department of Neurology, Erasmus Medical Centre, Rotterdam, The Netherlands; <sup>8</sup>Brain Research Institute, University of Vienna, Austria; <sup>9</sup>Department of Animal Science, Biomedical Primate Research Centre, Rijswijk, The Netherlands

YSK, PS, SAJ contributed equally to this work  
HPMB and BAH share senior authorship

*J Immunol* 2008, 180: 1326-1337



## ABSTRACT

The recombinant human myelin oligodendrocyte glycoprotein (MOG)-induced experimental autoimmune encephalomyelitis (EAE) model in the common marmoset is characterized by 100% disease incidence, a chronic disease course, and a variable time interval between immunization and neurological impairment. We investigated whether monkeys with fast and slow disease progression display different anti-MOG T or B-cell responses and analyzed the underlying pathogenic mechanism(s). The results show that fast progressor monkeys display a significantly wider specificity diversification of anti-MOG T-cells at necropsy than slow progressors, especially against MOG34-56 and MOG74-96. MOG34-56 emerged as a critical encephalitogenic peptide, inducing severe neurological disease and multiple lesions with inflammation, demyelination, and axonal injury in the central nervous system (CNS). Although EAE was not observed in MOG74-96-immunized monkeys, weak T-cell responses against MOG34-56 and low grade CNS pathology were detected. When these cases received a booster immunization with MOG34-56 in IFA, full-blown EAE developed. MOG34-56-reactive T-cells expressed CD3, CD4 or CD8, and CD56, but not CD16. Moreover, MOG34-56-specific T-cell lines displayed specific cytotoxic activity against peptide-pulsed B-cell lines. The phenotype and cytotoxic activity suggest that these cells are natural killer-cytotoxic T lymphocytes (NK-CTL). These results support the concept that cytotoxic cells may play a role in the pathogenesis of multiple sclerosis.

## INTRODUCTION

Multiple sclerosis (MS) is a chronic progressive inflammatory demyelinating disease of the human central nervous system (CNS). The pathological hallmark of MS is the lesion, being in the majority of cases a sharply demarcated demyelinated area in the CNS white matter (WM) that expresses a variable degree of inflammation, axonal injury, gliosis and remyelination<sup>1,2</sup>. Although the trigger of MS is not known, it is generally believed that lesion formation involves the synergistic action of cellular and humoral autoimmune reactions directed against components of the myelin sheath<sup>3</sup>. Anti-myelin autoimmune reactions may be induced by viruses that share cross-reactive T- and B-cell epitopes with myelin antigen (Ag), a phenomenon known as molecular mimicry<sup>4</sup>.

In response to the requirement for a useful preclinical model for the efficacy evaluation of new biopharmaceutical agents for the treatment of MS, we have developed a chronic progressive experimental autoimmune encephalomyelitis (EAE) model in the New World primate species, the common marmoset (*Callithrix jacchus*). This EAE model has several intriguing aspects that makes it also a highly useful disease

model for basic research, including the 100% incidence despite the outbred nature, the chronic progressive course (reviewed in<sup>5,6</sup>), and the heterogeneous pathology present in WM and grey matter (GM) that ranges from early active to chronic inactive/remyelinating lesions<sup>6-8</sup>. Moreover, using serially applied magnetic resonance imaging (MRI) sequences, brain lesions can be visualized and characterized in relation to the expression of an overt neurological deficit<sup>9-11</sup>.

Several lines of evidence point to a critical role of autoimmune reactions directed against myelin oligodendrocyte glycoprotein (MOG) in the induction of chronic progressive EAE. Marmosets immunized with a chimeric protein combining myelin basic protein (MBP) and proteolipid protein (PLP) developed clinical EAE only after the spreading of the autoimmune reaction to MOG has taken place<sup>12</sup>. Moreover, the development of chronic progressive EAE in both Biozzi ABH mice<sup>13</sup> and marmosets<sup>14</sup> is impaired when the animals were immunized with MOG-deficient mouse myelin.

The marmoset EAE model induced with recombinant human (rh) MOG1-125 (rhMOG) is characterized by a 100% disease incidence but variable clinical course. The high susceptibility of marmosets to this model maps to an invariant major histocompatibility complex (MHC) class II molecule, Cja-DRB\*W1201, which emerged as a dominant restriction element for the activation of CD4<sup>+</sup> T-cells specific for the epitope MOG24-36<sup>15</sup>. The monomorphic allele is present and expressed in each monkey<sup>16,17</sup>. Independently from us, Villoslada et al. showed by adoptive transfer that MOG24-36-reactive T-cells induce mild inflammatory CNS pathology<sup>18</sup>.

The aim of the current study was to analyze autoimmune mechanisms underlying the variable clinical course. Hence, we investigated whether the rate of disease progression in the rhMOG-induced EAE model is associated with particular anti-MOG T- or B-cell response patterns. Furthermore, we examined the phenotype and function of T-cells involved in the induction of neurological impairment. We found that fast progressor monkeys displayed a broad T-cell repertoire with responses to epitopes encompassed within MOG34-56 and/or MOG74-96. Marmosets immunized with MOG34-56 in complete Freund's adjuvant (CFA) developed CNS inflammation and widespread demyelination in the WM and GM, which may be caused by cytotoxic activity of infiltrated T-cells. In support of this, MOG34-56-specific T-cell lines (TCL) were found to express markers of natural killer-cytotoxic T lymphocytes (NK-CTL) (CD3<sup>+</sup>, CD4<sup>+</sup> or CD8<sup>+</sup>, CD56<sup>+</sup>, and CD16<sup>-</sup>) and to lyse peptide-pulsed, autologous as well as allogeneic EBV-transformed B-cell lines.

## MATERIALS AND METHODS

### Animals

All monkeys included in the current study were purchased from two purpose-bred colonies, one being kept at the Biomedical Primate Research Centre (Rijswijk, The Netherlands) and the second at the German Primate Center (Göttingen, Germany). Individual data of all monkeys used in this study are listed in Table 1. Monkeys were included in the study only after a complete physical, hematological, and biochemical check-up had been performed. The reported experiments span a period of about six years. During the experiments, the monkeys were initially housed individually in spacious cages with padded shelter provided on the floor and were under intensive veterinary care. Since 2005, pair housing became the standard within the BPRC. The daily diet during the study consisted of commercial food pellets for New World monkeys (Special Diet Services, Witham, Essex, UK), supplemented with rice, raisins, peanuts, marshmallows, biscuits, fresh fruit, grasshoppers, and maggots. Drinking water was provided ad libitum.

### Ethics

In accordance with the Dutch law on animal experimentation, all study protocols and experimental procedures were reviewed and approved by the Institute's Ethics Committee before the experiments could be started.

### RhMOG-induced EAE

A recombinant protein encompassing the extracellular domain of human MOG (rhMOG) was produced in *Escherichia coli* and purified as previously described<sup>19</sup>. RhMOG-induced EAE was evoked in a total of 23 monkeys by injection into the dorsal skin of 600 µl stable emulsion containing 100 µg of rhMOG in 300 µl of buffered saline and 300 µl of CFA (Difco Laboratories, Detroit, MI) under ketamine anesthesia (40 mg/kg; AST Pharma, Oudewater, The Netherlands) as described previously<sup>15</sup>.

### MOG peptide-induced EAE

All MOG peptides for immunization and cell culture were purchased from prof. A. Ben Nun (Weizmann Institute of Sciences, Rehovot, Israel) or from ABC Biotechnology (London, UK). EAE was induced with synthetic peptides that represent amino acids 34 to 56 (MOG34-56) and 74 to 96 (MOG74-96) of the human MOG extracellular domain. The monkeys were immunized with 100 µg of MOG peptide dissolved in 300 µl of buffered saline and 300 µl of CFA as previously described<sup>15</sup>. Monkeys that did not develop overt neurological deficit (score  $\geq 2.0$ ) within 28 days received booster immunizations with the same amount of peptide in incomplete Freund's adjuvant (IFA)

**Table 1. Overview of monkeys included in this study.**

<b>Monkey</b>	<b>Twin pair<sup>a</sup></b>	<b>Sex<sup>b</sup></b>	<b>Age<sup>c</sup></b>	<b>Immunization</b>	<b>Experiment</b>
KK		M	32	rhMOG	
QI		M	31	rhMOG	
QK		M	25	rhMOG	
QR		F	29	rhMOG	
QQ		M	28	rhMOG	
Mi009		M	26	rhMOG	
Mi010		M	26	rhMOG	
Mi011		M	26	rhMOG	
Mi020		M	28	rhMOG	
Mi021		M	30	rhMOG	
Mi022		M	48	rhMOG	
Mi062		M	24	rhMOG	
Mi065		M	23	rhMOG	
Mi069		M	20	rhMOG	
9501		M	35	rhMOG	
9505		M	54	rhMOG	
9601		M	25	rhMOG	
9814		M	15	rhMOG	
9819		M	15	rhMOG	
9841		M	21	rhMOG	
9853		F	22	rhMOG	
9854		M	22	rhMOG	
M9902		M	20	rhMOG	
M0131		M	24	MOG34-56	1
M0167		M	20	MOG34-56	1
M0178		M	20	MOG34-56	1
M0182		M	19	MOG34-56	1
M02075	Twin	M	22	MOG34-56	2
M02076	Twin	M	22	MOG74-96	2,A
M02078	Twin	M	23	MOG34-56	2
M02079	Twin	M	23	MOG74-96	2,A
M02087	Twin	M	22	MOG74-96	2,A
M02088	Twin	M	22	MOG34-56	2

Monkey	Twin pair <sup>a</sup>	Sex <sup>b</sup>	Age <sup>c</sup>	Immunization	Experiment
M02120	Twin	M	21	MOG34-56	2
M02121	Twin	M	21	MOG74-96	2,A
M03017	Twin	M	37	MOG34-56	3
M03018	Twin	M	37	MOG74-96+ MOG34-56	3,B
M03026	Twin	M	37	MOG34-56	3
M03027	Twin	M	37	MOG74-96+ MOG34-56	3,B
M03032	Twin	M	37	MOG34-56	3
M03033	Twin	M	37	MOG74-96+ MOG34-56	3,B

<sup>a</sup> Twin pairs are indicated by 'Twin'

<sup>b</sup> M, Male; F, Female.

<sup>c</sup> Age in months of the monkeys at the start of the experiment

at time points indicated in figure 2 and 6. Ag-adjuvant emulsion was prepared by gentle stirring of the PBS/oil mixture at 4°C for at least 1 h.

### Clinical scoring

Clinical signs were scored twice daily by trained observers using a previously described semiquantitative scale<sup>20</sup>. Briefly, 0 = no clinical signs; 0.5 = apathy, loss of appetite, altered walking pattern without ataxia; 1 = lethargy, anorexia, tail paralysis, tremor; 2 = ataxia, optic disease; 2.5 = para- or monoparesis, sensory loss, brain stem syndrome; 3 = para- or hemiplegia; 4 = quadriplegia; and 5 = spontaneous death attributable to EAE. A score of 2 or higher reflects an overt neurological deficit. Monkeys were sacrificed for ethical reasons once complete paralysis of hind limbs (score  $\geq$  3.0) was observed or at the predetermined endpoint of the study. Moreover, monkeys were weighed three times per week. As in rodent EAE models, body weight serves as a reliable surrogate disease marker in the marmoset. Body weight data are depicted as a separate disease parameter above the clinical score graphs.

### Ex vivo analysis of T-cell responses

The maximum blood sample that can be collected in a month from primates at the BPRC should not exceed 1% of the body weight. For an average adult marmoset weighing 350 grams, this equals a maximum monthly blood sample of 3.5 ml. Hence,

volumes of up to 1.5 ml at 2-weeks interval were collected into heparinized Vacutainer tubes (Greiner, Sölingen, Germany). Peripheral blood mononuclear cells (PBMC) were isolated from heparinized venous blood using lymphocyte separation medium (LSM®, ICN Biomedical Inc., Aurora, OH). Moreover, cell suspensions were prepared from aseptically removed axillary (ALN), inguinal (ILN), and cervical (CLN) lymph nodes and spleen. PBMC, lymph node, and spleen cells were cultured in triplicate for the detection of proliferative responses towards rhMOG and a panel of MOG peptides as previously described<sup>15</sup>. In some assays, PLP peptide 139-151 (PLP139-151), recombinant human MBP, and recombinant human  $\alpha$ B-crystallin (both provided by Dr. J.M. van Noort, TNO-Preventie en Gezondheid, Leiden, The Netherlands) were included. OVA served as control Ag in all studies. All Ag were tested at 5  $\mu$ g/ml. After 48 h of culture, 0.5  $\mu$ Ci of tritiated thymidine (<sup>3</sup>H]Thy) was added per well, and incorporation of the radiolabel was determined after 18 h using a matrix 9600 beta-counter (Packard 9600; Packard Instrument Company, Meriden, CT). Results are expressed as the mean stimulation index (SI). SI values above 2.0 were considered to be relevant.

### **Flow cytometry and CFSE labeling**

To determine the phenotype of proliferating cells, 4 x 10<sup>6</sup> viable mononuclear cells (MNC) from ALN were suspended in 1 ml PBS and incubated for 7 min at room temperature with carboxyfluorescein diacetate succinimidyl ester (CFSE, final concentration 1.5  $\mu$ M; Fluka, Deisenhofen, Germany). The labeled cells were cultured for 7 days with peptides under the standard conditions described above. For flow cytometric analysis we used the following commercially available, labeled monoclonal antibodies (mAb) directed against human CD markers: anti-CD3 with PerCP or Alexa Fluor 700 label (BD Biosciences), APC-labeled anti-CD4 (DAKO, Glostrup, Denmark), biotinylated anti-CD8 (Serotec, Düsseldorf, Germany), anti-CD56 with PE-Cy7 label, anti-CD16-PE, and streptavidin PE-Cy7 or streptavidin PerCP (BD Biosciences). Flow cytometric analysis was performed on a FACSort flow cytometer using FACSDiva software (BD Biosciences). First, viable cells were gated using the live/dead fixable violet viability stain (Invitrogen, Molecular Probes, Carlsbad, CA). Within the viable cell gate, lymphocytes/monocytes were selected using forward and side scatter. Within the lymphocyte/monocyte gate CD3<sup>+</sup> cells were selected. The CD3<sup>+</sup> population in the CFSE experiment consisted of CD4<sup>+</sup> cells (48-70%) and CD8<sup>+</sup> cells (12-18%). Within each gated subpopulation the percentage of cells with CFSE dilution was calculated.

### **Cytotoxicity assay**

Autologous and allogeneic peptide-pulsed <sup>51</sup>chromium-labeled, Epstein-Barr virus (EBV)-transformed B-cell lines were used as target cells to test the cytotoxic potential of MOG peptide-specific TCL. In brief, 10<sup>6</sup> B-cells were incubated for 60 min at 37°C

with  $^{51}$ chromium and pulsed with 100  $\mu$ g MOG34-56 or MOG74-96 and subsequently washed thoroughly with PBS. Peptide pulsed B-cells were mixed with effector T-cells at 1:1, 1:4, and 1:16 ratio in U-well microtiter plates and cultured for 5 h at 37°C in culture medium, after which 100  $\mu$ l of the supernatant was collected to determine the amount of radiolabel in a gamma-counter. Controls consisted of peptide-pulsed target cells without T-cells (spontaneous release) or peptide-pulsed target cells lysed with 1% Triton X-100 (maximum release). Results are expressed as % killing using the formula:  $(\text{T-cell induced} - \text{spontaneous})/(\text{maximal} - \text{spontaneous}) \times 100$ .

### **Generation of MOG peptide-reactive T-cell lines**

At necropsy, cell suspensions were prepared from spleen, ALN, ILN, and CLN. MNC of rhMOG- or MOG peptide-immunized marmosets were stimulated *ex vivo* with rhMOG, MOG34-56, or MOG74-96 to establish specific TCL. Briefly, MNC ( $10^6$ /well) were seeded into 24-well plates (Greiner) and stimulated with 10  $\mu$ g/ml rhMOG, MOG34-56, or MOG74-96. Every 2 or 3 days, half of the culture supernatant was replaced with fresh medium containing 20 U/ml rh interleukin (IL)-2 (Proleukin, Chiron Corporation, Emeryville, CA) and split when needed. After 14 to 21 days of culture, part of the cells were transferred into 96-well flat-bottom plates (Greiner) and tested for reactivity with a panel of 23-mer MOG peptides<sup>15</sup>. Lethally irradiated (50 gray) EBV-transformed marmoset B-cells from stably growing lines maintained in 75-cm<sup>2</sup> tissue culture flasks (Greiner) were used as antigen presenting cell (APC). Lines of interest were characterized by the expression of T-cell specific cell surface markers by flow cytometry using cross-reactive mAb raised against human CD markers<sup>21</sup>. Isotype controls were kindly provided by J. Miller (Chemicon International, South Hampton, UK).

### **B-cell responses**

Venous blood samples were centrifuged and the plasma supernatants were collected and stored frozen at -20°C until further analysis. Ab binding to myelin proteins (rhMOG, MBP,  $\alpha$ B-crystallin, and HPLC-purified human PLP) or to a panel of overlapping 23-mer MOG peptide sequences was determined using ELISA<sup>22</sup>. Bound Ab was detected using polyclonal alkaline phosphatase-conjugated goat-anti-monkey IgM  $\mu$ -chain (Rockland, Gilbertsville, PA) or rabbit-anti-human IgG (Abcam, Cambridge, UK). Ab specific for discontinuous MOG epitopes are considered particularly pathogenic<sup>23</sup>. To distinguish between Ab reactivity against discontinuous and linear epitopes, serum samples were preincubated with a mixture of all overlapping MOG peptides (10  $\mu$ g/ml for each peptide) for 1 h at 37°C before probing them for reactivity with rhMOG coated onto ELISA plates. As an internal control, the MOG54-76 peptide was left out of the peptide mix used for preincubation because in previous studies this peptide was found to contain dominant B-cell epitopes. The results of the Ab assays are expressed as the fold increase of light

absorbance at 405 nm compared with the reactivity with OVA as an irrelevant antigen or compared to the reactivity in preimmune sera of the same monkeys.

### **Post mortem examination**

Monkeys selected for necropsy were first deeply sedated by intramuscular injection of ketamine (50 mg/kg), and subsequently euthanised by the infusion of pento-barbital sodium (Euthesate®; Apharmo, Duiven, The Netherlands). Brain, spinal cord, spleen, ILN, ALN, and CLN were removed. Representative parts of all organs were snap frozen in liquid nitrogen or fixed in 4% buffered formalin. Frozen tissues were stored at – 80°C. After at least 7 days of fixation in formalin, the tissues were transferred into buffered saline containing sodium azide for stabilization before MRI<sup>11</sup>.

To assess the total lesion load in the brain, MR images were made of formalin-fixed brains as described previously<sup>11,20</sup>. Both frozen and fixed tissues were examined with histological and immunohistochemical techniques as previously described<sup>20,24,25</sup>.

### **MRI procedures**

Brains of MOG34-56- and MOG74-96-immunized animals were analyzed by MRI. MRI experiments were performed post mortem on a 6.3 T horizontal bore MRI scanner (Varian, Palo Alto, USA). The formalin-fixed brains were submerged in a perfluoropolyether (Fomblin, Ausimont, NJ) for susceptibility matching. The following parameters were used in all experiments: field of view, 2.5×2.5 cm<sup>2</sup>; matrix, 128×128; slice thickness, 1 mm; number of slices, 20. T2-weighted (T2W) images were collected using a spin-echo sequence with the following parameters: repetition time, 4 s; echo time, 35 ms; number of signal averages, 8. T<sub>2</sub>-maps were recorded with a multiecho sequence using the following parameters: repetition time, 8 s; echo spacing, 20 ms; echo train length, 8; number of signal averages, 4. Diffusion tensor images were made using a pulsed field gradient spin echo sequence with the following parameters: repetition time, 4 s; echo time, 35 ms; number of signal averages, 8. Diffusion weighting was applied in 10 directions with the following pulsed field gradient parameters:  $\Delta$ , 20 ms;  $\delta$ , 10 ms; diffusion gradient ( $G_{diff}$ ), 0; and 120 millitesla/meter (mT/m), resulting in b-value of 0 and 1717 s/mm<sup>2</sup>.

### **Image analysis**

First, WM was segmented manually. In the WM, lesions were identified as regions with a T<sub>2</sub> value 10% above the normal appearing white matter (NAWM). Average T<sub>2</sub>, apparent diffusion coefficient, and fractional anisotropy values were determined for lesions and NAWM. Image analysis was done using Mathematica (Wolfram Research Europe Ltd, Oxfordshire, UK).

## Statistics

The relation between a broad T-cell response and fast disease progression (see data in Table 2) was analyzed using Kaplan-Meier survival analysis. Statistical significance of differences between groups was calculated using the log rank test. Because four potential contrasts could be chosen for this analysis,  $p$  values were considered statistically significant when  $< 0.05/4 = 0.0125$  (Bonferroni correction).

Results of  $T_2$  relaxation time, fractional anisotropy, and apparent diffusion coefficient were analyzed by a two population (independent)  $t$  test.

## RESULTS

### Disease course and autoimmune reactions in rhMOG-immunized monkeys

Table 2 gives a summary of data obtained from 23 rhMOG-immunized marmosets. Clinical scores are depicted in figure 1 showing that in 100% of the monkeys clinical EAE was induced but that the time interval between EAE induction and the expression of an overt neurological deficit varied considerably. Of the 23 examined monkeys, 20 were sacrificed after they had developed an EAE score  $\geq 2$ . Three monkeys were withdrawn from their respective experiments without neurological impairment. One monkey (QK) had experienced serious body weight loss and was sacrificed pre-term to avoid a sudden deterioration of the clinical state, as has been observed in rhesus monkeys in which immunization with MOG34-56 induced acute onset EAE<sup>26</sup>. Two monkeys (Mi020 and Mi021) were sacrificed with mild signs of EAE (score 0.5) as they reached the end of the experiment. The time interval between EAE induction and the development of hemiplegia/paraplegia (EAE score of 3) varied from 34 to 139 days (mean 73 days) (Table 2). Notably, serial MRI in selected monkeys reveals ample disease activity within the CNS WM during the asymptomatic interval, which apparently does not lead to an overt neurological deficit<sup>10,27</sup>. We have taken advantage of this unique outbred model to test whether monkeys with a fast or slow disease progression rate display different Ab and T-cell response patterns.

### Antibodies

Serum reactivity with rhMOG protein was detected in all monkeys (Table 2). The anti-MOG IgG Ab reactivity was directed against linear epitopes within three main regions, namely MOG4-26, MOG24-46, and MOG54-76. Analysis of immune sera that were collected at two week intervals during the entire disease course revealed that the first upcoming Ab reactivity was against MOG54-76. The anti-rhMOG Ab reactivity at necropsy was reduced by  $>95\%$  when the immune sera were preincubated with a mix of the complete MOG peptide panel before the binding to rhMOG-coated ELISA plates

was tested. However, when MOG54-76 was left out of the peptide mix the reduction of serum reactivity with rhMOG was <10% (data not shown). These data indicate that the MOG54-76 peptide contains one or more important recognition sites for rhMOG-induced Ab. Ab reactivities towards MBP and  $\alpha$ B-crystallin were infrequently observed (data not shown). In summary, we observed no obvious association between disease progression and the number of MOG peptides recognized by IgG molecules present in necropsy sera (Table 2).

### T-cell responses

RhMOG-induced TCL generated from ILN, ALN, or spleen of slow and fast disease progressors were tested for reactivity with a panel of MOG peptides. In accordance with previously published data<sup>15</sup> a proliferative response against the peptide MOG24-36 was found in all monkeys (Table 2). Besides this ubiquitous reactivity with MOG24-36, individual monkeys displayed a variable reactivity with other MOG peptides. When the monkeys were ranked according to the total disease duration, it was evident that fast progressor monkeys displayed a broader T-cell reactivity with the MOG peptide panel than slow progressor monkeys (Table 2). The relation between a broader T-cell response with faster disease progression is highly significant (Figure 1;  $p < 0.0125$ ).

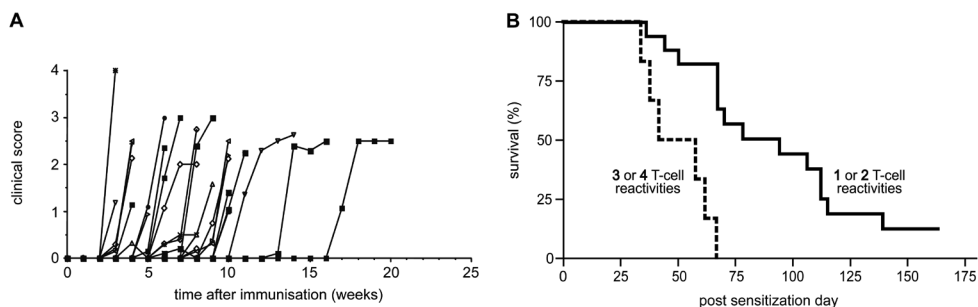


**Figure 1. Association of disease progression with T-cell reactivity diversification in rhMOG-induced EAE.**

A, The EAE course of 23 unrelated monkeys (Table 1) that received a single immunization with 100  $\mu$ g rhMOG in CFA is shown. Note that the disease incidence is 100% but that the time interval between EAE induction and the expression of an overt neurological deficit varies clearly between individual monkeys. B, Kaplan-Meier plot shows survival curves of monkeys with a narrow (one or two peptides recognized) or broad (three or four peptides recognized) T-cell epitope diversification. The difference between both groups is highly significant ( $p < 0.001$ ; log rank test).

**Table 2. T-cell and antibody responses against rhMOG and MOG peptides in rhMOG-immunized marmosets.**

Monkey	Sex <sup>a</sup>	Sacrificed (psd)	EAE score	T-cell reactivity (MOG peptides) <sup>b</sup>			Ab <sup>c</sup> reactivity		
							rhMOG	pMOG <sup>d</sup>	
QQ	M	34	3	24-36	54-76	<b>74-96</b>	+	0	
Mi022	M	36	5	24-36	<b>64-86</b>		+	0	
KK	M	38	3	24-36	<b>34-50</b>	94-110	+	7	
QR	F	42	3	24-36	<b>34-50</b>	<b>64-86</b>	+	5	
M9902	M	44	3.5	24-36	94-110		+	6	
QI	M	50	2	24-36			+	6	
9601	M	58	3	24-36	4-11	12-21	<b>24-46</b>	+	8
Mi011	M	62	3	24-36	4-11	<b>34-50</b>	+	1	
9854	M	67	2.5	24-36	54-76	<b>74-96</b>	+	3	
9853	F	67	3	24-36			+	3	
Mi069	M	67	2.5	24-36	54-76		+	7	
Mi065	M	67	2.5	24-36			+	7	
9501	M	70	3	24-36			+	8	
9814	M	78	2.5	24-36			+	1	
9819	M	94	3	24-36			+	5	
Mi010	M	106	3	24-36			NT <sup>e</sup>		
Mi009	M	112	2.5	24-36			NT <sup>e</sup>		
9841	M	112	2	24-36			+	1	
9505	M	115	3	24-36	<b>64-86</b>		+	1	
Mi062	M	139	3	24-36			+	7	
Mean (n=23)		73							
QK <sup>f</sup>	M	50	0.5	24-36			+	6	
Mi020 <sup>f</sup>	M	155	0	24-36			+	5	
Mi021 <sup>f</sup>	M	163	0.5	24-36	<b>74-96</b>		+	8	

<sup>a</sup> M, Male; F, Female<sup>b</sup> MOG peptides of interest are indicated in bold<sup>c</sup> Antibody reactivity was tested in necropsy serum<sup>d</sup> For the serum reactivity with MOG peptides only the number of recognized peptides is given<sup>e</sup> NT, not tested<sup>f</sup> Marmosets with positive MRI, no or mild clinical EAE

## Chapter 3.1

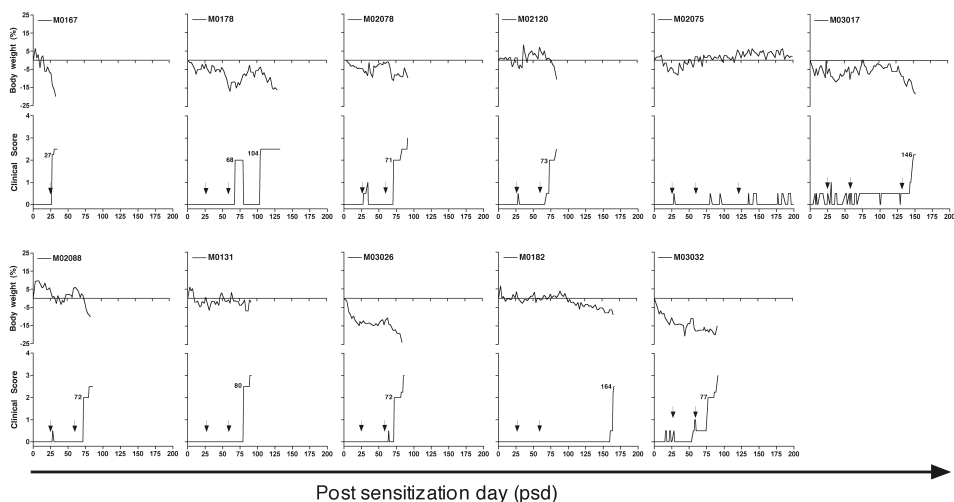


**Figure 2. Clinical course of MOG34-56 induced EAE.**

Eleven marmosets were immunized with 100  $\mu$ g MOG34-56 in CFA. Monkeys without overt signs of EAE at the end of a pre-determined episode of  $\pm$  28 days received one, two, or three booster immunizations with 100  $\mu$ g MOG34-56 in IFA (arrows). Clinical scores and changes in body weight (percentage compared with day 0) as a surrogate disease parameter of individual monkeys are shown. Ten of the 11 monkeys were sacrificed with a clinical score of  $\geq$  2.5, whereas one monkey was sacrificed at the end of a 200-day observation period without neurological signs. Numbers in the figures represent the time point (psd) when overt neurological signs (score  $\geq$  2) were first observed.

### Characterization of potentially encephalitogenic MOG peptides

To determine the contribution of individual MOG peptide-specific T-cell reactivities to the EAE pathogenesis in marmosets, we have taken advantage of a unique biological feature of this model. Marmoset twins develop *in utero* as stable bone marrow chimeras due to the shared placental blood stream<sup>28</sup>. This implies that the T-cells of both twins are educated in the same thymic environment and that similar mixed populations of bone marrow-derived elements are seeded into the peripheral tissues and organs of both siblings. Hence, despite the different genetic background, such nonidentical twin siblings can be regarded as immunologically similar.

Of the three peptides that were most frequently recognized by T-cells from fast progressor monkeys, MOG34-56, MOG54-76, and MOG76-96 (Table 2), we chose MOG34-56 and MOG76-96 for the immunization of chimeric twins. Because we were mainly interested in T-cell responses, MOG54-76 was not included for further analyses as this peptide is also a B-cell epitope (see above).

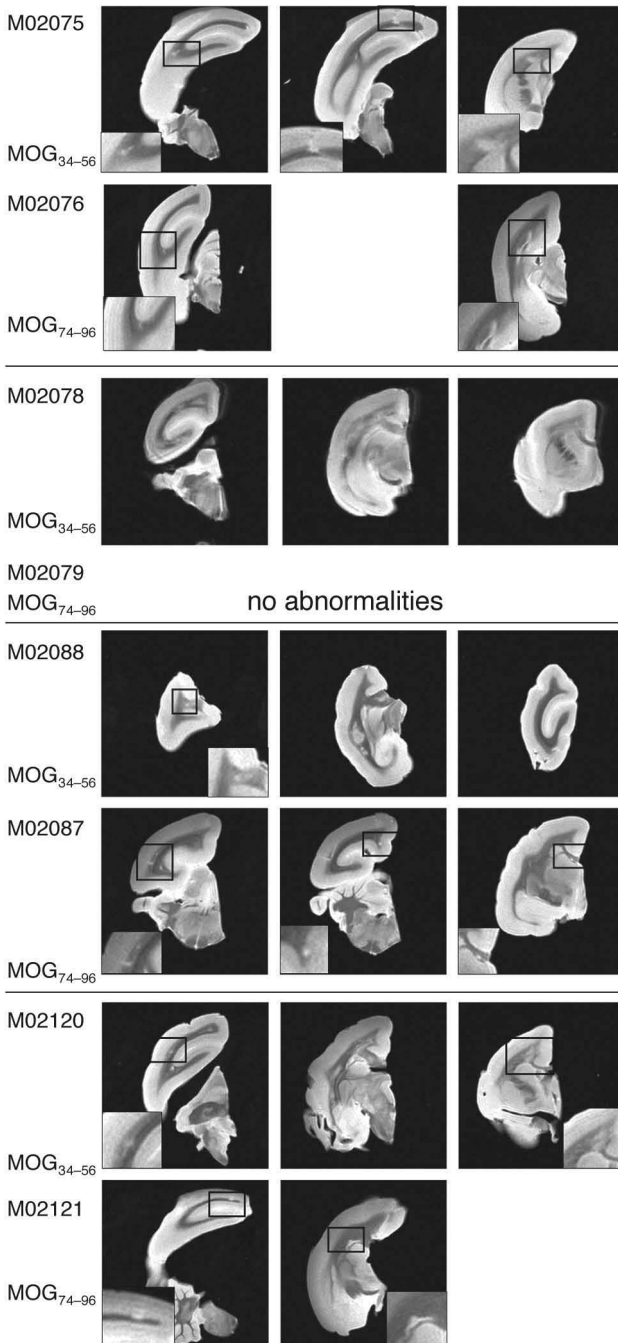


**Figure 3. MRI reveals white matter pathology in MOG34-56-immunized monkeys.**

High contrast T2W images of formalin-fixed brains were recorded to assess the total lesion load. Corresponding slices from twins of which one sibling was immunized with MOG34-56 and the other with MOG74-96 are shown. The pictures clearly illustrate white matter pathology in MOG34-56-immunized monkeys that displayed overt neurological signs. This was negligible in the MOG34-56-immunized monkey (M02075) and in all four MOG74-96 monkeys in which overt neurological signs did not develop. Magnification of the lesions shown in the corner are indicated by boxes.

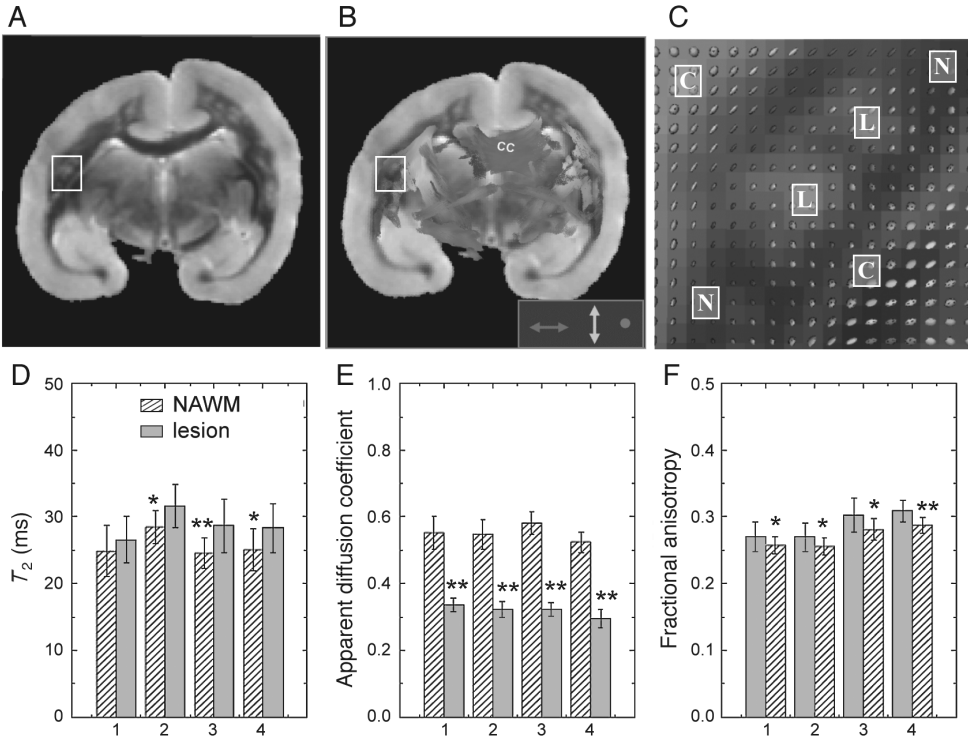


**Figure 4. Diffusion tensor imaging of MOG34-56-induced brain lesions.**

The disruption of the normally restricted orientation (anisotropic) of water diffusion in white matter was used as an indirect MRI measure of tissue destruction in formalin-fixed brains. Brains from the four MOG34-56-immunized monkeys in experiment 1 (see Table 1) were used for this analysis. A tomographic section of the brain of monkey M0167 is depicted as a representative example. A, High contrast T2W images were made to visualize hyperintense structural abnormalities. B, The (disturbance of) fiber direction within the white matter is visualized with the standard color codes (red, left ==> right; blue, superior ==> inferior; green, anterior ==> posterior). C, The ellipsoid representation of fiber orientation within a lesion-rich area (white square) shows a round shape in the cortical (C) and lesion (L) area whereas these are more unidirectional in the compact white matter. D-F, Mean values of the total lesion (grey bars) and white matter (hatched bars) area of four monkeys (M0131, M0167, M0178, and M0182) are shown. The depicted quantitative parameters are as follows: 1) the mean of all voxels for T2 relaxation times (D), which is higher in the lesions than in the NAWM due to increased water content; 2) the degree of fractional anisotropy (E), which is decreased due to destruction of compact myelin; and 3) and the apparent diffusion coefficient (F), which is slightly higher in lesions than in NAWM. Data are mean  $\pm$  SD. \*  $P < 0.05$ , \*\*  $P < 0.001$ . See page 311 for a full-color representation of this figure.

### MOG34-56-induced EAE

A total of 11 monkeys were immunized in three separate experiments with MOG34-56/CFA followed by booster immunizations on post sensitization days (psd) 28, 56, and ~125 with MOG34-56/IFA until overt clinical signs of EAE were detectable. The individual EAE scores depicted in figure 2 show a heterogeneous clinical picture. One monkey (M0167) developed EAE associated with marked weight loss within 30 days after EAE induction. In two monkeys (M0182 and M03017) EAE developed only after psd 145 and one monkey (M02075) was sacrificed at psd 200 with only mild symptoms (score 0.5). In the remaining 7 monkeys, overt neurological deficits were first observed around psd 75. Interestingly, in three monkeys (M0178, M03026, and M03032) we observed optic neuritis, which remitted spontaneously within two weeks.

T2W MR images were made of the formalin-fixed brains of all monkeys to visualize the spatial distribution and size of lesions. Contrast in T2W images is mainly based on differences in water content caused, for example, by inflammation. Hence, altered signal intensity in the *in vivo* T2W images of a tissue mainly reflects inflammation. However, T2W images of formalin-fixed tissues, can also be used to assess the extent of myelin destruction<sup>11</sup>. In figure 3 the post mortem brain MR images of four twins (Table 1; Experiment 2) are depicted, illustrating that significant lesion formation has taken place in the MOG34-56-immunized monkeys.

The loss of a highly organized compact myelin structure in a demyelinated lesion causes a reduction of the directional diffusivity of water, which can be visualized in diffusion tensor images (Figure 4A)<sup>10</sup>. To obtain an overall picture of the lesion pathology, MR images of the total fixed brain were recorded. More specific, the directional diffusivity (fractional anisotropy) of water in lesions and NAWM was determined. Figure 4B and 4C depict one slice as an illustrative example that shows the disturbed organization of WM in the T<sub>2</sub> lesion, suggesting that compact myelin has disappeared. Figure 4E shows the mean fractional anisotropy values of all T<sub>2</sub> lesions throughout the brain of four MOG34-56-immunized marmosets; these were substantially lower in the lesions than of the perilesional NAWM, indicating the ubiquitous loss of compact WM.

Pathological changes in the brain and spinal cord were also examined by histology. Figure 5 shows dramatic demyelination in the spinal cord WM area of a MOG34-56-immunized monkey. At the time of necropsy demyelination was still taking place. The lesions were heavily infiltrated with T-cells and macrophages that contained phagocytosed myelin debris. Axonal pathology was clearly present. Significant demyelination was also observed in the spinal cord grey matter areas. Within these areas, activated microglia cells as well as infiltrating macrophages were detected.

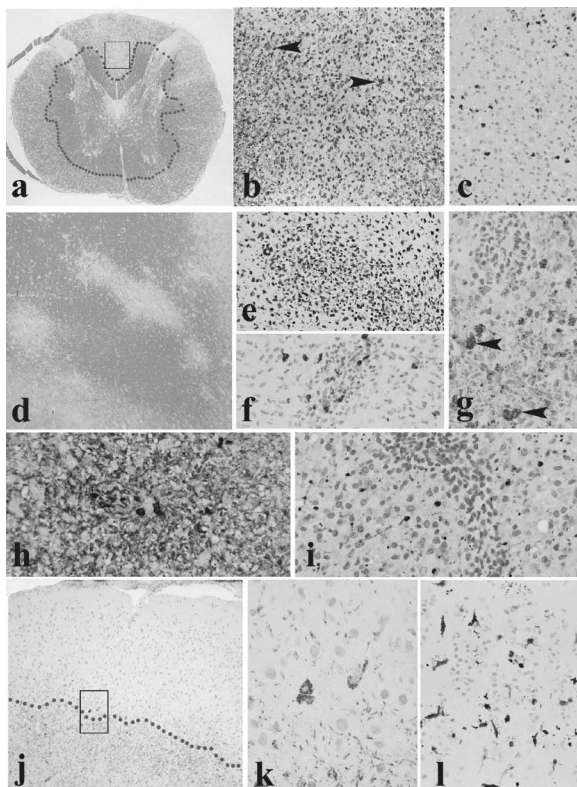


**Figure 5. MOG34-56 induces inflammation and demyelination in the CNS.**

A, Luxol fast blue staining (original magnification x23) reveals that in this cross-section of spinal cord > 50% of the white matter has been demyelinated (blue line, border with normal white matter) and is remyelinating. Magnified views of the rectangle are shown in B and C. B, CNPase staining (original magnification x160) confirms demyelination and remyelination. Arrowheads point at oligodendrocyte cell bodies in the lesion centre. C, CD3 staining (original magnification x160) shows the presence of T lymphocytes in this area. D, Luxol fast blue staining (original magnification x38) indicates the presence of demyelinating lesions in the corpus callosum. E, MRP-14 positive macrophages are present in these lesions (E, original magnification x99) together with CD3 positive T lymphocytes (F, original magnification x200). G, PLP staining (original magnification x310) reveals PLP degradation products in macrophages (arrowheads). H, IgM staining (original magnification x290) shows plasma cells and Ig deposition on myelin. I, Axonal injury (axonal spheroids) in these white matter lesions is visualized by amyloid precursor protein staining (original magnification x275). In addition to spinal cord and brain white matter lesions, prominent cortical demyelination is also present. J, PLP staining (original magnification x50) reveals subpial demyelination. The meningeal lining is at the upper part of the figure, the blue lining marks the border of the demyelinated cortex, and a magnified view of the area inside the rectangle is shown in K. K, The area inside the rectangle in J (original magnification x990) in which microglial cells with uptake of PLP-positive myelin degradation products can be found. L, These activated microglial cells (original magnification x185) also stain positively with MRP-14, being an early activation marker of macrophages. See page 312 for a full-color representation of this figure.

**MOG74-96-induced EAE**

To test the encephalitogenic potential of the MOG74-96 peptide, the twin siblings of seven of the 11 MOG34-56-immunized monkeys were immunized with MOG74-96. Two separate experiments, denoted A and B, were done comprising four and three monkeys, respectively (Table 1).

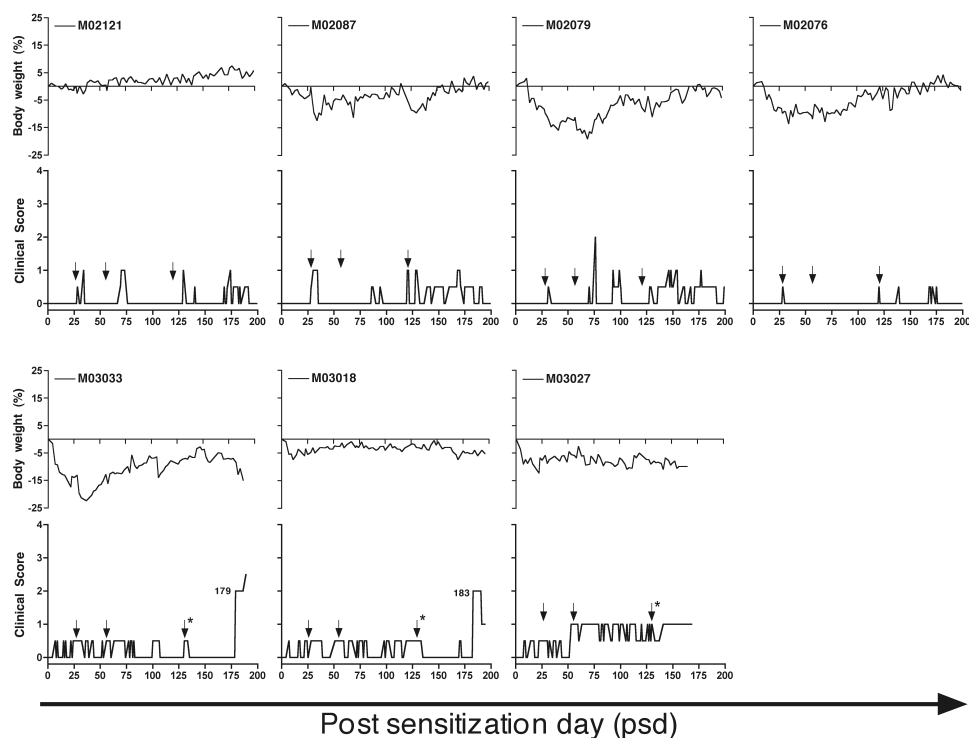


**Figure 6. Immunization with MOG34-56/IFA induces full blown EAE in MOG74-96 sensitized marmosets.**

Seven marmosets, twin siblings of the monkeys in figure 2 (see Table 1) were immunized with 100  $\mu$ g MOG74-96 in CFA. Monkeys without overt signs of EAE (score < 2) at the end of a pre-determined episode of  $\pm$  28 days received three booster immunizations with 100  $\mu$ g MOG74-96 in IFA (arrows). Clinical scores and changes in body weight (percentage compared with day 0) as surrogate disease parameter of individual monkeys are shown. Because none of the monkeys developed overt neurological deficit within the pre-determined observation period of 125 days, three (M03033, M03018, and M03027) received the third booster immunization of 100  $\mu$ g MOG34-56 in IFA (arrow with an asterisk), resulting in full blown EAE in two monkeys (M03033 and M03018). Numbers in the figures represent the time point (psd) when overt neurological signs were first observed.

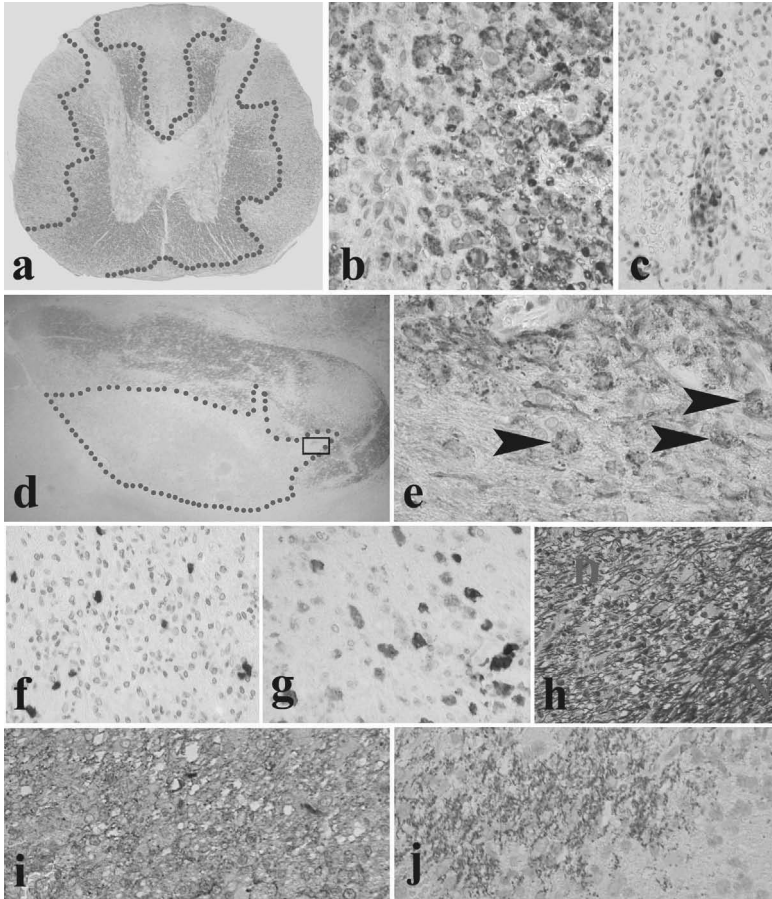


**Figure 7. Pathology of MOG34-56-boosted EAE in MOG74-96-immunized monkeys.**

Pathology present in the spinal cord of monkey M03033 is shown in A-C; pathology in the optic tract is shown in D-J. A, Staining for luxol fast blue (original magnification x20) reveals demyelinated areas (bordered by blue dotted line) in the spinal cord white matter. B, Late active demyelination (original magnification x350) is shown by the presence of PLP-positive degradation products in macrophages. C, Besides demyelination, inflammation of the lesions is characterized by the presence of CD3<sup>+</sup> lymphocytes (original magnification x150). D, Luxol fast blue staining (original magnification x45) shows large demyelinated lesions (borders indicated by dotted line) in the optic tract. Magnified views of the rectangular area are shown in E-J. E, Staining for PLP (original magnification x350) reveals the presence of PLP degradation products in macrophages (arrowheads). F, The optic tract lesions contained CD3<sup>+</sup> lymphocytes (original magnification x150). G, Single macrophages are stained positively for MRP-14 (original magnification x150). H, A bielschowsky stain for axons (original magnification x150) shows a reduced density of axonal fibers in the demyelinated area (D) compared to the surrounding NAWM (N). I, Staining for IgM (original magnification x300) and complement C9 (J, original magnification x300) shows deposition in the demyelinated areas. See page 313 for a full-color representation of this figure.

*Experiment A.* In the first experiment (monkeys M02121, M02076, M02079, and M02087), overt neurological disease did not develop during the 200-day observation period. However, mild signs of EAE (score 0.5) were observed (Figure 6).

To test whether monkeys immunized with MOG74-96 displayed pathological changes within the CNS WM, high definition T2W images were made of the formalin-fixed brains from all four monkeys. In three monkeys clear abnormalities, albeit of moderate severity, were detected in the brain WM, namely one large periventricular lesion in M02076, two large lesions in M02121, and several small lesions in M02087 (Figure 3).

Histological examination confirmed the presence of mild demyelination in frontal regions in the brain of two monkeys that were scored positive with MRI, i.e. M02076 and M02121. Interestingly, very little inflammatory activity was detected within these lesions (data not shown). In monkey M02087 no brain lesions were found, indicating that the abnormalities observed with MRI do not represent areas of inflammatory demyelination.

*Experiment B.* In the second experiment essentially the same results were obtained after the subsequent immunizations with MOG74-96, namely significant weight loss associated with only mild clinical signs. The mild CNS pathology observed in experiment A was associated with the appearance of low-level T-cell reactivity against MOG34-56 (see next paragraph). To amplify this low-level response, all three MOG74-96-immunized monkeys were given a single booster immunization with MOG34-56 in IFA. This induced overt neurological signs in two of the three monkeys within a few weeks (Figure 6). This observation contrasts with the situation in rhesus monkeys where booster immunization with MOG34-56 in IFA did not induce EAE, although this species is much more susceptible to EAE than marmosets<sup>26</sup>. In the third monkey (M03027), EAE scores fluctuating between 0.5 and 1.0 were recorded from psd 50 onwards. After the boost with MOG34-56, the disease stabilized at EAE score of 1. The monkey was finally sacrificed at psd 168 for histological analysis of the CNS.

The T2W post mortem images showed dramatic CNS pathology. Apart from large areas with increased T2W signal intensity, likely due to demyelination, the most remarkable feature was the presence of large “black holes” in the WM (data not shown). Histological analysis demonstrated comparable pathological changes as in MOG34-56-immunized monkeys. Brain and spinal cord contained large demyelinated lesions with infiltrated T-cells and activated macrophages and microglia (Figure 7).

### **Autoantibodies in MOG peptide-induced EAE cases**

Plasma samples prepared from venous blood collected at 7-day intervals from the first immunization and at necropsy were tested with ELISA for the presence of IgM and IgG Ab against rhMOG and MOG peptides. Only total IgG responses were tested, because IgG subclasses are not described for the marmoset. Figure 8 shows the results for IgG at

necropsy, which were representative for IgM and the data of the 7-day interval plasma.

The main Ab response in MOG34-56-immunized monkeys was against MOG24-46. In some monkeys we also found antibodies against MOG34-56 and rhMOG. In two MOG34-56-immunized monkeys a diversification of the Ab response to MOG54-76 was found (Figure 8A). Because this peptide, which is a dominant B-cell epitope in rhMOG-induced EAE, has only two overlapping amino acids with the immunizing peptide, it may be that this reactivity is caused by epitope spreading.

The dominant response in MOG74-96-immunized monkeys was against the immunizing peptide; but in the monkeys from experiment B, which were boosted with MOG34-56 in IFA, low-level Ab reactivity against rhMOG and MOG24-46 was also detected (Figure 8B).

### T-cell reactivity in MOG peptide-induced EAE

PBMC, isolated at 2-week intervals after immunization, and MNC from lymphoid organs were cultured with rhMOG and a MOG peptide panel to test proliferation. Moreover, cells of ALN from the twins of experiment 3 (Table 1) were CFSE labeled and

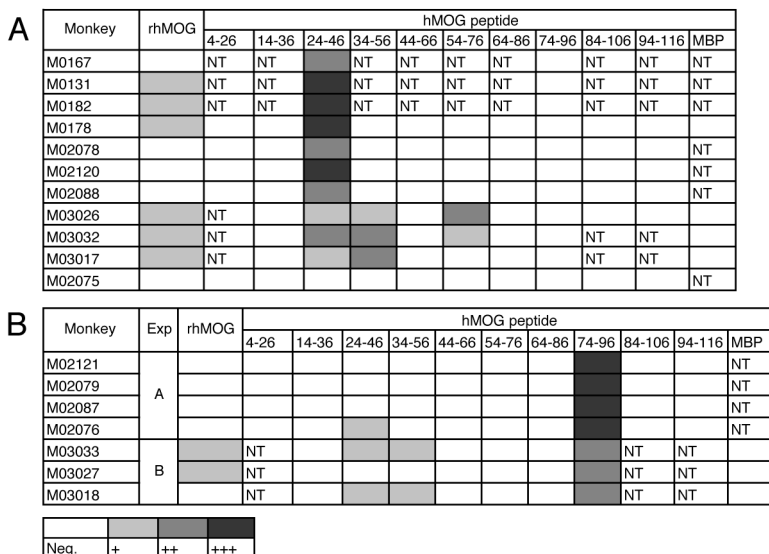


**Figure 8. Diversification of antibody reactivity in MOG34-56 and MOG74-96-immunized monkeys.** Plasma of MOG34-56 (A) and MOG74-96 (B) immunized monkeys were collected at necropsy and tested with ELISA for IgG reactivity with rhMOG and the panel of 23-mer peptides that covers the extracellular domain of MOG (1-125). Results are expressed as fold increase of OD relative to pre-immune marmoset serum. Neg., <2; +, 2 to <4; ++, 4 to <8; +++, >8. NT, not tested due to lack of material.

subsequently stimulated for 7 days with the immunizing peptides for the phenotyping of proliferating cells, visualized by the dilution of the fluorescent dye.

**Proliferative responses in MOG34-56-immunized monkeys**

In all monkeys, PBMC proliferation was found against MOG34-56 (Figure 9A). The proliferative response in PBMC remained low, rarely exceeding an SI of 5.0. As expected, much higher responses were found in the lymphoid organs collected at

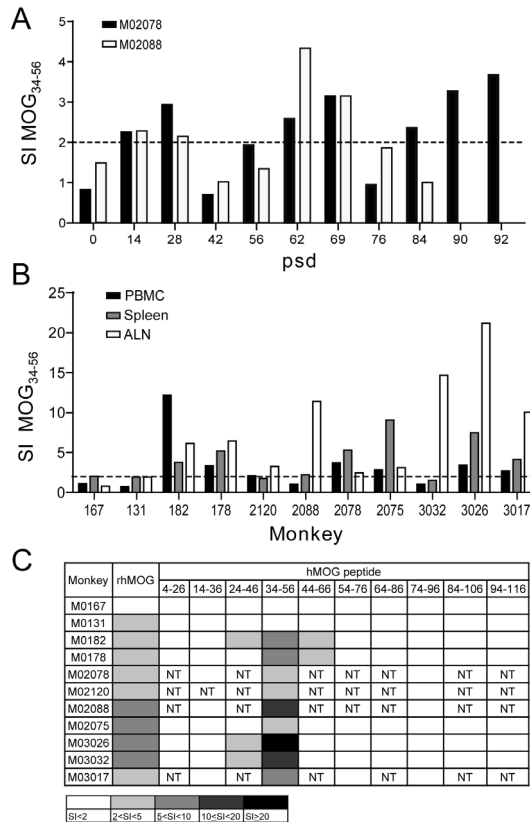


**Figure 9. T-cell proliferation remains confined to the immunizing peptide MOG34-56.**

Eleven marmosets were immunized with MOG34-56 in CFA (psd 0) followed by booster immunizations with MOG34-56 in IFA at psd 28, 56, and ~ 125. PBMC collected at different time points and MNC of secondary lymphoid organs collected at necropsy were probed for their proliferative response against the MOG peptide panel. Only responses above an SI of 2 (dotted line) are considered positive. Proliferative responses were found against MOG34-56. A, PBMC data from two representative monkeys. B, High responses were found in ALN and spleen at necropsy. C, Summary table of proliferative responses of ALN cells from all 11 monkeys against rhMOG and the MOG peptide panel. NT, not tested.

necropsy. The highest responses were mostly found in ALN and spleen (Figure 9B), while lower proliferation was found in ILN (data not shown). Only in monkey M02088 proliferation could be detected in CLN (data not shown). Cells of ALN (Figure 9C), spleen and ILN (data not shown) also proliferated against rhMOG and peptides overlapping with MOG34-56.

### **Proliferative responses in MOG74-96-immunized monkeys**

In PBMC from MOG74-96-immunized monkeys proliferation against MOG74-96 was found (Figure 10A-B). In addition, from psd 104 proliferation against MOG34-56 was detectable (Figure 10A-B). The response to MOG34-56 could be amplified by a booster immunization with MOG34-56 in IFA (Figure 10B). At necropsy, MNC of MOG74-96-immunized animals proliferated against MOG74-96, but not against MOG34-56 (Figure 10C). The three monkeys challenged with MOG34-56 at the third booster displayed a reduced response against MOG74-96 and increased proliferation against MOG34-56 (Figure 10C). Cells of ALN collected at necropsy also proliferated against rhMOG (Figure 10D).

### **Phenotype of MOG34-56- and MOG74-96-reactive T-cells**

MNC from ALN, which contained the highest proliferative response, were stained with the fluorescent dye CFSE and subsequently cultured with the respective peptides. After 7 days, cells were harvested and stained with fluorescein-labeled mAb used for the phenotyping of human MNC subsets that are known to cross-react with marmoset MNC<sup>21</sup>. Proliferating cells were identified by dilution of CFSE. MOG34-56 stimulation of MNC from MOG34-56-immunized monkeys induced CFSE dilution in both CD4<sup>+</sup> and CD8<sup>+</sup> T-cell subsets (Figure 11A). However, the percentage of divided CD4<sup>+</sup> cells was about twice as high as that of divided CD8<sup>+</sup> cells. Figure 11B shows the CFSE dilution in MNC cultures of monkeys immunized with MOG74-96 and boosted with MOG34-56 (experiment B). Proliferation of cells stimulated with MOG34-56 or with MOG74-96 was found in both the CD4<sup>+</sup> and the CD8<sup>+</sup> T-cell subsets.

### **Cytotoxic activity of MOG34-56- and MOG74-96-specific T-cell lines**

It was very difficult to generate stable TCL from the peptide-immunized monkeys from experiment 3 (Table 1), although we used the same method as successfully applied for the generation of stable TCL from rhMOG-immunized marmosets<sup>15</sup>. Most lines collapsed after two or three rounds of restimulation with peptide-pulsed B-cell lines. Stable TCL could only be obtained of three monkeys, i.e. the twins M03017 and M03018 and the monkey M03033. Cytolytic activity towards autologous MOG peptide-pulsed APC by MOG-reactive TCL from MS patients has been described<sup>29</sup>. Hence, we hypothesized that MOG peptide-specific T-cells from the marmoset might exert cytotoxic activity and

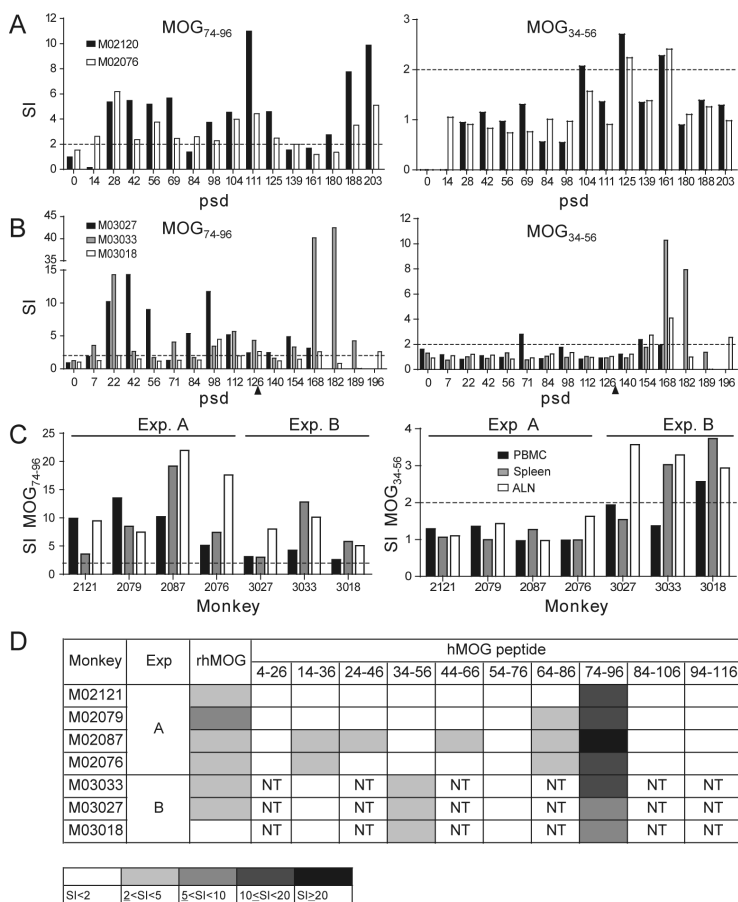


**Figure 10. Amplification of anti-MOG34-56 T-cell responses in MOG74-96-immunized animals after a booster with MOG34-56 in IFA.**

Four marmosets were immunized with MOG74-96 in CFA (psd 0) followed by immunizations with MOG74-96 in IFA at psd 28, 56, and 119 (experiment A). Three marmosets were immunized with MOG74-96 in CFA (psd 0) followed by two booster immunizations with MOG74-96 in IFA at psd 28 and 56. At psd 130 the monkeys received a booster with MOG34-56 in IFA (arrowhead) (experiment B). PBMC were collected at different time points and probed for their proliferative response against MOG74-96 and MOG34-56. Only responses above an SI of 2 (dotted line) are considered positive. A, Proliferation of PBMC of two representative monkeys of experiment A. Proliferative responses were mainly directed against MOG74-96, although after psd 100 also responses above an SI of 2.0 against MOG34-56 were detected. B, Proliferation of PBMC of the monkeys of experiment B. Proliferative responses were mainly directed against MOG74-96, although after the booster immunization with MOG34-56 in IFA proliferative responses against this peptide increased. C, Proliferation of MNC collected at necropsy. The monkey codes are given on the x-axis. The monkeys of experiment A show high responses to MOG74-96, whereas the monkeys of experiment B show increased responses to MOG34-56. D, Summary table of proliferative responses of ALN MNC from all 7 monkeys against rhMOG and the MOG peptide panel.

kill the peptide-pulsed B-cell lines that were used as APC. To test this hypothesis, the phenotype and cytolytic activity of MOG peptide-specific TCL were determined.

MOG34-56- and MOG74-96-specific TCL contained a CD3<sup>+</sup> cell population that consisted of a mixture of CD4<sup>+</sup>CD8<sup>-</sup>, CD4<sup>-</sup>CD8<sup>+</sup>, and CD4<sup>+</sup>CD8<sup>+</sup> cells (data not shown). A significant fraction of the TCL, ranging from 14.8 to 78.9%, expressed the NK-CTL marker CD56 (Figure 11C).

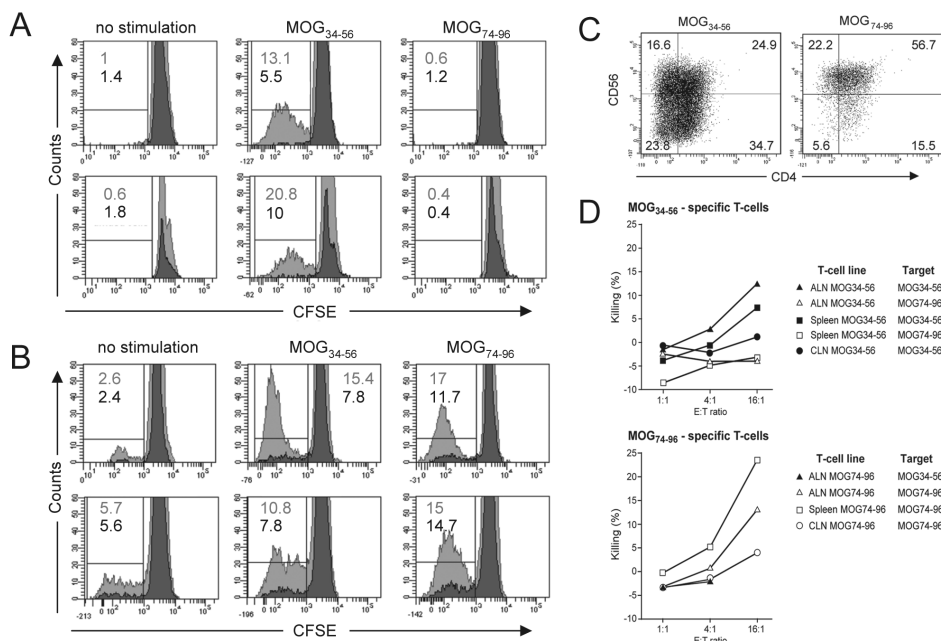


**Figure 11. MOG34-56- and MOG74-96-reactive T-cells show an NK-CTL like phenotype and activity.**

A-B, Freshly isolated MNC of ALN from EAE-affected marmosets were labeled with the fluorescent probe CFSE and subsequently cultured for 7 days with MOG34-56 or MOG74-96. Harvested cells were stained for CD3, CD4, and CD8 and analyzed by flow cytometry. The percentages of proliferated CD3<sup>+</sup>CD4<sup>+</sup> (light shading) and CD3<sup>+</sup>CD8<sup>+</sup> (dark shading) living cells under 3 stimulatory conditions are shown: without stimulant, with MOG34-56, or with MOG74-96. Data are shown for MOG34-56-immunized monkeys (M03017 and M03032) (A) and monkeys sensitized against MOG74-96 and finally boosted with MOG34-56 (M03018 and M03027) (B). C-D, Short-term T-cell lines (TCL) (effector cells) from 3 monkeys (M03017, M03018, and M03033) against MOG34-56 and MOG74-96 were established from MNC of spleen, ALN, and CLN. Shown are the data of M03018. C, Viable CD3<sup>+</sup> cells of MOG34-56- or MOG74-96-specific TCL derived from ALN of M03018 were stained for CD4 and CD56. D, The specific cytotoxicity was tested against <sup>51</sup>Cr labeled autologous EBV-transformed B-cell lines (target cells), which were untreated or pulsed with MOG34-56 or MOG74-96. Shown is the % killing by MOG34-56-specific TCL (top) and MOG74-96-specific TCL (bottom). TCL were cultured with MOG34-56-pulsed autologous B-cell lines (closed symbols) or MOG74-96-pulsed autologous B-cell lines (open symbols).

Cytolytic activity of the three stable lines was tested with peptide-pulsed EBV-transformed autologous and allogeneic B-cell lines as target cells. The results in figure 11D show the peptide-specific cytotoxicity of MOG34-56 or MOG74-96 induced TCL from M03018 against autologous B-cell lines. MOG34-56-specific TCL were cytotoxic for MOG34-56-pulsed B-cells and MOG74-96-specific TCL killed MOG74-96-pulsed B-cells. MOG34-56 and MOG74-96-specific TCL of M03018 could also kill, respectively, MOG34-56 and MOG74-96-pulsed B-cell lines of M03033 (data not shown). No cytotoxicity of the MOG34-56- and MOG74-96-specific TCL against nonpulsed B-cells was observed (data not shown).

To collect phenotypical data from more monkeys, TCL that were stored frozen after three rounds of peptide stimulation and expansion on IL-2 were thawed. Reactivation was performed by a single round of peptide-specific stimulation using EBV-transformed B-cells as APC, followed by 8 days expansion on IL-2. This yielded seven MOG34-56-specific TCL derived from five monkeys (M03017, M03018, M03026, M03027, and M03033) and two MOG74-96-specific TCL derived from two monkeys (M03017 and M03027). The CD3<sup>+</sup> population of MOG34-56-specific TCL consisted of 30.9% (range 11-58%) CD4<sup>+</sup> cells, 11.4% (range 3-19%) CD8<sup>+</sup> cells, and 54.2% (range 37-80%)

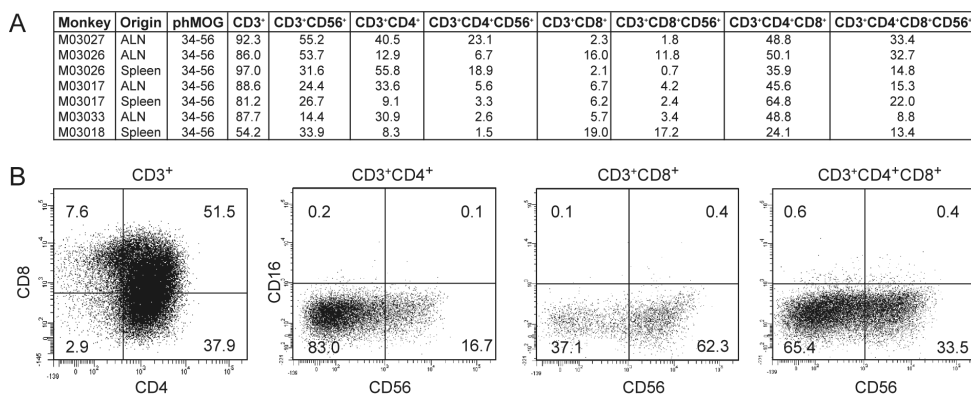


**Figure 12. Phenotype of MOG34-56-specific T-cell lines.**

Seven T-cell lines (TCL), which were frozen after three rounds of antigenic stimulation and expansion on IL-2, were thawed and restimulated with MOG34-56 presented by autologous EBV-transformed B-cells. After 8 days expansion on IL-2, the phenotype of these lines was determined by FACS analysis. Vital CD3<sup>+</sup> lymphocytes were analyzed for CD4 and CD8 expression. This resulted in CD4<sup>+</sup>, CD8<sup>+</sup> and CD4/CD8 double positive populations. CD16 and CD56 expression was determined in these populations. The percentages of T-cell subpopulations in all 7 lines is given in table A. The dot plots in B depict a representative example, being the MOG34-56-specific TCL derived from the ALN of M03017. Numbers in the quadrants represent percentages of the subpopulation described above each dot plot.

CD4<sup>+</sup>CD8<sup>+</sup> double positive cells. The high proportions of CD4/CD8 double positive cells is not an artifact of the freeze/thawing procedure, as this subpopulation is also found in peptide-stimulated cultures of freshly isolated lymph node and spleen cells. CD56 expression was most pronounced on single CD8<sup>+</sup> T cells (62%; range 33-91%), followed by 45% (range 18-69%) of the double positive cells and 32% (range 9-58%) of the single CD4<sup>+</sup> cells. In none of the subpopulations was CD16 expression observed (Figure 12). The CD3<sup>+</sup> population of two additional MOG74-96-specific TCL consisted of 10.6% (1.8/19.4) CD4<sup>+</sup> cells, 38.7% (63.4/13.9) CD8<sup>+</sup> cells, and 48.3% (32.3/64.2) double positive cells. All three subpopulations expressed significant CD56 levels, respectively 50.4% (79.5/21.2) of the CD4<sup>+</sup>, 82.1% (96.9/76.3) of the CD8<sup>+</sup>, and 72.1% (93.4/50.8) of the CD4<sup>+</sup>CD8<sup>+</sup> populations (data not shown).

## DISCUSSION

Several aspects of EAE in common marmosets make it a unique experimental model of MS, in particular the outbred nature, the genetic and immunological proximity to humans, and the remarkable neuropathological similarity with the disease in humans [for review<sup>6</sup>]. The disease typically follows a progressive course that can last from several weeks to more than a year<sup>20</sup>. Of the many components of CNS myelin with proven encephalitogenic capacity in mice, MOG appeared to be the most critical for the induction of chronic progressive disease in Biozzi ABH mice and marmosets<sup>13,30</sup>. This prompted us to investigate the MOG-induced autoimmune mechanisms that drive progression of the disease using a rhMOG-induced EAE model.

We have previously shown in a relatively small group of monkeys that the 100% EAE prevalence maps to the invariant MHC class II molecule *Caja-DRB\*W1201*, which is involved in the activation of MOG24-36 specific encephalitogenic T-cells<sup>15</sup>. Although the presence of *Caja-DRB\*W1201* in the MHC repertoire of each individual monkey at the genomic level was already known for several years<sup>16</sup>, it was only recently reported that mRNA transcripts of this allele are indeed expressed in APC of all tested monkeys<sup>17</sup>.

With regard to MOG-induced autoimmune mechanisms involved in the progression of rhMOG-induced EAE, we report here several novel findings that in part contrast with published data. The current results show that monkeys displaying a relatively broad reactivity of their lymph node T-cells with a MOG peptide panel developed neurological deficit significantly earlier than monkeys with a more restricted reactivity profile. By contrast, we observed no association between the reactivity profile of immune sera with the MOG peptide panel and the rate of EAE progression. Hence, we conclude that the different time spans between EAE induction and the expression of neurological signs is associated with a diversification of proliferative T-cell responses against MOG epitopes

beyond MOG24-36. Our interpretation of this finding is that fast progressor monkeys may be (genetically predisposed) high responders to peptides processed from rhMOG and presented to encephalitogenic T-cells present in the normal repertoire. We have chosen MOG34-56 and MOG74-96 for further examination since these peptides were detected in most fast progressor monkeys. Moreover, strong T-cell reactivity to these peptides is found in rhMOG-induced EAE models<sup>15,31</sup>.

Ten of 11 monkeys immunized with MOG34-56/CFA developed overt clinical EAE, although the susceptibility of individual monkeys varied, as reflected by the number of booster immunizations needed for EAE induction. In our previous study we reported that in monkeys immunized with peptide MOG14-36, only CD4<sup>+</sup> Th1-cells were induced together with mild inflammatory CNS pathology<sup>15</sup>. Our current data show that in MOG34-56-immunized monkeys, CD4<sup>+</sup> as well as CD8<sup>+</sup> T-cells are activated and that many inflammatory/demyelinating lesions are formed in the WM and, in some monkeys, also in the GM. Moreover, MOG34-56 induced TCL phenotypically resembled NK-CTL and displayed specific cytotoxic activity towards peptide-pulsed B-cell lines. The observation that essentially the complete clinical and pathological picture of rhMOG-induced EAE was reproduced in monkeys immunized with a single 23-mer peptide contrasts with data from Genain and colleagues showing that the development of full blown EAE depends on anti-MOG Ab recognizing discontinuous epitopes, and that full-blown EAE cannot be induced with MOG peptides<sup>32</sup>.

Monkeys sensitized against the peptide MOG74-96 did not show overt neurological signs, although we observed clinical EAE scores up to 1 as well as low-level CNS inflammation and demyelination by both MRI and histology. Furthermore, we detected low-level T-cell proliferation against MOG34-56. These data indicate that mild EAE may have been induced by *in vivo* activation of MOG34-56-reactive T-cells. This assumption is supported by the observation that a single booster immunization of the monkeys with MOG34-56 in IFA induced overt neurological signs within a few weeks in two out of three monkeys. This observation cannot be explained by cross-reactivity between the two peptides, as neither TCL nor immune sera from MOG34-56-immunized monkeys cross-reacted with MOG74-96 and vice versa. Hence, we conclude that in the MOG74-96-immunized monkeys MOG34-56-reactive T-cells had been recruited from the resting state, indicating that limited epitope spreading had taken place.

We like to propose as the underlying mechanism that MOG34-56-reactive (memory) T-cells present in the naive repertoire are activated by APC carrying myelin Ag from the lesions to draining lymph nodes. This concept is supported by previously reported findings. First, the ubiquitous autoreactivity against MOG14-36 induces CNS infiltration of T-cells and macrophages, which may trigger initial CNS WM damage<sup>15,18</sup>. Second, myelin-loaded APC can be found localized in the CLN and spleen of EAE-affected monkeys<sup>33</sup>. We have not (yet) been able to directly demonstrate induction of autoreactive

T-cells by myelin-loaded APC present within the CLN. However, the localization in T-cell areas of the lymph nodes creates the conditions needed for such a functional interaction. Third, data from the rhesus monkey EAE model show that MOG34-56-reactive T-cells present in the naive repertoire can be activated by immunization with a 23-mer peptide derived from the major capsid protein (UL86) of human cytomegalovirus (CMV; CMV UL86981-1003)<sup>26</sup>. The CMV of common marmosets has not been isolated and characterized yet. However, assuming that CMV-induced memory T-cells do occur in the natural repertoire of common marmosets, as is the case in humans as well as rhesus monkeys, it is tempting to speculate that T-cells present in lymph nodes and spleen may be activated by myelin-loaded APC draining from the EAE-affected CNS<sup>33</sup>.

The mechanisms underlying the dramatic CNS pathology upon immunization with MOG34-56 remain to be fully elucidated. Our data demonstrate that the induction of NK-T-cell like cytotoxic activity represents at least one of the pathogenic mechanisms. The cytotoxicity assay shown in figure 11 was performed with a mixture of CD56<sup>+</sup> cells, namely CD4<sup>+</sup>, CD8<sup>+</sup>, and CD4<sup>+</sup>CD8<sup>+</sup>. The phenotype of the cells (CD3<sup>+</sup>CD4<sup>+</sup> and/or CD8<sup>+</sup>CD56<sup>+</sup>CD16<sup>-</sup>) as well as the capacity to lyse peptide-pulsed, autologous and allogeneic, B-cell lines are suggestive of an NK-T-cell like activity. Interestingly, a similar activity has been observed for anti-MOG T-cell-lines from MS patients<sup>29</sup>. The possible involvement of such cells in the pathogenesis of MS has been reported by several groups<sup>34,35</sup>. We are currently exploring further the different cell subsets involved and the cytotoxic effector mechanisms, both *ex vivo* and *in situ*.

In conclusion, we report an association between disease progression in the rhMOG- induced EAE model in marmosets with the diversification of the anti-MOG T-cell response. In addition to a T-cell response against MOG24-36, which is present in all monkeys and is the presumed trigger of the disease, T-cell responses against MOG34-56 and MOG74-96 are detectable in monkeys with a rapid disease progression. MOG34-56 displays potent encephalitogenic activity leading to inflammation and tissue destruction in the CNS, most likely via the activation of cytotoxic T-cells with a NK-CTL-like phenotype. In our view the marmoset EAE model offers a unique experimental setting to further unravel the pathogenic mechanisms and to develop novel therapeutic approaches targeting these mechanisms, including the cytotoxic activity.

## ACKNOWLEDGEMENTS

We thank Fred Batenburg for excellent biotechnical assistance and daily care of the monkeys; Jaco Bakker, Leo van Geest, and Gerco Braskamp for expert veterinary care; Tom Haaksma and Dr. Ivanela Kondova for autopsy of the monkeys; Boudewijn Ouwerling for laboratory work; and Henk van Westbroek for the artwork.

## REFERENCES

1. Noseworthy JH et al. Multiple sclerosis. *N Engl J Med* 343:938-952 (2000)
2. Compston A et al. Multiple sclerosis. *Lancet* 359:1221-1231 (2002)
3. Sospedra M et al. Immunology of multiple sclerosis. *Annu Rev Immunol* 23:683-747 (2005)
4. Sospedra M et al. Molecular mimicry in multiple sclerosis. *Autoimmunity* 39:3-8 (2006)
5. 't Hart BA et al. A new primate model for multiple sclerosis in the common marmoset. *Immunol Today* 21:290-297 (2000)
6. 't Hart BA et al. Modelling of multiple sclerosis: lessons learned in a non-human primate. *Lancet Neurol* 3:588-597 (2004)
7. Pomeroy IM et al. Demyelinated neocortical lesions in marmoset autoimmune encephalomyelitis mimic those in multiple sclerosis. *Brain* 128:2713-2721 (2005)
8. Merkler D et al. Differential macrophage/microglia activation in neocortical EAE Lesions in the marmoset monkey. *Brain Pathol* 16:117-123 (2006)
9. 't Hart BA et al. Broad spectrum immune monitoring in immune-mediated inflammatory disorders. *Drug Discov Today* 10:1348-1351 (2005)
10. 't Hart BA et al. MRI-guided immunotherapy development for multiple sclerosis in a primate. *Drug Discov Today* 11:58-66 (2006)
11. Blezer EL et al. Quantitative MRI-pathology correlations of brain white matter lesions developing in a non-human primate model of multiple sclerosis. *NMR Biomed* 20:90-103 (2007)
12. McFarland HI et al. Determinant spreading associated with demyelination in a nonhuman primate model of multiple sclerosis. *J Immunol* 162:2384-2390 (1999)
13. Smith PA et al. Native myelin oligodendrocyte glycoprotein promotes severe chronic neurological disease and demyelination in Biozzi ABH mice. *Eur J Immunol* 35:1311-1319 (2005)
14. Jagessar SA et al. Autoimmunity against myelin oligodendrocyte glycoprotein is dispensable for the initiation although essential for the progression of chronic encephalomyelitis in common marmosets. *J Neuropathol Exp Neurol* 67:326-340 (2008)
15. Brok HP et al. Myelin/oligodendrocyte glycoprotein-induced autoimmune encephalomyelitis in common marmosets: the encephalitogenic T cell epitope pMOG24-36 is presented by a monomorphic MHC class II molecule. *J Immunol* 165:1093-1101 (2000)
16. Antunes SG et al. The common marmoset: a new world primate species with limited Mhc class II variability. *Proc Natl Acad Sci USA* 95:11745-11750 (1998)
17. Doxiadis GG et al. Reactivation by exon shuffling of a conserved HLA-DR3-like pseudogene segment in a New World primate species. *Proc Natl Acad Sci USA* 103:5864-5868 (2006)
18. Villoslada P et al. Frequency, heterogeneity and encephalitogenicity of T cells specific for myelin oligodendrocyte glycoprotein in naive outbred primates. *Eur J Immunol* 31:2942-2950 (2001)
19. Kerlero de Rosbo N et al. Predominance of the autoimmune response to myelin oligodendrocyte glycoprotein (MOG) in multiple sclerosis: reactivity to the extracellular domain of MOG is directed against three main regions. *Eur J Immunol* 27:3059-3069 (1997)
20. 't Hart BA et al. Histopathological characterization of magnetic resonance imaging-detectable brain white matter lesions in a primate model of multiple sclerosis: a correlative study in the experimental autoimmune encephalomyelitis model in common marmosets (*Callithrix jacchus*). *Am J Pathol* 153:649-663 (1998)
21. Brok HP et al. An extensive monoclonal antibody panel for the phenotyping of leukocyte subsets in the common marmoset and the cotton-top tamarin. *Cytometry* 45:294-303 (2001)
22. Boon L et al. Prevention of experimental autoimmune encephalomyelitis in the common marmoset (*Callithrix jacchus*) using a chimeric antagonist monoclonal antibody against human CD40 is associated with altered B cell responses. *J Immunol* 167:2942-2949 (2001)
23. Brehm U et al. Epitope specificity of demyelinating monoclonal autoantibodies directed against the human myelin oligodendrocyte glycoprotein (MOG). *J Neuroimmunol* 97:9-15 (1999)

## Chapter 3.1

24. Laman JD et al. Protection of marmoset monkeys against EAE by treatment with a murine antibody blocking CD40 (mu5D12). *Eur J Immunol* 32:2218-2228 (2002)
25. Laman JD et al. Expression of accessory molecules and cytokines in acute EAE in marmoset monkeys (*Callithrix jacchus*). *J Neuroimmunol* 86:30-45 (1998)
26. Brok HP et al. The human CMV-UL86 peptide 981-1003 shares a crossreactive T-cell epitope with the encephalitogenic MOG peptide 34-56, but lacks the capacity to induce EAE in rhesus monkeys. *J Neuroimmunol* 182:135-152 (2007)
27. 't Hart BA et al. Suppression of ongoing disease in a nonhuman primate model of multiple sclerosis by a human-anti-human IL-12p40 antibody. *J Immunol* 175:4761-4768 (2005)
28. Haig D. What is a marmoset? *Am J Primatol* 49:285-296 (1999)
29. Van der Aa A et al. Functional properties of myelin oligodendrocyte glycoprotein-reactive T cells in multiple sclerosis patients and controls. *J Neuroimmunol* 137:164-176 (2003)
30. Heijmans N et al. Antibodies to native myelin oligodendrocyte glycoprotein are critical for severe chronic experimental autoimmune encephalomyelitis and demyelination in mice and marmosets. *J Neuroimmunol* 178:52 (Abstract) (2006)
31. Kerlero de Rosbo N et al. Rhesus monkeys are highly susceptible to experimental autoimmune encephalomyelitis induced by myelin oligodendrocyte glycoprotein: characterisation of immunodominant T- and B-cell epitopes. *J Neuroimmunol* 110:83-96 (2000)
32. von Büdingen HC et al. Frontline: Epitope recognition on the myelin/oligodendrocyte glycoprotein differentially influences disease phenotype and antibody effector functions in autoimmune demyelination. *Eur J Immunol* 34:2072-2083 (2004)
33. de Vos AF et al. Transfer of central nervous system autoantigens and presentation in secondary lymphoid organs. *J Immunol* 169:5415-5423 (2002)
34. Vergelli M et al. A novel population of CD4+CD56+ myelin-reactive T cells lyses target cells expressing CD56/neural cell adhesion molecule. *J Immunol* 157:679-688 (1996)
35. Antel JP et al. Non-MHC-restricted cell-mediated lysis of human oligodendrocytes in vitro: relation with CD56 expression. *J Immunol* 160:1606-1611 (1998)

## 3.2

### **Induction of progressive demyelinating autoimmune encephalomyelitis in common marmoset monkeys using MOG34-56 peptide in incomplete Freund adjuvant**

S. Anwar Jagessar<sup>1,2</sup>, Yolanda S. Kap<sup>1,2,3</sup>, Nicole Heijmans<sup>1</sup>, Nikki van Driel<sup>1</sup>, Linda van Straalen<sup>4</sup>, Jeffrey J. Bajramovic<sup>4</sup>, Herbert P.M. Brok<sup>5</sup>, Erwin L.A. Blezer<sup>6</sup>, Jan Bauer<sup>7</sup>, Jon D. Laman<sup>2,3</sup>, and Bert A. 't Hart<sup>1,2,3</sup>

<sup>1</sup>Department of Immunobiology, Biomedical Primate Research Centre, Rijswijk, The Netherlands; <sup>2</sup>MS Centre ErasMS, Rotterdam, The Netherlands; <sup>3</sup>Department of Immunology, Erasmus Medical Centre, Rotterdam, The Netherlands; <sup>4</sup>Alternatives Unit, Biomedical Primate Research Centre, Rijswijk, The Netherlands; <sup>5</sup>Animal Science Department, Biomedical Primate Research Centre, Rijswijk, The Netherlands; <sup>6</sup>Image Sciences Institute, University Medical Centre Utrecht, The Netherlands; <sup>7</sup>Brain Research Institute, Medical University, Vienna, Austria

SAJ and YSK contributed equally to this work

*J Neuropathol Exp Neurol* 2010, 69: 372-385



## ABSTRACT

Experimental autoimmune encephalomyelitis (EAE) in the Neotropical primate common marmoset (*Callithrix jacchus*) is a relevant autoimmune animal model of multiple sclerosis. T-cells specific for peptide 34 to 56 of myelin oligodendrocyte glycoprotein (MOG34-56) have a central pathogenic role in this model. The aim of this study was to assess the requirement for innate immune stimulation for activation of this core pathogenic autoimmune mechanism. Marmoset monkeys were sensitized against synthetic MOG34-56 peptide alone or in combination with the nonencephalitogenic peptide MOG74-96 formulated in incomplete Freund's adjuvant (IFA), which lacks microbial compounds. EAE development was recorded by monitoring neurological signs, brain magnetic resonance imaging, and longitudinal profiling of cellular and humoral immune parameters. All monkeys developed autoimmune inflammatory/demyelinating central nervous system disease characterized by massive brain and spinal cord demyelinating white matter lesions with activated macrophages and CD3<sup>+</sup> T-cells. Immune profiling *ex vivo* demonstrated the activation of mainly CD3<sup>+</sup>CD4<sup>+</sup>8<sup>+</sup>CD56<sup>+</sup> T-cells against MOG34-56. Upon *ex vivo* stimulation, these T-cells produced more interleukin 17A compared with Th1 cytokines (e.g. interferon- $\gamma$ ) and displayed peptide-specific cytolytic activity. These results indicate that the full spectrum of marmoset EAE can be induced by sensitization against a single MOG peptide in IFA lacking microbial compounds for innate immune activation and by eliciting antigen-specific T-cell cytolytic activity.

## INTRODUCTION

Multiple sclerosis (MS) is a chronic neurological disease affecting the central nervous system (CNS) of 1 per 1,000 young adults in the moderate climate areas of the United States and Europe<sup>1</sup>. During the past decades, understanding of the immunopathogenic mechanisms that drive the disease has advanced considerably, resulting in the development of several effective disease-modifying agents<sup>2</sup>. However, the few successes are in contrast to a long list of treatments that failed to reproduce the beneficial effects in animal models of MS when tested in MS patients. The poor translation of scientific data to the clinic is in part attributed to the wide gaps between human patients and animal models<sup>3,4</sup>.

Limitations of the current MS models in inbred and specific pathogen free laboratory rodent strains include the lack of genetic diversity and exposure to environmental pathogens, both of which have a strong influence on the developing immune system<sup>5</sup>. Moreover, persistent latent infections with herpesviruses that have a strong impact on the

aging of the human immune system do not occur in rodents<sup>6</sup>. Finally, rodents are most often used at young adult ages (8-12 weeks). Non-human primates do not have these limitations because they are long-lived and are housed under conventional conditions in social groups where a high genetic and microbiological diversity is maintained.

The common marmoset (*Callithrix jacchus*) is a small Neotropical primate that provides a valid preclinical MS model. The model reproduces the progressive clinical course and approximates the neuropathological complexity of human MS<sup>7,8</sup>. The parallel clinicopathological features of this model and the close genetic, immunological, and microbiological similarities of humans and marmosets create an attractive experimental system for the dissection of critical pathogenic mechanisms that are promising candidate targets for MS therapy<sup>9</sup>.

We previously demonstrated that autoimmunity against the extracellular domain of myelin oligodendrocyte glycoprotein (MOG), a quantitatively minor component of CNS myelin, is critical for the activation of the pathogenic mechanisms that drive experimental autoimmune encephalomyelitis (EAE) progression in Biozzi ABH mice<sup>10</sup> and marmosets<sup>11</sup>. The immunopathogenic mechanisms elicited by human MOG were unraveled in marmosets immunized with recombinant human MOG (rhMOG), a recombinant protein representing the extracellular domain (residues 1-125) of human MOG<sup>12</sup>. Whereas the 100% incidence of EAE induction could be mapped to the activation of T helper 1 cells specific for the peptide MOG24-36<sup>13</sup>, T-cells directed against epitopes encompassed within peptide MOG34-56 were found to play a critical role in the progression of rhMOG-induced EAE<sup>12</sup>.

Having identified the activation of MOG34-56 T-cells as a core pathogenic autoimmune mechanism in the marmoset EAE model, we set out to investigate the minimum activation requirements. We report that marmosets sensitized against MOG34-56 peptide in incomplete Freund's adjuvant (IFA), a formulation that lacks microbial antigens (Ag) for innate immune activation, all developed severe clinical EAE, which is characterized by marked inflammation and primary demyelination in the CNS. Immune profiling supports a key pathogenic role for CD3<sup>+</sup>CD4<sup>+</sup>/8<sup>+</sup>CD56<sup>+</sup> T-cells, with pro-inflammatory and cytolytic capacities. Although antibodies (Ab) against the immunizing peptides were formed, these failed to bind intact rhMOG, arguing against a direct pathogenic role. Our present results challenge the concept that innate immune mechanisms triggered by microbial compounds in the Ag inoculum are a necessary prerequisite to break T-cell tolerance leading to EAE. The possibility of inducing EAE without the need for complete Freund's adjuvant (CFA), which induces necrotizing skin lesions that cause serious discomfort to the animals, also implies a major refinement of the model.

## MATERIALS AND METHODS

### Animals

The monkeys included in this study originated from purpose-bred colonies of the Biomedical Primate Research Centre (BPRC), Rijswijk, The Netherlands, and the German Primate Centre (DPZ), Göttingen, Germany. Monkeys purchased from DPZ had been housed for at least 6 months in the BPRC before use. Individual data for all monkeys are listed in Table 1. Before inclusion in the study, the monkeys received complete physical, haematological, and biochemical examination, and during the study, they remained under veterinary care. Monkeys were housed in pairs in spacious cages enriched with branches and toys and with padded shelter provided on the floor. The daily diet consisted of commercial food pellets for New World monkeys (Special Diet Services, Witham, Essex, UK), supplemented with rice, raisins, peanuts, marshmallows, biscuits, fresh fruit, grasshoppers, and maggots. Drinking water was provided ad libitum.

**Table 1. Overview of marmosets used in this study and their response to EAE.**

Experiment	Monkey	Sex <sup>a</sup>	Age <sup>b</sup>	Immunization MOG peptide	Clinical EAE signs	Lesions on MRI
1	M03138	F	36	34-56 + 74-96	Yes	Yes
	M03139	F	36	34-56 + 74-96	Yes	Yes
	M04033	F	31	34-56 + 74-96	Yes	Yes
	M04034	F	31	34-56 + 74-96	Yes	Yes
2A	M03162	M	47	34-56 + 74-96	Yes	Yes
	M05056	M	27	34-56 + 74-96	Yes	Yes
	M05082	M	25	34-56 + 74-96	Yes	Yes
	M06012	M	20	34-56 + 74-96	Yes	Yes
	M06017	M	21	34-56 + 74-96	Yes	Yes
2B	9847	M	105	34-56	Yes	Yes
	M05047	M	30	34-56	Yes	Yes
	M06006	M	29	34-56	Yes	Yes
	M06018	M	21	34-56	Yes	Yes
	M06020	M	21	34-56	Yes	Yes

<sup>a</sup> F, female; M, male

<sup>b</sup> Age in months at the start of the experiment

EAE, experimental autoimmune encephalomyelitis; MOG, myelin oligodendrocyte glycoprotein; MRI, magnetic resonance imaging

### **Ethics**

In accordance with the Dutch law on animal experimentation, all study protocols and experimental procedures were reviewed and approved by the Institute's Ethics Committee before the start of experiments.

### **Antigens**

The human MOG extracellular domain (rhMOG) was expressed as an unglycosylated recombinant protein in *Escherichia coli* and purified, as previously described<sup>14</sup>. Synthetic MOG peptides based on the human MOG sequence used for immunization and cell culture were purchased from ABC Biotechnology (London, UK) and Cambridge Research Biochemicals (Cleveland, UK).

### **Induction of EAE**

EAE was induced with 100 µg MOG34-56 or with the mixture of 100 µg MOG34-56 and 100 µg MOG74-96. For each immunization, the monkeys were injected into the dorsal skin with the MOG peptide dissolved in 300 µl PBS (Invitrogen, Gibco BRL, Glasgow, UK) and emulsified with 300 µl IFA (Difco Laboratories, Detroit, MI). The inoculum was injected into the inguinal and axillary regions of the dorsal skin divided over 4 spots of 150 µl each. Ag-adjuvant emulsions were prepared by gentle stirring the peptide/oil mixture at 4°C for at least 1 h. Monkeys that failed to develop serious neurological deficits (score ≥ 2.0; see next paragraph) within 28 days received re-challenges at 4-weeks interval with the same dose of peptide(s) in IFA until EAE developed.

### **Clinical scoring**

Clinical signs were scored daily by two trained independent observers, as described<sup>7</sup>. Briefly: 0 = no clinical signs; 0.5 = apathy, loss of appetite, altered walking pattern without ataxia; 1 = lethargy, anorexia, loss of tail tonus, tremor; 2 = ataxia, optic disease; 2.5 = para- or monoparesis, sensory loss, brain stem syndrome; 3 = para- or hemiplegia; 4 = quadriplegia; 5 = spontaneous death attributable to EAE. Monkeys were sacrificed for ethical reasons once complete paralysis of one or both hindlimbs (score ≥ 3.0) was observed or at a predetermined endpoint.

To obtain an objective surrogate disease marker, the monkeys were weighed three times per week. This was performed without sedation using the Perspex cylinder with which adequately trained monkeys were captured from the home cage.

### **Post mortem examination**

At the time of necropsy, the monkeys were first deeply sedated with ketamine (50 mg/ml PBS) (Produlab Pharma, Raamsdonkveer, The Netherlands) injected intramuscularly at a dose of 100 µl/kg body weight; they were subsequently euthanised

by infusion of pentobarbital sodium (Euthesate; Apharmo, Duiven, The Netherlands). Brain, spinal cord, spleen, cervical lymph nodes (CLN), inguinal lymph nodes (ILN), and axillary lymph nodes (ALN) were aseptically removed. Small parts of all organs were snap-frozen in liquid nitrogen and stored at -80°C for immunohistochemistry. One brain hemisphere was fixed for at least 7 days in 4% buffered formalin and subsequently transferred into buffered saline with sodium azide (Sigma-Aldrich, Gillingham, UK) to allow stabilization before magnetic resonance imaging (MRI). To assess the total brain lesion load, MR images were made of formalin-fixed brains as described<sup>15</sup>. After MRI, the tissues were examined with histological and immunohistochemical techniques as described<sup>7,12</sup>.

### **Magnetic resonance imaging**

MR brain images were acquired from live animals and post mortem formalin-fixed brains. *In vivo* MRI experiments were performed on the two animals that had no clear overt clinical scores and were still alive at the end of the protocol (i.e. M06006 and M06012). Experiments were performed on a 4.7-T horizontal bore MRI scanner (Varian, Palo Alto, CA). T2-weighted (T2W) images (field of view, 40 x 40 mm; matrix, 128x 128; zero-filled, 256 x 256; slice thickness, 1 mm; number of experiments, 2) were collected using a spin-echo sequence with a repetition time of 2.75 s and an echo time of 30 ms. Post mortem images were obtained on a 9.4-T MRI scanner (Varian). Formalin-fixed brains were submerged in a perfluoropolyether (Fomblin, Fluortek AB, Knivsta, Sweden) for susceptibility matching. T2W images (field of view, 25 x 25 mm; matrix, 256 x 256; zero-filled, 512 x 512; slice thickness, 0.75 mm; number of experiments, 2) were collected using a spin-echo sequence with a repetition time of 2.6 s and an echo time of 20 ms.

### **Assays for innate immune stimulatory activity**

The immunizing peptides MOG34-56 and MOG74-96 and IFA were screened for contamination with ligands of Toll-like receptors (TLR) using human endothelial kidney (HEK293) cells transfected with human TLR2, TLR3, TLR4, or TLR5 and HEK293XL cells transfected with TLR7, TLR8, TLR9, or TLR10 (all from InvivoGen, San Diego, CA). The cell lines were cotransfected using Polyfect (Qiagen Benelux, Venlo, The Netherlands) with a reporter vector expressing luciferase under the control of an NF-κB-responsive promoter (pNifty2-luc; InvivoGen). Stably transfected clones were selected and used in bioassays. Cells were plated in flat-bottom 96-wells plates (Greiner Bio-one, Frickenhausen, Germany) at a density of  $1 \times 10^5$  cells/well and were stimulated with individual MOG peptides, IFA, or a mix of MOG peptide and IFA. After 16 h incubation at 37°C, the cells were lysed in 50 µl Steady Glo luciferase buffer (Promega Benelux, Leiden, The Netherlands) for 10 min, and bioluminescence was measured

using a Packard 9600 Topcount Microplate Scintillation & Luminescence Counter (Packard Instrument Company, Meriden, CT). As a positive control for NF- $\kappa$ B-mediated activation (i.e. the presence of the pNifty2-luc vector), 25 ng/ml tumor necrosis factor (TNF)- $\alpha$  (Peprotech, London, UK) was used. Positive controls for TLR2 and TLR4 activation were lipopolysaccharide (100 ng/ml); TLR3, polyriboinosinic polyribocytidylic acid (Poly(I:C)) (20  $\mu$ g/ml); TLR5, flagellin (1  $\mu$ g/ml); TLR7, an adenine derivate (CL-087) (1  $\mu$ g/ml); TLR8, a thiozoloquinolone derivate (CL-075) (1  $\mu$ g/ml); TLR9, synthetic oligonucleotides that contain unmethylated CpG (ODN2006) (2  $\mu$ mol/ml). No ligands are known for TLR10, but TLR10 expression in the transfected HEK293 cell lines was confirmed with Western blot (data not shown). The TLR-specific ligands were obtained from InvivoGen.

For cytokine production assays, CD14<sup>+</sup> cells isolated from buffy coats of healthy human donors with MACS beads (Miltenyi Biotech, Auburn, CA) were cultured for 7 days with 20 ng/ml macrophage colony-stimulating factor (PeproTech) to differentiate them into macrophages. Culture supernatants of macrophages and peripheral blood mononuclear cells (PBMC) also isolated from buffy coats were collected after 24 h stimulation with both immunizing MOG peptides and IFA to measure cytokine production.

### **Mononuclear cell and T-cell line preparation**

The maximum monthly blood volume that can be collected from marmosets is 1% of the body weight, which is 3.5 ml for an average adult monkey of 350 g. Longitudinal immune monitoring was performed using 1 ml of venous blood collected at 2-weeks interval from the femoral vein into heparinized vacutainers (Greiner, Sölingen, Germany). At necropsy mononuclear cell (MNC) suspensions were also prepared from aseptically removed ALN, ILN, and spleen. MNC and PBMC were isolated using lymphocyte separation medium (LSM, ICN Biomedical Inc, Aurora, OH).

T-cell lines (TCL) were generated from MNC isolated from spleen and ALN by alternate stimulation with MOG34-56 or MOG74-96 and recombinant human IL-2 (Proleukin, Emeryville, CA), as described previously<sup>13</sup>. Lethally irradiated (70 Gy) Epstein-Barr virus (EBV)-transformed autologous marmoset B-lymphoblastoid cells (B-LCL)<sup>16</sup> from stably growing lines maintained in 75-cm<sup>2</sup> tissue culture flasks (Greiner Bio-one, Frickenhausen, Germany) were used as antigen presenting cells (APC). TCL displaying Ag specificity were characterized with cross-reactive monoclonal Ab raised against human CD markers<sup>17</sup>.

### **Ex vivo analysis of T-cell responses**

The PBMC and MNC suspensions were assayed in triplicate for proliferation against rhMOG (10  $\mu$ g/ml) and a panel of MOG peptides (each 10  $\mu$ g/ml)<sup>12,13</sup>. Proliferation was

assessed by the incorporation of [<sup>3</sup>H]-thymidine (0.5 µCi/well) (PerkinElmer, Boston, MA) during the final 18 h of a 64 h culture using a matrix 9600 β-counter (Packard Instrument Company). Results are expressed as stimulation index (SI), that is, the ratio of radiolabel incorporation in stimulated versus unstimulated cultures. SI values greater than 2.0 were considered positive.

Flow cytometry and carboxyfluorescein succinimidyl ester (CFSE) assay phenotyping of proliferating cells were performed as described<sup>12</sup>. In brief, PBMC and MNC from ALN and spleen were suspended in 1 ml PBS and incubated for 7 min at room temperature with the fluorescent vital dye CFSE (final concentration 1.5 µM; Fluka, Deisenhofen, Germany), followed by culturing for 7 days at 37°C with or without Ag. Harvested cells were stained with labeled monoclonal Ab raised against the following human CD markers<sup>17</sup>: anti-CD3 (BD Biosciences, San Diego, CA), anti-CD4 (DAKO, Glostrup, Denmark), anti-CD8-biotin (Serotec, Düsseldorf, Germany), anti-CD56, anti-CD16, and streptavidin PE-Cy7 or streptavidin PerCP (BD Biosciences). Viable cells were gated using violet viability stain (Invitrogen, Molecular Probes, Carlsbad, CA). Within each gated subpopulation the percentage of cells with CFSE dilution was calculated. Flow cytometric analysis was performed on a FACS LSRII flow cytometer using FACSDiva software 5.0 (BD Biosciences).

For cytokine analyses, supernatants of PBMC, ALN, and spleen cells were collected after a 48 h stimulation with rhMOG or a panel of overlapping MOG peptides. Supernatants were assayed according to manufacturers' instructions with commercial ELISA kits for monkey TNF-α, monkey interferon-γ (IFN-γ) (U-Cytech, Utrecht, The Netherlands) and human cross-reactive IL-17A (eBioscience, San Diego, CA). Culture supernatants of human macrophages and PBMC stimulated with MOG34-56 and MOG74-96 peptides and IFA were assayed with human IL-6, IL-12p40+p70, TNF-α, and IL-1β (U-Cytech, Utrecht, The Netherlands) ELISA kit.

For cytotoxicity assays, autologous B-LCL labelled with <sup>51</sup>Chromium (PerkinElmer) were pulsed with peptides of interest and used as target cells to test cytolytic activity of MOG peptide-specific TCL, as described previously<sup>12</sup>. Controls consisted of peptide-pulsed <sup>51</sup>Chromium-labeled target cells without T-cells (i.e. spontaneous release) or peptide-pulsed <sup>51</sup>Chromium-labeled target cells lysed with 1% Triton X-100 (Sigma-Aldrich, Steinheim, Germany) (maximum release). To test whether the cytolytic activity was perforin mediated, T-cells were pre-incubated with 28 nmol/l concanamycin A (Sigma-Aldrich) for 2 h at 37°C. After extensive washing, the cells were mixed with peptide-pulsed <sup>51</sup>Chromium-labeled target cells. Results are expressed as percentage killing: (T-cell induced release – spontaneous release)/(maximal release – spontaneous release) x 100%.

### **Autoantibody detection**

Venous blood samples were centrifuged and plasma supernatants were collected and stored at -20°C until further analysis. Ab binding to rhMOG (or to a panel of overlapping 23-mer pMOG (residues 1-125) sequences was determined using ELISA, as described<sup>18</sup>. Bound IgG Ab was detected using polyclonal alkaline phosphatase-conjugated rabbit-anti-human IgG (Abcam, Cambridge, UK). The results of the Ab assays are expressed as fold increase of light absorbance at 405 nm compared with the reactivity present in preimmune sera of the same monkeys.

### **Statistical analysis**

A high variation in the disease course and associated immune parameters between individual animals is inherent to the outbred nature of this model. Statistical evaluation of data was performed using unpaired t-test when this was possible and relevant; values of  $p < 0.05$  were considered significant. For the immune assays, values above the mean background  $\pm 2$  SD for T-cell proliferation ( $SI \geq 2$ ) and Ab production (fold increase  $\geq 2.0$ ) were considered positive.

## **RESULTS**

### **Lack of innate immune activation by peptide/IFA constituents**

The TLR and Nodlike receptor families of pathogen recognition receptors comprise important mediators for the activation of innate immune mechanisms, which have been considered essential for EAE induction in most rodent models and are engaged by microbial compounds in CFA<sup>19,20</sup>. To determine the presence of possible innate immune stimulatory activity, the synthetic MOG peptides and IFA used for immunization were probed for stimulation of human macrophages and PBMC and TLR-transfected HEK293 cells.

Macrophages and PBMC were incubated with IFA, MOG34-56, and MOG74-96 in PBS, or MOG34-56/IFA emulsion. Culture supernatants were assayed for IL-6, IL-12p40+p70, and TNF- $\alpha$ . No significant levels of these cytokines were detected (Figure 1A). No IL-1 $\beta$  was detected in the supernatants, indicating that this signature cytokine of the inflammasome pathway was also not activated under the conditions tested. The IFA and MOG peptides were also tested for the activation of the NF- $\kappa$ B-driven luciferase reporter gene in HEK293 cells transfected with human TLR2, TLR3, TLR4, TLR5, TLR7, TLR8, TLR9, or TLR10; no cell stimulation was detected in any of these assays (Figure 1B).

Because tissue injury from skin injection of peptide/IFA emulsion may elicit danger signals that can activate APC and because skin flora microbes might infect the inoculum

site despite appropriate cleaning, we also compared CFA and IFA immunization for EAE in EAE-susceptible Biozzi ABH and C57BL/6 mice. The mice were first immunized with human MOG34-56 in CFA or in IFA with additional intraperitoneal pertussis toxin.

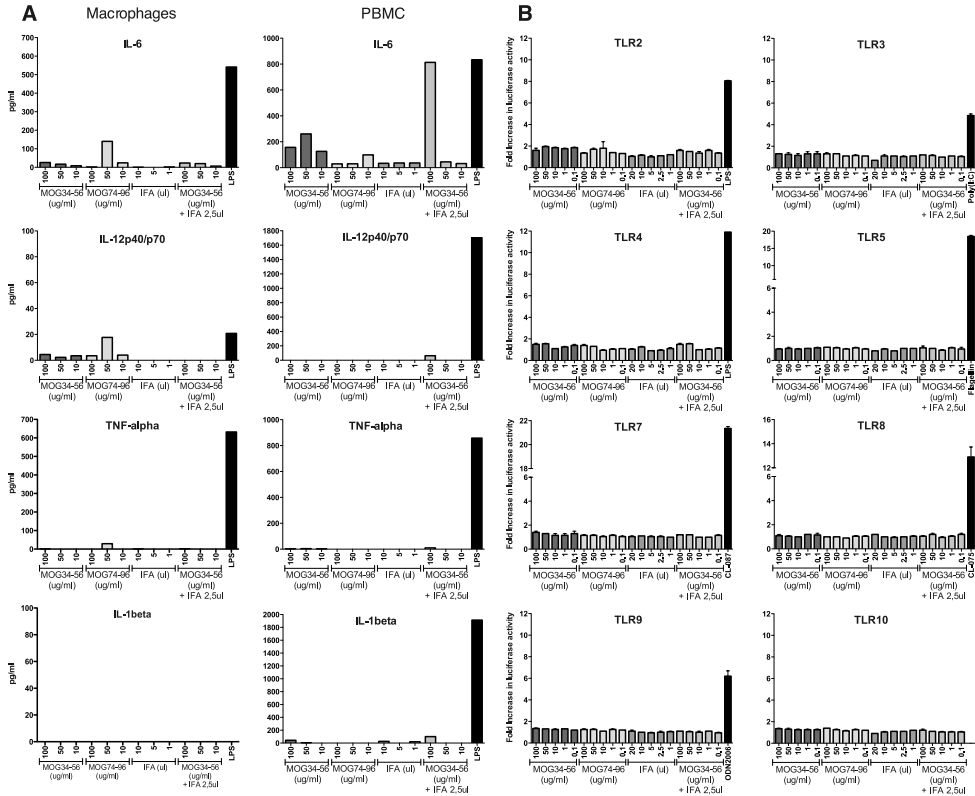


**Figure 1. MOG34-56 and MOG74-96 are not contaminated with known pattern recognition receptor ligands.**

A, Human CD14<sup>+</sup> cells were isolated and differentiated to macrophages. The macrophages (left panel) and human peripheral blood mononuclear cells (PBMC) (right panel) were incubated with MOG34-56, MOG74-96, incomplete Freund's adjuvant (IFA), or lipopolysaccharide (LPS) (500 ng/ml). The supernatants were tested for the presence of IL-6, IL-12p40/p70, TNF- $\alpha$  and IL-1 $\beta$  by ELISA. Data are shown from 1 of 2 experiments performed. B, Toll like receptor (TLR) activity of the MOG peptides was assessed in human endothelial kidney 293 (HEK293) cell lines stably transfected with human TLR2, TLR3, TLR4, TLR5, TLR7, TLR8, TLR9, and TLR10 and the NF- $\kappa$ B luciferase reporter gene. The TLR expressing cell lines were incubated with the MOG peptides, IFA, or MOG plus IFA. Responses are expressed as fold increase of luciferase activity (mean  $\pm$  SD). Peptide-stimulated HEK293 cells are compared with unstimulated cells. Fold increases greater than 2 were considered positive. In both assays, the peptides and IFA did not reveal significant stimulatory activity. Data from 2 of 6 experiments are pooled.

Booster immunizations were with MOG34-56 in IFA plus intraperitoneal pertussis toxin. Only sensitization against MOG34-56 was observed in CFA-induced (mild) EAE, whereas this was not observed in MOG34-56/IFA-immunized mice (data not shown).

Together, these data confirm that the peptides used for EAE induction are not contaminated with ligands for innate antigen receptors

### **Clinical disease**

The intracutaneous injection of the peptide/IFA emulsion elicited only moderate redness at the injection sites attributable to a moderate inflammatory reaction to local injury of the injected skin. In the first experiment, 4 female marmoset monkeys were immunized with a mixture of equal amounts of MOG34-56 and MOG74-96 in IFA. In a second experiment, the same immunization protocol was repeated in 5 males (Experiment 2A). In parallel, another 5 males were immunized with only 100 µg MOG34-56 in IFA (Experiment 2B). Figure 2 shows that the 4 monkeys in experiment 1 had onset of clinical signs almost simultaneously around psd 85, i.e. shortly after the third rechallenge immunization. Disease development in the 5 animals in experiment 2A was more heterogeneous: One monkey (M06017) developed EAE after one rechallenge; two monkeys (M05056 and M05082) needed two rechallenges; and one monkey (M03162) needed three rechallenges before clinical disease (score  $\geq 2.0$ ) developed. One monkey (M06012) recovered within a few days after a short episode of neurological signs after the second rechallenge and maintained a mild EAE score of 0.5 for the remainder of the 160-day observation period.

The 5 animals immunized only with MOG34-56 in IFA (experiment 2B) also developed heterogeneous EAE courses consisting of hindlimb paralysis and ataxia along with body weight loss. Because omission of MOG74-96 did not markedly alter the courses, this is consistent with our previous observation that MOG34-56 (given in CFA) was a more relevant Ag for EAE induction and progression. One monkey in this group (M05047) developed EAE after a single immunization. M06018 and 9847 needed two immunizations, and M06020 required three immunizations for development of overt neurological disease. M06006 recovered within a few days after a short episode of neurological signs after the second immunization. Thus, EAE can be induced in marmosets with a single MOG peptide in an adjuvant formulation that does not contain microbial compounds that stimulate innate antigen immune receptors.

### **Brain MRI**

Increased signal intensity in T2W images of an EAE-affected marmoset brain recorded *in vivo* usually reflects edema caused by inflammation, whereas a hyperintense region in post mortem T2W images usually represents a demyelinated lesion<sup>7,15</sup>. *In vivo* T2W brain images confirmed the presence of brain lesions in the two monkeys (M06012

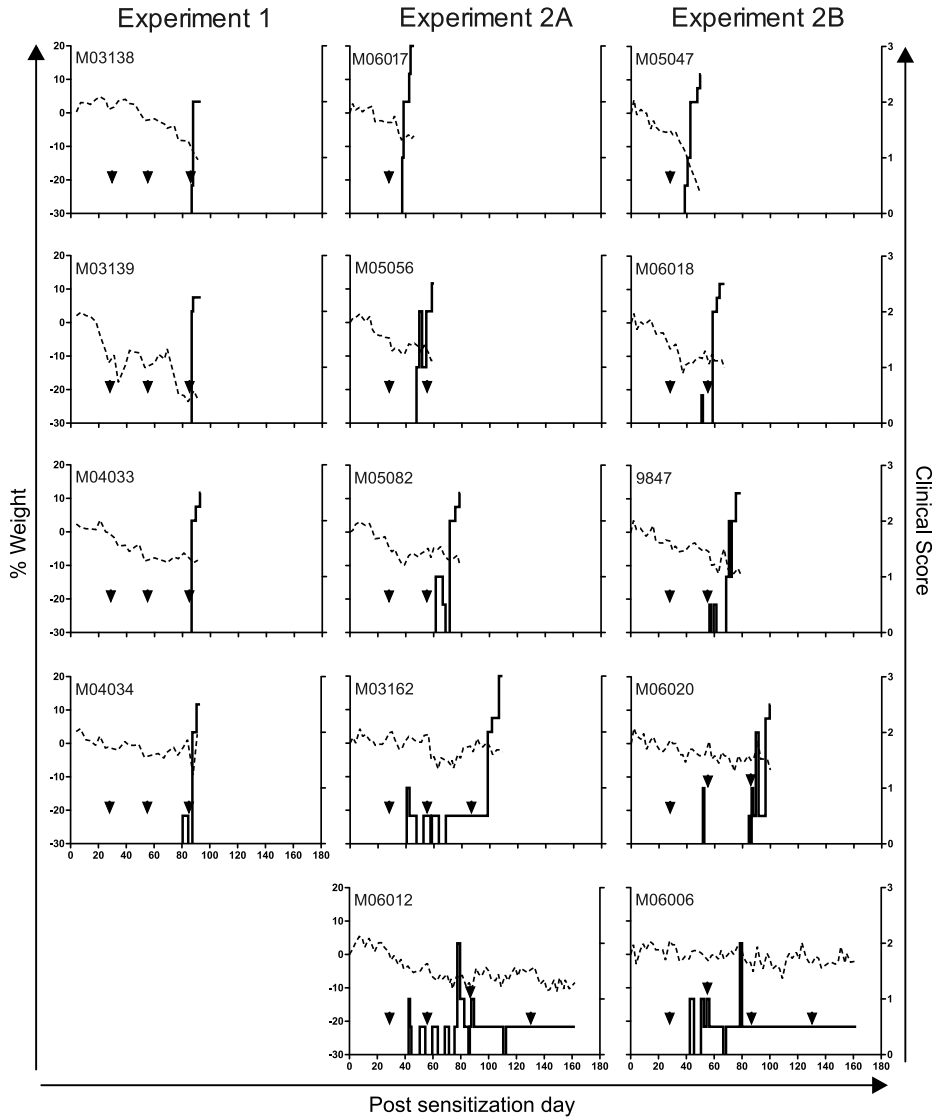


**Figure 2. Monkeys immunized with MOG peptide in IFA all developed clinical EAE.**

In 2 experiments, 4 female (Experiment 1) and 5 male (Experiment 2A) marmosets were immunized with MOG34-56 and MOG74-96 emulsified in IFA (post sensitization day 0). A third group of 5 male monkeys was immunized with only MOG34-56 in IFA (Experiment 2B). At the indicated time points (arrows) challenges were given with the same antigen preparations. The graphs depict the clinical scores (right y-axis, solid line) and the percentage body weight loss compared with day 0 (left y-axis, dotted line).

and M06006) from experiment 2 that had exhibited relapsing/remitting disease but had scores of 0.5 at the time of necropsy (Figure 3A). At the MRI level, the lesions induced with MOG34-56 in IFA do not display marked differences from those induced using CFA<sup>12</sup>.

High-definition T2W post mortem brain images of all 5 EAE monkeys induced with MOG34-56 in IFA displayed variable lesion loads (Figure 3B). In particular, there were numerous large and confluent lesions in monkey M05047 and M06006. The T2 hyperintensity was not confined to the white matter because it also affected leukocortical regions.

### **Histology and immunohistochemistry**

Representative histological and immunohistochemical findings are shown in figure 4. The brain and spinal cord sections showed many demyelinated lesions containing infiltrating CD3<sup>+</sup> T-cells and activated macrophages. Proteolipid protein (PLP) and MRP14 staining in lesions showed macrophages containing degraded PLP products. Spinal cord sections also showed that staining for immunoglobulin overlapped with that of complement C9neo staining, a marker of complement-mediated tissue injury. Thus, the lesions induced in monkeys immunized with MOG34-56 in IFA are highly similar to those induced by immunization with MOG34-56 in CFA<sup>12</sup>.

### **T-cell reactivities and cytokine production**

Immune parameter profiles varied among individual animals reflecting the genetic variation of this outbred model. Spleen and CLN drain the brain<sup>21</sup>, whereas ALN and ILN drain the peptide/IFA inoculation sites. The MNC isolated from blood and lymphoid organs from the 4 animals in experiment 1 were tested for proliferation against MOG34-56, MOG74-96, and rhMOG (Figure 5A). In PBMC from 3 of 4 monkeys (except M03138), proliferation was detected against both MOG34-56 and MOG74-96; T-cell proliferation in PBMC against rhMOG was observed only in M04034. Spleen MNC from monkey M03139 showed reactivity against the tested MOG peptides, and proliferation against rhMOG was detected only in M03139 and M04033. Proliferation responses in MNC from the pooled lymph nodes paralleled those in PBMC. In 9 of the 10 monkeys from experiment 2, proliferation against the immunizing peptide(s) was detected in at least one of the analyzed compartments, but no T-cell proliferation was detected in monkey M05056 (Figure 5A).

We next analyzed the T-cell phenotypes of the cells that displayed specific proliferation against MOG34-56. In the model induced with MOG34-56/CFA, the main proliferation response against MOG34-56 mapped to a subset of CD3<sup>+</sup> T-cells expressing CD4 and/or CD8 in combination with CD56<sup>12</sup>. Specific proliferation of T-cells in PBMC, spleen, and ALN against MOG34-56 was mainly observed in the CD4/CD8 double-positive fraction

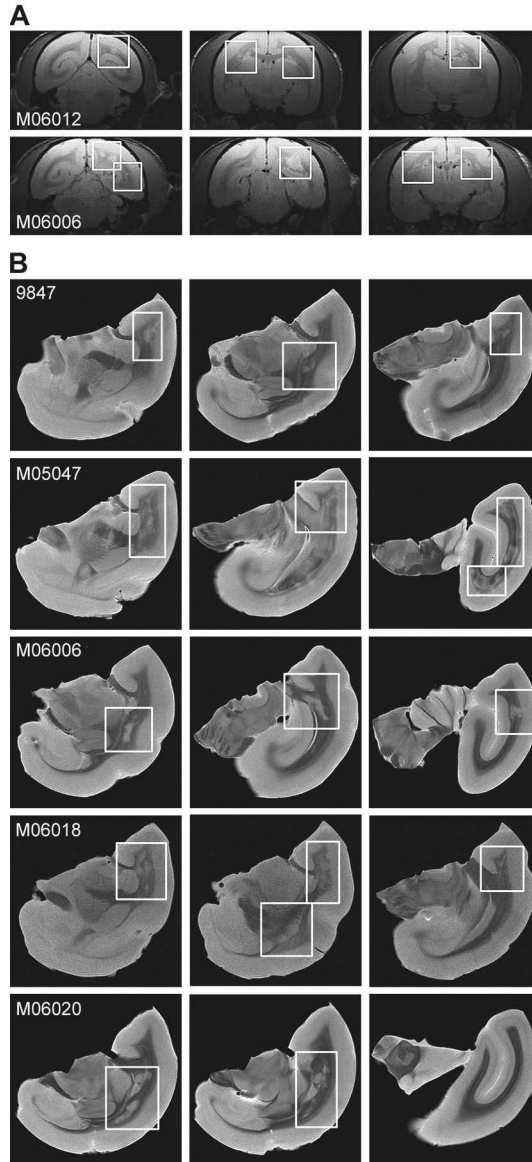


**Figure 3. T2-weighted magnetic resonance brain images confirm inflammation despite clinical remission in 2 animals and show lesion load distribution in post mortem brains.**

Lesions framed in white lines are sharply demarcated areas of increased signal intensity. A, Brain imaging of the 2 monkeys that were in remission at the time of death (see Figure 2) demonstrated CNS white matter lesions before death. B, High-resolution T2-weighted images were made of complete formalin-fixed brains to assess the total lesion load.

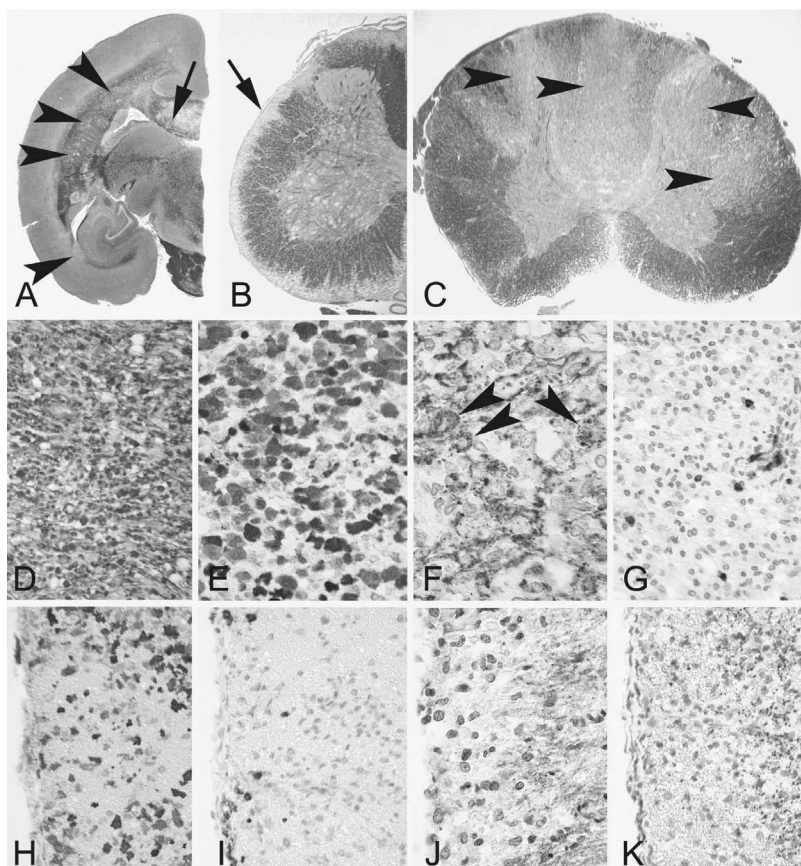


**Figure 4. MOG34-56 in IFA induces demyelination and inflammation in brain and spinal cord.**

Hyperintense white matter areas that were detected in T2-weighted images were analyzed with histology and immunohistochemistry. Brain of M05047 (A, D-G) and spinal cord of 9847 (B,C, H-K) are shown as representatives. A, Luxol fast blue-Periodic acid-Schiff (LFB-PAS) staining (original magnification x4) shows multiple large demyelinating lesions (arrowheads). The lesion in the corpus callosum (arrow) is enlarged in figures D-G. B, Subpial demyelination in spinal cord demonstrated with LFB-PAS (original magnification x25). The arrow indicates the area enlarged in H-K. C, Multiple large focal lesions are also seen in the spinal cord (arrowheads; original magnification x25). D, Enlargement of the area indicated with arrow in panel A. LFB-PAS (original magnification x125) staining shows late active demyelination and the presence of PAS-positive macrophages. E, Macrophage immunostaining using the macrophage marker MRP14 (original magnification x400). F, Immunostaining for myelin PLP (original magnification x500) shows macrophages containing phagocytosed PLP positive fragments (arrowheads). G, Immunostaining for CD3 (original magnification x200) shows that the lesions contain few T-cells. H-K, (original magnification x200) H, Subpial spinal cord area immunostained for MRP14 shows the presence of macrophages. I, CD3 immunostaining shows some meningeal T lymphocytes. J, K, Staining for immunoglobulin (J) reveals deposition in a pattern that overlaps with that of complement factor C9neo (K). See page 314 for a full-color representation of this figure.

with or without CD56 expression (Figure 5B). However, ALN also showed increased proliferation of CD3<sup>+</sup>CD4<sup>+</sup> and CD3<sup>+</sup>CD4<sup>+</sup>CD56<sup>+</sup> cells. The highest T-cell proliferation was observed in the spleen and ALN compared with the PBMC.

Freshly isolated PBMC, spleen, and ALN cells were stimulated for 48 h with rhMOG and overlapping MOG peptides, after which culture supernatants were collected for detection of IL-17A, IFN- $\gamma$ , and TNF- $\alpha$  cytokine levels (Figure 6). In experiment 2A, a high level of the Th17 signature cytokine IL-17A was measured in spleen cell cultures of all animals after stimulation with rhMOG or MOG34-56 and in 3 of 5 monkeys after MOG74-96 stimulation. IL-17A was produced only in PBMC cultures of M06012; in 3 monkeys, we observed production by ALN cells. In experiment 2B, there was marked IL-17A production from rhMOG-stimulated PBMC of 2 monkeys (9847, M06006), in spleen cell cultures of 3 monkeys (9847, M06018, and M06020) upon stimulation with rhMOG and MOG34-56, and in ALN cells of 2 monkeys (9847 and M06020) after stimulation

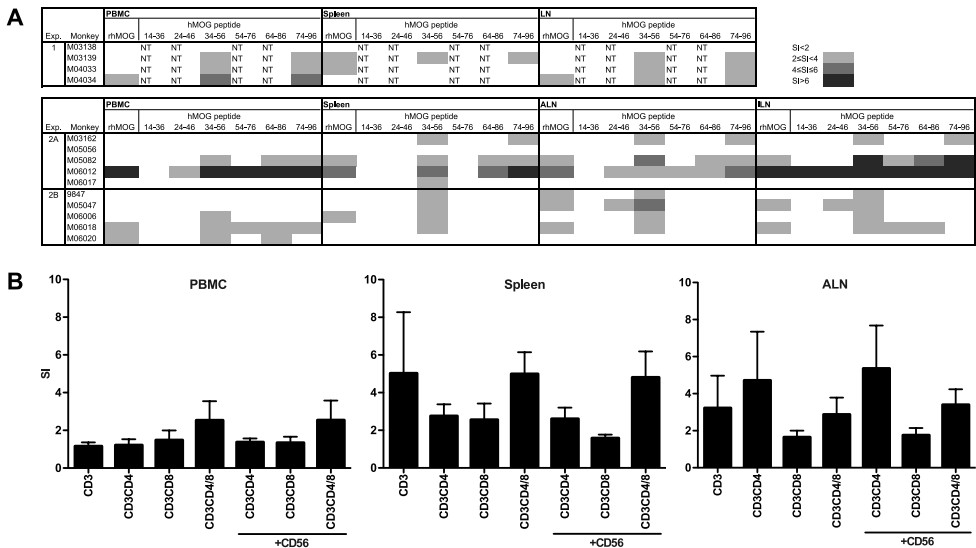


**Figure 5. Ex vivo MOG34-56 stimulation induces proliferation in the CD3<sup>+</sup>CD4/CD8<sup>+</sup>CD56<sup>+</sup> fraction.** Mononuclear cells (MNC) from blood, spleen, axillary lymph nodes (ALN), and inguinal lymph nodes (ILN) were collected at necropsy and tested for ex vivo reactivity with recombinant human MOG and the panel of 23-mer overlapping MOG peptides. A, Proliferation was determined by [<sup>3</sup>H]-thymidine incorporation and expressed as stimulation index (SI) relative to unstimulated cultures. Data are presented in graded grey scale. B, CFSE labelled MNC of animals in experiment 2 were cultured for 7 days with MOG34-56. Harvested cells were analyzed by flow cytometry to determine phenotype of MOG34-56-reactive cells. Data were pooled from monkeys that displayed clinical signs at the time of sacrifice (n=8). Mean  $\pm$  SEM is given for each subset. SI greater than or equal to 2 is considered significant. NT, not tested.

with MOG34-56 and/or rhMOG. Variable profiles of IFN- $\gamma$  and TNF- $\alpha$  production were detected in all 3 groups, i.e. they were absent in ALN cells cultures and present in PBMC and in spleen cell cultures of only some monkeys.

### T-cell lines

TCL were generated from spleen and ALN against MOG34-56 and MOG74-96. There were high expansion rates of TCL specific for MOG74-96, whereas those against MOG34-56 collapsed after a few (range 4-6) restimulations. One possible explanation for this may be that MOG34-56 T-cells killed the peptide-presenting B-LCL APC; this is similar to MOG-specific T-cells from MS patients<sup>22</sup>.

The specific cytolytic activity of MOG34-56 and MOG74-96 TCL was tested using autologous <sup>51</sup>Chromium-labeled B-LCL presenting either peptide. The MOG34-56-induced TCL lysed target cells pulsed with MOG34-56 more effectively than they lysed target cells pulsed with MOG74-96 (Figure 7A). Conversely, MOG74-96-induced TCL lysed target cells pulsed with MOG74-96 more effectively than those pulsed with MOG34-56. Cytolysis was completely abrogated when the T-cells were preincubated with concanamycin A (Figure 7B), indicating that the cytolytic activity is largely dependent on granule exocytosis<sup>23</sup>.

These data show that immunization with MOG34-56 activates CD4<sup>+</sup> and CD8<sup>+</sup>T-cells,

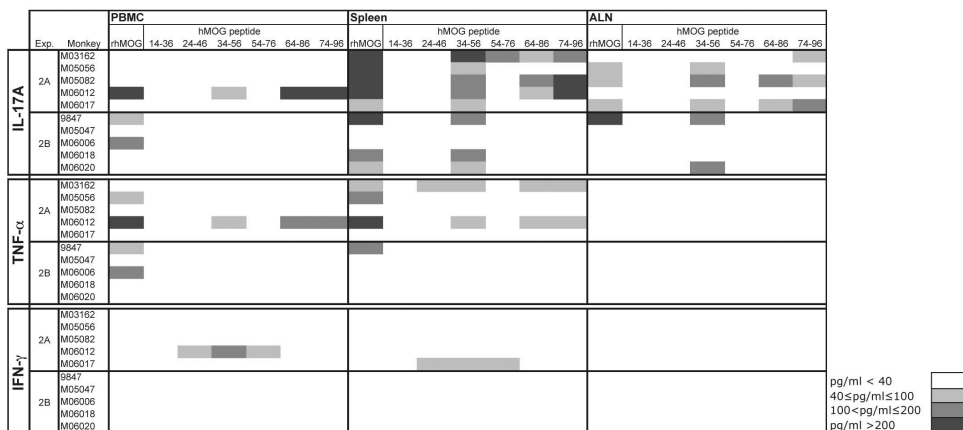


**Figure 6. Ex vivo production of IL-17A, TNF- $\alpha$ , and IFN- $\gamma$  by rhMOG and MOG peptide-stimulated mononuclear cells (MNC).**

MNC from blood, spleen, and axillary lymph nodes (ALN) from experiment 2A and 2B monkeys were cultured for 48 h with rhMOG and a panel of MOG peptides. Culture supernatants were tested for the presence of the cytokines.

including CD3<sup>+</sup>CD56<sup>+</sup> cells expressing both CD4 and CD8. Bulk cultures stimulated with MOG34-56 display specific cytolytic activity toward peptide-pulsed B-LCL and produce a higher level of the Th17 signature cytokine IL-17A than of the Th1 signature cytokine IFN- $\gamma$ . Whether these activities are all exerted by the same subset of T-cells remains to be determined.

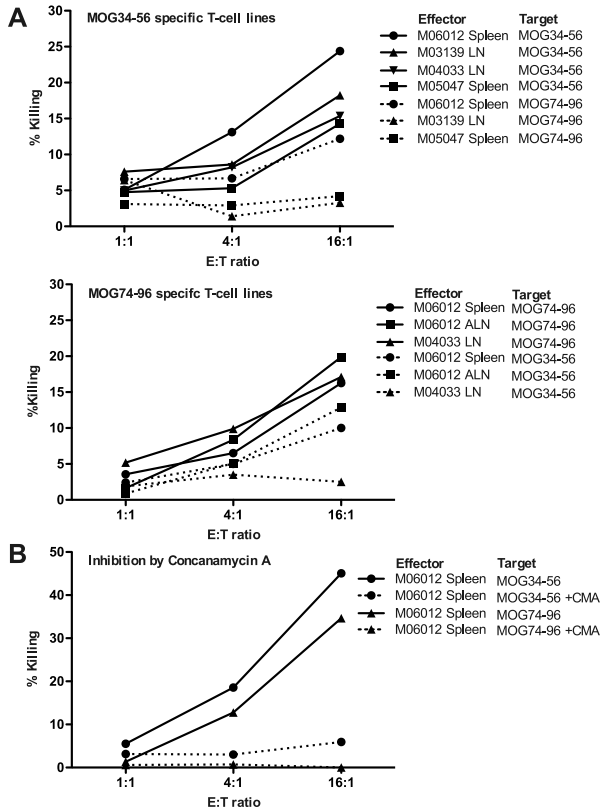


**Figure 7. MOG-peptide reactive T-cell lines have cytolytic activity that can be blocked by concanamycin A.**

Short-term T-cell lines against MOG34-56 and MOG74-96 were obtained from spleen, axillary lymph nodes (ALN), and pooled lymph nodes (LN) by stimulation with peptide-pulsed autologous Epstein-Barr virus (EBV)-transformed B-cells. A, Cytolytic activity of specific T-cell lines (effector cells [E]) was tested using <sup>51</sup>Chromium-labeled EBV-transformed B-cells as target cells (T) that were pulsed with MOG34-56 or MOG74-96 or without antigen. Specific lysis of target cells is expressed in percentage killing. Dotted lines indicate background killing with irrelevant peptide. The cytolytic activity of MOG34-56-induced lines is peptide-specific. B, Before cytotoxicity testing, the effector cells were incubated with concanamycin A (CMA) to inhibit cytolytic activity based on granule exocytosis<sup>23</sup>.

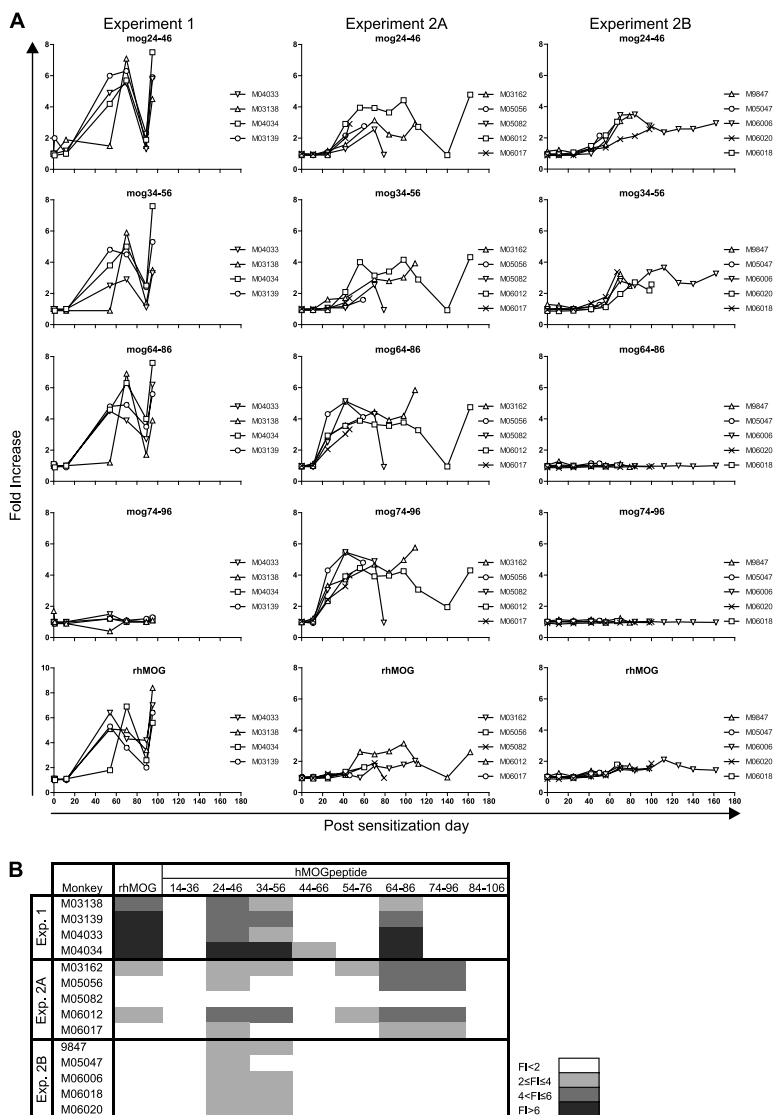


**Figure 8. Plasma IgG antibody binding to MOG peptides and rhMOG.**

IgG antibody levels in plasma samples collected from monkeys immunized with MOG34-56 and MOG74-96 (experiment 1 and 2A) or with only MOG34-56 (experiment 2B). Antibody responses were measured by ELISA to rhMOG and a panel of overlapping MOG peptides in plasma samples collected every 4 weeks during the entire study (A) and at necropsy (B). IgG responses are expressed in fold increase; plasma levels are compared with preimmune plasma. Fold increase greater than 2 is considered positive.

### Autoantibody response

Plasma samples were tested for the presence of IgG binding to plate-bound rhMOG or overlapping sets of MOG peptides (Figure 8A). Figure 8B shows anti-MOG IgG levels in necropsy plasma. All monkeys in experiment 1 and 2A, immunized with MOG34-56 and MOG74-96, showed IgG reactivity with MOG24-46, MOG34-56, and MOG64-86. In all 4 female monkeys in experiment 1, serum IgG reactivity was directed against rhMOG, but not to MOG74-96. Remarkably, sera from monkeys in experiment 2A also contained IgG against MOG74-96, but IgG binding with rhMOG was only observed in M03162 and M06012, albeit at a low levels. Interestingly, necropsy plasma of 2 monkeys from experiment 2A contained IgG against MOG54-76, a dominant B-cell epitope in the rhMOG-induced EAE model (Figure 8B)<sup>13</sup>. Because the overlap of this peptide with MOG34-56 is only marginal (i.e. 2 amino acids), this Ab specificity was likely generated in response to demyelination. Sera from marmosets sensitized against MOG34-56 alone (Experiment 2B) only showed reactivity to the immunizing peptide and the overlapping peptide MOG24-46. There were no detectable IgG Ab levels against rhMOG, demonstrating that in monkeys immunized with MOG34-56/IFA, production of autoantibodies binding to MOG protein was not a requirement for mediating demyelination<sup>24</sup>.

## DISCUSSION

We report here that 14 of 14 marmosets from an outbred colony develop overt clinical EAE associated with CNS inflammation, demyelination, and axonal damage upon sensitization against MOG34-56 in IFA or MOG34-56 combined with the nonencephalitogenic peptide MOG74-96 in IFA.

Although CFA is a powerful tool for EAE induction, there are also several major disadvantages. It is notorious for the induction of granulomas at inoculation sites and in body organs (liver, lung), causing serious discomfort to immunized animals. The potent systemic stimulatory effect of CFA also causes a strong enlargement of lymphoid organs, haemopoietic dysfunction, and disruption of lymph node architecture<sup>25,26</sup>. CFA also has a strong systemic immune-stimulatory effect mediated by its component mycobacteria that may overwhelm more subtle immune regulatory mechanisms, such as causing Th1 skewing of cellular autoimmune reactions<sup>25</sup>. Collectively, these arguments warrant the determination of whether use of CFA is mandatory for induction of EAE in marmosets or if it can be replaced with the less noxious Ag formulation with IFA.

Immune profiling of the marmosets that were immunized with MOG peptides in IFA revealed induction of cellular and humoral autoreactivity against the sensitizing peptide as well as rhMOG protein in several cases. These results imply that EAE induction in

this new EAE model relies on the activation of adaptive immune mechanisms without the need for simultaneously activating innate immune mechanisms by microbial compounds in the inoculum, as is required in rodent models. These findings suggest that the activation requirements for MOG34-56-reactive T-cells present in the mature immune repertoire of adult (2 – 5 years) marmosets living under conventional conditions differ profoundly from those for the activation of MOG34-56-reactive T-cells present in the immature repertoire of young-adult (8 – 12 weeks) specific pathogen free laboratory mice.

Our *in vitro* experiments confirm that the components of the peptide/IFA inoculum lack innate immune stimulatory activity via receptors for pathogen-associated molecular patterns, such as TLR and Nodlike receptors, which relay danger signals to engage innate immune activation of APC. However, we cannot conclude that EAE induction in this model occurs entirely without involvement of innate immune mechanisms. Quite obviously, APC present at the injection site of the peptide/IFA emulsion can be activated by danger signals released from the injured skin and from the IFA action. Unlike the EAE model induced with CFA, however, the autoreactive T-cells would have to migrate from the lymph nodes where they are activated to the CNS in the absence of the strong systemic innate immune activation signals elicited by CFA. This might be explained by a recent report that IL-17A producing CCR6<sup>+</sup> T-cells have the capacity to enter the resting noninflamed CNS via the choroid plexus and the cerebrospinal fluid<sup>27</sup>. Interestingly, IL-17A producing T-cells are prominent in the MOG34-56/IFA induced EAE model but seem less prominent in the Th1-dominated models induced with CFA<sup>13,28</sup>. Our serial brain MRI studies demonstrate that the first signs of cerebral inflammation in MOG34-56/IFA immunized monkeys are often detected around the lateral ventricles is noteworthy in this context (data not shown).

The observation that autoantibodies against intact MOG are not directly involved in the generation of demyelination in monkeys immunized with only MOG34-56 in IFA is another discrepancy between the CFA-independent and CFA-dependent EAE model in marmosets and rodents. Although Ab against the immunizing peptides were consistently found in the current study, we detected Ab binding to non-glycosylated recombinant MOG1-125, a prerequisite for demyelination, only in some animals<sup>28</sup>. This was clearly demonstrated by von Büdingen et al<sup>28,29</sup> who reported that immunization with (pooled) MOG peptides in CFA, supported by intravenous *Bordetella pertussis* particles, incited only mild inflammatory EAE in marmosets. Induction of robust EAE associated with demyelination required supplementary infusion of Ab against conformational MOG epitopes<sup>28</sup>.

The close immunologic similarities between humans and marmosets suggest parallels between T-cell mediated immunopathogenic processes between MS and the MOG34-56/IFA induced EAE model. The phenotype (CD3<sup>+</sup>CD4/8<sup>+</sup>CD56<sup>+</sup>) and

cytolytic activity of the MOG34-56-reactive marmoset T-cells are reminiscent of the finding of CD4<sup>+</sup>CD56<sup>+</sup> cytolytic T-cells in MS patients, although they may use a different cytotoxic mechanism. Cytolysis of human oligodendrocytes was found to be major histocompatibility complex (MHC)-independent<sup>30,31</sup> and to involve interaction of NKG2D on CD4 cells with NKG2D ligands (MICA/B) on the target cells<sup>32</sup>. By contrast, the peptide-specific and concanamycin A-sensitive cytolytic activity of the marmoset T-cells suggests that the cytolytic mechanism resembles that of classical MHC class I-restricted cytotoxic T-cells. Interestingly, another group reported that MOG-reactive T-cells cloned from blood of MS patients, but not those from the blood of healthy controls, display cytolytic activity towards autologous target cells pulsed with MOG peptides 1-22, 34-56, and 74-96<sup>22</sup>. Although oligodendrocytes normally lack detectable MHC expression, MHC class I molecules are induced under inflammatory conditions rendering them as potential targets for killing by CD3<sup>+</sup>CD8<sup>+</sup> cytotoxic T-lymphocytes in EAE and MS<sup>33</sup>.

In conclusion, we present a new EAE model in which MS-like clinical disease and pathological alterations are induced by immunization with a single peptide formulated with IFA. This novel model represents a major improvement for ethical, practical, and mechanistic reasons. First, the model definitively proves that the presence of microbial ligands for innate antigen receptors in the inoculum is not essential for induction of autoimmune disease in a species closely related to man. Second, replacement of CFA with IFA substantially reduces the discomfort to the animals, a central aim of biomedical research in non-human primates<sup>34</sup>. Third, the model is more useful for the study of the subtle regulatory networks that keep autoreactive T- and B-cells in check and maintain homeostasis within the CNS because these are often overwhelmed by the strong systemic Th1-skewed immune stimulation by the bacterial Ag in CFA. Fourth, refinement of the model by use of IFA may reduce the attrition rate of experimental therapies by reducing the occurrence of both false-positive and false-negative studies. As an example, the disappointing effect of anti-IL-12p40 Ab (ustekinumab) therapy in MS<sup>35</sup> contrasts sharply with the impressive results obtained in two marmoset EAE models<sup>36,37</sup>. In retrospect, it seems possible that these remarkably discrepant effects might be explained by the Th1-skewing effect of CFA (which is absent in MS) on the immunopathogenic process. Finally, preclinical immunotherapy studies with novel biologicals targeting immunity in EAE models induced are often hampered by the strong stimulation of neutralizing Ab formation by CFA. This complication is removed in our new model. Based on the latter two arguments, we believe that the new model is highly useful for immunotherapy development.

## ACKNOWLEDGEMENTS

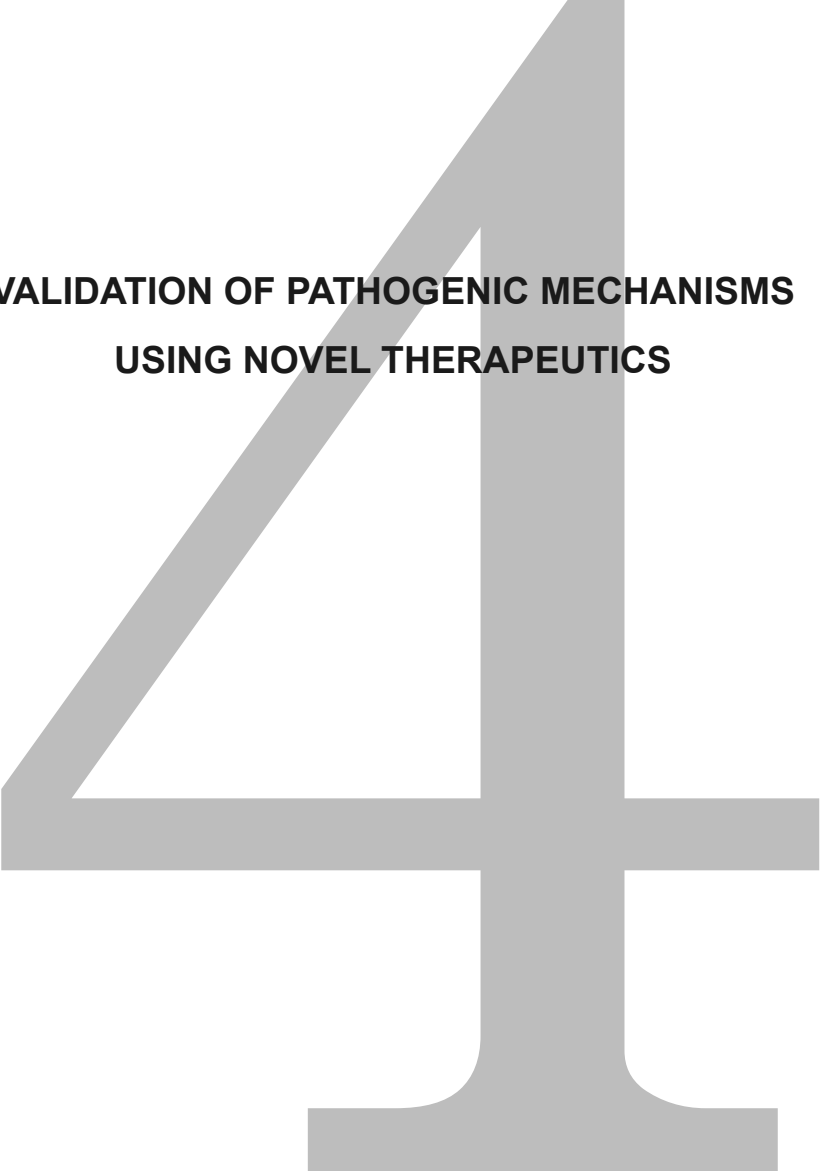
We thank Fred Batenburg, Mariska van Etten and Tom Haaksma for their excellent biotechnical assistances. Prof. Rogier Q. Hintzen (MS neurologist at the Erasmus Medical Center and MS Centre ErasMS Rotterdam) is thanked for critical reading of the manuscript. The study was supported by a grant from the European Committee under framework program 6, contract number QLRI-CT-2002-02758 (EUPEAH; Glucocorticoid hormone programming in early life and its impact on adult health). The authors also acknowledge fruitful discussions within the COST Action BM0603 Inflammation in Brain Disease Neurinfnet, and networking support from COST.

## REFERENCES

1. Compston A et al. Multiple sclerosis. *Lancet* 372:1502-1517 (2008)
2. Lopez-Diego RS et al. Novel therapeutic strategies for multiple sclerosis-a multifaceted adversary. *Nat Rev Drug Discov* 7:909-925 (2008)
3. 't Hart BA et al. The use of animal models to investigate the pathogenesis of neuroinflammatory disorders of the central nervous system. *Curr Opin Neurol* 16:375-383 (2003)
4. 't Hart BA et al. Evaluating the validity of animal models for research into therapies for immune-based disorders. *Drug Discov Today* 9:517-524 (2004)
5. Adams AB et al. Heterologous immunity: an overlooked barrier to tolerance. *Immunol Rev* 196:147-160 (2003)
6. Koch S et al. Cytomegalovirus infection: a driving force in human T cell immunosenescence. *Ann N Y Acad Sci* 1114:23-35 (2007)
7. 't Hart BA et al. Histopathological characterization of magnetic resonance imaging-detectable brain white matter lesions in a primate model of multiple sclerosis: a correlative study in the experimental autoimmune encephalomyelitis model in common marmosets (*Callithrix jacchus*). *Am J Pathol* 153:649-663 (1998)
8. 't Hart BA et al. Modelling of multiple sclerosis: lessons learned in a non-human primate. *Lancet Neurol* 3:588-597 (2004)
9. Feldmann M et al. Design of effective immunotherapy for human autoimmunity. *Nature* 435:612-619 (2005)
10. Smith PA et al. Native myelin oligodendrocyte glycoprotein promotes severe chronic neurological disease and demyelination in Biozzi ABH mice. *Eur J Immunol* 35:1311-1319 (2005)
11. Jagessar SA et al. Autoimmunity against myelin oligodendrocyte glycoprotein is dispensable for the initiation although essential for the progression of chronic encephalomyelitis in common marmosets. *J Neuropathol Exp Neurol* 67:326-340 (2008)
12. Kap YS et al. Fast progression of recombinant human myelin/oligodendrocyte glycoprotein (MOG)-induced experimental autoimmune encephalomyelitis in marmosets is associated with the activation of MOG34-56-specific cytotoxic T cells. *J Immunol* 180:1326-1337 (2008)
13. Brok HP et al. Myelin/oligodendrocyte glycoprotein-induced autoimmune encephalomyelitis in common marmosets: the encephalitogenic T cell epitope pMOG24-36 is presented by a monomorphic MHC class II molecule. *J Immunol* 165:1093-1101 (2000)
14. Kerlero de Rosbo N et al. Predominance of the autoimmune response to myelin oligodendrocyte glycoprotein (MOG) in multiple sclerosis: reactivity to the extracellular domain of MOG is directed against three main regions. *Eur J Immunol* 27:3059-3069 (1997)

15. Blezer EL et al. Quantitative MRI-pathology correlations of brain white matter lesions developing in a non-human primate model of multiple sclerosis. *NMR Biomed* 20:90-103 (2007)
16. Antunes SG et al. The common marmoset: a new world primate species with limited Mhc class II variability. *Proc Natl Acad Sci USA* 95:11745-11750 (1998)
17. Brok HP et al. An extensive monoclonal antibody panel for the phenotyping of leukocyte subsets in the common marmoset and the cotton-top tamarin. *Cytometry* 45:294-303 (2001)
18. Boon L et al. Prevention of experimental autoimmune encephalomyelitis in the common marmoset (*Callithrix jacchus*) using a chimeric antagonist monoclonal antibody against human CD40 is associated with altered B cell responses. *J Immunol* 167:2942-2949 (2001)
19. Darabi K et al. The third signal in T cell-mediated autoimmune disease? *J Immunol* 173:92-99 (2004)
20. Visser L et al. Proinflammatory bacterial peptidoglycan as a cofactor for the development of central nervous system autoimmune disease. *J Immunol* 174:808-816 (2005)
21. de Vos AF et al. Transfer of central nervous system autoantigens and presentation in secondary lymphoid organs. *J Immunol* 169:5415-5423 (2002)
22. Van der Aa A et al. Functional properties of myelin oligodendrocyte glycoprotein-reactive T cells in multiple sclerosis patients and controls. *J Neuroimmunol* 137:164-176 (2003)
23. Kataoka T et al. Concanamycin A, a powerful tool for characterization and estimation of contribution of perforin- and Fas-based lytic pathways in cell-mediated cytotoxicity. *J Immunol* 156:3678-3686 (1996)
24. Mesleh MF et al. Marmoset fine B cell and T cell epitope specificities mapped onto a homology model of the extracellular domain of human myelin oligodendrocyte glycoprotein. *Neurobiol Dis* 9:160-172 (2002)
25. Billiau A et al. Modes of action of Freund's adjuvants in experimental models of autoimmune diseases. *J Leukoc Biol* 70:849-860 (2001)
26. de Vos AF et al. Severe T-cell depletion from the PALS leads to altered spleen composition in common marmosets with experimental autoimmune encephalomyelitis (EAE). *J Neuroimmunol* 161:29-39 (2005)
27. Reboldi A et al. C-C chemokine receptor 6-regulated entry of TH-17 cells into the CNS through the choroid plexus is required for the initiation of EAE. *Nat Immunol* 10:514-523 (2009)
28. von Büdingen HC et al. Frontline: Epitope recognition on the myelin/oligodendrocyte glycoprotein differentially influences disease phenotype and antibody effector functions in autoimmune demyelination. *Eur J Immunol* 34:2072-2083 (2004)
29. von Büdingen HC et al. Immune responses against the myelin/oligodendrocyte glycoprotein in experimental autoimmune demyelination. *J Clin Immunol* 21:155-170 (2001)
30. Vergelli M et al. A novel population of CD4+CD56+ myelin-reactive T cells lyses target cells expressing CD56/neural cell adhesion molecule. *J Immunol* 157:679-688 (1996)
31. Antel JP et al. Non-MHC-restricted cell-mediated lysis of human oligodendrocytes in vitro: relation with CD56 expression. *J Immunol* 160:1606-1611 (1998)
32. Saikali P et al. NKG2D-mediated cytotoxicity toward oligodendrocytes suggests a mechanism for tissue injury in multiple sclerosis. *J Neurosci* 27:1220-1228 (2007)
33. Hoftberger R et al. Expression of major histocompatibility complex class I molecules on the different cell types in multiple sclerosis lesions. *Brain Pathol* 14:43-50 (2004)
34. Chapman K et al. Preclinical safety testing of monoclonal antibodies: the significance of species relevance. *Nat Rev Drug Discov* 6:120-126 (2007)
35. Segal BM et al. Repeated subcutaneous injections of IL12/23 p40 neutralising antibody, ustekinumab, in patients with relapsing-remitting multiple sclerosis: a phase II, double-blind, placebo-controlled, randomised, dose-ranging study. *Lancet Neurol* 7:796-804 (2008)
36. Brok HP et al. Prevention of experimental autoimmune encephalomyelitis in common marmosets using an anti-IL-12p40 monoclonal antibody. *J Immunol* 169:6554-6563 (2002)
37. 't Hart BA et al. Suppression of ongoing disease in a nonhuman primate model of multiple sclerosis by a human-anti-human IL-12p40 antibody. *J Immunol* 175:4761-4768 (2005)



A large, bold, gray number '4' is centered on the page. The number is composed of a diagonal stroke from the top-left to the middle-right, a horizontal stroke from the middle-left to the middle-right, and a vertical stroke from the top-right to the bottom-right. The bottom of the vertical stroke is rounded and flares out into a wide, flat base.

**VALIDATION OF PATHOGENIC MECHANISMS  
USING NOVEL THERAPEUTICS**



# 4.1

## **Effects of early IL-17A neutralization on disease induction in a primate model of experimental autoimmune encephalomyelitis**

Yolanda S. Kap<sup>1,2,3</sup>, S. Anwar Jagessar<sup>1,2</sup>, Nikki van Driel<sup>1</sup>, Erwin Blezer<sup>4</sup>,  
Jan Bauer<sup>5</sup>, Marjan van Meurs<sup>2,3</sup>, Paul Smith<sup>1</sup>, Jon D. Laman<sup>2,3</sup>, and  
Bert A. 't Hart<sup>1,2,3</sup>

<sup>1</sup>Department of Immunobiology, Biomedical Primate Research Centre, Rijswijk, The Netherlands; <sup>2</sup>Department of Immunology, Erasmus Medical Centre, Rotterdam, The Netherlands; <sup>3</sup>MS Centre ErasMS, Rotterdam, The Netherlands; <sup>4</sup>Image Sciences Institute, University Medical Center Utrecht, Utrecht, The Netherlands; <sup>5</sup>Brain Research Institute, University of Vienna, Austria

*J Neuroimmune Pharmacol (in press)*



## ABSTRACT

We report on the effect of antibody-mediated neutralization of IL-17A in a non-human primate experimental autoimmune encephalomyelitis (EAE) model induced with recombinant human myelin oligodendrocyte glycoprotein (rhMOG). We tested a human-anti-human IL-17A-antibody in two doses (3 and 30 mg/kg) against placebo (PBS). The treatment was started one day before EAE induction and continued throughout the experiment. Although all monkeys developed clinically evident EAE, the onset of neurological signs was delayed in some monkeys from both treatment groups. Total CNS lesion volumes, demyelination, or inflammation did not differ between the different groups. Immune profiling revealed an altered distribution of IL-17A-producing cells in the lymphoid organs of mAb treated monkeys. Comparable numbers of IL-17A-producing cells were observed in the brain. RhMOG-induced T-cell proliferation in the lymph nodes was slightly reduced after anti-IL-17A antibody treatment. To summarize, we found that anti-IL-17A antibody as a single treatment from disease induction leads to a modestly, albeit not significantly, delayed neurological disease progression in the marmoset EAE model. This suggests a role of IL-17A in late stage disease in the marmoset EAE model, but IL-17A may not be the dominant pathogenic cytokine.

## INTRODUCTION

Multiple sclerosis (MS) is a progressive neurological disease of unknown origin characterized by the progressive accumulation of inflammation and degeneration in the grey and white matter of the central nervous system (CNS). The accumulation of injury involves a combined cellular and humoral autoimmune attack on the protective myelin sheaths around axons leading to disturbed saltatory pulse conduction<sup>1,2</sup>. This immunopathogenic process is modeled in experimental autoimmune encephalomyelitis (EAE), an experimental disease induced in genetically susceptible laboratory animals including mice, rats, guinea pigs, and monkeys. The EAE model in common marmosets, a small-sized Neotropical primate, combines a remarkable clinical and neuropathological similarity with MS and a high genetic and immunological proximity to humans<sup>3</sup>. The model is therefore exquisitely suitable for translational research into immunopathogenic mechanisms and the efficacy evaluation of therapeutic antibodies (Ab), which because of their high target specificity do not cross-react with lower species. The marmoset EAE model forms a bridge narrowing the gap between EAE models and MS<sup>4,5</sup>.

Research conducted in the past years has shown that the 100% disease incidence and variable progression rate of neurological deficit is associated with the mobilization of highly reactive T-cells present in the normal repertoire with variable specificities for

myelin oligodendrocyte glycoprotein (MOG)<sup>6,7</sup>. Whereas disease induction could be mapped to the Caja-DRB1\*W1201 restricted activation of T helper (Th) 1 cells specific for MOG24-36<sup>8</sup>, the rate of disease progression appeared to be regulated by natural-killer like T-cells specific for MOG34-56<sup>6,7</sup>. Further research confirmed that this T-cell subset is able to induce clinical signs and pathology in the CNS white and grey matter without the support of innate antigen receptor ligands in the inoculum or autoantibodies against rhMOG or the inducing peptides<sup>7</sup>. These data led to the hypothesis that MOG34-56-specific T-cells have a central pathogenic role in the regulation of disease progression in the marmoset EAE model.

The most obvious immunological characteristics of MOG34-56-specific T-cell lines generated from EAE-affected monkeys were specific cytolytic activity towards MOG34-56-pulsed target cells and production of IL-17A<sup>6,7</sup>. However, typical Th1 cell-derived cytokines, such as IFN- $\gamma$  or TNF- $\alpha$ , that are abundantly produced by MOG24-36-specific Th1 cells involved in EAE initiation<sup>8</sup> were not produced by MOG34-56-specific T-cells<sup>7</sup>. This may well be due to the fact that for the activation of encephalitogenic Th1 cells in mice as well as in marmosets strong bacterial adjuvants are needed, i.e. complete Freund's adjuvant (CFA)<sup>9</sup>. By contrast, our data in the marmoset EAE model demonstrates that encephalitogenic T-cells specific for MOG34-56 can also be activated by immunization with MOG34-56 in incomplete Freund's adjuvant (IFA)<sup>7</sup>.

These observations prompted us to test whether Ab-mediated neutralization of IL-17A modulates disease progression in the EAE model in marmosets, elicited by a single immunization with recombinant protein of the extracellular domain of human MOG (MOG1-125) in CFA. The most prevalent disease course in this model is clinically characterized by the appearance of progressively accumulating motor defects after an episode of variable length, during which MRI-detectable lesions do not lead to evident neurological symptoms<sup>6,8</sup>. A typical relapsing-remitting disease course is only occasionally observed. Our previous studies have revealed that intervention with an Ab against the shared p40 subunit of IL-12 and IL-23 has a clear beneficial effect in the rhMOG-induced EAE model<sup>10,11</sup>. This supports an important pathogenic role of IL-12 and IL-23, which may be exerted via the inhibition of IL-17A production, as IL-23 promotes IL-17A production<sup>12</sup>.

Here, we report that prophylactic treatment with anti-IL-17A monoclonal antibody (mAb) at doses achieving plasma through levels above 1  $\mu\text{g/ml}$  induced a moderate delay of EAE onset. These data indicate that IL-17A is only one of several cytokines driving progression of the marmoset EAE model to clinically evident neuroinflammatory disease; absence of IL-17A being possibly compensated by Th1 cytokines that are abundantly produced in the rhMOG/CFA model.

## MATERIALS AND METHODS

### Animals

The common marmoset monkeys used in this study were randomly selected from the outbred colony kept at the Biomedical Primate Research Centre (Rijswijk, The Netherlands) under conventional and not specific pathogen free conditions. Animals were only included after a complete physical, hematological, and biochemical check-up had been performed. During the study, monkeys were pair-housed in spacious cages and remained under intensive veterinary care. The daily diet consisted of commercial food pellets for New World monkeys (Special Diet Services, Witham, Essex, UK), supplemented with rice, raisins, peanuts, marshmallows, biscuits, fresh fruit, grasshoppers, and maggots. Drinking water was provided ad libitum. In accordance with the Dutch law on animal experimentation, all study protocols and experimental procedures have been reviewed and approved by the Institute's Ethics Committee.

The study comprised 22 male and 2 female monkeys (M05011 and M04049). The average age of the monkeys was  $33 \pm 16$  months, which is adult age for marmosets. The average body weight was  $377 \pm 35$  gram.

### RhMOG-induced EAE

EAE was induced by immunization with a recombinant protein encompassing the extracellular domain of human MOG residues 1-125 (rhMOG), which was produced in *Escherichia coli* and purified as previously described<sup>13</sup>. The inoculum, containing 100 µg rhMOG in 300 µl phosphate buffered saline (PBS) emulsified with 300 µl CFA containing mycobacterium butyricum (Difco Laboratories, Detroit, MI), was injected at four locations into the dorsal skin under ketamin anesthesia (40 mg/kg; AST Pharma, Oudewater, The Netherlands).

Clinical signs were scored daily by two independent observers using a previously documented semi-quantitative scale<sup>14</sup>: 0 = no evident clinical signs; 0.5 = apathy, loss of appetite, altered walking pattern without ataxia; 1 = lethargy, anorexia, tail paralysis, tremor; 2 = ataxia, optic disease; 2.25 = monoparesis; 2.5 = paraparesis, sensory loss; 3 = para- or hemiplegia. For ethical reasons monkeys were sacrificed before or once complete paralysis of hind limbs (score  $\geq 3.0$ ) was observed, or at the pre-determined endpoint of the study (post sensitization day (psd) 113). Body weight measurements of conscious monkeys, which is used a surrogate disease marker, were performed three times per week.

Monkeys selected for necropsy were first deeply sedated by intramuscular injection of ketamin (50 mg/kg) and subsequently euthanised by infusion of pento-barbital sodium (Euthesate®; Apharmo, Duiven, The Netherlands).

### **Reactivity and dosing regimen of anti-IL-17A mAb**

The test substance was produced by UCB Celltech (UK) as a humanized IgG4κ mAb specific for human IL-17A, coded as 497.g2. The mAb has been extensively characterized *in vitro* in terms of bioassay, affinity for IL-17A, and cross reactivity against marmoset IL-17A. The affinity of the mAb with marmoset IL-17A is two fold lower than with human IL-17A when assessed by Biacore and four fold less potent in a bioassay compared to humans.

The animals were subcutaneously injected once a week starting one day before immunization until the predetermined end of the study at day 113. Animals were randomly assigned to three experimental groups. Eight animals received 3 mg/ml/kg anti-IL-17A mAb diluted in PBS, eight animals were injected with 30 mg/ml/kg anti-IL-17A mAb diluted in PBS, and eight control animals received sterile PBS (1 ml/kg) as placebo treatment. All animals received the same volume per kg body weight. One monkey (M04063) in the 30 mg/kg anti-IL-17A mAb dose group succumbed at psd 69 unexpectedly without prior signs of EAE and was therefore excluded from further analyses. Autopsy revealed that the cause of death was not related to the test substance or EAE, but to perforation of the gastro-intestinal tract by plant material, possibly originating from the branches used for cage enrichment.

### **Blood sampling and plasma levels of anti-IL-17A mAb**

Venous blood was collected into heparinized vacutainers (Greiner, Sölingen, Germany) under ketamin anesthesia (40 mg/kg) at psd 0, 6, 34, 62, and at necropsy.

After centrifugation plasma was collected and stored frozen at -20°C until analysis of test substance levels was performed. Test substance plasma levels were determined by ELISA. Microtitre plates were coated with human IL-17A (R&D Systems, Minneapolis, MN) at 0.5 µg/mL in PBS overnight, blocked with PBS/1% BSA, glazed with PBS/5% lactose/0.1% BSA, dried, sealed in foil pouches, and stored at 2-8°C. The standard curve was prepared by making serial doubling dilutions of the 497.g2 top standard (starting at 200 ng/mL) in PBS/1% BSA/1% BGG/1% human plasma. 50 µL of each standard, interassay control, and sample (diluted at least 1/100) were added to the appropriate wells containing 50 µL PBS/1% BSA/1% BGG. The interassay control concentrations were nominally 80, 20, and 8 ng/mL. Standards, interassay control, and samples were tested in duplicate. The plate was covered and incubated with agitation at RT for two hours. The plate was washed with PBS/0.1% Tween-20 four times and incubated with goat anti-human Kappa-HRP conjugate (1/10000) in PBS/1% BSA/1% BGG at RT for 30 min. The plate was washed again with PBS/0.1% Tween-20 four times and incubated with 100 µL tetramethyl benzidine substrate for 10 min. The reaction was stopped with 50 µL/well of 2.5 M H<sub>2</sub>SO<sub>4</sub> and measured at 450 nm (and 630 nm as a reference).

## **MRI**

Post mortem magnetic resonance images (MRI) of one brain hemisphere were recorded to assess differences in the CNS lesion load between treated and control monkeys<sup>15</sup>. Half of the brain collected at necropsy was fixed in 4% buffered formalin and transferred into buffered saline containing sodium azide after two weeks.

MRI experiments were performed on a 9.4 T horizontal bore MRI scanner (Varian, Palo Alto, CA). The formalin-fixed brains were submerged in a non-magnetic oil (Fomblin; perfluorinated polyether, Solvay Solexis, Weesp, The Netherlands) to prevent unwanted susceptibility artifacts.

The following quantitative images were obtained (field of view, 2.5×2.5 cm<sup>2</sup>; matrix, 256×256; slice thickness, 0.75 mm; number of slices, 41; number of experiments, 2):

- T<sub>2</sub>-maps, which were calculated from the images obtained of a multi echo sequence using the following parameters: repetition time, 4000 ms; echo spacing, 14.75 ms; echo train length, 4. T<sub>2</sub>-maps were the result of a mono-exponential fit of the MRI signal intensities as a function of TE. The T2-weighted images with TE of 14.75 ms were used for region of interest (ROI) analyses.
- Magnetization transfer ratio (MTR) maps were calculated from two T1-weighted spin echo images with and without a magnetization transfer-saturation pulse, with  $MTR=100*[(Munsaturated-Msaturated)/Munsaturated]$ . Repetition time, 1675 ms; echo time, 23 ms; MT-pulse, 8.19 ms gaussian shaped pulse, nominal flip angle 1000, offset - 9.4 kHz.

ROI were defined using the free available Medical Image Processing, Analysis and Visualization (MIPAV version 4.3.0, National Institutes of Health, Bethesda, MD) package. ROI of lesions, defined as areas with abnormal increased signal intensities, were automatically outlined in all T2-weighted images containing white matter structures using the level-set method of MIPAV. Volumes, T2, and MTR values were calculated from these ROI.

## **Histology and immunohistochemistry**

Frozen and fixed tissues were processed for histological and immunohistochemical techniques as previously described<sup>16,17</sup>.

Demyelination was visualized by staining myelin and myelin degradation products with Klüver Barrera method (Luxol Fast Blue with Periodic Acid-Schiff). Inflammation was visualized by staining infiltrating cells with hematoxylin and eosin. Of each animal 8 sections, approximately 6 cm<sup>2</sup> in total, were analysed.

Snap-frozen sections of the brain, spleen, and axillary (ALN), inguinal (ILN), and cervical lymph nodes (CLN) were used to determine the number of IL-17A-producing cells. Sections of 6 µm were thaw mounted on gelatin/chrome alum coated glass slides and stored overnight in humidified atmosphere. Next day, sections were air-dried for

1 h at RT. Within 2 weeks sections were fixed at RT in fresh acetone containing 0.02% H<sub>2</sub>O<sub>2</sub>. After air-drying, sections were washed with PBS containing 0.05% Tween-20 (Sigma-Aldrich Chemie, Zwijndrecht, The Netherlands) and incubated with 1% blocking reagent (TSA HRP kit, Invitrogen, Molecular Probes, Carlsbad, CA) at RT for 1 h. After blocking, sections were incubated for 1 h with a primary Ab against IL-17A (eBio64Cap17, eBiosciences, San Diego, CA). All incubations were performed at RT and between incubations sections were washed with 1% blocking reagent. Primary Ab was detected by incubation for 1 h with biotinylated rabbit anti-mouse IgG (DAKO, Glostrup, Denmark) and streptavidin-HRP (TSA HRP kit, Invitrogen) for 30 min, both diluted in 1% blocking reagent. Sections were incubated for 10 min with tyramide-biotin dissolved in amplification buffer (TSA HRP kit, Invitrogen) containing 0.15% H<sub>2</sub>O<sub>2</sub>. Next, sections were again incubated for 30 min with streptavidin-HRP. To reveal peroxidase activity, sections were incubated with AEC (3-amino-9-ethylcarbazole, Sigma) substrate for 10 min resulting in a bright red precipitate. Sections were counterstained with hematoxylin and embedded with glycerol-gelatin. In control stainings in which the first Ab was omitted or using an isotype control, no immunopositive cells could be detected. For the lymph nodes, the number of IL-17A-producing cells is the mean of the number of IL-17A positive cells of three non-adjacent sections.

### **Analysis of T-cell reactivities**

T-cell responses against different antigens were analysed *ex vivo* as described previously<sup>8</sup>. Briefly, PBMC were isolated by density gradient centrifugation over lymphocyte separation medium (Axis-Shield PoC AS, Oslo, Norway). Mononuclear cell (MNC) suspensions were prepared from aseptically removed spleen and ALN. Cells were cultured in triplicate for detection of proliferative responses towards rhMOG and a panel of MOG peptides. All antigens were tested at 5 µg/ml. After 48 h of culture, 0.5 µCi/well of tritiated thymidine ([<sup>3</sup>H]Thy) was added and incorporation of radiolabel was determined after 18 h using a matrix 9600 β-counter (Packard 9600; Packard Instrument Company, Meriden, CT). Results are expressed as the mean stimulation index (SI), which is defined as the counts per minute (cpm) of stimulated cells divided by the cpm of unstimulated cells. SI values above 2.0 were considered to be relevant.

The phenotype of proliferating cells was determined as described previously<sup>6</sup>. Briefly, 4x10<sup>6</sup> viable MNC from ALN or spleen were suspended in 1 ml PBS and incubated for 7 min at RT with CFSE (final concentration 1.5 µM; Fluka, Deisenhofen, Germany). Labeled MNC were cultured for 7 days with rhMOG or MOG peptides. For flow cytometric analysis we used the following commercially available labeled mAb directed against human CD markers: Alexa Fluor 700-labeled anti-CD3 (BD Biosciences), APC-labeled anti-CD4 (DAKO), biotinylated anti-CD8 (Serotec, Düsseldorf, Germany), and

streptavidin PerCP (BD Biosciences). Flow cytometric analysis was performed on a FACSort using FACSDiva software (BD Biosciences).

## Statistics

Log Rank test, One-way Anova, and Student's t-test were performed to statistically analyse the results. Results were considered statistically different at  $p < 0.05$ .

## RESULTS

### Plasma levels of anti-IL-17A mAb in rhMOG-immunized monkeys

The marmosets included in the study were randomly assigned to three treatment groups. The control group ( $n=8$ ) received 1 ml/kg PBS and the two treatment groups received anti-IL-17A mAb at 3 mg/ml/kg ( $n=8$ ) or 30 mg/ml/kg ( $n=7$ ). The test substances were subcutaneously administered once per week starting one day before immunization. Plasma levels of the anti-IL-17A mAb were determined 7 days after each administration (Figure 1). As expected, plasma concentrations of the mAb in the 3 mg/kg mAb dose group were about 10-fold lower compared to the 30 mg/kg mAb dose group. In two animals (M04099 and M03144) of the 3 mg/kg mAb dose group plasma mAb trough levels, measured one week after administration, were remarkably low, i.e. below 1  $\mu\text{g/ml}$  at psd 34, while these were above 1  $\mu\text{g/ml}$  in all the other monkeys of this group. In the 30 mg/kg mAb dose animals the plasma levels of the test substance were above 10  $\mu\text{g/ml}$  from psd 6 throughout the experiment.

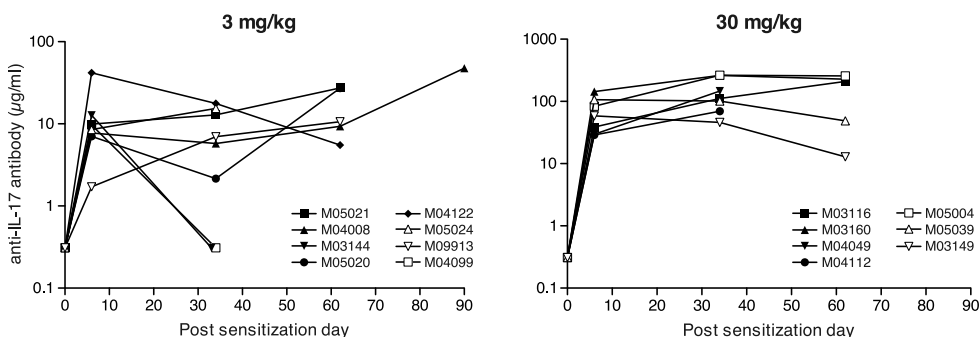
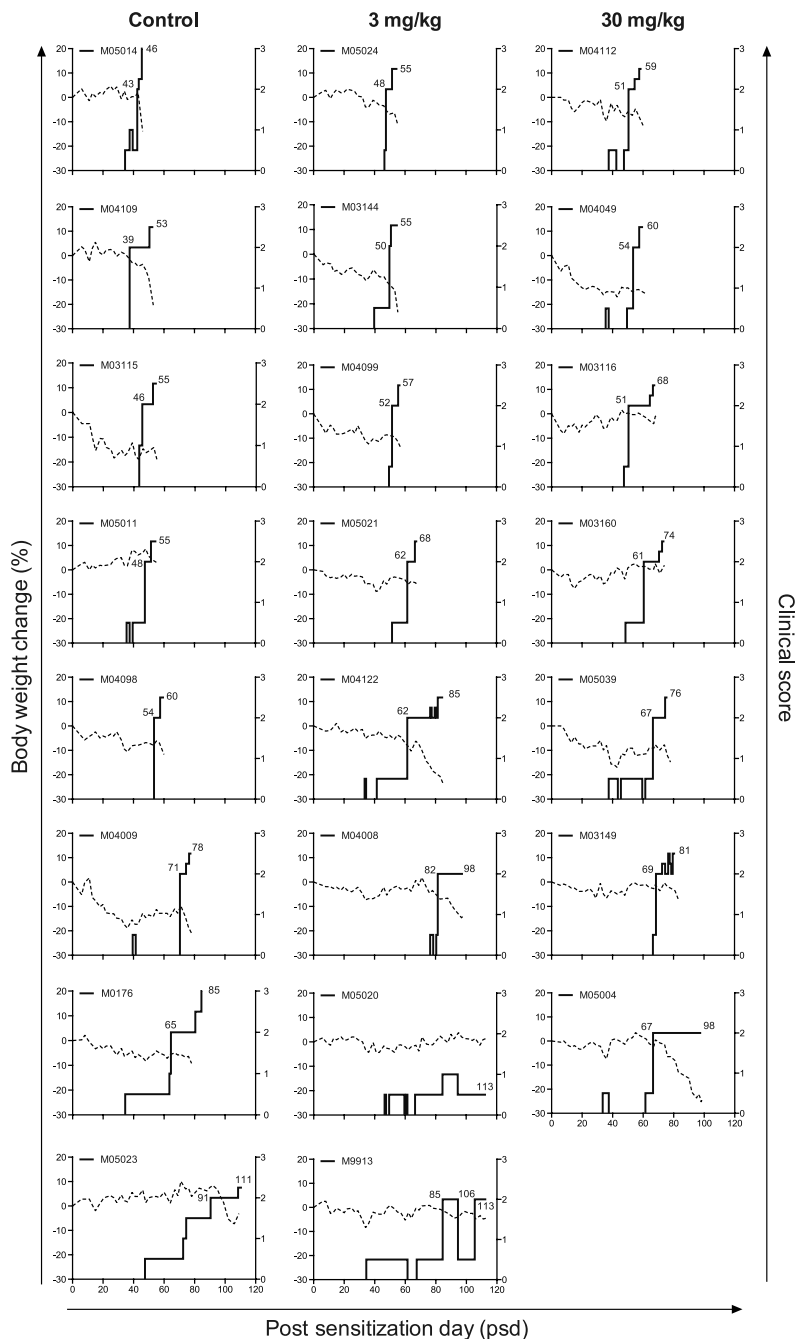


**Figure 1. Plasma levels of anti-human IL-17A mAb were sustained during the study.**

Once a week, animals received a subcutaneous injection with 1 ml/kg PBS (not shown), 3 mg/kg anti-IL-17A mAb (left graph), or 30 mg/kg anti-IL-17A mAb (right graph) starting one day before immunization. Plasma was collected from venous blood at several time points during the study and anti-IL-17A mAb levels in plasma were determined by ELISA. The y-axes have log scales. M04099 and M03144 of the low antibody dose group were not able to sustain a trough level of the antibody above 1  $\mu\text{g/ml}$ .



### Clinical signs after anti-IL-17A mAb treatment

EAE was induced by a single immunization with rhMOG emulsified in CFA. The course of clinical signs in individual animals is depicted in figure 2. Solid lines represent clinical scores and dotted lines represent percentage body weight loss, serving as a surrogate disease marker in this model. The figure shows a similar disease course in the monkeys that developed full-blown clinical EAE. Three monkeys from the 3 mg/kg mAb dose group and one monkey in the 30 mg/kg mAb dose group did not reach the stage of hind-limb paralysis (score 3) within the pre-determined observation period of 113 days. In the 3 mg/kg mAb dose group one monkey (M05020) did not develop any signs of EAE within the pre-defined observation period. A second monkey of this group (M9913) reached EAE score 2 around psd 85, remitted, and developed a second episode of EAE score 2 (psd 106), which remained present until the end of the observation period. Two monkeys (M04008 and M05004) had to be sacrificed for ethical reasons with EAE score 2 due to serious body weight loss. It is noteworthy that the two monkeys with the lowest anti-IL17A mAb plasma levels at day 34 (M03144 and M04099) were amongst the first monkeys to be sacrificed.

The EAE progression-rate to overt neurological deficit was defined as the time interval between the day of rhMOG/CFA immunization (psd 0) and the first day that clinical score 2 was observed. At the level of this parameter we observed a delayed EAE progression in the 3 mg/kg mAb dose group (mean psd 69.3; range 48–113) compared to the placebo group (mean psd 57.1; range 39–91) and the 30 mg/kg mAb dose group (mean psd 60.0; range 51–69). It is noteworthy that the variation between animals of this parameter was much lower in the 30 mg/kg mAb dose group (18 days) than in the placebo group (52 days) and the 3 mg/kg mAb dose group (> 65 days).

The disease progression from EAE score 2 (=ataxia) to the ethical end-point at score 3.0 (=paraplegia) or excessive body weight loss (> 20%) was more rapid in placebo group monkeys (mean 10.8 days, range 3–20) than in monkeys from the 3 mg/kg mAb (mean 12.9, range 5–28) and 30 mg/kg mAb (mean 13.7, range 6–31) dose group. Statistical evaluation of both disease phases (score 0 to 2 and score 2 to > 2) was done by survival analysis, but no significant differences were found (Figure 3).

In summary, these data show a moderate inhibitory effect of the Ab treatment on the EAE course, although differences between the groups did not reach statistical significance.

### Figure 2. Clinical score and body weight loss of rhMOG-immunized marmosets.

Shown are the clinical score (solid line, right y-axis) and the body weight change in percentages compared to day 0 (dotted line, left y-axis) of the placebo group (left graphs), the low dose group (middle graphs), and the high dose group (right graphs). Numbers in the figure represent the time points (psd) when neurological signs (score  $\geq 2$ ) were first observed and the day of sacrifice.

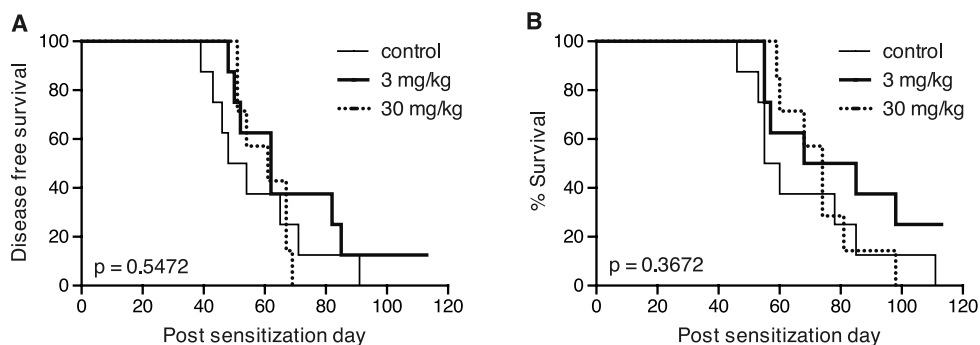


**Figure 3. Survival curves.**

Survival time to score 2 (A) and survival time to day of sacrifice (B) are shown. P-values indicated in the graph are the results of comparing three groups. Comparing the survival to the day of sacrifice of the control group versus only the 3 mg/kg group resulted in a p-value of 0.1610. When two animals of the 3 mg/kg group with low anti-IL-17A mAb plasma levels (M04099 and M03144) are included in the control group instead of the 3 mg/kg group, the p-value is 0.0428. According to the Bonferroni correction this is not significant, but it is highly suggestive for a delay in disease progression.

### Effect of anti-IL-17A mAb on white matter lesion load

Prior to sectioning for histological examination, post mortem T2-weighted MR images were made of the formalin-fixed cerebral hemispheres to visualize and quantitate the total lesion load. The analysed parameters were lesion volume,  $T_2$ , and MTR values of white matter lesions. In fixed brains an increased  $T_2$  signal reflects demyelination, while a reduction of MTR values correlates well with the intensity of macrophage infiltration<sup>15</sup>.

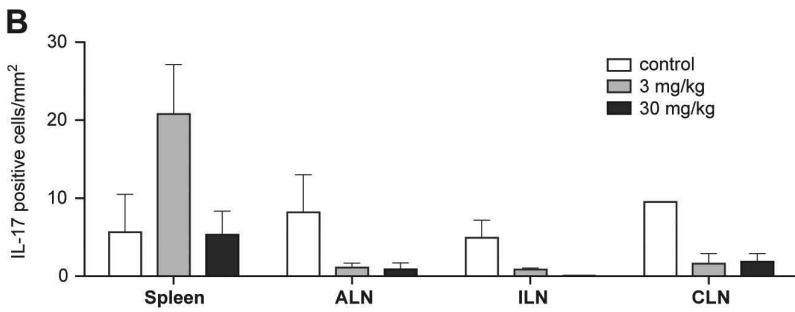
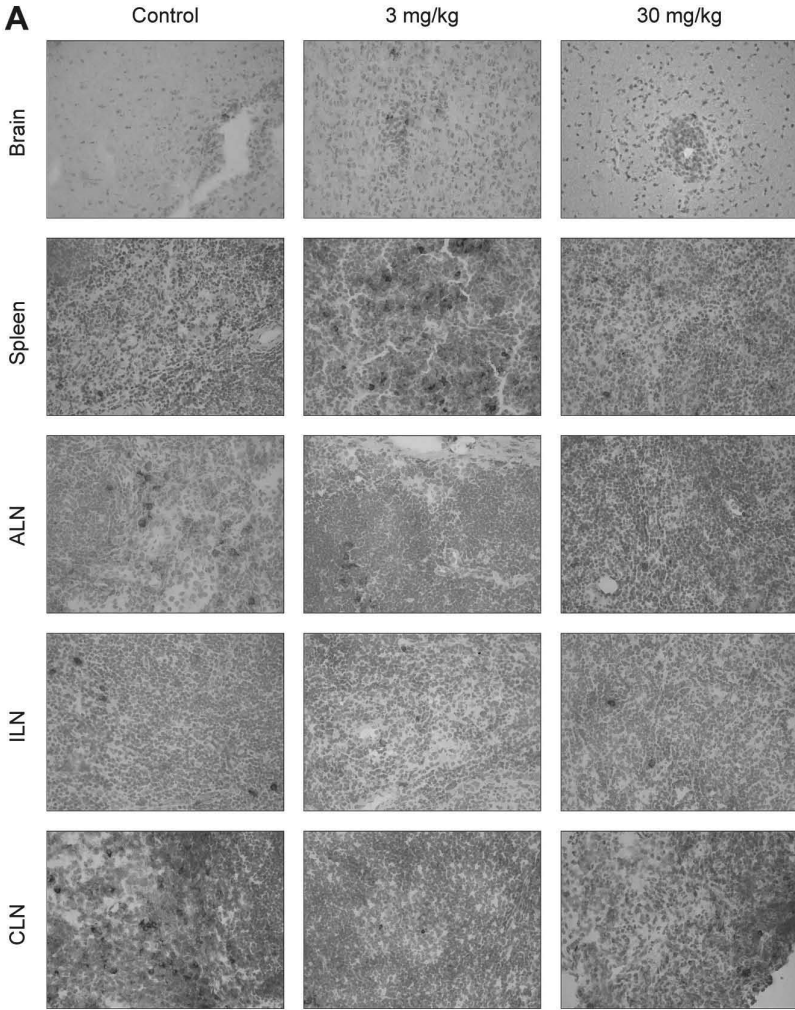
Significant differences were not observed between the three groups (Table 1). In the analysed hemispheres of two animals of the control group cerebral white matter lesions were absent. White matter lesion volumes were slightly increased in the 30 mg/kg mAb dose group compared to the placebo group. Monkey M05004 had clinical score 2 for a long time, which might explain the high lesion load. The lesions in the 3 and 30 mg/kg mAb dose group had a slightly higher  $T_2$  and lower MTR value compared to placebo (Table 1).

These results were confirmed by the quantitative histology data (Table 1). Both inflammation and demyelination were moderately increased, although not significant, in the two mAb treated groups compared with the placebo group.

For the correct interpretation of these data it is pertinent to emphasize that lesion formation in this model starts well before neurological deficits can be observed. Moreover, most animals were sacrificed at the stage of clinically evident EAE, which occurred at different time intervals after immunization. It may therefore not be surprising that major effects of the mAb treatment on the CNS pathology were not observed, neither in positive nor in negative direction.

**Table 1. White matter lesion parameters.**

Animal	WM lesions assessed by MRI			Histology		
	Volume (mm <sup>3</sup> )	T2 (ms)	MTR	# Inflammatory lesions/cm <sup>2</sup>	# Demyelinating lesions/cm <sup>2</sup>	Demyelination %
<b>Control</b>						
M0176	87	28.0	31.3	16	4.7	1.5
M03115	597	24.0	32.0	20	9.2	1.5
M04009	150	29.7	30.3	15	3.7	0.8
M04098	0	-	-	1	0.2	0
M04109	163	26.0	32.1	19	5.3	1.6
M05011	2	23.2	35.9	3	1.0	0.1
M05014	0	-	-	0	0.0	0
M05023	449	27.9	31.2	60	6.2	1.3
<b>Mean</b>	<b>181</b>	<b>26.5</b>	<b>32.1</b>	<b>17</b>	<b>3.8</b>	<b>0.9</b>
<b>SEM</b>	<b>79</b>	<b>1.0</b>	<b>0.8</b>	<b>7.9</b>	<b>1.3</b>	<b>0.3</b>
<b>3 mg/kg</b>						
M03144	483	29.9	29.9	32	7.7	1.6
M04008	135	27.6	29.2	25	9.8	1.6
M04099	113	26.6	33.9	11	1.7	0.3
M04122	354	27.6	31.2	45	12.0	2.4
M05020	178	26.1	33.3	19	3.3	0.4
M05021	30	29.3	30.9	5	2.0	0.2
M05024	642	27.5	31.2	52	11.0	2
M9913	321	25.9	29.7	13	4.3	3.3
<b>Mean</b>	<b>282</b>	<b>27.5</b>	<b>31.2</b>	<b>25</b>	<b>6.5</b>	<b>1.5</b>
<b>SEM</b>	<b>73</b>	<b>0.5</b>	<b>0.6</b>	<b>5.9</b>	<b>1.5</b>	<b>0.4</b>
<b>30 mg/kg</b>						
M03116	39	27.0	32.8	6	2.5	0.3
M03149	304	31.9	28.7	5	1.0	0.2
M03160	50	32.8	28.6	45	8.7	1.1
M04049	212	25.9	32.3	68	4.7	1.1
M04112	354	27.6	31.2	34	8.7	3
M05004	1261	25.8	29.7	52	8.8	3.4
M05039	715	27.1	31.5	18	3.2	0.7
<b>Mean</b>	<b>419</b>	<b>28.3</b>	<b>30.7</b>	<b>33</b>	<b>5.4</b>	<b>1.4</b>
<b>SEM</b>	<b>165</b>	<b>1.1</b>	<b>0.6</b>	<b>9.1</b>	<b>1.3</b>	<b>0.5</b>



### IL-17A expression in the brain and lymphoid organs

To assess the effect of anti-IL-17A mAb treatment on *in situ* expression of IL-17A, cryosectioned brains and lymphoid organs were examined with immunohistochemistry. In the brains of control and anti-IL-17A mAb treated animals IL-17A-positive cells were found in the perivascular space or in the vicinity of blood vessels (Figure 4A). No differences were observed between placebo and anti-IL-17A mAb treated animals.

IL-17A-producing cells in secondary lymphoid organs were mainly found in the red pulp of the spleen and in the medulla of the lymph nodes. We observed a trend towards higher numbers of IL-17A-producing cells in the spleen of animals dosed with 3 mg/kg anti-IL-17A mAb compared to animals that had received placebo or 30 mg/kg mAb, although the differences were not significant (Figure 4A-B). By contrast, we detected lower numbers of IL-17A-producing cells in the ALN, ILN, and CLN in both treatment groups compared to the placebo group (Figure 4A-B). Taken together, these data suggest that the anti-IL-17A mAb treatment caused altered distribution of IL-17A-producing cells over the different lymphoid compartments.

### Effect of anti-IL-17 mAb on T-cell proliferation

Cellular immune parameters of the three groups were examined to underpin the observed *in vivo* effects of the IL-17A mAb. To this end, PBMC and MNC of spleen and ALN were tested for proliferation against rhMOG and a panel of 23-mer overlapping MOG peptides.

Similar to previous studies<sup>6</sup>, proliferation of PBMC during the disease course and at necropsy was low and remained confined to the immunizing rhMOG protein and a few peptides, i.e. MOG14-36, MOG24-46, and MOG34-56 (Figure 5). No clear differences were observed between the three groups.

More robust proliferative responses were observed in the lymphoid organs, especially in the ALN and spleen. Figure 5 shows that in most animals the highest proliferative response was against rhMOG followed by peptides MOG14-36 and MOG24-46. MNC from the ALN of the anti-IL-17A mAb treated groups displayed a lower proliferative response against rhMOG and MOG peptides than MNC from

### Figure 4. Differential expression of IL-17A in the brain and lymphoid organs.

IL-17A expression was detected by immunohistochemistry. Panel A (original magnification x200) shows representative examples of each group for brain, spleen, and axillary (ALN), inguinal (ILN), and cervical (CLN) lymph nodes. Panel B shows the number of IL-17A-positive cells per mm<sup>2</sup> (mean  $\pm$  sem). Only one CLN of the control group was analyzed. No IL-17A-producing cells were detected in the ILN of the 30 mg/kg treated group. Statistical differences between the numbers of IL-17A-positive cells were analysed by One-Way Anova. Results were considered statistically different at  $p < 0.05$ . No statistical differences were found between the three groups. See page 315 for a full-color representation of this figure.

ALN of the placebo group (Figure 5). No differences between the three groups were observed in the spleen (Figure 5).

Next, we analysed the phenotype of the rhMOG responsive cells using the CFSE fluorescent dye dilution technique in combination with cell phenotyping for surface markers. RhMOG responsive CD3<sup>+</sup>CD4<sup>+</sup> and CD3<sup>+</sup>CD8<sup>+</sup> cells with CFSE dye dilution were visualized by flow cytometry. The percentages of CD3<sup>+</sup>CD4<sup>+</sup> and CD3<sup>+</sup>CD8<sup>+</sup> cells determined by fluorescent dye dilution did not differ significantly between placebo and anti-IL-17A mAb treated groups (data not shown), suggesting that the treatment with anti-IL-17A mAb did not cause a skewing of the CD4/CD8 ratio of rhMOG-specific T cells.

In conclusion, treatment with the anti-IL-17A mAb did not exert an obvious effect on the quality or quantity of the cellular autoimmune reactions. However, we like to emphasize again that the analysed lymphoid organs were collected at different time intervals after the EAE induction, creating a possible bias in the data.

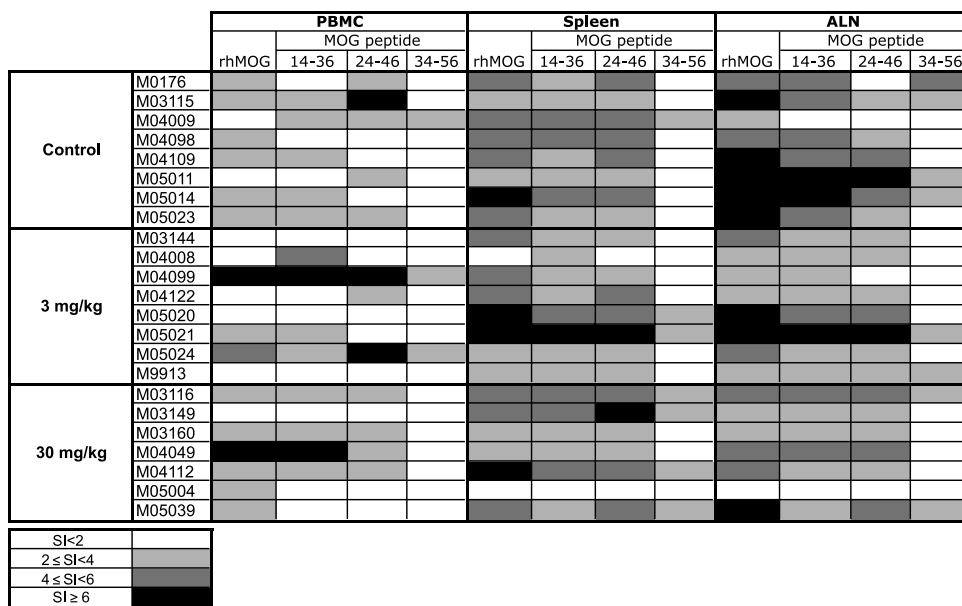


**Figure 5. T-cell responses after anti-IL-17A mAb treatment.**

PBMC and mononuclear cells isolated from the axillary lymph node (ALN) and spleen at necropsy were tested for proliferation against rhMOG and MOG peptides. The stimulation index (SI) was calculated by dividing the counts per minute (cpm) of stimulated wells by cpm of unstimulated wells. The stimulation index is divided into groups with different shading as indicated in the figure.

## DISCUSSION

Key pathogenic elements for EAE development in rhMOG-immunized marmosets comprise CD40, IL-12, and IL-23<sup>10,18-20</sup>. We have shown that a mAb against the shared p40 subunit of IL-12 and IL-23 caused profound suppression of disease symptoms when dosed from disease induction. One possible mechanism of action could have been a reduction in IL-17A that is one of the downstream cytokines from IL-23. However, the modest effect of an anti-IL-17A mAb in the current study indicates that a reduction in IL-17A does not account for the activity of IL-12p40 mAb and that other cytokines, perhaps IL-12 directly or other cytokines downstream of IL-12 and/or IL-23, are more important in the induction phase of this non-relapsing model.

The results of the current study demonstrate that prophylactic treatment with an anti-IL-17A mAb induced only a moderate extension of the disease-free time interval after EAE induction. Furthermore, immune parameters of the disease, such as T-cell proliferation against rhMOG or MOG peptides was only somewhat reduced, whereas also a marginal aggravation of CNS pathology was observed. However, the variations were all within the normal range of variation in this outbred model and may also be attributable to the longer survival. Using immunohistochemistry only a few IL-17A-positive cells could be detected in the brains of placebo and treated-monkeys, but no significant differences between groups were observed. The number of IL-17A-positive cells was increased in the spleen in the 3 mg/kg group and decreased in the axillary and inguinal lymph nodes of both groups compared to placebo animals. The higher number of IL-17A-producing cells in the spleen of monkeys that have been treated with anti-IL-17A mAb compared to placebo monkeys may be explained by feedback regulation. The observation that IL-17A receptor deficient mice produce more IL-17A<sup>21</sup> indicates that IL-17A production may be regulated by a negative feedback loop. In conclusion, the current results fail to show a robust effect of the anti-IL-17A mAb treatment on the EAE course in rhMOG/CFA-immunized marmosets.

The moderate protection against EAE induction is in agreement with data reported by some groups in mouse EAE models. Also in IL-17A<sup>-/-</sup> mice<sup>22</sup>, in mice treated with anti-IL-17A mAb<sup>12,23,24</sup>, and in mice vaccinated against IL-17A<sup>25</sup> only moderately delayed onset of clinical signs has been observed. However, other groups have demonstrated more robust effects of IL-17A on the EAE course in mice. Examples are by vaccination with IL-17A-OVA complexes that induce IL-17A blocking Ab<sup>26</sup> or adoptive transfer of IL-17<sup>+</sup> and IL-17<sup>-</sup> T-cells<sup>12,22,27</sup>. Furthermore, in the chronic-relapsing EAE model in Biozzi ABH mice, prophylactic dosing with an anti-IL-17A mAb produced a small delay in onset of the acute phase of disease, whereas treatment with the mAb started after the acute phase or during the secondary-progressive phase was very efficacious, and could even reverse the chronic motor disability (Smith, unpublished observations). Other groups

suggested that Th17 cells are not pathogenic at all<sup>28</sup> or that besides Th17 cells, Th1 cells are also essential in EAE<sup>29-31</sup>.

How can it be explained that IL-17A neutralization does not fully protect against EAE in the rhMOG-induced marmoset model? One possible explanation is the high complexity of the model. Unraveling of the pathogenic mechanisms showed that the disease is initiated by Th1 cells specific for MOG24-36, which induce small inflammatory lesions<sup>8</sup>. The moderate inflammatory injury caused by Th1 cells can be dramatically amplified by Ab against conformational epitopes of MOG<sup>32</sup>, which are clearly produced in the rhMOG model. Another subset of highly reactive T-cells with natural killer-cytotoxic T-lymphocyte characteristics and specific for MOG34-56 becomes involved at a later stage in the disease<sup>6</sup>. Our previously reported studies in marmoset EAE models induced with MOG34-56 in CFA<sup>6</sup> or IFA<sup>7</sup> demonstrated that the same clinical and pathological end-points can be reached via different immunopathogenic routes. It can thus be envisaged that after neutralization of IL-17A in the complex rhMOG/CFA-induced model other pathogenic mechanisms, such as Th1 cells, may come into play. It could also be possible that Th1 and Th17 cells act in different phases of the disease. In the previously reported study in the rhMOG-induced marmoset EAE model it was observed that Th1 cells specific for MOG24-36 are engaged in EAE induction, whereas MOG34-56 specific T-cells, which produce mainly IL-17A, mediate disease progression<sup>6,7</sup>. This suggests that, consistent with the results in the Biozzi ABH mouse model, neutralizing IL-17A in a later phase of the disease is more effective.

Yet, another possible explanation is that IL-17A, although being the signature cytokine of Th17 cells, is not the dominant pathogenic factor produced by Th17 cells. This explanation is supported by data in mice. IL-12/IL-23p40<sup>-/-</sup> mice are completely resistant to EAE, whereas only clinical scores and not the disease incidence is reduced in IL-17<sup>-/-</sup> mice<sup>22,33-35</sup>. Moreover, treatment of mice with anti-IL-23 mAb prevented either EAE induction or relapse, in contrast to the anti-IL-17A mAb treatment that blocked relapse, but had a smaller effect on the induction phase<sup>24</sup>. This may suggest that other Th17 cytokines induced by IL-23 may be pathogenetically more relevant than IL-17A in the induction phase, such as IL-21 or IL-22 (reviewed in:<sup>36</sup>). In addition, Chen et al. suggested that IL-23 may also directly activate macrophages to produce inflammatory cytokines, such as IL-6, IL-1, and TNF- $\alpha$ , which may cause inflammation and demyelination even when IL-17A is neutralized<sup>24</sup>.

Is there a place for an IL-17A neutralizing antibody in the treatment of MS? Axtell et al. reported that on the basis of clinical response to IFN- $\beta$  two groups may be distinguished in the MS patient population. Responsiveness to IFN- $\beta$  treatment requires a Th1 cytokine profile, whereas cases with a Th17 dominated cytokine profile are non-responders to IFN- $\beta$  treatment<sup>37</sup>. It is tempting to speculate on the basis of these and our data that non-responder cases to IFN- $\beta$  treatment in the MS population may benefit

from treatment with IL-17A antibody. The ideal study design to obtain proof-of-principle may be a parallel effectivity analysis in the marmoset EAE model, where in one sibling of a chimeric twin EAE is induced with MOG34-56 in CFA, which is a Th1 prone model, and in the other twin sibling with MOG34-56 in IFA, which is a more Th17 prone disease<sup>6,7</sup>.

In summary, we found that treatment with anti-IL-17A mAb induces a moderate delay of clinical EAE in marmosets, but that EAE is not completely abrogated. This suggests a pathogenic role for IL-17A in the marmoset EAE model and maybe in MS, but IL-17A may not be the only key pathogenic cytokine.

## ACKNOWLEDGEMENTS

The authors like to thank Fred Batenburg for excellent biotechnical assistance and daily care of the monkeys, Jaco Bakker DVM, Gerco Braskamp DVM and Merei Keehnen DVM for expert veterinary care, Tom Haaksma and Dr. Ivanela Kondova for autopsy of the monkeys. The authors thank Henk van Westbroek for the artwork.

## REFERENCES

1. Sospedra M et al. Immunology of multiple sclerosis. *Annu Rev Immunol* 23:683-747 (2005)
2. Compston A et al. Multiple sclerosis. *Lancet* 372:1502-1517 (2008)
3. 't Hart BA et al. Clinical, pathological, and immunologic aspects of the multiple sclerosis model in common marmosets (*Callithrix jacchus*). *J Neuropathol Exp Neurol* 68:341-355 (2009)
4. 't Hart BA et al. Modelling of multiple sclerosis: lessons learned in a non-human primate. *Lancet Neurol* 3:588-597 (2004)
5. Kap YS et al. Experimental Autoimmune Encephalomyelitis in the Common Marmoset, a Bridge Between Rodent EAE and Multiple Sclerosis for Immunotherapy Development. *J Neuroimmune Pharmacol* 5:220-230 (2010)
6. Kap YS et al. Fast progression of recombinant human myelin/oligodendrocyte glycoprotein (MOG)-induced experimental autoimmune encephalomyelitis in marmosets is associated with the activation of MOG34-56-specific cytotoxic T cells. *J Immunol* 180:1326-1337 (2008)
7. Jagessar SA et al. Induction of progressive demyelinating autoimmune encephalomyelitis in common marmoset monkeys using MOG34-56 peptide in incomplete Freund adjuvant. *J Neuropathol Exp Neurol* 69:372-385 (2010)
8. Brok HP et al. Myelin/oligodendrocyte glycoprotein-induced autoimmune encephalomyelitis in common marmosets: the encephalitogenic T cell epitope pMOG24-36 is presented by a monomorphic MHC class II molecule. *J Immunol* 165:1093-1101 (2000)
9. Billiau A et al. Modes of action of Freund's adjuvants in experimental models of autoimmune diseases. *J Leukoc Biol* 70:849-860 (2001)
10. Brok HP et al. Prevention of experimental autoimmune encephalomyelitis in common marmosets using an anti-IL-12p40 monoclonal antibody. *J Immunol* 169:6554-6563 (2002)
11. 't Hart BA et al. Suppression of ongoing disease in a nonhuman primate model of multiple sclerosis by a human-anti-human IL-12p40 antibody. *J Immunol* 175:4761-4768 (2005)

12. Langrish CL et al. IL-23 drives a pathogenic T cell population that induces autoimmune inflammation. *J Exp Med* 201:233-240 (2005)
13. Kerlero de Rosbo N et al. Predominance of the autoimmune response to myelin oligodendrocyte glycoprotein (MOG) in multiple sclerosis: reactivity to the extracellular domain of MOG is directed against three main regions. *Eur J Immunol* 27:3059-3069 (1997)
14. 't Hart BA et al. Preclinical assessment of therapeutic antibodies against human CD40 and human interleukin-12/23p40 in a nonhuman primate model of multiple sclerosis. *Neurodegener Dis* 5:38-52 (2008)
15. Blezer EL et al. Quantitative MRI-pathology correlations of brain white matter lesions developing in a non-human primate model of multiple sclerosis. *NMR Biomed* 20:90-103 (2007)
16. 't Hart BA et al. Histopathological characterization of magnetic resonance imaging-detectable brain white matter lesions in a primate model of multiple sclerosis: a correlative study in the experimental autoimmune encephalomyelitis model in common marmosets (*Callithrix jacchus*). *Am J Pathol* 153:649-663 (1998)
17. Laman JD et al. Expression of accessory molecules and cytokines in acute EAE in marmoset monkeys (*Callithrix jacchus*). *J Neuroimmunol* 86:30-45 (1998)
18. Boon L et al. Prevention of experimental autoimmune encephalomyelitis in the common marmoset (*Callithrix jacchus*) using a chimeric antagonist monoclonal antibody against human CD40 is associated with altered B cell responses. *J Immunol* 167:2942-2949 (2001)
19. Laman JD et al. Protection of marmoset monkeys against EAE by treatment with a murine antibody blocking CD40 ( $\mu$ 5D12). *Eur J Immunol* 32:2218-2228 (2002)
20. 't Hart BA et al. Treatment with chimeric anti-human CD40 antibody suppresses MRI-detectable inflammation and enlargement of pre-existing brain lesions in common marmosets affected by MOG-induced EAE. *J Neuroimmunol* 163:31-39 (2005)
21. Smith E et al. IL-17A inhibits the expansion of IL-17A-producing T cells in mice through "short-loop" inhibition via IL-17 receptor. *J Immunol* 181:1357-1364 (2008)
22. Komiyama Y et al. IL-17 plays an important role in the development of experimental autoimmune encephalomyelitis. *J Immunol* 177:566-573 (2006)
23. Hofstetter HH et al. Therapeutic efficacy of IL-17 neutralization in murine experimental autoimmune encephalomyelitis. *Cell Immunol* 237:123-130 (2005)
24. Chen Y et al. Anti-IL-23 therapy inhibits multiple inflammatory pathways and ameliorates autoimmune encephalomyelitis. *J Clin Invest* 116:1317-1326 (2006)
25. Rohn TA et al. Vaccination against IL-17 suppresses autoimmune arthritis and encephalomyelitis. *Eur J Immunol* 36:2857-2867 (2006)
26. Uyttenhove C et al. Development of an anti-IL-17A auto-vaccine that prevents experimental autoimmune encephalomyelitis. *Eur J Immunol* 36:2868-2874 (2006)
27. Jager A et al. Th1, Th17, and Th9 effector cells induce experimental autoimmune encephalomyelitis with different pathological phenotypes. *J Immunol* 183:7169-7177 (2009)
28. Haak S et al. IL-17A and IL-17F do not contribute vitally to autoimmune neuro-inflammation in mice. *J Clin Invest* 119:61-69 (2009)
29. O'Connor RA et al. Cutting edge: Th1 cells facilitate the entry of Th17 cells to the central nervous system during experimental autoimmune encephalomyelitis. *J Immunol* 181:3750-3754 (2008)
30. Lees JR et al. Host T Cells Are the Main Producers of IL-17 within the Central Nervous System during Initiation of Experimental Autoimmune Encephalomyelitis Induced by Adoptive Transfer of Th1 Cell Lines. *J Immunol* 180:8066-8072 (2008)
31. Kroenke MA et al. IL-12- and IL-23-modulated T cells induce distinct types of EAE based on histology, CNS chemokine profile, and response to cytokine inhibition. *J Exp Med* 205:1535-1541 (2008)
32. Genain CP et al. Antibody facilitation of multiple sclerosis-like lesions in a nonhuman primate. *J Clin Invest* 96:2966-2974 (1995)

33. Becher B et al. Experimental autoimmune encephalitis and inflammation in the absence of interleukin-12. *J Clin Invest* 110:493-497 (2002)
34. Gran B et al. IL-12p35-deficient mice are susceptible to experimental autoimmune encephalomyelitis: evidence for redundancy in the IL-12 system in the induction of central nervous system autoimmune demyelination. *J Immunol* 169:7104-7110 (2002)
35. Cua DJ et al. Interleukin-23 rather than interleukin-12 is the critical cytokine for autoimmune inflammation of the brain. *Nature* 421:744-748 (2003)
36. Fouser LA et al. Th17 cytokines and their emerging roles in inflammation and autoimmunity. *Immunol Rev* 226:87-102 (2008)
37. Axtell RC et al. T helper type 1 and 17 cells determine efficacy of interferon-beta in multiple sclerosis and experimental encephalomyelitis. *Nat Med* 16:406-412 (2010)



## 4.2

### **Late B-cell depletion with a human anti-human CD20 IgG1κ mAb halts the development of experimental autoimmune encephalomyelitis in marmosets**

Yolanda S. Kap<sup>1,2,3</sup>, Nikki van Driel<sup>1</sup>, Erwin Blezer<sup>4</sup>, Paul W.H.I. Parren<sup>5</sup>,  
Wim K. Bleeker<sup>5</sup>, Jon D. Laman<sup>2,3</sup>, Jenny L. Craigen<sup>6</sup>, and Bert A. 't Hart<sup>1,2,3</sup>

<sup>1</sup>Department of Immunobiology, Biomedical Primate Research Centre, Rijswijk, The Netherlands; <sup>2</sup>Department of Immunology, Erasmus Medical Centre, Rotterdam, The Netherlands; <sup>3</sup>MS Centre ErasMS, Rotterdam, The Netherlands; <sup>4</sup>Image Sciences Institute, University Medical Center Utrecht, Utrecht, The Netherlands; <sup>5</sup>Genmab, Utrecht, The Netherlands; <sup>6</sup>GlaxoSmithKline Discovery, BioPharm R&D, Stevenage, United Kingdom

*J Immunol (in press)*



## ABSTRACT

Depletion of CD20<sup>+</sup> B-cells has been related to reduced clinical activity in relapsing-remitting multiple sclerosis. The underlying mechanism is not understood as serum IgG levels were unaltered by the treatment. We report the effect of late B-cell depletion on cellular and humoral immune mechanisms in a preclinical MS model, i.e. experimental autoimmune encephalomyelitis (EAE) in the common marmoset. We used a novel human-anti-human CD20 IgG1 $\kappa$  monoclonal antibody (HuMab 7D8) that cross-reacts with marmoset CD20. EAE was induced in fourteen marmosets by immunization with recombinant human myelin oligodendrocyte glycoprotein (rhMOG) in CFA. After 21 days, B-cells were depleted in seven monkeys by HuMab 7D8 and seven control monkeys received PBS. Humab 7D8 induced profound and long-lasting B-cell depletion from PBMC and lymphoid organs throughout the observation period of 106 days. Whereas all control monkeys developed clinically evident EAE, overt neurological deficits were substantially reduced in three HuMab 7D8 treated monkeys and four HuMab 7D8 treated monkeys remained completely asymptomatic. The effect of HuMab 7D8 was confirmed on magnetic resonance images, detecting only small lesions in HuMab 7D8 treated monkeys. The infusion of HuMab 7D8 arrested the progressive increase of anti-MOG IgG antibodies. Although CD3<sup>+</sup> T-cell numbers in lymphoid organs were increased, their proliferation and cytokine production were significantly impaired. Most notable were the substantially reduced mRNA levels of IL-7 and pro-inflammatory cytokines (IL-6, IL-17A, IFN- $\gamma$ , TNF- $\alpha$ ). In conclusion, B-cell depletion prevents the development of clinical and pathological signs of EAE, which is associated with impaired activation of MOG-reactive T-cells in lymphoid organs.

## INTRODUCTION

Recent clinical trials in multiple sclerosis (MS) with the chimeric CD20 monoclonal antibody (mAb) rituximab (Rituxan) have triggered renewed interest in the pathogenic relevance of B-cells. Treatment of relapsing-remitting MS (RRMS) with rituximab led to sustained peripheral B-cell depletion, reduced relapse rate, and reduced numbers of brain white matter (WM) lesions<sup>1-3</sup>. B-cell depletion by rituximab also reduced the lesion volume enlargement in primary progressive MS but had only a modest effect on disease progression<sup>4</sup>. Rituximab not only depletes B-cells from peripheral blood, but also from cerebrospinal fluid and cerebral perivascular spaces<sup>5-7</sup>.

Traditionally, B-cells were thought to contribute to MS mainly via the production of autoantibodies, which upon binding to myelin sheaths initiate Ab-dependent cell-mediated cytotoxicity and complement-dependent cytotoxicity<sup>8</sup>. Autoantibodies directed

against myelin proteins, such as myelin oligodendrocyte glycoprotein (MOG), have been isolated from MS patients<sup>9,10</sup> and healthy controls<sup>11</sup>. Autoantibodies were found to amplify demyelination in mouse<sup>12</sup>, rat<sup>13</sup>, and non-human primate<sup>14</sup> experimental autoimmune encephalomyelitis (EAE) models. Furthermore, evidence for antibody- and complement-mediated demyelination has been described in type II MS lesions<sup>15</sup>. Recently, B-cells were detected in ectopic lymphoid structures in the meninges of MS brains, although their putative pathogenic role in these structures is still unknown<sup>16,17</sup>.

The fact that plasma cells do not express CD20 and were therefore not depleted by anti-CD20 mAb, likely explains the lack of reduction in total IgG serum<sup>2,3</sup>. It has therefore been suggested that the clinical effect of depleting B-cells in RRMS may be due to interference with other B-cell functions, such as antigen presentation and cytokine production, leading to impaired activation of T-cells and macrophages<sup>2,3</sup>. Reduced numbers of T-cells have been reported in the cerebrospinal fluid after B-cell depletion, but not in blood<sup>4,6</sup>. Because access to body fluids or organs other than blood for immune profiling is limited in MS patients and healthy controls, we chose to investigate the effect of B-cell depletion on T-cell activation in lymphoid organs in a relevant animal model of MS, EAE in the common marmoset<sup>18,19</sup>.

The recombinant human MOG (rhMOG)-induced EAE model in the common marmoset is a relevant model for the purpose of this study, because both autoantibodies and anti-MOG T-cells are induced. Autoantibodies contribute significantly to the pathogenic process in this marmoset EAE model<sup>14,20</sup>. However, full development of evident neurological disease does not strictly depend on the presence of autoantibodies, because T-cells specific for the MOG34-56 epitope can induce demyelination<sup>21,22</sup>. These highly pathogenic T-cells, which are activated in the rhMOG-induced EAE model, express CD56, are cytotoxic, and produce IL-17A<sup>21,22</sup>. Cytotoxic CD56<sup>+</sup> MOG-specific T-cells are also present in MS<sup>23,24</sup>. In marmosets, these T-cells can be activated by a very mild immunization protocol that only includes MOG34 56 emulsified in incomplete Freund's adjuvant (IFA), suggesting that anti-MOG T-cells are highly pathogenic and important in the pathogenic process<sup>22</sup>.

In recent years, a panel of fully human CD20 Ab was generated in Ig transgenic mice<sup>25</sup>. This panel included ofatumumab and HuMab 7D8, which both bind to a unique membrane-proximal CD20 epitope, comprising the small and large extracellular loops. Ofatumumab and HuMab 7D8 display superior CD20 binding and complement dependent cytotoxicity compared to rituximab<sup>25-28</sup>.

In the current study, we have induced profound B-cell depletion by weekly infusion of the human-anti-human CD20 mAb HuMab 7D8 starting three weeks after the EAE induction by a single immunization with rhMOG formulated in complete Freund's adjuvant (CFA). The treatment was started simultaneously in all animals well after immunization (i.e. at week three) to avoid interference with induction of the immunopathogenic

process but before the onset of overt clinical EAE. Neurological signs in the used model appear between four and 16 weeks after immunization with rhMOG/CFA<sup>21</sup>. The earliest responders display clinical signs already within four weeks, suggesting that the autoimmune mechanisms needed for the induction of lesions and neurological deficit can be induced within four weeks after immunization.

We report that this semi-therapeutic treatment schedule with HuMab 7D8, when autoantibody production is already ongoing, impaired the development of neurological deficit. The immunological correlates of this remarkable therapeutic effect were arrest of already initiated autoantibody production and impaired activation of autoreactive T-cells in lymphoid organs, read-out by reduced proliferation and pro-inflammatory cytokine production in lymphoid organs. These data obtained in a valid preclinical model of MS contribute to a better understanding of the elusive mechanism underlying the clinical effect of B-cell depletion in RRMS.

## MATERIALS AND METHODS

### Animals

The common marmoset monkeys used in this study were purchased from two outbred colonies, respectively kept at the Biomedical Primate Research Centre (Rijswijk, The Netherlands) or the German Primate Centre DPZ (Göttingen, Germany). Only animals that were declared healthy after the veterinarian's physical, hematological, and biochemical check-up were included. Monkeys were pair-housed in spacious cages and under intensive veterinary care throughout the study. The daily diet consisted of commercial food pellets for New World monkeys (Special Diet Services, Witham, Essex, UK), supplemented with rice, raisins, peanuts, marshmallows, biscuits, fresh fruit, and grasshoppers. Drinking water was provided *ad libitum*. According to the Dutch law on animal experimentation, all study protocols and experimental procedures have been reviewed and approved by the Institute's Ethics Committee.

Twelve marmosets were used to find an effective dose (pharmacokinetics/-dynamics (PK/PD)) and fourteen marmosets were used for efficacy assessment in the EAE model (Table 1). The average body weight distribution of monkeys selected for the EAE experiment was the same for the control ( $367 \pm 30$  gram) and treatment group ( $332 \pm 41$  gram).

### RhMOG-induced EAE

EAE was induced with a recombinant protein encompassing the extracellular domain of human MOG residues 1-125 (rhMOG), which was produced in *Escherichia coli* and purified as previously described<sup>29</sup>. The inoculum contained 100 µg rhMOG in 300 µl phosphate buffered saline (PBS) and was emulsified in 300 µl CFA containing

**Table 1. Overview of monkeys included in the pharmacokinetic/pharmacodynamic (PK/PD) study and the EAE study.**

PK study						
Nr	Monkey	Sex <sup>a</sup>	Age <sup>b</sup>	Treatment	Concentration (mg/kg)	Day of sacrifice
1	M05051	F	34	Placebo		7
2	M06050	F	22			62
3	Mi013024	M	40			7
4	Mi013212	M	34			62
5	M06028	F	26	HuMab 7D8	10 (one dose)	7
6	M06067	F	22		62	
7	Mi012698	M	49		7	
8	Mi013067	M	26		62	
9	M06047	F	23	HuMab 7D8	20 (one dose)	7
10	Mi012964	M	53			62
11	Mi013294	M	34			7
12	Mi013362	F	30			62
EAE						
	Monkey	Sex <sup>a</sup>	Age <sup>b</sup>	Treatment	Concentration (mg/kg)	
	M02052	M	84	Placebo		
	M06061	M	31			
	M06081 <sup>c</sup>	M	28			
	M07021	M	24			
	M07029	M	24			
	M07048	M	21			
	M07080	M	20			
	M04096	M	56	HuMab 7D8	Single dose of 20 mg/kg followed by a weekly dose of 5 mg/kg	
	M05073	M	43			
	M06055	M	31			
	M07012	M	26			
	M07075	M	21			
	M07085	M	20			
	M07095	M	19			

<sup>a</sup> F, Female; M, Male<sup>b</sup> Age in months at the start of the experiment<sup>c</sup> M06081 died on psd 33 without EAE

*Mycobacterium butyricum* (Difco Laboratories, Detroit, MI) by gentle stirring for at least 1 h at 4°C. The emulsion was injected at four locations into the dorsal skin under alfaxalone anesthesia (10 mg/kg; alfaxon; Vetoquinol, Den Bosch, The Netherlands).

Clinical signs were scored daily by two independent observers using a previously described semi-quantitative scale<sup>30</sup>. Briefly, 0 = no clinical signs; 0.5 = apathy, altered walking pattern without ataxia; 1 = lethargy, tail paralysis, tremor; 2 = ataxia, optic disease; 2.25 = monoparesis; 2.5 = paraparesis, sensory loss; 3 = para- or hemiplegia. Overt neurological deficit starts at score 2. For ethical reasons monkeys were sacrificed once complete paralysis of limbs (score  $\geq 3.0$ ) was observed, or at the pre-determined endpoint of the study, i.e. post sensitization day (psd) 106. Body weight measurements of conscious monkeys, which is used as a surrogate disease marker, were performed three times per week.

### **CD20 treatment**

HuMab 7D8 is a human IgG1k mAb<sup>25</sup> (Genmab, Utrecht, The Netherlands) directed against human CD20 and cross-reactive with marmoset CD20 (data not shown).

The PK/PD study comprised 12 marmosets. Four monkeys received a single i.v dose of 10 mg/kg HuMab 7D8 from a 2.86 mg/ml stock solution. Four marmosets received a single i.v dose of 20 mg/kg HuMab 7D8 from a 12.18 mg/ml stock solution. Four control animals received 1 ml/kg sterile PBS.

The EAE study comprised 14 marmosets. Seven monkeys received a single i.v. dose of 20 mg/kg HuMab 7D8 21 days after immunization. To maintain plasma levels above 5-10  $\mu\text{g/ml}$  of HuMab 7D8, 5 mg/kg was administered i.v. every week for the duration of the study. Seven control animals received 1 ml/kg sterile PBS.

### **Blood sampling, cell numbers, and plasma levels**

For the initial PK/PD study, 50  $\mu\text{l}$  blood was collected in 450  $\mu\text{l}$  citrated PBS at 5, 15, 30, 60, 120, and 240 min. After 1, 3, 7, and 34 days 500  $\mu\text{l}$  blood was collected in heparinized vacutainers (Greiner, Sölingen, Germany) under alfaxalone anesthesia (10 mg/kg). After centrifugation, plasmas were collected and stored frozen at -20°C until analysis of test substance levels was performed.

Every two weeks during the EAE study, 1.5 ml venous blood was collected into EDTA vacutainers (Greiner) under alfaxalone anesthesia (10 mg/kg). The alternating weeks, 50  $\mu\text{l}$  blood was collected in 450  $\mu\text{l}$  PBS/EDTA without sedation. The number of red and white blood cells was measured on a Sysmex XT-2000iV (Sysmex, Norderstedt, Germany).

Plasma levels of HuMab 7D8 were determined by ELISA, in which an idiotypic specific mouse mAb (Genmab MS3001-009) was used for capture and a mouse anti-human IgG (Fc-specific) HRP conjugated mAb (MH16-1, CLB, Amsterdam, The Netherlands) for detection. The quantification limit was 1  $\mu\text{g/ml}$  in plasma.

## Necropsy

Monkeys selected for necropsy were first deeply sedated by intramuscular injection of alfaxalone (10 mg/kg). Maximum volume of blood was collected into EDTA or heparinized vacutainers and subsequently the marmoset was euthanised by infusion of pento-barbital sodium (Euthesate®; Apharmo, Duiven, The Netherlands).

Spleen and lymph nodes from several anatomical locations were collected aseptically and cut into four pieces, which were processed for cell culture, fixed in buffered formalin, snap-frozen in liquid nitrogen, or processed for RNA extraction with RNAlater (Sigma, St. Louis, MO). Half of the brain and spinal cord was stored in formalin and the other half was snap-frozen in liquid nitrogen. Femur was collected in PBS for isolation of bone-marrow cells.

## Magnetic resonance imaging (MRI)

One cerebral hemisphere collected at necropsy was fixed in 4% buffered formalin and two weeks later transferred into buffered saline containing sodium azide to allow stabilization of MR relaxation time characteristics<sup>31</sup>. High-contrast post mortem MR images were recorded on a 9.4 T horizontal bore NMR spectrometer (Varian, Palo Alto, CA), equipped with a quadrature coil (RAPID, Biomedical, Rimpf, Germany). Brains were submerged in non-magnetic oil (Fomblin; perfluorinated polyether, Solvay Solexis, Weesp, The Netherlands) to prevent unwanted susceptibility artifacts.

On a sagittal scout image, 41 contiguous coronal slices of 0.75 mm were defined covering the complete brain, with the following characteristics: field of view, 25x25 mm; matrix, 256x256; zero-filled, 512x512; voxel volume,  $7.15 \times 10^{-3} \text{ mm}^3$ , two transitions. The following MRI data sets were collected:

- $T_2$  maps were calculated by a mono-exponential fitting of six spin echo images with increasing TE. TR, 2650 ms; TE, 10+5x10 ms. The second image of this series, i.e. TE, 20 ms, was used for Region of Interest (ROI) determination.
- MTR maps were calculated from two T1W spin echo images with and without a Magnetization Transfer saturation pulse. Magnetization transfer ratio (MTR) values represent the percentage decrease in MR signal intensity as a result of this pulse. TR, 1675 ms; TE, 23 ms; MT-pulse: 8.19 ms gaussian shaped pulse, nominal flip angle 1000, offset -9.4kHz.

Calculations of  $T_2$  and MTR were done with a homemade software package developed in MATLAB (v. 7.2 The Mathworks Inc., Natick, MA). ROI were defined using the free available Medical Image Processing, Analysis and Visualization package (MIPAV version 4.3.0., National Institutes of Health, Bethesda, MD). WM lesions were defined as areas with abnormal high signal intensities in the WM. The total volume of WM lesions was determined for the complete hemisphere.

### Anti-MOG Ab detection

Ab binding to rhMOG and MOG54-76 was determined using ELISA as described<sup>21</sup>. Bound IgM Ab was detected using alkaline phosphatase-conjugated goat-anti-monkey IgM (Rockland Immunochemicals, Gilbertsville, PA) and bound IgG Ab was detected using polyclonal alkaline phosphatase-conjugated rabbit-anti-human IgG (Abcam, Cambridge, UK). The results of the Ab assays are expressed relative to a standard curve of pooled necropsy plasma from three rhMOG/CFA-immunized control marmosets of this study. The Ab concentration in pooled plasma was arbitrarily defined as 350 when OD = 1 and ELISA data of 10- and 100-fold diluted test samples were fitted to a four-parameter hyperbolic function, using home-made software ADAMSEL (dr. E. Remarque, BPRC, The Netherlands).

### Procedures and assays for quantification of cellular immune response

- *MNC isolation*: Mononuclear cell (MNC) suspensions from PBMC, spleen, and bone marrow were isolated by density gradient centrifugation over lymphocyte separation medium (Axis-Shield PoC AS, Oslo, Norway). Cell suspensions from axillary (ALN), inguinal (ILN), lumbar (LLN), and cervical (CLN) lymph nodes were isolated by gently pressing the organ through a nylon mesh and washed with RPMI medium.
- *Phenotyping with flow cytometry*: To enable visualization of residual CD20 expressing cells in the circulation or lymphoid organs of monkeys treated with HuMab 7D8, MNC were subjected to an Ab stripping protocol aimed at removal of HuMab 7D8. Cells ( $2 \times 10^6$ ) were incubated with 5 ml acidic buffer (50 mM glycine-HCl, 5 mM KCl, 130 mM NaCl, pH 3) for 4 min at RT and subsequently washed and used for flow cytometry. The flow cytometry protocol used to phenotype MNC involved staining of dead cells using violet viability stain (Invitrogen, Molecular Probes, Carlsbad, CA) for 25 min at RT. Subsequently, cells were incubated with CD3-AF700 (SP34-2, BD Biosciences, San Diego, CA), CD20-PE (H299, Beckman Coulter, Fullerton, CA), CD40-FITC (B-B20, Abcam, Cambridge, MA), CD4-APC (MT310, Zebra Bioscience, Enschede, The Netherlands), and CD8-biotin (LT-8, Serotec, Düsseldorf, Germany) for 30 min at 4°C. CD8-positive cells were visualized by incubation with streptavidin-PerCP (BD Biosciences) for 30 min at 4°C. Finally, cells were fixed in 1% cytofix (BD Biosciences). Flow cytometric analysis was performed on a FACS LSRII using FACSDiva software (BD Biosciences).
- *Proliferation*: Proliferation of MNC was assayed as previously described<sup>32</sup>. Briefly, cells were cultured in triplicate at a cell density of  $2 \times 10^5$  per well in 96-wells U-bottom plates with rhMOG, MOG peptides, OVA, and ConA. All antigens were tested at 5 µg/ml. After 48 h culture, 50 µl supernatant was harvested for cytokine ELISA and 0.5 µCi/well of tritiated thymidine ( $^3\text{H}$ Thy) was added to the cells. Incorporation of

radiolabel was determined after 18 h using a matrix 9600  $\beta$ -counter (Packard 9600; Packard Instrument Company, Meriden, CT).

- *Phenotyping of proliferating cells*: This was performed by CFSE vital dye dilution assay as described elsewhere<sup>21</sup>.
- *Cytokine detection with ELISA*: Due to limitation of sample volume and availability of cross-reactive ELISA reagents we chose to assay for three cytokines. The production of IL-17A, IFN- $\gamma$ , and IL-12p40/p70 was measured in culture supernatants with commercial ELISA according to manufacturers instructions (U-Cytech, Utrecht, The Netherlands).
- *Cytokine detection with quantitative PCR (qPCR)*: RNA was isolated using RNeasy minikit (Qiagen, Hilden, Germany) and cDNA was synthesized using RevertAid First Strand cDNA Synthesis Kit (Fermentas, St. Leon-Rot, Germany) according to the manufacturers instructions. Random hexamer primers were used for cDNA synthesis. Expression levels of mRNA were determined by quantitative PCR using iTaq supermix with ROX and CFX96 Real-Time System (both from Bio-Rad, Hercules, CA). Primer and probes used are listed in table 2. Probes were obtained from the Universal Probe Library set for human (Roche, Indianapolis, In). Transcript levels were normalized against the reference gene abelson (ABL)<sup>33</sup>.

### Immunohistochemistry

Spleen and lymph nodes obtained at necropsy were snap-frozen in liquid nitrogen and stored in -80°C. Frozen spleen and lymph node sections of 6  $\mu$ m were cut and thaw mounted on gelatin/chrome alum coated glass slides. Slides were kept overnight at RT

**Table 2. Primer and probe combinations for qPCR.**

Gene	Forward primer	Reverse primer	Probe
ABL	CAGAGAAGGTCTATGAACTCATGC	GGTGGATTCAGCAAAGGAG	GCAGTGGA
CD3	AGGCAAGAGTGTGTGAGAACTG	GATGCAGATGTCCACTATGACAA	GGAGGTGG
CD19	CAGCCCCGTCTTATAGAAACC	CACTGTCCGGCTCCTCATAG	AGAAGAGGA
IL-17A	CCTCATTGGTGTCACTGCTG	TGCAATTCCTGCCTTCACTA	GCTGCTGA
IFN- $\gamma$	GGAGAGAGGAGGGTGACAGA	TTGGATGCTCTGGTTGTCTTTA	CAGAGCCA
TNF- $\alpha$	GGACGAGCTCTCCAAGGACT	GCACTCGGGATTTCGAGAAG	GGCCCTGG
IL-7	TGCACCAGCAAGGTAAAGA	CCAAACTCTTTGTCCGGTTGG	TGCCCTGG
IL-4	CTAAACGGCTGGACAGGAA	CCTTCACAGGACAGGAGTTCA	CAGCCTGG
IL-6	CCAATCTGGATTCAATGAGGA	AACTCCAAAAGACCAAGTGGTGA	GCCTGCTG
IL-10	GTTGCCTTCAGCAGAGTGAA	GCAACCCAGGTAACCCCTTAAA	TGCTGGAG
IL-1 $\beta$	TGGTCCTAACAGATGAAGTGC	GTAGTGCTGGCGGGAGAGT	GACCTGGA

in a humidified atmosphere. After air-drying the slides for 1 h, they were fixed in fresh acetone containing 0.02% (v/v) H<sub>2</sub>O<sub>2</sub>. Acetone fixed slides were air-dried for 10 min and subsequently washed in PBS. Tissue sections were incubated with primary Ab overnight at 4°C in a humidified atmosphere. Primary Ab were mouse-anti-human CD20 (clone L26, Dako, Glostrup, Denmark), mouse-anti-human CD40 (clone B-B20, Chemicon, Billerica, MA), and rabbit anti-human CD3 (Dako). Incubations with secondary and tertiary reagents were performed for 1 h at RT. Between incubation steps the slides were washed twice with PBS. Detection of primary unlabelled Ab was followed by incubation with donkey-anti-mouse or goat-anti-rabbit, both biotin labeled. This was followed by incubation with HRP-labelled avidin-biotin-complex (Vectastain ABC, Vector laboratories, Burlingame, CA). HRP activity was revealed by incubation for 10 min at RT with 3-amino-9-ethyl-carbozole (AEC; Sigma, Zwijndrecht, The Netherlands), leading to a bright red precipitate. CD40 expression was enhanced with the tyramide signal amplification kit (Invitrogen, Carlsbad, CA). Incubation with isotype-matched primary Ab of irrelevant specificity and omission of the primary Ab served as negative controls.

### Statistics

Data are presented as mean ± sem of 6 control and 7 treated marmosets. Statistical analysis was performed using Prism 5.0b for Mac OS X. Survival was analysed using Log-Rank test. Other data was analysed using the Mann-Whitney U test.  $p < 0.05$  was considered statistically significant.

## RESULTS

### Dose-finding and PK/PD of HuMab 7D8

The effective Ab dose for maximum B-cell depletion from blood and lymph nodes was determined in twelve marmosets. Groups of 4 monkeys each received a single i.v. injection with placebo (PBS) or HuMab 7D8 at a dose of 10 mg/kg or 20 mg/kg (Table 1). At the indicated time points during the first (Figure 1A) and subsequent days (Figure 1B), small venous blood volumes were withdrawn for plasma isolation in which HuMab 7D8 levels were determined, respectively. As expected, all placebo-treated monkeys scored negative in the assay (data not shown). The average HuMab 7D8 levels in the 10 mg/kg and 20 mg/kg dose group measured in the 5 min blood sample were 56 and 181 µg/ml, respectively. The plasma concentration was maintained at trough level above 10 µg/ml during the following seven days.

Predictably, the CD20 molecule on B-cells in the treated group may be bound by HuMab 7D8 and therefore could not bind the anti-CD20 Ab conjugate used in flow cytometry. Because anti-CD19 mAb cross-reacted only poorly with marmosets, we have

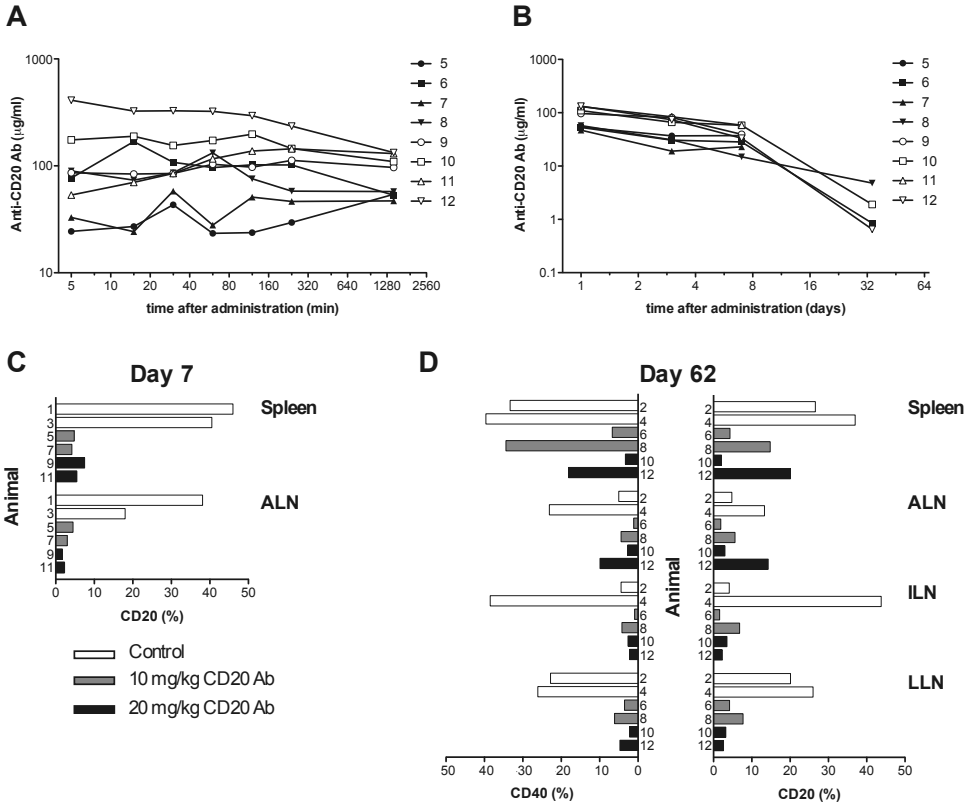


**Figure 1. A single dose of the human anti-human CD20 antibody HuMab 7D8 induces profound and long-lasting B-cell depletion in naive marmosets.**

A-B, Circulating plasma levels of HuMab 7D8 were determined at 5, 15, 30, 60, 120, and 240 min (A) and 1, 3, 7, and 34 days (B) after administration of HuMab 7D8. Animals received a single dose of 10 mg/kg (closed symbols, Table 1) or 20 mg/kg (open symbols, Table 1). Plasma levels of the antibody (y-axis) are shown in log-scale. Plasma levels of the 20 mg/kg group were higher until day 34. C-D, Seven or 62 days after administration of HuMab 7D8, two animals of each group (Table 1) were sacrificed and CD20 expression was determined in lymphoid organs by flow cytometry. White bars, control; grey bars 10 mg/kg HuMab 7D8; black bars, 20 mg/kg HuMab 7D8. Cells underwent a stripping procedure to remove the *in vivo* administered HuMab 7D8 from cells. Shown are the animal numbers on the y-axis (corresponding to Table 1) and the percentage living CD20<sup>+</sup> or CD40<sup>+</sup> cells on the x-axis. At day 7, the percentage of CD20<sup>+</sup> B-cells was lower in both treatment groups (C). At day 62, animal 8 (Mi013067) and animal 12 (Mi013362) showed higher percentages of CD20<sup>+</sup> and CD40<sup>+</sup> B-cells than the other treated animals (D).

also determined CD40-expressing cells as surrogate marker for B-cell depletion. CD20 is a pan-B-cell marker expressed throughout the B-cell lineage with the exception of plasma cells. CD40 is expressed besides on activated antigen presenting cells (DC and macrophages) also on resting and activated mature B-cells, but not on plasma cells.

Seven days after the single administration of HuMab 7D8, two animals of each group were sacrificed (Table 1) and the extent of B-cell depletion from spleen and ALN was assessed by flow cytometry. The profound depletion of CD20<sup>+</sup> cells by both doses of HuMab 7D8 is depicted in Figure 1C. The remaining six animals were sacrificed 62 days after HuMab 7D8 administration (Table 1). Figure 1D shows that even two months after the administration of a single HuMab 7D8 dose reduced percentages of CD20<sup>+</sup> and CD40<sup>+</sup> cells were found in all lymphoid organs. However, the figure also shows that in one monkey of each group (nr 8/Mi013067 and nr 12/Mi013362) insufficient B-cell depletion or partial repletion of B-cells had occurred in the spleen and ALN at that time (Figure 1D).

### **Anti-CD20 mAb effectively depletes B-cells throughout the EAE experiment**

Fourteen unrelated marmosets were immunized with rhMOG in CFA. Seven animals were randomly selected for treatment with HuMab 7D8 from psd 21 and seven animals for placebo treatment with PBS (Table 1). Based on the PK/PD data we chose to induce complete B-cell depletion with a single loading dose of 20 mg HuMab 7D8 per kg body weight followed by a weekly intravenous maintenance dose of 5 mg/kg. This dosing regimen aimed at a plasma trough level of 5-10 µg/ml, which was previously described to be sufficient for sustained biological activity *in vivo*<sup>34</sup>.

Plasma levels of HuMab 7D8 were measured every week at seven days after intravenous administration of HuMab 7D8 or PBS. The plasma level of HuMab 7D8 remained above 5 µg/ml, with the exception of one time point (day 42) in one monkey (M07075) (Figure 2A). Every two weeks, percentages of CD20<sup>-</sup> and CD40<sup>-</sup> expressing cells in PBMC were determined by flow cytometry to confirm B-cell depletion by HuMab 7D8. Seven days after the first dose of HuMab 7D8, i.e. 28 days after immunization, CD20<sup>+</sup> and CD40<sup>+</sup> cells were almost completely depleted compared to the control group (Figure 2B, Supplemental Figure 1). Throughout the study, the percentage of CD20 remained at very low level in the treatment group, except at psd 84. At this time point, six of the seven animals, M07095 being the only exception, contained elevated numbers of CD20<sup>+</sup> cells in PBMC. However, as CD40 expression remained low at this time point we assume that these might be immature B-cells repleting the peripheral compartment (Figure 2B, Supplemental Figure 1).

At necropsy, the percentage of CD20<sup>+</sup> and CD40<sup>+</sup> cells present in PBMC, spleen, bone marrow, and lymph nodes were determined by flow cytometry. In the HuMab 7D8 treatment group, CD20<sup>-</sup> and CD40<sup>-</sup> expressing cells were detected, but the levels were

still significantly lower than in the control group (Figure 2C, Supplemental Figure 2). Also, the expression of CD19, assessed in spleen and ALN by qPCR, was significantly lower in the treatment group (Figure 2D).

In conclusion, the chosen HuMab 7D8 dosing regimen induced profound and persistent B-cell depletion from blood and lymphoid organs.

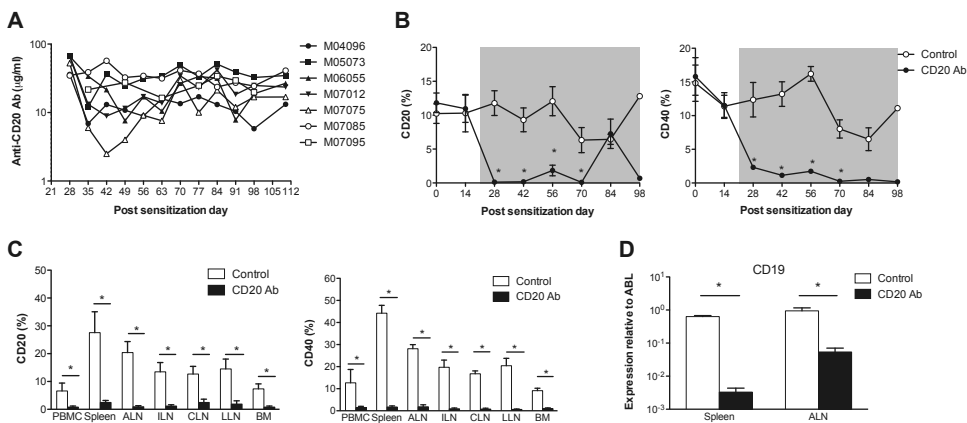


**Figure 2. B-cells are depleted significantly from blood and lymphoid organs in the marmoset EAE model.**

A, Treatment with HuMab 7D8 was started 21 days after immunization with rhMOG in CFA. Plasma levels of circulating HuMab 7D8 were determined at the indicated time points during the study and are shown in log-scale (y-axis). B, CD20 and CD40 expression in PBMC was determined by flow cytometry throughout the study. Shown are the percentages of living CD20<sup>+</sup> or CD40<sup>+</sup> cells of total measured cells. The treatment period is indicated as grey-shaded box. Open symbols represent the control animals and closed symbols the treated animals. CD20 was not removed with the stripping procedure, because the number of available PBMC was too small. CD40 was used to confirm B-cell depletion. At post sensitization day (psd) 28, 42, 56, and 70 a significant lower percentage of B-cells was observed in treated animals compared to control animals. It is of note that the number of animals decreased during the study: the number of control animals was 6 until day 42; at psd 56, 70, 84, 98, CD20 and CD40 expression were analysed in 5, 4, 2, and 1 control animals, respectively; the number of HuMab 7D8 treated animals remained seven during the study. C, At necropsy, CD20 and CD40 expression was determined in PBMC and lymphoid organs by flow cytometry. White bars are control animals and black bars are treated animals. Cells underwent a stripping procedure to remove anti-CD20 Ab from cells. Shown are the percentages viable CD20<sup>+</sup> cells and CD40<sup>+</sup> cells that were gated from the total analysed cell number using the live/dead marker (mean ± sem). B-cells were depleted significantly from PBMC and lymphoid organs. D, CD19 mRNA expression was determined by quantitative PCR and normalized to expression levels of abelson (ABL) gene. Shown are mean ± sem. y-axis is in log-scale. CD19 mRNA expression was significantly decreased in treated animals, confirming B-cell depletion. \* p < 0.05 compared to the control group using Mann-Whitney U test.

**B-cell depletion prevents the development of clinical signs**

Six of the seven control animals developed clinically evident EAE characterized by overt neurological signs above EAE score 2 from psd 55 onward (Figure 3A). One control animal died unexpectedly at psd 33 without any detectable neurological signs (M06081). The most likely cause of death deduced from pathology examination was cardiac failure. Therefore, this monkey was excluded from further analysis. Four of the six control animals were sacrificed with at least one paralyzed limb (hemi- /paraplegia; score = 3). M02052 was sacrificed with clinical score 2.25, because of persistent optic neuritis, which started at psd 48, and excessive weight loss. M07048 was sacrificed at the predetermined end-point psd 106 after three short-lasting episodes of ataxia (Figure 3A).

In contrast, four of the seven animals treated with HuMab 7D8 failed to develop detectable neurological signs (Figure 3A). The remaining three treated animals developed neurological signs only for one day (M07075 and M07095) or two separate days (M04096). Paralysis was observed in none of the treated animals and all animals were sacrificed with clinical score 0 or 0.5 at the predetermined end-point psd 106 (Figure 3A). The curves for disease-free survival (i.e. time to EAE score 2.0) and overall survival (time to end-point) show that the clinical differences between the two groups are highly significant (Figure 3B). In conclusion, late B-cell depletion abrogated the development of neurological signs.

**B-cell depletion prevents (MRI-detectable) CNS pathology**

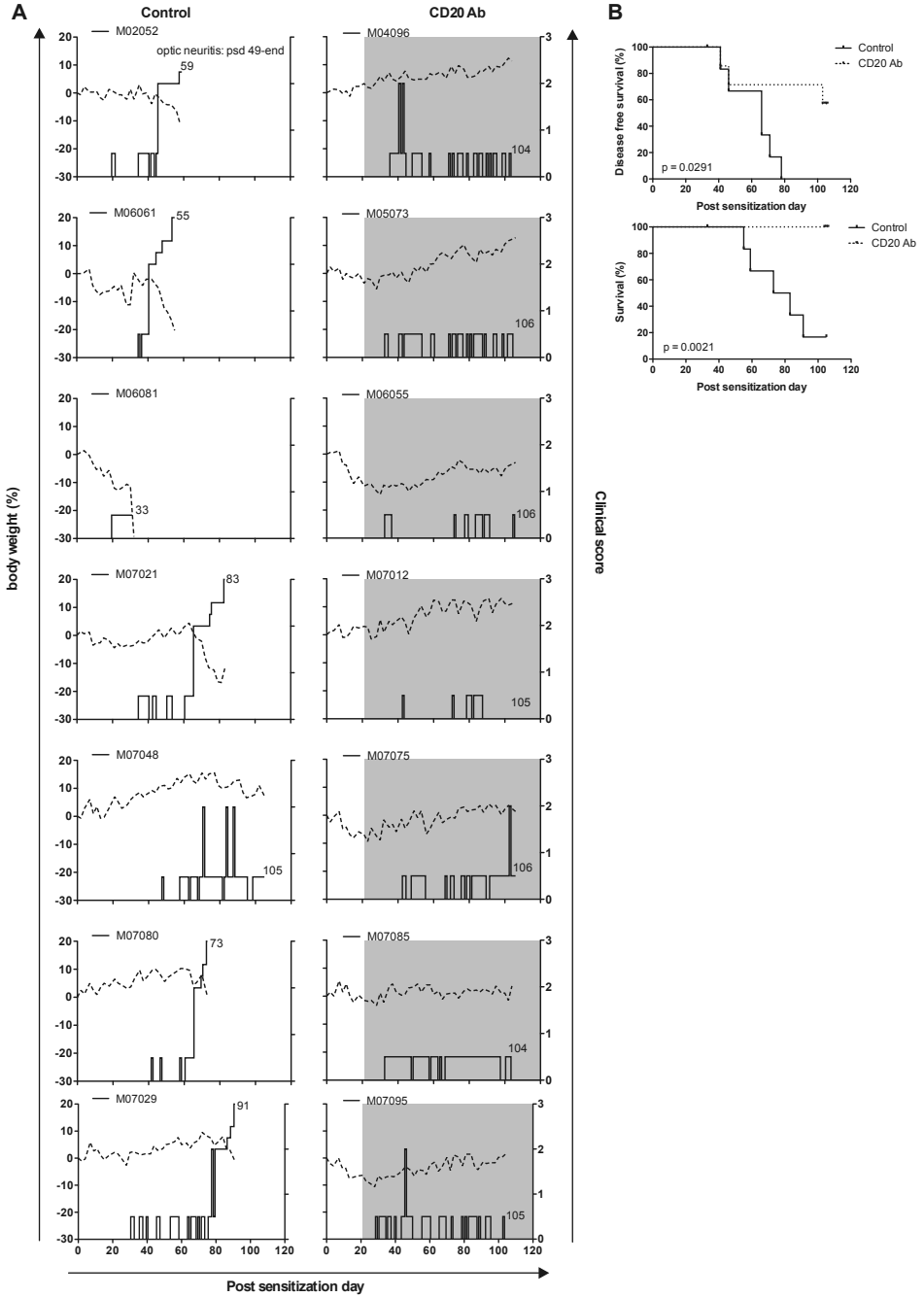
MRI sequences of fixed hemispheres were recorded to confirm that B-cell depletion not only prevented the development of neurological signs, but also of brain lesions. Figure 4A and B show representative examples of T2-weighted (T2W) images and MTR images of two control and two HuMab 7D8 treated marmosets. Figure 4C shows that the lesion load is significantly lower in the HuMab 7D8 treated group than in the control group. No lesions could be observed in three of the seven treated monkeys and only very small lesions in four of the seven treated monkeys. A lower T2 and a higher MTR of lesions in the treatment group suggest that the tissue damage was less in the HuMab 7D8 treated animals compared to the control animals (Figure 4C).

In conclusion, these data show that B-cell depletion significantly reduced EAE-associated brain pathology.

**B-cell depletion results in reduction of plasma autoantibodies**

The immunological hallmark and most widely accepted biomarker of B-cell contribution in the EAE model is the production of autoantibodies. To obtain evidence whether B-cell functionality is eliminated completely in HuMab 7D8 treated monkeys, we measured plasma levels of IgM and IgG against rhMOG and MOG54-76 every

Chapter 4.2



two weeks and at the start of the treatment. Antibodies against MOG54-76 were measured, because this peptide comprises a dominant B-cell epitope of anti-MOG Ab generated in the rhMOG-induced EAE model<sup>21</sup>. IgM levels peaked in both groups at psd 28 and declined after that (data not shown). The levels of rhMOG- or MOG54-76-specific IgG were clearly higher in the control group than in the HuMab 7D8 treated group (Figure 5A). Until psd 28, i.e. 7 days after the start of the treatment, IgG levels were comparable between both groups. After psd 28, IgG levels did not increase further in the treatment group, whereas more than a 10-fold increase was detected in the control group (Figure 5A). The area under the curves was calculated for each individual animal and group means were calculated. Figure 5B shows that IgG autoantibodies against rhMOG and MOG54-76 were significantly lower in the treatment group compared to the control group. Also at necropsy, significant reduction of autoantibodies was observed (Figure 5C).

### Effect of B-cell depletion on cell numbers, T-cell phenotype, and proliferation

To test the systemic effect of B-cell depletion on the cellular immune compartment in the marmoset EAE model, we first analysed the distribution of leukocyte and lymphocyte subsets. Figure 6A shows the variation of white blood cell, lymphocyte, neutrophil, and monocyte numbers in PBMC in both groups. Increased numbers of monocytes were observed in the treatment group (Figure 6A). At necropsy, we also observed increased absolute numbers of white blood cells, lymphocytes, neutrophils, and monocytes in the treatment group, although not significant (Figure 6B). It is of note, that the cell numbers at necropsy are determined at different/individual time points, i.e. the day each animal is sacrificed with full-blown EAE in the control group and the end of the study for treated animals.

### Figure 3. Late B-cell depletion prevents the development of neurological signs.

A, the clinical scores of control (left column) and treated (right column) animals are depicted. Post sensitization day (psd) is indicated on the x-axis. Dotted lines indicate the percentage of body weight loss compared to the day of immunization (left y-axis). Solid lines indicate clinical score (right y-axis). The treatment period is indicated with a grey-shaded box. The day of sacrifice of individual monkeys is indicated in the figure with cyphers. Monkey M06081 succumbed without neurological deficit from cardiac failure. Of the six remaining control animals five developed sustained neurological signs (clinical score  $\geq 2$ ). Control animal M07048 developed neurological signs for three independent days, but post mortem MRI analysis confirmed the presence of substantial brain white matter demyelination (Figure 4). Four of the seven HuMab 7D8 treated animals developed no neurological signs and three of the seven developed neurological signs for only one or two days. B, shows the survival curves. The upper panel shows the disease free survival, meaning the time until the animals developed EAE score 2. The lower panel is the survival time until the day of sacrifice, which was the humane or pre-determined end-point. B-cell depletion significantly increased both types of survival ( $p < 0.05$  Log Rank).

During the study and at necropsy, the phenotype of lymphocytes was analysed by flow cytometry to assess the effect of B-cell depletion on the T-cell compartment. We observed no effect on the CD3 percentage or the CD4/CD8 ratio in PBMC throughout the observation period (Figure 6C). At necropsy, however, higher percentages of CD3<sup>+</sup> cells were observed in PBMC, spleen, and lymph nodes (Figure 6D). Although we like to emphasize that this is a percentage and not an absolute number and may be caused by depletion of the B-cell population, CD3 mRNA levels were also significantly increased in the ALN (Figure 6E). The CD4/CD8 ratio was not changed in PBMC or lymphoid organs at necropsy (data not shown).

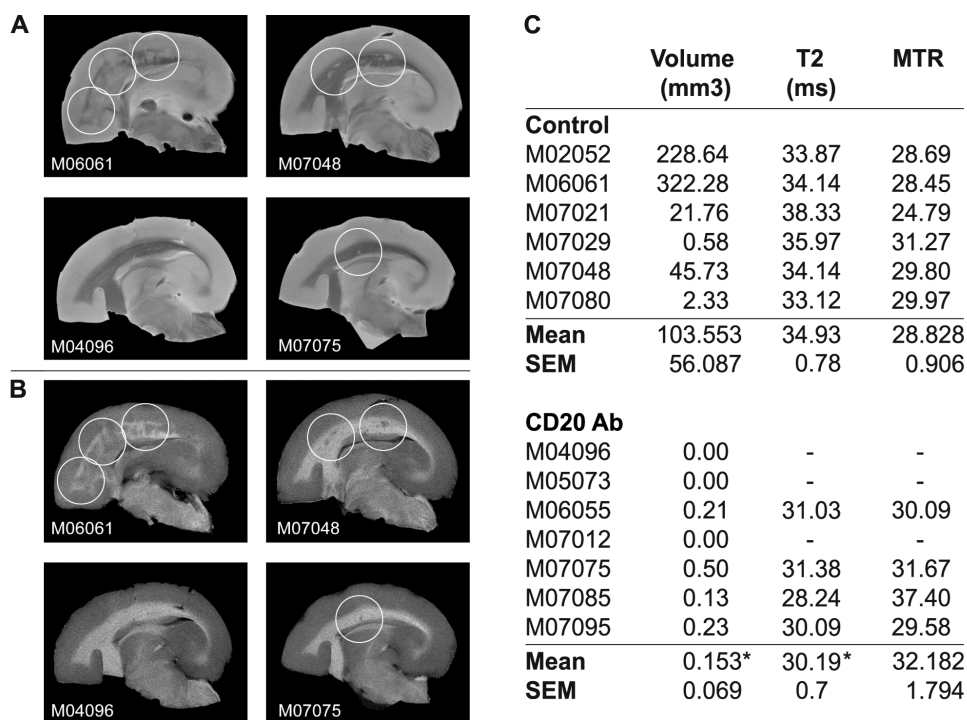


**Figure 4. Reduced cerebral white matter lesion load in B-cell depleted EAE marmosets.**

Formalin-fixed hemispheres were analysed with MRI for volume (mm<sup>3</sup>), T2 signal intensity (ms), and MTR (% reduction in signal intensity) of white matter lesions. T2W images were used to calculate the volume (mm<sup>3</sup>). Representative examples of T2W images (A) and MTR images (B) of two control and two HuMab 7D8 treated animals are shown. White lines encircle the lesions. C, B-cell depletion significantly reduced the volume of white matter lesions. Lower T2 and higher MTR within the lesions of the HuMab 7D8 treated animals suggest less damage within the lesions of treated animals. \*  $p < 0.05$  compared to the control group using Mann-Whitney U test.

Next, we analysed the effect of B-cell depletion on proliferation and cytokine production. At necropsy, we observed a higher level of proliferation in PBMC from the treatment group stimulated with rhMOG, MOG peptides 24-46 and 34-56, or ConA (Figure 7A). By contrast, the proliferative responses of MNC from monkeys in the

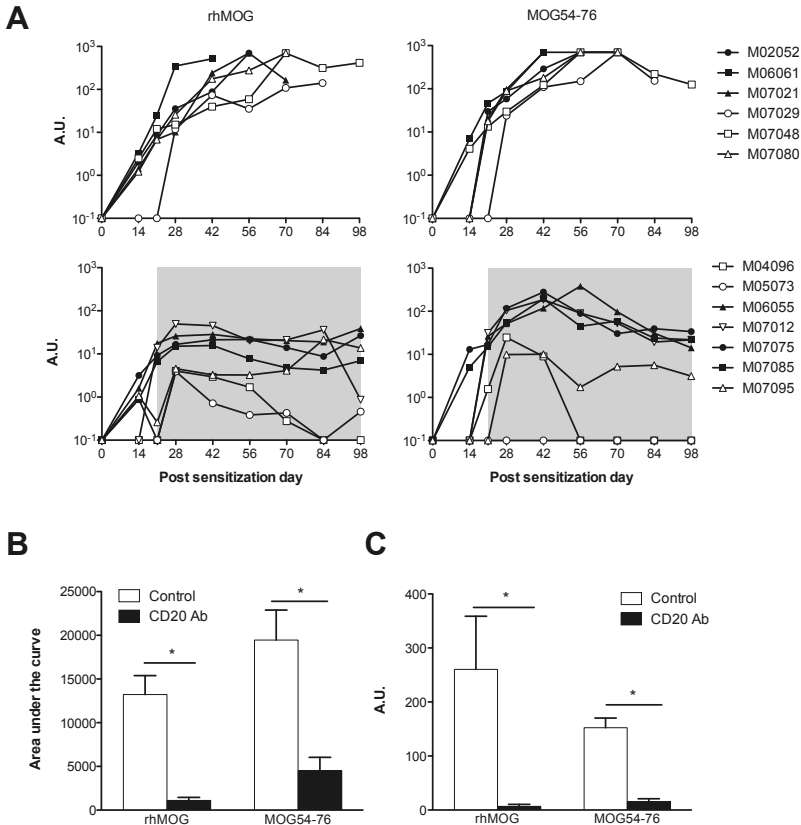


**Figure 5. Reduced plasma levels of IgG after B-cell depletion.**

Plasma IgG levels against rhMOG and MOG54-76, being the dominant binding site of anti-MOG IgG Ab, were determined by ELISA. Recorded OD values were transformed into arbitrary units (A.U., y-axis, log-scale) using home-made software. A, The upper panel shows the control animals and the lower panel shows the HuMab 7D8 treated animals with the treatment period indicated as grey-shaded box. Post sensitization day is shown on the x-axis. Shown are the IgG levels of individual animals. B, Area under the curve was calculated for each individual animal and is depicted as mean  $\pm$  sem. Plasma IgG levels against rhMOG and MOG54-76 were significantly reduced after B-cell depletion. Shown is mean  $\pm$  sem. C, Reduced IgG levels were also observed in treated animals at necropsy, which reflects peak of the disease in control animals. Results are depicted as mean  $\pm$  sem. \*  $p < 0.05$  compared to the control group using Mann-Whitney U test.

treatment group to these antigens were lower in spleen, ALN, and LLN. It is of note that also the background proliferation and the response to OVA and ConA were reduced in these organs (Figure 7A). No differences were observed in ILN or CLN (data not shown).

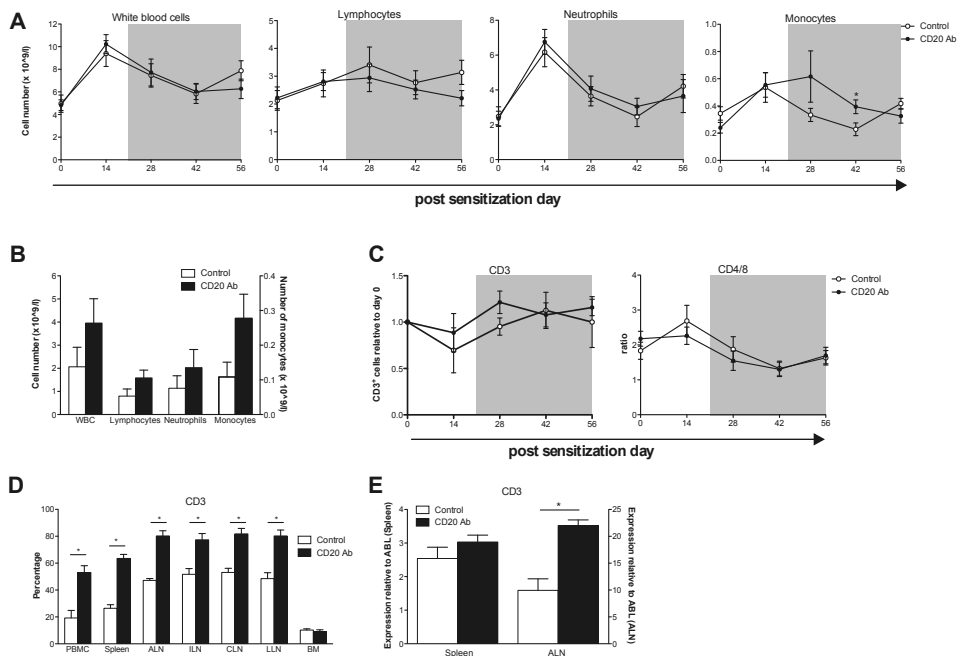


**Figure 6. Hematological effects of B-cell depletion.**

A-B, The absolute number of white blood cells, lymphocytes, neutrophils, and monocytes was determined during the study (A) and at necropsy (B). The grey-shaded box indicates the treatment period. Shown are mean  $\pm$  sem. The results of day 56 are the mean of five instead of six control animals. At psd 42, a significantly higher number of monocytes was recorded in the treatment group compared to the control group. At necropsy, higher numbers of all analysed cell types were observed in the treatment group, although differences were not significant. The higher number of lymphocytes at necropsy may be compensatory for the loss of B-cells. C, During the study the percentages of CD3<sup>+</sup> cells were analysed by flow cytometry. Shown is the change in CD3<sup>+</sup> cell frequencies relative to the day of immunization. No difference in CD3<sup>+</sup> cells or CD4/CD8 ratio was observed throughout the study. Shown are the mean  $\pm$  sem until day 56, since after psd 56 we started to take control animals out of the study. The grey-shaded area indicates the treatment period. D, At necropsy, significant increase of CD3<sup>+</sup> cell percentage was observed by flow cytometry in PBMC and secondary lymphoid organs, but not in bone marrow. E, At necropsy, CD3 mRNA expression in spleen (left y-axis) and ALN (right y-axis) was analysed by qPCR and normalized to the expression levels of abelson (ABL) gene. Shown is the mRNA expression of CD3 relative to ABL (mean  $\pm$  sem). CD3 mRNA was significantly increased in ALN, but not in spleen. \* p < 0.05 compared to the control group.

The phenotype of the cells in spleen and ALN that proliferated against rhMOG was assessed with the CFSE dilution assay. We observed that depletion of CD20<sup>+</sup> cells led to reduced proliferation of both CD4<sup>+</sup> and CD8<sup>+</sup> T-cells from ALN and, albeit to a lesser extent, from spleen (Figure 7B and data not shown).

In conclusion, the late depletion of B-cells has profound effects on the T-cell compartment. The most obvious effect observed in blood at necropsy was increment of monocyte numbers. CD3<sup>+</sup> T-cells were also increased in blood and all analysed secondary lymphoid organs. The activity assessment showed that proliferation was increased in blood but decreased in the secondary lymphoid organs.

### Reduced cytokine production after B-cell depletion

The rhMOG-induced protein levels of interleukin (IL)-12 (p40/p70), IL-17A, and IFN- $\gamma$  were analysed in supernatant of rhMOG-stimulated MNC cultures. We observed IL-17A production by splenocytes in four of the six control animals, and by MNC from

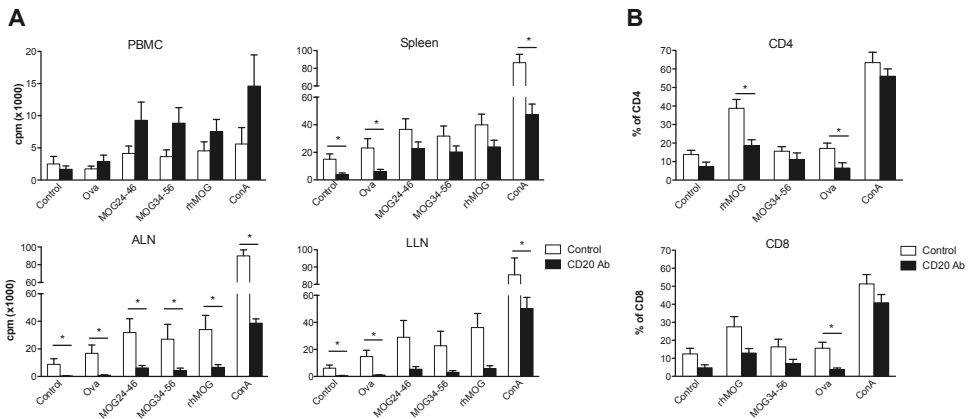


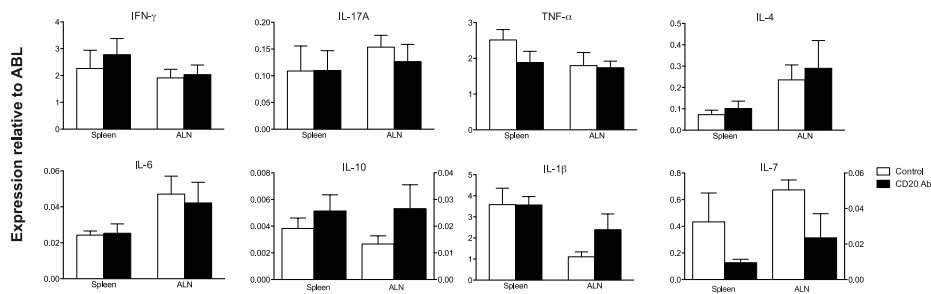
**Figure 7. Increased T-cell proliferation in blood versus reduced T-cell proliferation in lymphoid organs after B-cell depletion.**

A, Proliferation at necropsy was assessed using the incorporation of 3[H]-thymidin. Shown are the mean  $\pm$  sem in counts per minute (y-axis). Proliferation in the spleen was assessed in six of the seven HuMab 7D8 treated animals, since the spleen of M05073 could not be analysed due to small cell numbers. Proliferation in the LLN was analysed in 4 animals of each group. Increased proliferation against rhMOG and MOG peptides was observed in PBMC of treated animals. In contrast, reduced general (no stimulation, OVA, ConA) and MOG-specific proliferation was observed in lymphoid organs of treated animals. B, Shows the percentage of dividing CD3<sup>+</sup>CD4<sup>+</sup> or CD3<sup>+</sup>CD8<sup>+</sup> cells in the ALN. Percentages of total measured events are shown in mean  $\pm$  sem. Reduced proliferation against rhMOG and OVA was observed in both T-cell compartments. \* p < 0.05 compared to the control group using Mann-Whitney U test.

**A**

		IL-17A					IFN- $\gamma$					IL-12							
		PBMC	Spleen	ALN	ILN	CLN	LLN	PBMC	Spleen	ALN	ILN	CLN	LLN	PBMC	Spleen	ALN	ILN	CLN	LLN
Control	M02052		84	98			215							65	162				
	M06061								88										
	M07021		36	220			28		50	67				163	120	41	33		
	M07029																		
	M07048		31												307				
	M07080		74						28					87					
CD20 Ab	M04096														76				
	M05073								242					220	235				
	M05055														74				
	M07012													123	24,5				
	M07075		61						105					99					
	M07085																		
M07095																			

**B**



**C**

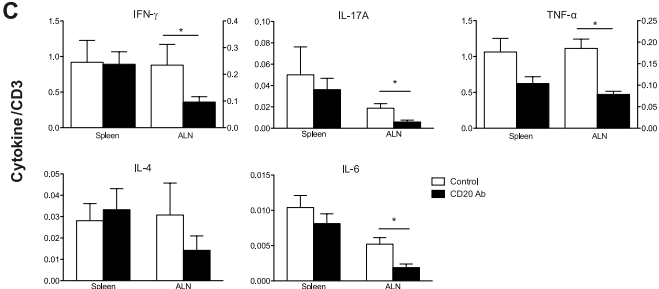


**Figure 8. Cytokine profiles in B-cell depleted and control EAE marmosets.**

A, The production of cytokine protein was determined with ELISA in supernatants of cells stimulated for 48 h with rhMOG or OVA. Shown are the cytokine concentrations (pg/ml) produced in response to rhMOG from which the OVA-induced cytokine production was subtracted. Cytokine levels in unstimulated cells were below 25 pg/ml. IL-17A was detected in four of the six control animals, but only in one of the seven treated animals. B-C, Cytokine gene transcript levels in tissue was also determined by qPCR and normalized to expression levels of abelson (ABL) gene. In the case of two y-axes, the left y-axis refers to the spleen and the right y-axis to the ALN. B, Shows the mRNA expression levels of the cytokines relative to ABL (mean  $\pm$  sem). No differences in mRNA levels of T-cell specific cytokines were observed, but IL-10 and IL-1 $\beta$  were increased in ALN of treated animals compared to controls. IL-7 mRNA levels were substantially reduced in spleen and ALN of treated animals compared to control animals. Since CD3 mRNA expression levels were significantly increased in the ALN of treated animals (Figure 6E), the levels of T-cell specific cytokines of Figure 8B were also expressed relative the CD3 mRNA levels of Figure 6E. This shows the cytokine mRNA levels per CD3 mRNA (mean  $\pm$  sem). The normalized values show in the ALN, but not in the spleen, significantly lower levels of IL-17A, IFN- $\gamma$ , TNF- $\alpha$ , and IL-6 (C). \*  $p < 0.05$  compared to the control group using Mann-Whitney U test.

ALN and LLN from 2 of the 6 control animals in response to stimulation with rhMOG. By contrast, we observed rhMOG-stimulated IL-17A production only in splenocytes of one of the seven B-cell depleted animals (Figure 8A). No such obvious differences between control and treated animals were observed for the production of IFN- $\gamma$  and IL-12 (Figure 8A).

Cytokine production in spleen and ALN was also analysed at the mRNA level. In treated animals, mRNA levels of IL-10 and IL-1 $\beta$  were increased in the ALN and IL-7 mRNA was reduced in both spleen and ALN compared to the control animals. This indicates that B-cells are an important source of IL-7 in the rhMOG-induced EAE model. No differences between treated and non-treated animals were observed for IL-17A, IFN- $\gamma$ , TNF- $\alpha$ , IL-6, and IL-4 (Figure 8B).

The data in the previous paragraph demonstrated that CD3<sup>+</sup> T-cell numbers are increased in the lymphoid organs of B-cell depleted monkeys, as was also reflected by increased CD3 mRNA levels in the ALN (Figure 6E). For this reason we chose to normalize the T-cell cytokine mRNA levels (IL-17A, IFN- $\gamma$ , TNF- $\alpha$ , IL-6, and IL-4) against CD3 instead of ABL. Indeed, the corrected data show reduced IL-17A, IFN- $\gamma$ , TNF- $\alpha$ , and IL-6 levels in the ALN of treated animals, suggesting less cytokine production per T-cell (Figure 8C).

In conclusion, the reduction of T-cell proliferation together with the reduced cytokine production in lymphoid organs indicates that the depletion of CD20<sup>+</sup> B-cells impairs the activity and/or pathogenic function of cellular autoimmune mechanisms.

### **B-cell depletion alters the composition of T-cell and B-cell areas in spleen and lymph nodes**

We have investigated in more detail the effect of B-cell depletion on the organization of spleen and ALN using haematoxylin/eosin (HE) staining and immunostaining of cryosections. The anti-CD20 Ab (clone L26) used for immunostaining recognizes an intracellular epitope of CD20<sup>35</sup>. Therefore, this Ab does not compete with the anti-CD20 Ab administered *in vivo*.

The HE staining of the spleen shows a similar structural organization in control and HuMab 7D8 treated animals. The spleen of all animals, except M04096, is composed of similar areas of white pulp (WP) and red pulp (RP) (Figure 9). In the control animals the WP consisted of T-cell and B-cell areas. In the HuMab 7D8 treated animals the WP consisted only of T-cells, even in the areas where B-cells were expected (Figure 9). M07095 showed a small area of CD20<sup>+</sup> and CD40<sup>+</sup> cells (data not shown), but in none of the other HuMab 7D8 treated animals CD20 or CD40 expressing B-cells were observed in the WP. A few CD40<sup>+</sup> cells were detected in the WP of HuMab 7D8 treated animals, but the morphology suggests that these were follicular dendritic cells or macrophages (Figure 9 insert).

The structure of the medulla and the cortex in the ALN was also similar in both groups as assessed by the HE staining (Figure 9). CD3 staining shows the normal structural organization in control animals. However, in the HuMab 7D8 treated animals the number

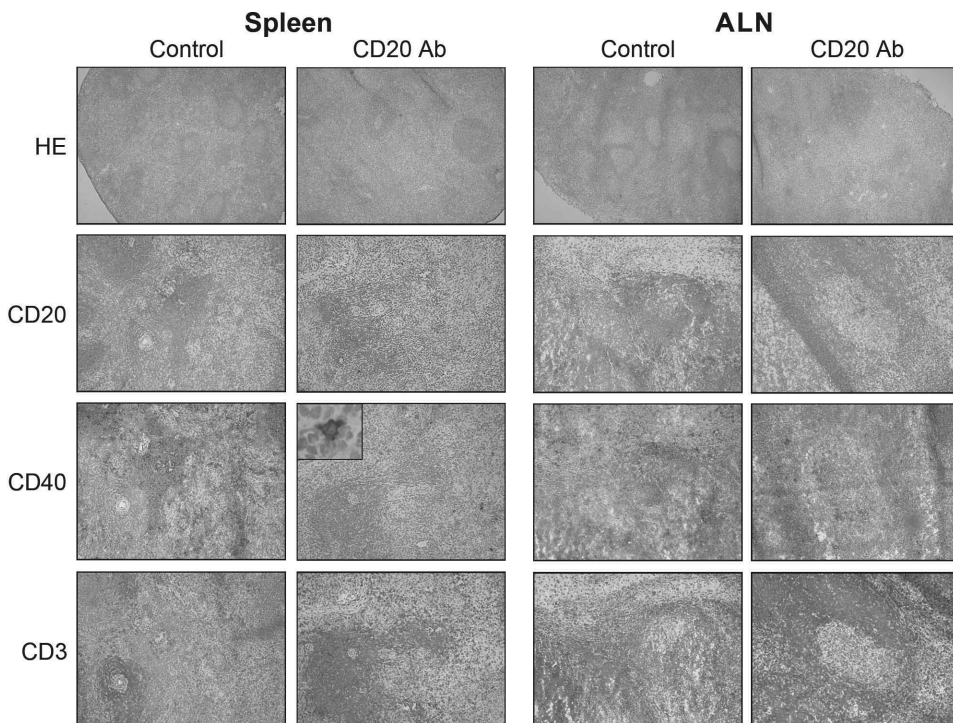


**Figure 9. Histological analysis of T-cell and B-cell areas in the spleen and ALN of B-cell depleted and control monkeys.**

Shown are representative examples of HE (original magnification x40), CD20 (original magnification x100), CD40 (original magnification x100), and CD3 (original magnification x100) staining on spleen (two left columns) and ALN (two right columns). The HE staining shows that the overall histology of the spleen and ALN was not changed by B-cell depletion. Spleen: The CD20 staining of the control animal shows a clearly demarcated B-cell area in the white pulp, which is also CD40<sup>+</sup>. CD40<sup>+</sup> cells are also present in the red pulp. The CD3 staining of the white pulp shows the CD3<sup>+</sup> T-cell area. In the B-cell depleted spleen no CD20<sup>+</sup> cells are present. A few CD40<sup>+</sup> cells are present, but these morphologically resemble follicular dendritic cells or macrophages (insert). The white pulp of the B-cell depleted animal seems to consist completely of T-cells. ALN: The ALN of the control animal contains a clearly demarcated CD20<sup>+</sup> area, which stains also CD40<sup>+</sup>. CD40<sup>+</sup> cells are also observed in the medulla. CD3<sup>+</sup> cells are confined to the T-cell areas of the cortex. In the ALN of B-cell depleted animals, the B-cell area is hypocellular with a few CD20<sup>+</sup> and CD40<sup>+</sup> cells, but the latter do not have the morphology of B-cells. The number of T-cells seems to be increased in the cortex of the ALN of B-cell depleted animals. See page 316 for a full-color representation of this figure.

of CD3<sup>+</sup> cells appeared to be increased in the cortex (Figure 9), which is in line with the increased CD3 mRNA expression (Figure 6E). A few CD20<sup>+</sup> cells were observed in M07075 and M07095, but in the other five HuMab 7D8 treated animals no CD20 staining was found. CD40 was detected in B-cell areas of the ALN of both control and HuMab 7D8 treated animals. However, in the HuMab 7D8 treated animals we observed that the B-cell areas were hypocellular compared to control animals. Furthermore, flow cytometry showed a reduced number of B-cells and also the morphology of the CD40<sup>+</sup> cells suggested that these cells were not B-cells.

These data demonstrate that the general structure of secondary lymphoid organs is not changed by B-cell depletion. In the spleen, the B-cell areas appeared to be filled with T-cells. In the ALN, T-cell numbers seemed to be increased in the T-cell areas and the B-cell areas were hypocellular and only contained CD40<sup>+</sup> non-B-cells.

## DISCUSSION

Clinical trials with a chimeric CD20 mAb have shown that depletion of B-cells has beneficial effects in RRMS, while autoantibody levels were unaffected<sup>2,3</sup>. This observation has raised questions on the exact immunopathogenic role of B-cells in MS. We have investigated in a non-human primate model of MS, i.e. EAE in the common marmoset, which immunopathogenic mechanisms are altered by B-cell depletion. As the chimeric anti-CD20 mAb (rituximab) does not cross-react with marmoset CD20 we used the fully human CD20 mAb HuMab 7D8<sup>25,26</sup>. In the first part of the current study, we have analysed the extent and duration of B-cell depletion after a single i.v. dose of HuMab 7D8 at 10 or 20 mg/kg. The results demonstrate the high potency of HuMab 7D8 in the marmoset as it induced profound and long-lasting depletion of B-cells from peripheral blood as well as lymphoid organs. In the second part of the study we have chosen a dosing regimen with a high loading dose of 20 mg/kg HuMab 7D8 for obtaining a robust B-cell depletion and thereby lowering the risk of inducing neutralizing Ab, followed by a 4-fold lower weekly maintenance dose at 5 mg/kg for maintaining maximum efficacy. The data show that the applied dosing schedule completely abrogated the typical MS-like clinical and pathological signs of this EAE model. This demonstrates the high *in vivo* efficacy of the Ab in this model and emphasizes the important role of B-cells in MS.

We observed substantially lower levels of rhMOG-specific IgG in marmosets treated with HuMab 7D8 compared to control animals, although the early stage production of IgM autoantibodies was unaffected. It is important to note that at the time that the HuMab 7D8 treatment was started, i.e. 21 days after immunization, the production of anti-MOG IgG production had already been initiated but had not reached peak levels. Peak levels of IgG autoantibody in the control group were reached about three weeks

later. The reported data suggest that the HuMab 7D8 treatment did not completely suppress anti-MOG IgG production but rather arrested the further increased production of anti-MOG IgG. The effect of B-cell depletion on autoantibody production in MS is unknown. Interestingly, in systemic lupus erythematosus (SLE) patients treatment with rituximab led to suppression of IgG autoantibody production, whereas no effect was observed on total IgG serum levels<sup>36</sup>.

The question is warranted whether the dramatic effect of HuMab 7D8 treatment on clinical scores and lesion formation in the marmoset EAE model can be completely attributed to the observed reduction of autoantibody levels. Previous research has shown that the EAE development in marmosets immunized with rhMOG in CFA involves the activation of cellular and humoral autoimmune mechanisms<sup>32</sup>. However, we would like to emphasize that autoantibodies do not have an essential influence on the EAE course, as lesions and neurological signs develop also in the absence of anti-MOG antibodies<sup>20-22</sup>. This is compatible with the finding that axonal injury in lesions is more linked to the presence of inflammation than of demyelination<sup>37</sup>. We like to postulate here that although the capacity of anti-MOG antibodies to amplify demyelination and mild clinical signs in the marmoset EAE model has been clearly demonstrated<sup>14,38</sup>, they are not an indispensable factor in the immunopathogenic process.

The current study shows that depletion of CD20<sup>+</sup> B-cells induced a few changes in peripheral blood, i.e. increased number of monocytes and increased proliferation of MNC against rhMOG and MOG peptides. A more profound effect was found in the lymphoid organs. The histological analysis of spleen and lymph nodes demonstrated that B-cell depletion dramatically altered the relative proportions of B-cells and T-cells. Where the complete depletion was expected, we had not anticipated the increase of T-cells. It can be assumed safely that the altered T/B ratio changes the environmental conditions under which the activation of the MOG34-56-reactive T-cells, which mediate the expression of neurological deficit, occurs<sup>21,22</sup>. The immune profiling of spleen and lymph nodes indeed confirmed that although these organs contain higher percentages of CD3<sup>+</sup> T-cells, proliferation of MOG (peptide)-reactive T-cells is impaired and cytokine production is skewed towards a more anti-inflammatory profile characterized by reduced IL-17A and IFN- $\gamma$  and increased IL-10. The strong reduction of IL-7 production in the B-cell depleted monkeys may be of particular interest as this is a crucial cytokine for the survival of IL-17A producing T-cells, which are thought to have a central pathogenic role in MS and EAE models<sup>39</sup>, including the EAE model in marmosets<sup>22</sup>. Impairment of T-cell activation has been put forward as a possible explanation for the clinical effect of B-cell depletion in RRMS<sup>2,3</sup>. Reduced T-cell activity after B-cell depletion has been observed in various experimental systems including naive mice, NOD mice, two mouse models for arthritis, and mice infected with *Listeria monocytogenes*<sup>40,41</sup>. Taken together, these data suggests that

the beneficial effect of systemic B-cell depletion may be mediated by mitigated T-cell activation in lymphoid organs.

In view of recent data on the pathogenic function of intra-CNS localized EBV-infected B-cells in MS<sup>42</sup>, although not confirmed by others<sup>43,44</sup>, it is tempting to speculate whether the clinical effect of the anti-CD20 Ab can be explained by the depletion of B-cells from the CNS. Several lines of evidence indicate that MOG34-56-specific T-cells, which have a key role in the clinical expression of EAE in marmosets, can be activated *ex vivo* by EBV-transformed B-cells<sup>21,22</sup>(Haanstra et al., manuscript in prep). Indeed, we have observed that the CD20<sup>+</sup> cells that are clearly present in the CNS of EAE-affected control marmosets cannot be detected in the anti-CD20 Ab-treated monkeys (not shown). We cannot exclude, however, that this is due to masking of CD20 by the therapeutic Ab. CD40 expression cannot be used as control, as this marker is strongly upregulated in the EAE-affected CNS and Ab for human CD19 do not cross-react with the marmoset counterpart<sup>45</sup>.

In conclusion, we have shown that B-cell depletion in the marmoset EAE model mitigated the activation of autoreactive T-cells. We like to postulate that this reduction in T-cell activation contributes to the remarkable clinical effect of B-cell depletion and we hypothesize that a similar T-cell change occurs in MS. It is difficult to prove this directly in MS patients since the T-cell activity in lymphoid organs cannot be examined. Current clinical trials support the idea that B-cell depletion is a major step in therapy development for RRMS patients. Future studies are warranted to elucidate further the antigen presenting function of B-cells, especially in the CNS, and to further investigate the organization of lymphoid organs after B-cell depletion.

## ACKNOWLEDGEMENTS

The authors like to thank Fred Batenburg, Mariska van Etten, and Martine Hoffmann for excellent biotechnical assistance and daily care of the monkeys, Jaco Bakker DVM, Gerco Braskamp DVM, and Merei Keehnen DVM for expert veterinary care, Tom Haaksma and Dr. Ivanela Kondova for autopsy of the monkeys. The authors thank Marjan van Meurs for help with *in situ* analysis, and Henk van Westbroek for the artwork.

## REFERENCES

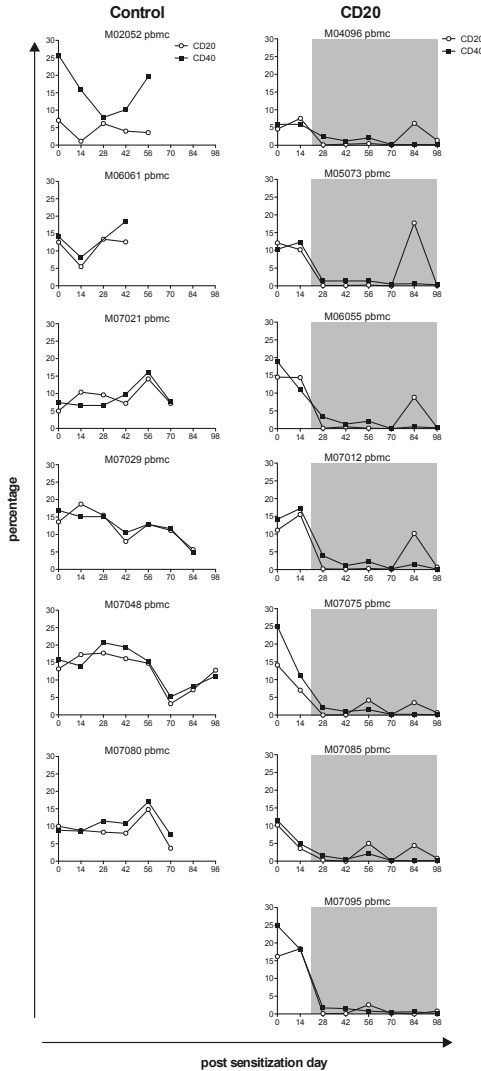
1. Stuve O et al. Clinical stabilization and effective B-lymphocyte depletion in the cerebrospinal fluid and peripheral blood of a patient with fulminant relapsing-remitting multiple sclerosis. *Arch Neurol* 62:1620-1623 (2005)
2. Bar-Or A et al. Rituximab in relapsing-remitting multiple sclerosis: a 72-week, open-label, phase I trial. *Ann Neurol* 63:395-400 (2008)
3. Hauser SL et al. B-cell depletion with rituximab in relapsing-remitting multiple sclerosis. *N Engl J Med* 358:676-688 (2008)
4. Hawker K et al. Rituximab in patients with primary progressive multiple sclerosis: Results of a randomized double-blind placebo-controlled multicenter trial. *Ann Neurol* 66:460-471 (2009)
5. Monson NL et al. Effect of rituximab on the peripheral blood and cerebrospinal fluid B cells in patients with primary progressive multiple sclerosis. *Arch Neurol* 62:258-264 (2005)
6. Cross AH et al. Rituximab reduces B cells and T cells in cerebrospinal fluid of multiple sclerosis patients. *J Neuroimmunol* 180:63-70 (2006)
7. Martin Mdel P et al. Depletion of B lymphocytes from cerebral perivascular spaces by rituximab. *Arch Neurol* 66:1016-1020 (2009)
8. Noseworthy JH et al. Multiple sclerosis. *N Engl J Med* 343:938-952 (2000)
9. Brehm U et al. Epitope specificity of demyelinating monoclonal autoantibodies directed against the human myelin oligodendrocyte glycoprotein (MOG). *J Neuroimmunol* 97:9-15 (1999)
10. Zhou D et al. Identification of a pathogenic antibody response to native myelin oligodendrocyte glycoprotein in multiple sclerosis. *Proc Natl Acad Sci USA* 103:19057-19062 (2006)
11. Haase CG et al. The fine specificity of the myelin oligodendrocyte glycoprotein autoantibody response in patients with multiple sclerosis and normal healthy controls. *J Neuroimmunol* 114:220-225 (2001)
12. Morris-Downes MM et al. Pathological and regulatory effects of anti-myelin antibodies in experimental allergic encephalomyelitis in mice. *J Neuroimmunol* 125:114-124 (2002)
13. Lington C et al. Augmentation of demyelination in rat acute allergic encephalomyelitis by circulating mouse monoclonal antibodies directed against a myelin/oligodendrocyte glycoprotein. *Am J Pathol* 130:443-454 (1988)
14. Genain CP et al. Antibody facilitation of multiple sclerosis-like lesions in a nonhuman primate. *J Clin Invest* 96:2966-2974 (1995)
15. Lucchinetti C et al. Heterogeneity of multiple sclerosis lesions: implications for the pathogenesis of demyelination. *Ann Neurol* 47:707-717 (2000)
16. Serafini B et al. Detection of ectopic B-cell follicles with germinal centers in the meninges of patients with secondary progressive multiple sclerosis. *Brain Pathol* 14:164-174 (2004)
17. Magliozzi R et al. Meningeal B-cell follicles in secondary progressive multiple sclerosis associate with early onset of disease and severe cortical pathology. *Brain* 130:1089-1104 (2007)
18. 't Hart BA et al. Modelling of multiple sclerosis: lessons learned in a non-human primate. *Lancet Neurol* 3:588-597 (2004)
19. Kap YS et al. Experimental Autoimmune Encephalomyelitis in the Common Marmoset, a Bridge Between Rodent EAE and Multiple Sclerosis for Immunotherapy Development. *J Neuroimmune Pharmacol* 5:220-230 (2010)
20. Jagessar SA et al. Autoimmunity against myelin oligodendrocyte glycoprotein is dispensable for the initiation although essential for the progression of chronic encephalomyelitis in common marmosets. *J Neuropathol Exp Neurol* 67:326-340 (2008)
21. Kap YS et al. Fast progression of recombinant human myelin/oligodendrocyte glycoprotein (MOG)-induced experimental autoimmune encephalomyelitis in marmosets is associated with the activation of MOG34-56-specific cytotoxic T cells. *J Immunol* 180:1326-1337 (2008)

22. Jagessar SA et al. Induction of progressive demyelinating autoimmune encephalomyelitis in common marmoset monkeys using MOG34-56 peptide in incomplete Freund adjuvant. *J Neuropathol Exp Neurol* 69:372-385 (2010)
23. Vergelli M et al. A novel population of CD4<sup>+</sup>CD56<sup>+</sup> myelin-reactive T cells lyses target cells expressing CD56/neural cell adhesion molecule. *J Immunol* 157:679-688 (1996)
24. Van der Aa A et al. Functional properties of myelin oligodendrocyte glycoprotein-reactive T cells in multiple sclerosis patients and controls. *J Neuroimmunol* 137:164-176 (2003)
25. Teeling JL et al. Characterization of new human CD20 monoclonal antibodies with potent cytolytic activity against non-Hodgkin lymphomas. *Blood* 104:1793-1800 (2004)
26. Teeling JL et al. The biological activity of human CD20 monoclonal antibodies is linked to unique epitopes on CD20. *J Immunol* 177:362-371 (2006)
27. Beum PV et al. Complement activation on B lymphocytes opsonized with rituximab or ofatumumab produces substantial changes in membrane structure preceding cell lysis. *J Immunol* 181:822-832 (2008)
28. Ruuls SR et al. Novel human antibody therapeutics: the age of the Umabs. *Biotechnol J* 3:1157-1171 (2008)
29. Kerlero de Rosbo N et al. Predominance of the autoimmune response to myelin oligodendrocyte glycoprotein (MOG) in multiple sclerosis: reactivity to the extracellular domain of MOG is directed against three main regions. *Eur J Immunol* 27:3059-3069 (1997)
30. 't Hart BA et al. Preclinical assessment of therapeutic antibodies against human CD40 and human interleukin-12/23p40 in a nonhuman primate model of multiple sclerosis. *Neurodegener Dis* 5:38-52 (2008)
31. Blezer EL et al. Quantitative MRI-pathology correlations of brain white matter lesions developing in a non-human primate model of multiple sclerosis. *NMR Biomed* 20:90-103 (2007)
32. Brok HP et al. Myelin/oligodendrocyte glycoprotein-induced autoimmune encephalomyelitis in common marmosets: the encephalitogenic T cell epitope pMOG24-36 is presented by a monomorphic MHC class II molecule. *J Immunol* 165:1093-1101 (2000)
33. Beillard E et al. Evaluation of candidate control genes for diagnosis and residual disease detection in leukemic patients using 'real-time' quantitative reverse-transcriptase polymerase chain reaction (RQ-PCR) - a Europe against cancer program. *Leukemia* 17:2474-2486 (2003)
34. Bleeker WK et al. Estimation of dose requirements for sustained *in vivo* activity of a therapeutic human anti-CD20 antibody. *Br J Haematol* 140:303-312 (2008)
35. Mason DY et al. Antibody L26 recognizes an intracellular epitope on the B-cell-associated CD20 antigen. *Am J Pathol* 136:1215-1222 (1990)
36. Vallerskog T et al. Treatment with rituximab affects both the cellular and the humoral arm of the immune system in patients with SLE. *Clin Immunol* 122:62-74 (2007)
37. Mancardi G et al. Demyelination and axonal damage in a non-human primate model of multiple sclerosis. *J Neurol Sci* 184:41-49 (2001)
38. McFarland HI et al. Determinant spreading associated with demyelination in a nonhuman primate model of multiple sclerosis. *J Immunol* 162:2384-2390 (1999)
39. Liu X et al. Crucial role of interleukin-7 in T helper type 17 survival and expansion in autoimmune disease. *Nat Med* 16:191-197 (2010)
40. Bouaziz JD et al. Therapeutic B cell depletion impairs adaptive and autoreactive CD4<sup>+</sup> T cell activation in mice. *Proc Natl Acad Sci USA* 104:20878-20883 (2007)
41. Hamel K et al. Suppression of Proteoglycan-Induced Arthritis by Anti-CD20 B Cell Depletion Therapy Is Mediated by Reduction in Autoantibodies and CD4<sup>+</sup> T Cell Reactivity. *J Immunol* 180:4994-5003 (2008)
42. Serafini B et al. Dysregulated Epstein-Barr virus infection in the multiple sclerosis brain. *J Exp Med* 204:2899-2912 (2007)

## Chapter 4.2

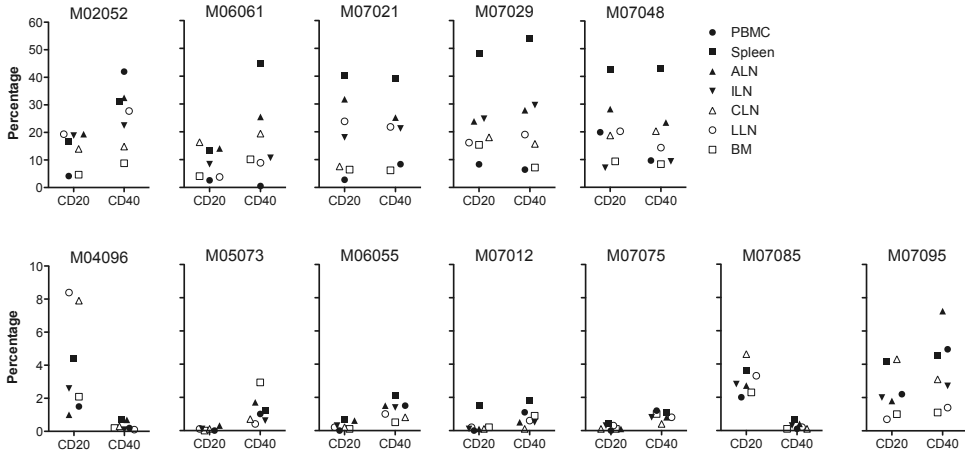
43. Willis SN et al. Epstein-Barr virus infection is not a characteristic feature of multiple sclerosis brain. *Brain* 132:3318-3328 (2009)
44. Sargsyan SA et al. Absence of Epstein-Barr virus in the brain and CSF of patients with multiple sclerosis. *Neurology* 74:1127-1135 (2010)
45. Kap YS et al. A monoclonal antibody selection for immunohistochemical examination of lymphoid tissues from non-human primates. *J Histochem Cytochem* 57:1159-1167 (2009)

SUPPLEMENTAL FIGURES



**Supplemental figure 1. B-cells are depleted from PBMC after treatment with HuMab 7D8.** CD20 and CD40 expression in PBMC was determined by flow cytometry every two weeks. Shown are the percentages of living CD20<sup>+</sup> (open symbols) and CD40<sup>+</sup> (closed symbols) cells of total measured cells. The left column are control animals, the right column are animals treated with HuMab 7D8, which was started 21 days after immunization. The treatment period is indicated as grey-shaded box. CD20 was not removed with the stripping procedure, because the number of available PBMC was too small. CD40 was used to confirm B-cell depletion.

Chapter 4.2



**Supplemental figure 2. B-cells are depleted from PBMC and lymphoid organs after treatment with HuMab 7D8.**

CD20 and CD40 expression in PBMC and lymphoid organs was determined by flow cytometry at necropsy. Shown are the percentages of living CD20<sup>+</sup> and CD40<sup>+</sup> cells of total measured cells. HuMab 7D8 was removed by a stripping procedure before flow cytometry staining. The upper row are control animals, the lower row are animals treated with HuMab 7D8, which was started 21 days after immunization. Note that the scale of the y-axis differs between the control and HuMab 7D8-treated animals. ALN, axillary lymph node (LN); ILN, inguinal LN; CLN, cervical LN; LLN, lumbar LN; BM, bone marrow.

# 4.3

## **Late CD20<sup>+</sup> B-cell depletion attenuates demyelination in the CNS white and grey matter of EAE-affected marmoset monkeys**

Yolanda S. Kap<sup>1,2,3</sup>, Jan Bauer<sup>4</sup>, Nikki van Driel<sup>1</sup>, Paul W.H.I. Parren<sup>5</sup>,  
Wim K. Bleeker<sup>5</sup>, Jon D. Laman<sup>2,3</sup>, Jenny L. Craigen<sup>6</sup>, Erwin Blezer<sup>7</sup> and  
Bert A. 't Hart<sup>1,2,3</sup>

<sup>1</sup>Department of Immunobiology, Biomedical Primate Research Centre, Rijswijk, The Netherlands; <sup>2</sup>Department of Immunology, Erasmus Medical Centre, Rotterdam, The Netherlands; <sup>3</sup>MS Centre ErasMS, Rotterdam, The Netherlands; <sup>4</sup>Brain Research Institute, University of Vienna, Austria; <sup>5</sup>Genmab, Utrecht, The Netherlands; <sup>6</sup>GlaxoSmithKline Discovery, BioPharm R&D, Stevenage, United Kingdom; <sup>7</sup>Image Sciences Institute, University Medical Center Utrecht, Utrecht, The Netherlands

*EB and BAH share senior authorship*

*Manuscript in preparation*



## ABSTRACT

This study aimed at investigating the effect of CD20<sup>+</sup> B-cell depletion on central nervous system grey and white matter demyelination in a relevant preclinical model of multiple sclerosis, i.e. experimental autoimmune encephalomyelitis (EAE) in common marmosets. EAE was induced in thirteen marmosets by immunization with myelin oligodendrocyte glycoprotein formulated in CFA. At 21 days post-immunization, B-cell depletion was induced by weekly treatment with HuMab 7D8, a human-anti-human CD20 antibody cross-reacting with marmoset CD20. *In vivo* MRI showed widespread brain white matter demyelination in control animals, which was absent in HuMab 7D8 treated animals. High-contrast post mortem MRI showed white matter lesions in four of seven HuMab 7D8 treated animals, but these were significantly smaller than in controls. The same technique revealed grey matter lesions in five of six control animals, while these were absent in HuMab 7D8 treated animals. Histology confirmed that inflammation and demyelination were substantially reduced in brain, spinal cord, and optic nerve of HuMab 7D8 treated monkeys. In conclusion, CD20<sup>+</sup> B-cell depletion by HuMab 7D8 profoundly reduced the development of grey and white matter pathology in the marmoset CNS. These data underline the central pathogenic role of B-cells in the induction of CNS pathology in the model.

## INTRODUCTION

Multiple sclerosis (MS) is a chronic autoimmune neurological disease characterized by inflammation and demyelination in the white matter (WM) and grey matter (GM) of the central nervous system (CNS)<sup>1,2</sup>. It is widely accepted that CNS pathology is caused by an autoimmune attack mediated by CD4<sup>+</sup> and CD8<sup>+</sup> T-cells, macrophages, and autoantibodies<sup>3</sup>. Recent studies have highlighted a prominent pathogenic role of B-cells in MS, which could not be explained by removal of the source of autoantibody production, suggesting other pathogenic mechanisms mediated by B-cells<sup>4,5</sup>. Depletion of B-cells with the chimeric CD20 monoclonal antibody rituximab reduced the relapse rate in patients with relapsing-remitting MS (RRMS)<sup>4-6</sup>. The remarkable clinical effect of B-cell depletion in RRMS was supported by the demonstration with magnetic resonance imaging (MRI) that the total number and volume of T2 lesions and the number of new gadolinium-enhancing brain WM lesions were reduced<sup>4,5</sup>.

The current study was undertaken to obtain proof-of-principle that B-cells are a valid target for antibody-mediated therapy aiming at the prevention of injury in the CNS WM as well as GM. We have investigated this in a valid preclinical MS model, i.e. experimental autoimmune encephalomyelitis (EAE) in common marmosets<sup>7,8</sup>.

This model is characterized by MS-like pathology affecting both WM and GM<sup>9,10</sup>. The experiment comprised two groups of monkeys in which progressive EAE was induced by a single immunization with rhMOG in CFA. In one group depletion of CD20<sup>+</sup> B-cells was induced at 21 days post-immunization using a human-anti-human CD20 antibody (HuMab 7D8)<sup>11,12</sup>. This induced profound and long-lasting depletion of CD20<sup>+</sup> B-cells from the circulation and lymphoid organs of marmosets (Kap et al., J Immunol, in press). The second group received placebo-treatment with an equivalent volume of phosphate buffered saline (PBS). Treatment was started late to model intervention in an ongoing immunopathogenic process, while achieving complete B-cell depletion before disease onset in early EAE responders<sup>13</sup>.

The immunological changes caused by CD20<sup>+</sup> B-cell depletion are reported separately (Kap et al., J Immunol, in press). Here, we report the dramatic effect on CNS pathology, i.e. that antibody-mediated depletion of CD20<sup>+</sup> B-cells profoundly reduced lesion development in the WM as well as the GM of the brain as assessed with MRI and histology. Also in the spinal cord and in the optic nerve of HuMab 7D8 treated monkeys we observed a significantly reduced intensity of inflammation and demyelination. These data support the central pathogenic role of B-cells in a valid preclinical model of MS and contribute to a better understanding of the therapeutic action of B-cell depleting monoclonal antibodies.

## **MATERIALS AND METHODS**

### **Animals**

Fourteen healthy adult common marmoset monkeys used in this study were randomly selected from the outbred colony kept at the Biomedical Primate Research Centre (Rijswijk, The Netherlands) (for individual data see Table 1). Only animals that were declared healthy after the veterinarian's physical, hematological, and biochemical check-up were included. The average body weights of the monkeys did not differ between the control and treatment group and was 367±30 gram and 332±41 gram, respectively. The monkeys were pair-housed under conventional conditions in spacious cages and were under intensive veterinary care throughout the study. The daily diet consisted of commercial food pellets for New World monkeys (Special Diet Services, Witham, Essex, UK), supplemented with raisins, marshmallows, biscuits, and fresh fruit. Drinking water was provided *ad libitum*. According to the Dutch law on animal experimentation, all study protocols and experimental procedures have been reviewed and approved by the Institute's Ethics Committee.

**RhMOG-induced EAE**

EAE was induced with a recombinant protein encompassing the extracellular domain of human MOG produced in *Escherichia coli* (residues 1-125; rhMOG) and purified as previously described<sup>14</sup>. The inoculum contained 100 µg rhMOG in 300 µl PBS emulsified with 300 µl complete Freund's adjuvant (CFA, containing *Mycobacterium butyricum*; Difco Laboratories, Detroit, MI). The emulsion was injected at four locations into the dorsal skin under alfaxalone anesthesia (10 mg/kg; alfaxan; Vetoquinol, Den Bosch, The Netherlands).

Clinical signs were scored daily by two independent observers using a previously described semi-quantitative scale<sup>15</sup>. Briefly, 0 = no clinical signs; 0.5 = apathy, altered walking pattern without ataxia; 1 = lethargy, tail paralysis, tremor; 2 = ataxia, optic

**Table 1. Overview of monkeys and their clinical score.**

Monkey	Pair	Sex <sup>a</sup>	Age <sup>b</sup>	Body weight <sup>c</sup>	Post sensitization day		
					Score 2	Score 3	End
Control							
M02052	1	M	84	307	46	-	59
M06061	2	M	31	306	41	54	55
M06081 <sup>d</sup>		M	28	283	-	-	33
M07021	3	M	24	339	66	83	83
M07029	4	M	24	377	78	91	91
M07048	5	M	21	316	71 <sup>e</sup> , 84 <sup>e</sup> , 88 <sup>e</sup>	-	105
M07080	6	M	20	322	66	73	73
CD20 Ab							
M04096	1	M	56	308	41 <sup>e</sup> , 43 <sup>e</sup>	-	104
M05073	2	M	43	430	-	-	106
M06055 <sup>d</sup>	2	M	31	333	-	-	106
M07012	3	M	26	330	-	-	105
M07075	4	M	21	374	103 <sup>e</sup>	-	106
M07085	5	M	20	273	-	-	104
M07095	6	M	19	347	46 <sup>e</sup>	-	105

<sup>a</sup> F, Female; M, Male

<sup>b</sup> Age in months at the start of the experiment

<sup>c</sup> Body weight (gram) at start experiment

<sup>d</sup> M06081 died on psd 33 without EAE. M06055 was added to pair 2 for MRI analysis

<sup>e</sup> Score 2 for 1 day

Survival time to score 2: p=0.0291; survival time to sacrifice with clinical signs: p=0.0021

disease; 2.25 = monoparesis; 2.5 = paraparesis, sensory loss; 3 = para- or hemiplegia. For ethical reasons monkeys were sacrificed once complete paralysis of hind-limbs (score  $\geq 3.0$ ) was observed, or at the pre-determined endpoint of the study, which was arbitrarily set at post sensitization day (psd) 106.

### **CD20 treatment**

HuMab 7D8 is a human IgG1 $\kappa$  monoclonal antibody (mAb) directed against human CD20<sup>11,12</sup> that cross-reacts with marmoset CD20 (data not shown). Seven marmosets received a single i.v. dose of 20 mg/kg HuMab 7D8 at psd 21 to induce robust B-cell depletion from blood and lymph nodes. To maintain plasma trough levels of HuMab 7D8 above 5-10  $\mu\text{g/ml}$ <sup>16</sup>, 5 mg/kg was administered i.v. every week. The seven control animals received 1 ml/kg sterile PBS (Table 1).

### ***In vivo* MRI**

T2 images are highly sensitive to the increased water content in lesions caused by vasogenic edema. The MTR value of a tissue is calculated from the ration of free and lattice-bound protons, Hence, reduction of MTR value of a tissue occurs when the tissue water content increases (inflammation) and when the density of tissue macromolecules decreases, such as by demyelination. T1-weighted (T1W) images were recorded to visualize active lesions with a more permeable blood-brain barrier. Increase of the T1W signal intensity by intravenously administered Gadolinium containing contrast agent (Gadovist), occurs when the paramagnetic probe leaks through the blood-brain barrier, which is more permeable by local production of inflammatory mediators.

Experiments were performed using a 4.7 T horizontal bore NMR spectrometer (Varian, Palo Alto, CA). After sedation with alfaxalone anesthesia (10 mg/kg; alfaxan; Vetoquinol, Den Bosch, The Netherlands) the animals were prepared for mechanical ventilation by an endotracheal intubation. A tail vein was cannulated for administration of a bolus of Gadovist (gadobutrol, Gd-BT-DO3A, Bayer Schering Pharma AG, Leverkusen, Germany).

Animals were immobilized in a specially designed stereotactic holder and placed in an animal cradle, which was inserted into the NMR spectrometer. During MR-experiments the animals were ventilated with isoflurane (1-2%) in N<sub>2</sub>O/O<sub>2</sub> (70/30). Expiratory CO<sub>2</sub> was monitored, and the body temperature was maintained at 37°C with a heated water pad. An infrared sensor (Nonin Medical Inc, Plymouth, Minnesota, USA) was attached to the animal hind paw for monitoring of heart rate and blood oxygen saturation. A homebuilt Helmholtz volume coil ( $\varnothing$  85 mm) and a self-made inductively coupled surface coil ( $\varnothing$  35 mm) were used for radio frequency (RF) transmission and signal reception, respectively.

On a sagittal scout image, 35 contiguous coronal slices of 1 mm were defined

covering the complete brain with the following characteristics: field of view, 40x40 mm; matrix, 128 x 128; zero-filled, 256 x 256; voxel volume,  $97 \times 10^{-3} \text{ mm}^3$ , two transitions. From these slices the following MRI data sets were collected (total duration of the experiments ~1.5 hrs):

- $T_2$  maps [ms]. Maps were obtained by a mono-exponential fit of five multi-echo images. TR, 2850 ms; TE, 15 + 4x15 ms. The second image in this series, i.e. TE, 30 ms, was used for Regions of Interest (ROI) determination.
- Magnetization Transfer Ratio (MTR) maps [% decrease in signal intensity]. Maps were calculated from two T1W gradient echo images with and without a MT-saturation pulse, with  $MTR = 100 * ((M_{\text{unsaturated}} - M_{\text{saturated}}) / M_{\text{unsaturated}})$ . TR, 680 ms; TE, 3.17 ms; MT-pulse: 12 ms gaussian shaped pulse, nominal flip angle  $500^\circ$ , offset – 4.7 kHz. Pixel-intensities display the percentage decrease in the MR signal intensity due to saturation pulse.
- Gadovist leakage images [% increase of signal intensity] were calculated from two T1W gradient echo images (TR=200 ms, TE=2.75 ms,  $\alpha=45^\circ$ ) before and after a bolus of 0.5 mmol/kg Gadovist (i.v. 10 min in circulation) with Gadovist leakage =  $100 * ((T1W_{\text{post Gadovist}} - T1W_{\text{pre-Gadovist}}) / T1W_{\text{pre-Gadovist}})$ . Pixel-intensities display the percentage increase in the MR signal intensity due to Gadovist leakage.

### Post mortem MRI

One cerebral hemisphere collected at necropsy was fixed in 4% buffered formalin and transferred into buffered saline containing sodium azide after two weeks to stabilize MR relaxation time characteristics<sup>17</sup>. High contrast post mortem MR images were recorded on a 9.4 T horizontal bore NMR spectrometer (Varian), equipped with a quadrature coil (RAPID, Biomedical, Rimpark, Germany). Formalin-fixed brains were submerged in a non-magnetic oil (Fomblin; perfluorinated polyether, Solvay Solexis, Weesp, The Netherlands) to prevent unwanted susceptibility artifacts.

T2 and MTR images were collected. An inversion recovery experiment was performed in which the signal from the GM was suppressed facilitating the detection of GM lesions. Image resolution was more than ten times higher than the resolution obtained with *in vivo* MRI. Next to the areas described above, GM Lesions, and normal appearing GM (NAGM) areas were also outlined.

On a sagittal scout image, 41 contiguous coronal slices of 0.75 mm were defined covering the complete brain, with the following characteristics: field of view, 25x25 mm; matrix, 256x256; zero-filled, 512x512; voxel volume,  $7.15 \times 10^{-3} \text{ mm}^3$ , two transitions. The following MRI data sets were collected:

- $T_2$  maps. These maps were calculated by a mono-exponential fitting of six spin echo images with increasing TE. TR, 2650 ms; TE, 10+5x10 ms. The second image of

this series, i.e. TE, 20 ms, was used for ROI determination.

- MTR maps. Maps were calculated from two T1W spin echo images with and without a MT-saturation pulse. TR, 1675 ms; TE, 23 ms; MT-pulse, 8.19 ms gaussian shaped pulse, nominal flip angle 1000, offset -9.4 kHz.
- Inversion recovery experiment in which the signal of the GM was suppressed. Fast spin echo sequence, TR, 4050 ms; echo train length, 9; echo spacing, 8.93 ms; effective TE, 17.86 ms; Inversion Time, 425 ms for GM suppression.

### Data evaluation MRI

Calculations of  $T_2$ , MTR, and Gadovist leakage were done with a homemade software package developed in MATLAB (v. 7.2 The Mathworks Inc., Natick, USA). ROI were defined using the free available Medical Image Processing, Analysis and Visualization (MIPAV version 4.3.0., National Institutes of Health, Bethesda, USA) package.

The following ROI were defined on T2W images for both *in vivo* (TE, 30 ms) and post mortem (TE, 20 ms) images:

- WM lesions: defined as areas with abnormal high signal intensities in the WM. WM lesions were outlined in the total brain.
- WM: the WM area was outlined in a predefined slice, i.e. the first caudal to rostral slice which showed a complete corpus callosum connection.
- GM: GM areas were outlined in the predefined slice as described for WM.
- Normal Appearing WM (NAWM): the NAWM area was calculated for the predefined slice with  $NAWM = WM - WM \text{ Lesions}$ .

For the post mortem images the following areas were also included:

- GM lesions were defined as areas with abnormal signal intensities on a combined T2W image and the inversion recovery experiment with suppression of the MR signal arising from GM. The latter experiment facilitates the detection of grey matter lesions. The total hemisphere was examined.
- Normal Appearing GM (NAGM). The NAGM area was calculated on the same predefined slice describe above with  $NAGM = GM - GM \text{ Lesions}$ .

### Histology and Immunohistochemistry

Frozen and fixed tissues were processed for histological and immunohistochemical techniques as previously described<sup>18,19</sup>.

### Statistics

Data are presented as mean  $\pm$  s.e.m. of 6 control and 7 treated marmosets. Statistical analysis was performed using Prism 5.0b for Mac OS X. Survival was analysed using Log-Rank test. Differences between control and treated marmosets were analysed

using the Mann-Whitney U test. Differences between WM lesions and WM or NAWM within the control group were analysed by the paired Student's t test.  $p < 0.05$  was considered statistically significant.

## RESULTS

### Clinical course and *in vivo* brain MRI recording

One monkey from the control (PBS-treated) group succumbed unexpectedly at psd 33 of cardiac failure and was therefore excluded from further analyses. The analysis of clinical EAE development in the remaining 6 control monkeys and 7 antibody-treated monkeys shows that depletion of CD20<sup>+</sup> B-cells significantly prevented the development of clinical signs (Table 1, survival time to score 2:  $p=0.0291$ ; survival time to sacrifice with clinical signs:  $p=0.0021$ ).

Before the start of the experiment, the animals were paired two-by-two based on age and body weight. Of each pair one monkey received control substance and one monkey the therapeutic antibody (for pairing see Table 1). The first MRI was planned before the start of the treatment, i.e. at psd 18. When at least one monkey of a pair had experienced evident neurological signs (clinical score  $\geq 2$ ) a second MRI was made of both paired monkeys to assess whether the two monkeys had a different brain lesion load.

At psd 18, none of the animals showed MRI detectable brain lesions, although the presence of small non-focal pathological alterations invisible with the applied MRI techniques could not be excluded (Figure 1A). In four pairs evident neurological signs (score 2 or higher) were first observed in the control monkey, whereas at that time the four paired HuMab 7D8 treated monkeys had no neurological signs (pair 2, 3, 4, 5). The MRI of the other two pairs were made because the treated animal (pair 6) or both animals (pair 1) displayed clinical score 2. In four of the six control animals, WM lesions were detected at the second MRI (Table 2, Figure 1A). Two control animals, i.e. M07021 and the asymptomatic monkey M07080, had no detectable brain WM lesions. In none of the HuMab 7D8 treated animals brain lesions were detected with MRI, although two animals (M04096 and M07095) had experienced a short episode of clinical score 2 (one day) only a few days before the MRI was made (Table 2).

### *In vivo* MRI analysis

Several clinically relevant MRI parameters were quantitated in WM, NAWM, GM, and WM lesion in the second MRI. The normal MRI characteristics of WM lesions in this model were found only in control animals, i.e. increased T2, decreased MTR, and increased Gadovist leakage compared to WM or NAWM (Table 3, Supplementary table 1).

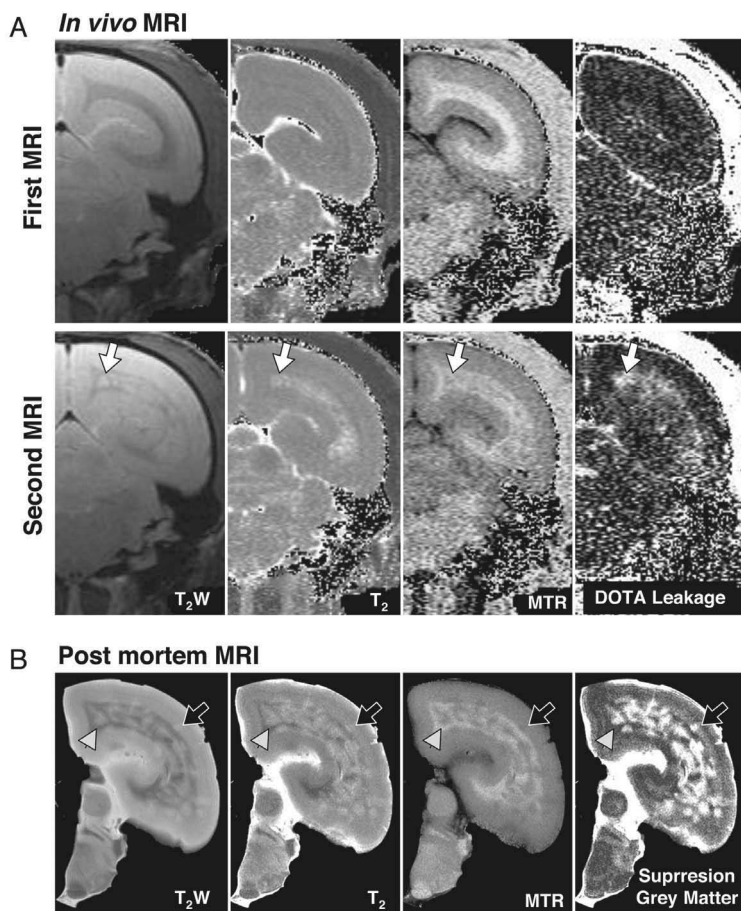


**Figure 1. Overview of MR images of one control EAE marmoset.**

The figure shows a typical example of a control animal (M06061) that developed severe EAE (Table 1). A, during the first MRI experiment, i.e. psd 18, no abnormalities were detected on the *in vivo* images (upper row). The second MRI (second row; see for psd Table 2) showed typical MRI abnormalities associated with the presence of white matter lesions, i.e. increase  $T_2$ , decreased MTR and increased DOTA leakage values. The white arrow points to a typical white matter lesion. B, this lesion (white arrowhead) can be even better appreciated on the post mortem images that are obtained with a more than ten times higher resolution. Grey matter lesions (black arrow) are also visible on the post mortem image, specifically on the image on which the signal arising from the grey matter is suppressed.  $T_2W$ ,  $T_2$ -weighted; MTR, Magnetization Transfer Ratio.

ROI were defined as follows: WM or GM area was outlined in a predefined slice, i.e. the first caudal to rostral slice which showed a complete corpus callosum connection; WM or GM lesions were defined as areas with abnormal signal intensities in the WM or GM. WM or GM lesions were outlined in the total brain; NAWM or NAGM area was calculated for the predefined slice with  $NAWM = WM - WM$  Lesions and  $NAGM = GM - GM$  lesion.

**Table 2. Brain WM lesion volume and day of recording of the second *in vivo* MRI.**

Pair	psd MRI	psd score 2	Control	Volume (mm <sup>3</sup> )	Volume (mm <sup>3</sup> )	CD20 Ab	psd score 2
1	48	46	M02052	22.4	0	M04096	41 <sup>a</sup> , 43 <sup>a</sup>
2	48	41	M06061	590.6	0	M05073	
					0	M06055	
3	73	66	M07021	0	0	M07012	
4	85	78	M07029	8.4	0	M07075	103 <sup>a</sup>
5	85	71 <sup>a</sup> , 84 <sup>a</sup> , 88 <sup>a</sup>	M07048	2.3	0	M07085	
6	50	66	M07080	0	0	M07095	46 <sup>a</sup>

<sup>a</sup> score 2 for 1 day

psd, post sensitization day

In controls, MTR is significantly lower in WM lesions compared to NAWM. Differences between NAWM of control and treated animals were not observed. The increment of T1 signal intensity by intravenous Gadovist was substantially lower in the WM of HuMab 7D8 treated animals than WM and NAWM of control animals, suggesting that in the control animals there is a higher overall increment of BBB permeability throughout the complete WM. This observation suggests that the WM of control animals is certainly not normal. Differences between both groups were not observed for the GM with respect to volume, T2, MTR, and Gadovist leakage.

Whereas the total volume of WM lesions was high in the control group, the fact that no lesions could be detected in the HuMab 7D8 treated monkeys precluded more detailed analysis (Table 3, Supplementary table 1).

In conclusion, these data demonstrate that late stage depletion of CD20<sup>+</sup> B-cells prevents the development of WM lesions that can be detected by *in vivo* MRI.

### Post mortem MRI of the brain

Animals were sacrificed at the peak of the disease or after a pre-determined time interval of 106 days in cases where the disease was less severe or absent (Table 1). To maximize the detection of EAE-associated pathology, we examined formalin-fixed hemispheres with high resolution MRI at 9.4 T field strength. On these post mortem images also GM lesions are detectable, especially when the MR signal of GM was suppressed (Figure 1).

The MRI scans revealed the presence of WM lesions in all six control animals with the normally observed characteristics, i.e. significantly increased T2 and significantly decreased MTR in WM lesions compared to WM or NAWM (Figure 1B). Interestingly,

small WM lesions were observed in four of the seven treated animals, but the average WM lesion volume of the treatment group was significantly lower than the control group (Table 4, Supplementary table 2). Note that the voxel volume of the post mortem images is more than ten times higher than for the *in vivo* images ( $7.2 \times 10^{-3}$  versus  $97.6 \times 10^{-3} \text{ mm}^3$ ) facilitating the detection of small lesions. Although four HuMab 7D8 treated animals contained WM lesions, their T2 values were significantly lower and the MTR values were higher compared to the lesions in control animals. Furthermore, T2 and MTR

**Table 3. Volume, T2, MTR, and Gadovist leakage during the second *in vivo* brain MRI.**

	Control	CD20 Ab
<b>Volume (mm<sup>3</sup>)</b>		
WM	51.0 ± 2.8	45.7 ± 2.8
GM	96.1 ± 3.3	97.2 ± 1.4
NAWM	43.6 ± 9.4	- <sup>b</sup>
WM lesion <sup>a</sup>	104.0 ± 97.4	0.00 ± 0.00 *
<b>T2 (ms)</b>		
WM	58.04 ± 2.62	55.53 ± 0.68
GM	59.76 ± 0.63	60.86 ± 0.84
NAWM	55.47 ± 0.68	- <sup>b</sup>
WM lesion	63.95 ± 3.06	- <sup>b</sup>
<b>MTR (% decrease signal intensity)</b>		
WM	42.33 ± 1.15	43.81 ± 0.51
GM	32.18 ± 0.17	32.01 ± 0.41
NAWM	42.97 ± 0.77	- <sup>b</sup>
WM lesion	36.48 ± 1.04 $\rho$	- <sup>b</sup>
<b>Gadovist leakage (% increase signal intensity)</b>		
WM	7.30 ± 1.03	6.02 ± 0.27
GM	7.98 ± 0.33	7.65 ± 0.25
NAWM	7.26 ± 1.01	- <sup>b</sup>
WM lesion	13.31 ± 2.91	- <sup>b</sup>

<sup>a</sup> Note that lesion volumes were determined in the total brain, whereas WM, GM, and NAWM values were only determined for a single pre-defined slice, i.e. the first caudal to rostral slice which showed the complete corpus callosum connection. Consequently WM lesion volumes can be larger than the WM/NAWM volume.

<sup>b</sup> Could not be determined, because of the absence of WM lesions

Shown are mean ± sem, \* P<0.05 compared to the control group with the Mann-Whitney U test.  $\rho$  P<0.05, Paired Student's t test was used to compare MTR values of WM lesions versus NAWM of the four control animals with WM lesions (Supplementary table 1).

values of WM lesions of treated animals did not significantly differ from WM or NAWM in these treated animals, which is the case in control animals. These data suggest that the lesions of treated animals contain less myelin damage.

Importantly, we detected considerable GM lesion formation in five of the six

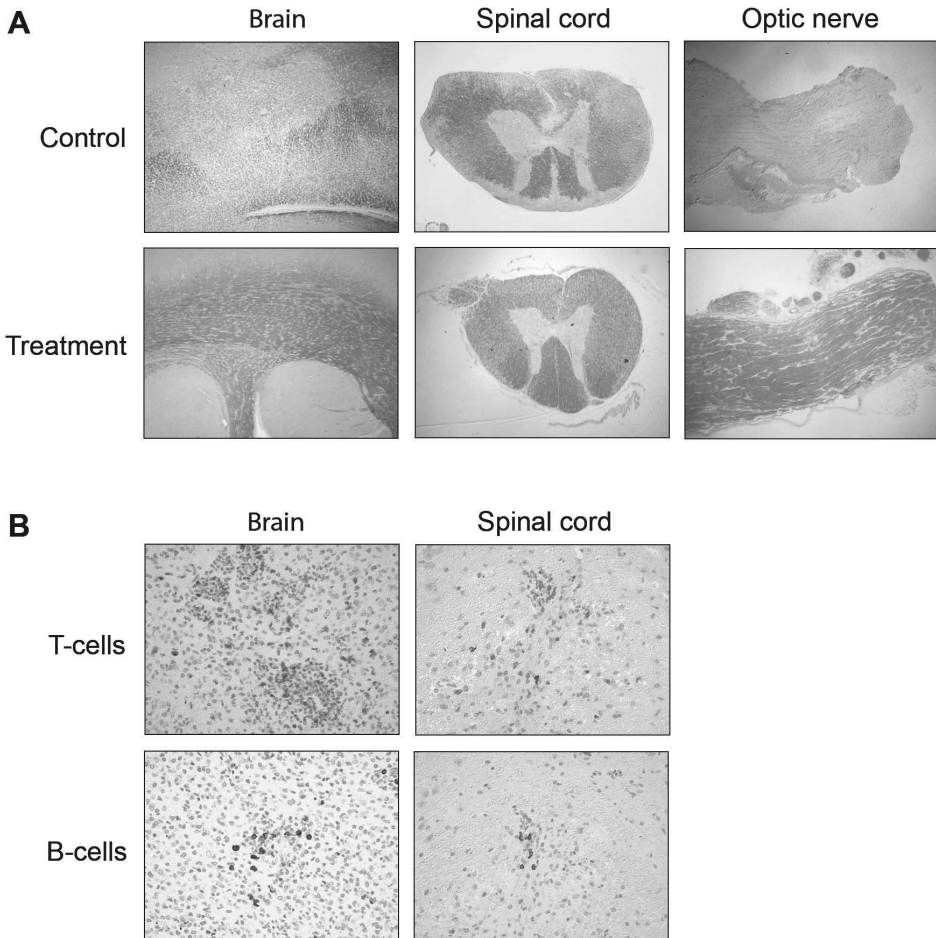


**Figure 2. Reduced demyelination and inflammation in the white matter after B-cell depletion.**

A, Luxol fast blue staining for myelin shows demyelination in the brain (original magnification x50), spinal cord (original magnification x25), and optic nerve (original magnification x25) of a representative control animal (upper panel). The lower panel shows the intact myelin pattern in brain, spinal cord, and optic nerve of treated animals. B, T-cells (upper panel) and B-cells (lower panel) were observed in brain and spinal cord lesions of control animals, but not in treated animals (original magnification x200). See page 317 for a full-color representation of this figure.

control animals, but in none of the HuMab 7D8 treated animals (Figure 1B, Table 4, Supplementary table 2). Relatively, differences in MR characteristics between GM lesions and surrounding unaffected tissue (GM/NAGM) was much lower than the differences observed for WM lesions versus WM/NAWM. In conclusion, the depletion of CD20<sup>+</sup> B-cells not only reduced the development of WM lesions, but also prevented the development of GM lesions.

**Table 4. Post mortem MRI of one brain hemisphere.**

	Control	CD20 Ab
<b>Volume (mm<sup>3</sup>)</b>		
WM	23.0 ± 1.9	18.8 ± 1.2
GM	36.4 ± 2.9	40.8 ± 1.5
NAWM	15.4 ± 2.4	17.1 ± 1.3
NAGM	35.1 ± 3.4	- <sup>b</sup>
WM lesion <sup>a</sup>	103.6 ± 56.1	0.2 ± 0.1 *
GM lesion <sup>a</sup>	9.7 ± 9.0	0.0 ± 0.0 *
<b>T2 (ms)</b>		
WM	29.56 ± 0.93	28.03 ± 0.96
GM	33.66 ± 1.11	34.81 ± 1.49
NAWM	28.45 ± 0.70	28.03 ± 0.96
NAGM	34.18 ± 1.20	- <sup>b</sup>
WM lesion	34.93 ± 0.78 $\rho$	30.19 ± 0.70 *
GM lesion	35.33 ± 1.27	- <sup>b</sup>
<b>MTR (% decrease signal intensity)</b>		
WM	33.98 ± 1.52	36.69 ± 0.34
GM	22.46 ± 0.22	22.25 ± 0.37
NAWM	35.40 ± 0.90	36.79 ± 0.58
NAGM	22.49 ± 0.27	- <sup>b</sup>
WM lesion	28.83 ± 0.91 $\rho$	32.18 ± 1.79
GM lesion	24.33 ± 0.78	- <sup>b</sup>

<sup>a</sup> Note that lesion volumes were determined in the total brain whereas WM, GM and NAWM values were only determined for a single pre-defined slice. See also table 3.

<sup>b</sup> could not be determined, because of the absence of GM lesions

Shown are mean ± sem, \* P < 0.05 compared to the control group with the Mann-Whitney U test.  $\rho$  P < 0.05, Paired Student's t test was used to compare MTR values of WM lesions versus NAWM of the six control animals with WM lesions.

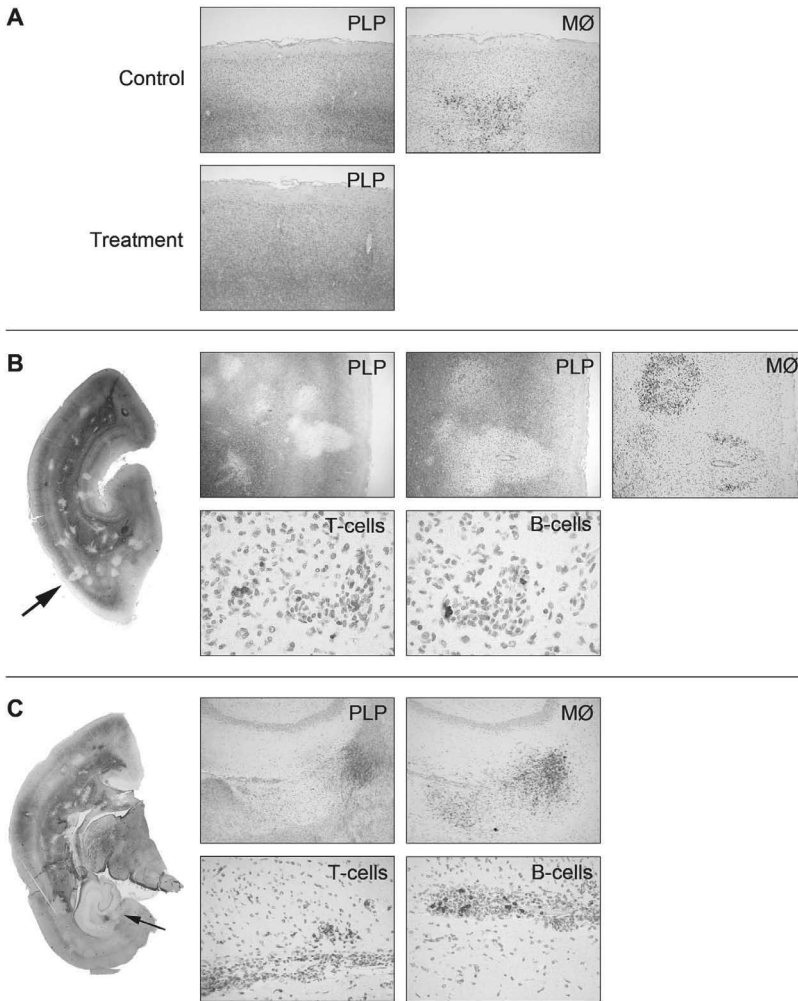


**Figure 3. B-cell depletion prevents the development of grey matter lesions.**

A, stainings for proteolipid protein and MRP14<sup>+</sup> macrophages show a large demyelinated lesion in cortical grey matter of a control animal (upper panel). No grey matter demyelination was observed in CD20<sup>+</sup> B-cell depleted animals (lower panel) (original magnification x500). B, Left hemisphere of a control animal is immunostained for PLP. The arrow points to a group of lesions that are depicted in the five smaller photographs. The first two photographs show the grey matter lesions in a PLP staining (original magnification x25 and x50). MRP14<sup>+</sup> staining shows an active lesion (upper lesion) with many (recently infiltrated) macrophages and an inactive lesion with macrophages only at the rim of the lesion (lower lesion). T-cells and B-cells were present in these lesions (original magnification x400). C shows a lesion in the hippocampus (arrow). Demyelination is shown by PLP staining. MRP14<sup>+</sup> macrophages, T-cells and B-cells were present in this lesion. See page 318 for a full-color representation of this figure.

### **Histology of CNS**

Figure 2 depicts the characteristic pathological aspects in WM of brain, spinal cord, and optic nerve that can be observed in the marmoset EAE model. Also the immunohistochemical detection of T- and B-cells is shown. To quantitate the beneficial effect of HuMab 7D8 we have determined the extent of WM demyelination in all three parts of the marmoset CNS. Histological analysis revealed actively demyelinating brain lesions in all control animals, even in the animals that had only small MRI detectable lesions on the post mortem images (M07029 and M07080). By contrast the small WM lesions that were detected with high contrast post mortem MRI in four HuMab 7D8 treated animals, showed limited or no histological signs of active demyelination (Table 5, Supplementary table 2). The extent of demyelination was significantly lower in the brain and spinal cord of treated animals compared to control animals. Demyelination in the optic nerve was observed in three of the six control animals, but in none of the treated animals (Figure 2A, Table 5).

Five of the six control animals contained prominent inflammation in the spinal cord. Spinal cord lesions were undetectable in the control animal that was sacrificed without clinical signs at the end of the study (M07048). Spinal cord lesions were also absent in four of the seven antibody-treated animals and very small-sized in three antibody-treated animals. Overall the severity of inflammation in spinal cord was significantly higher in control animals than in the HuMab 7D8 treated animals. Inflammation in the optic nerve was detected in four of the six control animals, but in none of the treated animals (Table 5). No T-cells and B-cells could be observed in the CNS of HuMab 7D8 treated animals, in contrast to control animals (Figure 2B).

A very important aspect of the marmoset EAE model, that distinguish it from the majority of rodent EAE models, is the demyelination in the cortical GM. Figure 3 shows that demyelination in the GM can be substantially more extensive than the usually focal demyelination in WM. Note that lesions in the depicted control animal were not only observed in the cortical GM (Figure 3B) but also in the hippocampus (Figure 3C). We have analysed the GM lesions that were detected with post mortem MRI in several control brain specimens, also with histology. In five control animals GM lesions were detected by MRI and in three of these animals this was confirmed by histology. Our histology analysis confirmed the observation with MRI, that no GM lesions had been formed in the HuMab 7D8 treated animals (Figure 3, Table 5, Supplementary table 2).

In conclusion, these data demonstrate that depletion of CD20<sup>+</sup> B-cells dramatically attenuated the development of MS-like pathology affecting WM and GM in different parts of the marmoset CNS, i.e. brain, spinal cord, and optic nerve.

**Table 5. Histology of brain, spinal cord, and optic nerve.**

	Brain		Spinal cord		Optic nerve	
	Demyelination <sup>a</sup>		Inflam- mation <sup>b</sup>	Demyelina- tion (%)	Inflam- mation <sup>b</sup>	Demyelina- tion <sup>a</sup>
	WM (%)	GM (%)				
<b>Control</b>						
M02052	27	1	1	13	+	+
M06061	42	5	3.2	36	+	+
M07021	2	0	2.3	44	-	-/+
M07029	3	0	1.7	64	-	-
M07048	9	0.5	0	0	-/+	-/+
M07080	5.5	0	1.3	37	-	-
<b>Mean</b>	14.75	1.08	1.583	32.33		
<b>SEM</b>	6.613	0.800	0.450	9.298		
<b>CD20 Ab</b>						
M04096	0	0	0	0	-	-
M05073	0	0	0	0	-	-
M06055	0	0	0	0	-	-
M07012	0	0	0	0	-	-
M07075	0	0	0.5	4	-	-
M07085	0	0	0.3	0	-	-
M07095	0	0	0.2	2	-	-
<b>Mean</b>	0 *	0	0.143 *	0.86 *		
<b>SEM</b>	0	0	0.075	0.595		

<sup>a</sup> Demyelination was visualized by staining myelin and myelin degradation products with Klüver Barrera (Luxol fast blue with periodic acid-Schiff) or proteolipid protein (PLP). Demyelination in the brain was determined as follows: brain sections stained for PLP were photographed at 2.5x magnification. Images were then imported in the Scion Image program (freeware downloaded from www.scioncorp.com), an image processing and analysis program based on NIH Image, developed at the National Institutes of Health, USA. In density slice mode, first the total area of the section was measured. After this, total WM (about 40 mm<sup>2</sup>) was measured and subtracted from the total area, resulting in the GM area (about 100 mm<sup>2</sup>). Lesions in WM and GM were selected by freehand mode and their size was measured. Finally the demyelination in WM or GM was calculated as percentage of total WM or GM. Eight sections of the spinal cord of each animal was analysed, which was approximately 6 cm<sup>2</sup> in total. Demyelination in optic nerve is quantified as: + = demyelination, +/- = some demyelination, - = no demyelination.

<sup>b</sup> Inflammation was visualized by staining infiltrating cells with hematoxylin and eosin, CD3, CD20, or MRP14. The inflammatory index of the spinal cord is given as the average number of inflamed bloodvessels/spinal cord cross section. Inflammation in optic nerve is assessed by staining macrophages with MRP14, + = macrophages present, +/- some macrophages present, - = no macrophages

\* P < 0.05 compared to the control group

## DISCUSSION

Clinical trials in RRMS patients have shown a marked clinical effect of CD20<sup>+</sup> B-cell depletion, namely marked reduction of relapse frequency associated with a decrease of contrast enhancing lesions in the cerebral WM<sup>4,5</sup>. The mechanism of action of the CD20<sup>+</sup> B-cell antibody was unexpected, as plasma IgG-levels were not depleted.

As a first step towards better understanding the presumed multifaceted pathogenic role of B-cells in CNS demyelinating disease, we have investigated the systemic effect of CD20<sup>+</sup> B-cell depletion in the rhMOG-induced EAE model in marmosets. The model is characterized by MS-like lesions developing in CNS WM and GM, which are induced by the synergistic action of autoreactive T-cells and autoantibodies<sup>8,9,13,20</sup>. We have used the antibody HuMab 7D8, a human CD20 specific monoclonal antibody with potent cytolytic activity that cross-reacts with marmosets<sup>11,12</sup>.

We report that the depletion of CD20<sup>+</sup> B-cells initiated well after EAE induction (psd 21) led to protection against evident clinical EAE and reduced volume of brain WM lesions. In addition, we observed suppression of demyelination in the optic nerve and in spinal cord, similar to the situation in a mouse EAE model<sup>21</sup>. Probably the most important finding in the current study is the complete abrogation of GM demyelination, which is a relatively recently recognized aspect of the complex MS pathology and which is thought to be clinically more relevant than lesions in the WM<sup>2,22</sup>. To our knowledge, this is the first documented evidence that demyelination of GM can be prevented with a CD20<sup>+</sup> B-cell depleting antibody. Finally, the depletion of CD20<sup>+</sup> B-cells also had a small but detectable effect on MRI parameters of the peri-lesional NAWM and NAGM.

The mechanisms underlying the dramatic effect of rituximab on the extent of demyelination in MS are unknown. We show here in the marmoset EAE model that demyelination of the CNS is profoundly reduced after depletion of CD20<sup>+</sup> B-cells. According to a widely supported concept, autoimmune demyelination in MS can take place in the absence (pattern 1 lesion) or presence (pattern 2 lesion) of IgG antibody binding to myelin<sup>23</sup>. This view is strongly supported by findings in the marmoset EAE model<sup>13,24-26</sup>. We have observed that animals treated with HuMab 7D8 had lower anti-rhMOG IgG levels in their circulation compared to the control animals (Kap et al., *J Immunol*, in press). This may partly explain the reduced demyelination observed in this study. In the rituximab trials in RRMS, no significant reduction of total serum IgG levels was found, although the specific effect on anti-myelin antibodies had not been determined<sup>4,5</sup>. The authors speculate that serum IgG levels were not affected by rituximab because plasma cells do not express CD20 and are therefore not depleted following short-term treatment by an anti-CD20 mAb<sup>27</sup>. The question is therefore warranted whether the clinical effect is mediated by another mechanism via which B-cells can induce demyelination. One possibility is that only long-lived plasma cells remain,

whereas short-lived (CD20<sup>+</sup>) plasma cells are depleted by the treatment. Indeed, this has been shown in a mouse arthritis model after anti-CD20 treatment<sup>28</sup>.

On the basis of our research in the marmoset EAE model we would like to coin an alternative mechanism, namely abrogation of antigen presentation by CD20<sup>+</sup> B-cells to pathogenic T-cells. We have previously reported that the expression of clinical signs of EAE is associated with the activation of a unique subset of cytotoxic IL-17A producing T-cells, which mediate widespread CNS demyelination in the absence of anti-MOG antibodies<sup>13,26</sup>. Separately, we have reported the observation in rhMOG-induced EAE in marmosets (the same animals as published in this paper) that late B-cell depletion by HuMab 7D8 significantly reduced T-cell proliferation and cytokine production in spleen and lymph nodes (Kap et al., *J Immunol*, in press). Importantly, we found no T-cells in the CNS of HuMab 7D8 treated animals (this report). Since demyelination in EAE affected marmosets can occur in the absence of autoantibodies, we propose that the abrogation of CNS pathology after B-cell depletion is mainly caused by the prevention of T-cell recruitment into the CNS.

In conclusion, B-cell depletion prevents the development of inflammation and demyelination in the WM and GM of the brain as well as in spinal cord and optic nerve. We show that CD20<sup>+</sup> B-cells have a central pathogenic role in inflammation and demyelination and are important in lesion development in all areas of the CNS. B-cell depletion reduced inflammation in WM of MS patients and thereby reduced the relapse rate. That B-cell depletion also reduced demyelination of GM may suggest that B-cell depletion will slow down the disease progression and have beneficial effects on long-term disease disability. These data underline the prominent pathogenic role of B-cells in the induction of widespread CNS pathology.

## **ACKNOWLEDGEMENTS**

The authors like to thank Fred Batenburg, Mariska van Etten, and Martine Hoffmann for excellent biotechnical assistance and daily care of the monkeys, Jaco Bakker DVM, Gerco Braskamp DVM, and Merei Keehnen DVM for expert veterinary care, Tom Haaksma and Dr. Ivanela Kondova for autopsy of the monkeys. The authors thank Henk van Westbroek for the artwork and Ed Remarque for statistics.

## REFERENCES

1. Compston A et al. Multiple sclerosis. *Lancet* 372:1502-1517 (2008)
2. Geurts JJ et al. Grey matter pathology in multiple sclerosis. *Lancet Neurol* 7:841-851 (2008)
3. Sospedra M et al. Immunology of multiple sclerosis. *Annu Rev Immunol* 23:683-747 (2005)
4. Hauser SL et al. B-cell depletion with rituximab in relapsing-remitting multiple sclerosis. *N Engl J Med* 358:676-688 (2008)
5. Bar-Or A et al. Rituximab in relapsing-remitting multiple sclerosis: a 72-week, open-label, phase I trial. *Ann Neurol* 63:395-400 (2008)
6. Hawker K et al. Rituximab in patients with primary progressive multiple sclerosis: Results of a randomized double-blind placebo-controlled multicenter trial. *Ann Neurol* 66:460-471 (2009)
7. 't Hart BA et al. Clinical, pathological, and immunologic aspects of the multiple sclerosis model in common marmosets (*Callithrix jacchus*). *J Neuropathol Exp Neurol* 68:341-355 (2009)
8. Kap YS et al. Experimental Autoimmune Encephalomyelitis in the Common Marmoset, a Bridge Between Rodent EAE and Multiple Sclerosis for Immunotherapy Development. *J Neuroimmune Pharmacol* 5:220-230 (2010)
9. 't Hart BA et al. Modelling of multiple sclerosis: lessons learned in a non-human primate. *Lancet Neurol* 3:588-597 (2004)
10. Pomeroy IM et al. Demyelinated neocortical lesions in marmoset autoimmune encephalomyelitis mimic those in multiple sclerosis. *Brain* 128:2713-2721 (2005)
11. Teeling JL et al. Characterization of new human CD20 monoclonal antibodies with potent cytolytic activity against non-Hodgkin lymphomas. *Blood* 104:1793-1800 (2004)
12. Teeling JL et al. The biological activity of human CD20 monoclonal antibodies is linked to unique epitopes on CD20. *J Immunol* 177:362-371 (2006)
13. Kap YS et al. Fast progression of recombinant human myelin/oligodendrocyte glycoprotein (MOG)-induced experimental autoimmune encephalomyelitis in marmosets is associated with the activation of MOG34-56-specific cytotoxic T cells. *J Immunol* 180:1326-1337 (2008)
14. Kerlero de Rosbo N et al. Predominance of the autoimmune response to myelin oligodendrocyte glycoprotein (MOG) in multiple sclerosis: reactivity to the extracellular domain of MOG is directed against three main regions. *Eur J Immunol* 27:3059-3069 (1997)
15. 't Hart BA et al. Preclinical assessment of therapeutic antibodies against human CD40 and human interleukin-12/23p40 in a nonhuman primate model of multiple sclerosis. *Neurodegener Dis* 5:38-52 (2008)
16. Bleeker WK et al. Estimation of dose requirements for sustained *in vivo* activity of a therapeutic human anti-CD20 antibody. *Br J Haematol* 140:303-312 (2008)
17. Blezer EL et al. Quantitative MRI-pathology correlations of brain white matter lesions developing in a non-human primate model of multiple sclerosis. *NMR Biomed* 20:90-103 (2007)
18. 't Hart BA et al. Histopathological characterization of magnetic resonance imaging-detectable brain white matter lesions in a primate model of multiple sclerosis: a correlative study in the experimental autoimmune encephalomyelitis model in common marmosets (*Callithrix jacchus*). *Am J Pathol* 153:649-663 (1998)
19. Laman JD et al. Expression of accessory molecules and cytokines in acute EAE in marmoset monkeys (*Callithrix jacchus*). *J Neuroimmunol* 86:30-45 (1998)
20. von Büdingen HC et al. Immune responses against the myelin/oligodendrocyte glycoprotein in experimental autoimmune demyelination. *J Clin Immunol* 21:155-170 (2001)
21. Matsushita T et al. Regulatory B cells inhibit EAE initiation in mice while other B cells promote disease progression. *J Clin Invest* 118:3420-3430 (2008)
22. Kutzelnigg A et al. Cortical lesions and brain atrophy in MS. *J Neurol Sci* 233:55-59 (2005)
23. Lucchinetti C et al. Heterogeneity of multiple sclerosis lesions: implications for the pathogenesis of demyelination. *Ann Neurol* 47:707-717 (2000)

24. Genain CP et al. Antibody facilitation of multiple sclerosis-like lesions in a nonhuman primate. *J Clin Invest* 96:2966-2974 (1995)
25. McFarland HI et al. Determinant spreading associated with demyelination in a nonhuman primate model of multiple sclerosis. *J Immunol* 162:2384-2390 (1999)
26. Jagessar SA et al. Induction of progressive demyelinating autoimmune encephalomyelitis in common marmoset monkeys using MOG34-56 peptide in incomplete Freund adjuvant. *J Neuropathol Exp Neurol* 69:372-385 (2010)
27. Tedder TF et al. Cloning of a complementary DNA encoding a new mouse B lymphocyte differentiation antigen, homologous to the human B1 (CD20) antigen, and localization of the gene to chromosome 19. *J Immunol* 141:4388-4394 (1988)
28. Huang H et al. Rituximab specifically depletes short-lived autoreactive plasma cells in a mouse model of inflammatory arthritis. *Proc Natl Acad Sci USA* 107:4658-4663 (2010)

**Supplementary table 1. Individual data of *in vivo* MRI of the second MRI experiment.**

	Volume (mm <sup>3</sup> )			
	WM	GM	NAWM	WM lesion <sup>a</sup>
<b>Control</b>				
M02052	49.93	84.45	47.63	22.39
M06061	56.93	91.89	15.99	590.58
M07021	40.89	92.19	<sup>b</sup>	0.00
M07029	55.03	99.24	53.22	8.42
M07048	57.59	105.59	57.59	2.34
M07080	45.65	103.15	-	0.00
<b>Mean</b>	51.01	96.09	43.61	103.96
<b>SEM</b>	2.75	3.26	9.43	97.39
<b>CD20</b>				
M04096	50.71	92.26	-	0
M05073	56.25	99.19	-	0
M06055	42.11	95.02	-	0
M07012	52.56	101.29	-	0
M07075	38.77	95.95	-	0
M07085	36.89	95.04	-	0
M07095	42.26	101.81	-	0
<b>Mean</b>	45.65	97.22	-	0.0
<b>SEM</b>	2.82	1.36	-	0.0
	T2 (ms)			
	WM	GM	NAWM	WM lesion
<b>Control</b>				
M02052	55.09	57.68	54.51	68.28
M06061	71.07	58.35	57.30	69.67
M07021	55.45	60.24	-	-
M07029	54.56	60.91	54.35	61.24
M07048	55.71	59.64	55.71	56.62
M07080	56.35	61.71	-	-
<b>Mean</b>	58.04	59.76	55.47	63.95
<b>SEM</b>	2.62	0.63	0.68	3.06
<b>CD20</b>				
M04096	55.66	58.79	-	-
M05073	53.27	60.34	-	-
M06055	55.51	60.28	-	-
M07012	56.82	59.70	-	-
M07075	58.70	65.68	-	-
M07085	54.55	60.19	-	-
M07095	54.21	61.00	-	-
<b>Mean</b>	55.53	60.86	-	-
<b>SEM</b>	0.68	0.84	-	-

(Supplementary table 1 continued)

	MTR (% decrease signal intensity)			
	WM	GM	NAWM	WM lesion
<b>Control</b>				
M02052	43.26	32.87	43.49	38.17
M06061	36.61	32.10	40.76	35.46
M07021	43.56	32.13	-	-
M07029	43.97	32.39	44.28	34.04
M07048	43.36	31.90	43.36	38.25
M07080	43.25	31.66	-	-
<b>Mean</b>	42.33	32.18	42.97	36.48
<b>SEM</b>	1.15	0.17	0.77	1.04
<b>CD20</b>				
M04096	43.95	32.57	-	-
M05073	44.83	32.60	-	-
M06055	45.17	32.68	-	-
M07012	43.65	32.30	-	-
M07075	40.96	29.59	-	-
M07085	43.91	32.35	-	-
M07095	44.15	31.97	-	-
<b>Mean</b>	43.81	32.01	-	-
<b>SEM</b>	0.51	0.41	-	-
	Gadovist leakage (% increase signal intensity)			
	WM	GM	NAWM	WM lesion
<b>Control</b>				
M02052	7.76	6.97	6.88	19.76
M06061	12.23	9.36	10.17	16.20
M07021	5.85	7.95	-	-
M07029	5.62	7.87	5.50	10.70
M07048	6.49	8.28	6.49	6.60
M07080	5.87	7.43	-	-
<b>Mean</b>	7.30	7.98	7.26	13.31
<b>SEM</b>	1.03	0.33	1.01	2.91
<b>CD20</b>				
M04096	5.72	7.43	-	-
M05073	7.22	8.18	-	-
M06055	5.39	6.53	-	-
M07012	5.87	8.08	-	-
M07075	5.66	7.08	-	-
M07085	6.83	8.27	-	-
M07095	5.47	7.95	-	-
<b>Mean</b>	6.02	7.65	-	-
<b>SEM</b>	0.27	0.25	-	-

<sup>a</sup> Note that lesion volumes were determined in the total brain whereas WM, GM, and NAWM values were only determined for a single pre-defined slice, i.e. the first caudal to rostral slice which showed the complete corpus callosum connection. Consequently WM Lesion volumes can be larger than the WM/NAWM volume.

<sup>b</sup> This parameter could not be determined, because of the absence of WM lesions

**Supplementary table 2. Post mortem MRI of individual animals.**

	Volume (mm <sup>3</sup> )					
	WM	GM	NAWM	NAGM	WM lesion <sup>a</sup>	GM lesion <sup>a</sup>
<b>Control</b>						
M02052	27.36	22.57	7.14	22.57	228.64	0.91
M06061	28.79	38.27	8.83	36.22	322.28	54.55
M07021	17.10	34.90	16.82	34.90	21.76	0.66
M07029	21.11	39.39	20.69	39.33	0.58	0.09
M07048	23.94	42.60	19.57	42.60	45.73	1.83
M07080	19.73	40.49	19.29	- <sup>b</sup>	2.33	0.00
<b>Mean</b>	23.00	36.37	15.39	35.12	103.55	9.67
<b>SEM</b>	1.85	2.95	2.41	3.41	56.09	8.98
<b>CD20</b>						
M04096	21.25	38.94	-	-	0.00	0.00
M05073	22.88	44.40	-	-	0.00	0.00
M06055	20.83	39.95	20.83	-	0.21	0.00
M07012	18.90	39.56	-	-	0.00	0.00
M07075	15.68	37.21	15.64	-	0.50	0.00
M07085	14.76	37.19	14.76	-	0.13	0.00
M07095	17.21	48.00	17.21	-	0.23	0.00
<b>Mean</b>	18.79	40.75	17.11	-	0.15	0.00
<b>SEM</b>	1.15	1.51	1.34	-	0.07	0.00
	T2 (ms)					
	WM	GM	NAWM	NAGM	WM lesion	GM lesion
<b>Control</b>						
M02052	31.14	31.15	27.91	31.15	33.87	35.41
M06061	31.33	32.52	29.41	32.48	34.14	35.45
M07021	27.37	33.27	27.27	33.27	38.33	30.65
M07029	30.01	37.12	29.90	37.12	35.97	37.99
M07048	31.42	36.85	30.33	36.85	34.14	37.15
M07080	26.10	31.03	25.90	31.03	33.12	-
<b>Mean</b>	29.56	33.66	28.45	34.18	34.93	35.33
<b>SEM</b>	0.93	1.11	0.70	1.20	0.78	1.27
<b>CD20</b>						
M04096	26.75	32.97	-	-	-	-
M05073	25.47	30.75	-	-	-	-
M06055	25.18	30.81	25.18	-	31.03	-
M07012	29.96	32.60	-	-	-	-
M07075	29.97	38.13	29.97	-	31.38	-
M07085	31.53	40.46	31.53	-	28.24	-
M07095	30.37	37.97	30.37	-	30.09	-
<b>Mean</b>	28.03	34.81	28.03	-	30.19	-
<b>SEM</b>	0.96	1.49	0.96	-	0.7	-

(Supplementary table 2 continued)

	MTR (% decrease signal intensity)					
	WM	GM	NAWM	NAGM	WM lesion	GM lesion
<b>Control</b>						
M02052	29.12	22.84	33.40	22.84	28.69	23.70
M06061	29.59	22.97	32.12	22.98	28.45	24.00
M07021	36.09	21.45	36.23	21.45	24.79	22.98
M07029	37.85	22.71	37.98	22.70	31.27	27.38
M07048	34.60	22.46	35.83	22.46	29.80	23.61
M07080	36.64	22.34	36.83	-	29.97	-
<b>Mean</b>	33.98	22.46	35.40	22.49	28.83	24.34
<b>SEM</b>	1.52	0.22	0.90	0.27	0.91	0.78
<b>CD20</b>						
M04096	36.70	22.27	-	-	-	-
M05073	37.04	22.63	-	-	-	-
M06055	35.56	20.86	35.56	-	30.09	-
M07012	35.94	21.54	-	-	-	-
M07075	37.89	23.47	37.90	-	31.67	-
M07085	37.67	23.33	37.67	-	37.40	-
M07095	36.04	21.65	36.04	-	29.58	-
<b>Mean</b>	36.69	22.25	36.79	-	32.18	-
<b>SEM</b>	0.34	0.37	0.58	-	1.79	-

<sup>a</sup> Note that lesion volumes were determined in the total brain whereas WM, GM and NAWM values were only determined for a single pre-defined slice, i.e. the first caudal to rostral slice which showed the complete corpus callosum connection. Consequently WM lesion or GM lesion volumes can be larger than the WM/NAWM or GM/NAGM volume.

<sup>b</sup> This parameter could not be determined, because of the absence of GM lesions



# 4.4

## **Role of amino-Nogo-A antagonism in oligodendrocyte differentiation and myelination in experimental demyelinating diseases**

Yi-Yang Yvonne Li<sup>1</sup>, Ryan Wang<sup>1</sup>, Yolanda S. Kap<sup>2,3,4</sup>, Yahui Zhang<sup>1</sup>, Ailian Liu<sup>1</sup>, Yonggang Zhao<sup>1</sup>, Maggie Song<sup>1</sup>, Lei Zhang<sup>1</sup>, Zailian Lu<sup>1</sup>, Rab K. Prinjha<sup>5</sup>, Yuchen Xu<sup>1</sup>, Jianfeng Xu<sup>1</sup>, Nikki van Driel<sup>2</sup>, Erwin Blezer<sup>6</sup>, Jan Bauer<sup>7</sup>, Matthew Cleveland<sup>8</sup>, Jens U. Wurthner<sup>8</sup>, Jim D. Faulkner<sup>8</sup>, Daniel Lee<sup>9</sup>, Hongtao Lu<sup>1</sup>, Bert A. 't Hart<sup>2,3,4</sup>, Jingwu Zhang<sup>1</sup>

<sup>1</sup>Department of Neuroimmunology, GlaxoSmithKline R&D Centre, Shanghai, China; <sup>2</sup>Department of Immunobiology, Biomedical Primate Research Centre, Rijswijk, The Netherlands; <sup>3</sup>Department of Immunology, Erasmus Medical Centre, Rotterdam, The Netherlands; <sup>4</sup>MS Centre ErasMS, Rotterdam, The Netherlands; <sup>5</sup>Epinova DPU, Immuno-Inflammation Centre of Excellence for Drug Discovery, GlaxoSmithKline; <sup>6</sup>Imaging Sciences Institute, University Medical Centre Utrecht, Utrecht, The Netherlands; <sup>7</sup>Brain Research Institute, University of Vienna, Austria; <sup>8</sup>GlaxoSmithKline, Biopharm R&D, Stevenage, UK; <sup>9</sup>Department of Translational Medicine, GlaxoSmithKline R&D Centre, Shanghai, China

YYL, RW, and YSK contributed equally to this work

*Submitted for publication*



## ABSTRACT

Nogo-A is a central nervous system myelin protein with two distinct domains, amino-Nogo-A and carboxyl Nogo66, which inhibits axonal outgrowth and promotes growth cone collapse. Here we show that antagonism of amino-Nogo-A ameliorated experimental autoimmune encephalomyelitis in marmosets. The treatment efficacy strongly correlated with markedly reduced levels of CNS demyelination. Axonal and myelin repair was further demonstrated with amino-Nogo-A antibody treatment in a lysophosphatidylcholine-induced demyelination model. The role of amino-Nogo-A was further validated *in vitro* as amino-Nogo-A, but not Nogo66, inhibited oligodendrocyte precursor cell differentiation and myelination in co-culture with dorsal root ganglion neurons and in organotypic cerebellar slices. Molecular analyses revealed that the underlying mechanism for the role of amino-Nogo-A on oligodendrocyte precursor cell differentiation and maturation involved the inhibition of Akt signaling pathway. The study provides new evidence supporting amino-Nogo-A antagonism as a potential therapeutic approach for multiple sclerosis and other demyelinating diseases through axon and myelin repair.

## INTRODUCTION

Multiple sclerosis (MS) is a chronic inflammatory and demyelinating disease affecting the central nervous system (CNS) characterized by focal white matter inflammation and the loss of the myelin sheath. It involves both cellular and humoral autoimmune attacks primarily targeting the myelin in the CNS resulting in demyelination, gliosis, and axonal injury as typically seen in MS lesions<sup>1</sup>. Substantial evidence supports that autoimmune inflammation in MS is associated with marked reduction in differentiation of oligodendrocyte precursor cells (OPC) and impairment in myelin tissue repair. It has been increasingly recognized that the reduced rate of remyelination in the MS brain is one of the major attributes to persistent demyelination and axon degeneration. The underlying mechanism is unclear and suggested to involve a potential blockade of OPC differentiation to mature and myelinating oligodendrocytes<sup>2,3</sup>. Key signaling molecules identified in the signaling pathways include, but not limited to, Akt, Fyn,  $\alpha$  or  $\beta$ 1 integrins, neuregulin, and Wnt<sup>4-8</sup>.

Nogo-A is a high molecular weight transmembrane protein expressed mainly in oligodendrocytes at all stages and is initially identified as a potent inhibitor for neurite outgrowth<sup>9-11</sup>. It is believed that the inhibitory effects of Nogo-A are mediated through both the C-terminal 66-residue extracellular domain (Nogo66) and the amino-terminal region<sup>12</sup>. Studies accumulated so far have indicated that Nogo66 plays a critical role

in the induction of growth cone collapse through interaction with Nogo-A receptor (NgR) while amino-Nogo-A appears to have a predominant inhibitory effect on neurite outgrowth via  $\beta 1$  integrins, thus preventing cell adhesion and spreading<sup>13,14</sup>. However, a specific receptor for amino-Nogo-A has not been identified. In rodent and marmoset spinal cord injury models, amino-Nogo-A antagonism was found to enhance axonal regeneration<sup>10,15-17</sup>, which was attributed to removal of the inhibitory role of amino-Nogo-A in neurite outgrowth. However, the role of amino-Nogo-A in oligodendrocyte biology and myelination is unknown. Notably, elevated Nogo-A expression was reported in chronic active demyelinating lesions of secondary progressive MS patients and elevated levels of the soluble form of Nogo-A in cerebrospinal fluid of MS patients<sup>18,19</sup>. A study by Karnezis et al. suggested that Nogo-A antagonism or its gene deficiency in rodents may confer protection in experimental autoimmune encephalomyelitis (EAE) as indicated by delayed disease onset and reduced disease severity<sup>20</sup>. However, the role and underlying mechanism of Nogo-A and its antagonism in demyelinating diseases is unknown. It is unclear whether the treatment efficacy observed in EAE with Nogo-A antagonism was mediated through axonal mechanism or potential remyelination mechanism.

In this study, we investigated our hypothesis that amino-Nogo-A plays a detrimental role in CNS myelination under pathological conditions where amino-Nogo-A is aberrantly expressed in injured myelin tissue. We first studied the antagonism of amino-Nogo-A in an EAE model in the common marmoset, as this non-human primate model closely resembles the essential clinical and pathological features of MS<sup>21,22</sup>. The effect of amino-Nogo-A antagonism was further evaluated in a non-inflammatory demyelinating model induced by lysophosphatidylcholine (LPC). An important aspect of this study was to delineate the mechanisms underlying the role of amino-Nogo-A and its antagonism in myelination and OPC differentiation at both cellular and molecular levels. These novel findings have important implications in the development of new treatment modality for MS by targeting the myelin repair mechanism.

## **MATERIALS AND METHODS**

### **Antibodies**

Amino-Nogo-A specific monoclonal antibodies (mAb) were generated by immunizing mice with a GST-amino-Nogo-A fusion protein. One of the resulting Ab (2A10) was characterized for its specificity by binding to an epitope encompassing amino acid residues 610-621 (VLPDIVMEAPLN) of human and rat amino-Nogo-A. The Ab binds to GST-amino-Nogo-A protein with high affinity ( $K_d = 0.8 - 1.0$  nM) and was effective in blocking amino-Nogo-A-mediated inhibition of neurite outgrowth. Amino-Nogo-A Ab was humanized using the best-fit CDR-grafting technique<sup>23</sup>. The resulting Ab retained

the same binding affinity to human amino-Nogo-A ( $K_d = 0.66$  nM). The Ab was tested in neurite outgrowth functional assay where it was shown to neutralize the inhibition induced by amino-Nogo-A. The parental mouse Ab against the same epitope was used in all experiments described here with the exception of marmoset EAE where the humanized version was used.

Ab used for immunoblot and immunohistochemistry experiments are as follows: rabbit anti-MBP, mouse anti-CNPase, mouse anti-NG2, mouse anti-GFAP, mouse anti-NeuN, rabbit anti-Olig2 and mouse anti-neurofilament H. They were all purchased from Millipore Chemicon (Billerica, MA).

### **Induction of EAE in marmosets**

The induction of marmoset EAE was performed as described<sup>22</sup>. Briefly, the animals of comparable age and body weight were immunized with a peptide corresponding to residues 34-56 of human myelin oligodendrocyte glycoprotein (MOG34-56), which was obtained from ABC Biotechnology (London, UK) or Cambridge Research Biochemicals (Cleveland, UK). The peptide was emulsified in phosphate buffered saline (PBS) and complete Freund's adjuvant (Difco Laboratories, Detroit, MI) as described previously<sup>22</sup>. Clinical signs were scored daily by two independent observers using a previously described semi-quantitative scale<sup>24</sup>. Briefly, 0 = no clinical signs; 0.5 = apathy, loss of appetite, altered walking pattern without ataxia; 1 = lethargy, anorexia, tail paralysis, tremor; 2 = ataxia, optic disease; 2.25 = monoparesis; 2.5 = paraparesis, sensory loss; 3 = para- or hemiplegia. Monkeys were sacrificed for ethical reasons once complete paralysis of hind limbs (score  $\geq 3.0$ ) was observed. Body weight measurements of conscious monkeys were performed three times per week. Monkeys selected for necropsy were first deeply sedated by intramuscular injection of ketamine (50 mg/kg, AST Pharma, Oudewater, The Netherlands) and subsequently euthanized by infusion of pentobarbital sodium (Euthesate, Apharmo, Duiven, The Netherlands). The marmoset EAE protocol was approved by the Institute's Ethics Committee.

### **Treatment of marmoset EAE with humanized amino-Nogo-A Ab**

Animals were intravenously (i.v.) injected with 30 mg/kg of humanized amino-Nogo-A Ab or PBS solvent under ketamine anesthesia (40 mg/kg). Treatment was given once a week starting one day before immunization until day 120 or day 168. Formalin fixed brains (8-10 slices) and spinal cords (8-10 cross sections) were embedded in paraffin and 5  $\mu$ m sections were cut. For basic classification of inflammation, demyelination, and axonal pathology, sections were stained with haematoxylin and eosin (H&E), Luxol fast blue (LFB) myelin stain, and Bielschowsky silver impregnation, respectively. Demyelination was measured by using a morphometric grid. In spinal cord, the demyelination was given as percentage of white matter of the spinal cord.

### **Lysophosphatidylcholine (LPC)-induced corpus callosum demyelination mouse model**

LPC-induced focal demyelination was performed as described<sup>25</sup>. All experimental and surgical procedures were performed according to protocols approved by IACUC of GSK R&D China. C57BL/6 mice were anesthetized with pentobarbital sodium (60 mg/kg) diluted in 0.9% sterile saline and positioned in a stereotaxic frame (RWD Life Science Co., Ltd, China). Two  $\mu$ l of 1% LPC (Sigma) was injected unilaterally into the corpus callosum using appropriate stereotaxic coordinates (1.42 mm anterior to bregma, 1.00 mm lateral to bregma, 2.25 mm deep from the skull surface) for 20 min, with a 10  $\mu$ l Hamilton syringe containing (Sigma, Gillingham, UK). The needle was kept in place for 10 min to reduce reflux up the needle track. Amino-Nogo-A Ab was then delivered locally at the indicated concentrations on day 3 post LPC injection. Three days after Ab injection, brains were collected and samples were prepared for histological analyses to assess demyelination.

### **Electron microscopy**

Brain tissues were immersed in 2.5% glutaraldehyde in 0.1 mol/L phosphate buffer (pH 7.4), post-fixed in 1% osmium tetroxide, dehydrated in ascending alcohols, and infiltrated and embedded in Epon 618 (Sigma), with each corpus callosum oriented for transverse axonal analysis. Sections were prepared at 1  $\mu$ m thickness from each block and stained with Toluidine blue. After examination under light microscopy, selected areas were trimmed for electron microscopy (EM). Ultra-thin sections (50-60 nm) were collected and stained with 3% uranyl acetate and lead citrate and then examined under a transmission electron microscope (Philips CM-120, Eindhoven, The Netherlands) at 100 kV.

### **Cerebellar slice culture**

The cerebellar slice culture was established as described<sup>26</sup>. Briefly, parasagittal slices of postnatal day 10 (P10) rat cerebellum were cut at 350  $\mu$ m using Leica VT1200 tissue Slicer (Leica Instruments, Wetzlar, Germany) and cultured on collagen-coated transwells (Costar, Lowell, MA) containing 50% basal medium with Earle's salts, 25% Hanks' buffered salt solution, 25% horse serum, and 5 mg/ml glucose (Invitrogen, Glasgow, UK). Demyelination was induced by LPC treatment at 0.5 mg/ml for 15-17 h followed by several washes. Amino-Nogo-A Ab or control Ab were added to the culture at indicated concentrations for 4 days. For whole-mount immunostaining, the slices were first blocked for 2-4 h with PBS containing 10% goat serum, 1% BSA, and 0.2% Triton X-100 at RT followed by primary and secondary Ab incubation overnight at 4°C. Images were captured using an Olympus BX60 microscope and Zeiss LSM confocal microscope.

### OPC differentiation assay

Cell suspension enriched for OPC were obtained from forebrain of 2-day old rat pups as described<sup>27</sup>. After repeated trituration, cells were pelleted, resuspended, and plated on poly-D-lysine (PDL)-coated T75 flasks. The resulting cultures were supplemented with the medium twice per week and subjected to a serial shake-off procedure after two weeks to obtain pure OPC. Specifically, the mixed glial cells were shaken initially for 1 h at 100 rpm to remove microglia and continuously shaken for 20–22 h at 37°C at 200 rpm to enrich OPC. OPC were collected by centrifugation at 1200 rpm for 5 min, resuspended in chemically defined basal medium (BDM). BDM consisted of DMEM supplemented with N2 medium (Invitrogen), glutamine (4 mM, Invitrogen), BSA (0.1 mg/ml, Sigma), hydrocortisone (20 nM, Sigma), selenium (30 nM, Sigma) and biotin (10 nM, Sigma). OPC were seeded in poly-ornithine-coated culture dishes and maintained in BDM supplemented with bFGF (10 ng/ml, Invitrogen) and PDGF (10 ng/ml, R&D systems, Minneapolis, MN) before experimental manipulation. Purity of OPC was >95% as quantified by A2B5<sup>+</sup> staining. To initiate OPC differentiation, OPC were cultured in BDM supplemented with triiodothyronine (30 nM, Sigma) and N-acetyl-L-cysteine (30 μM, Sigma) to differentiate into MBP<sup>+</sup> mature oligodendrocytes for 3-5 days.

### Construction of Nogo-A RNAi

Cloning and lentiviral vector packaging of small hairpin RNA (shRNA) was done using the Lenti-X shRNA Expression System (Clontech, Mountain view, CA). Synthesized shRNA oligonucleotides with designed BamHI and EcoRI sticky ends were annealed and cloned to the pLVX-shRNA2 plasmid. Sequences of rat Nogo-A shRNA are GATCCGCACCCACAGCAAACACTTTTCCTTCAAGAGAGGAAAGTGTGGTGGTGCTTTTGG (sense) and AATTCAAAAAGCACCACAGCAAACACTTTTCCTTCTTGAAGGAAAGTGTGGTGGTGGCG (antisense). Sequences of non-targeting control shRNA are GATCCTCGCTTACCGATTTCAGAATGGTTCAAGAGACCATTCTGAATCGGTAAGCGATTTTTG (sense) and AATTCAAAAATCGCTTACCGATTTCAGAATGGTCTTGAACATTCTGAATCGGTAAGCGAG (antisense). To package the lentiviral vectors containing the shRNA, pLVX-shRNA2 carrying Nogo-A or control shRNA and the Lenti-XHT Packaging Mix were cotransfected into HEK293T cells. Packaging cell supernatant was collected 48 h later and concentrated by centrifugation as previously described<sup>28</sup>. RNAi lentiviruses carrying green fluorescent protein (GFP) were generated to determine the transfection efficiency. Oligodendrocytes were infected with lentivirus at 3 m.o.i. per cell and approximately 50% of transfected oligodendrocytes were GFP positive. Cell viability was not altered by shRNA transfection.

### **Immunocytochemistry**

Cells were fixed in 4% paraformaldehyde and then incubated with indicated primary Ab overnight at 4°C<sup>29</sup>. After several washes, samples were incubated with appropriate Alexa-labeled secondary Ab (Molecular Probes, Carlsbad, CA) for 2 h. They were then mounted in VectaMount (Victor, Burlingame, CA) and visualized by Olympus BX60 fluorescence microscopy.

### **Co-culture of oligodendrocytes with DRG**

The co-culture system was established using a protocol as described<sup>30</sup>. Briefly, dorsal root ganglions (DRG) were dissected from rat embryos E14-16. After papain (30 U/ml, Sigma) and collagenase (200 µg/ml, Sigma) digestion for 15 min, the dissociated cells were plated onto 96-well plates coated with poly-D-lysine and laminin (Invitrogen) at a density of  $5 \times 10^4$  cells/well. The resulting neurons were cultured for 2 weeks in Neurobasal medium (Invitrogen) supplemented with 5% fetal bovine serum, in the presence of nerve growth factor (25 ng/ml, Invitrogen). To remove contaminating fibroblasts and glial cells, the cultures were pulsed every 3 days for a total of three times with 30 µM 5-fluorodeoxyuridine (Sigma). Enriched populations of OPC were obtained from P0 rats as described above. The enriched OPC (>95% pure) were added to DRG culture for 4-5 h followed by amino-Nogo-A treatment in the presence or absence of amino-Nogo-A Ab. Co-culture was maintained for another 3 days before the cells were fixed and immunostained for Cellomics analysis.

### **Western blot analysis**

Protein extraction from either cerebellar slice culture or OPC culture was carried out using RIPA lysis buffer (50 mM Tris-HCl, pH 7.5; 1 mM EDTA; 1 mM EGTA; 1 mM sodium orthovanadate; 50 mM sodium fluoride; 0.1% 2-mercaptoethanol; 1% Triton X-100, and 1% protease inhibitor cocktail (Roche, Indianapolis, IN)). Protein concentration was determined by BCA method (Pierce) and 10-15 µg of protein were separated on SDS-PAGE, transferred to PVDF membranes, and blotted with Ab specific for MBP, Tuj-1, Akt/pAkt and Nogo-A, using actin as a loading control. Signals were detected by enhanced chemiluminescence (Millipore).

### **CNPase activity assay**

CNPase activity was measured by a fluorometric assay as previously described<sup>31</sup>. Nicotinamide adenine dinucleotide 2', 3'-cyclic monophosphate (2', 3'-cNADP) was used as a substrate. Briefly, 5 µl of protein homogenate from cerebellar slice culture were added to 100 µl of a reaction mixture composed of 0.2 M MES buffer, pH 6.0; 1.0 mM 2',3'-cyclic NADP (Sigma); 30 mM MgCl<sub>2</sub>; 1.0 mM disodium EDTA; 1.5 mM glucose-

6-phosphate; 0.3% BSA and 23 µg/ml glucose-6-phosphate dehydrogenase (140 U/rag, Sigma). The fluorescence of the NADPH formed in the reaction was measured at an emission wavelength of 460 nm after excitation at 360 nm (Molecular Device).

### Neurite outgrowth assay

Cerebellar granule neurons (CGN) were isolated from day 7 postnatal mice as described<sup>10</sup>. PDL-coated 96-well plates were cultured for 7 days. Soluble amino-Nogo-A was added (5 µg/ml) to the indicated wells while myelin was coated onto the plate (0.5 µg/well) and unbound myelin was washed off by PBS before seeding CGN. Amino-Nogo-A Ab or its isotype control Ab was added at concentrations of 1, 5, and 20 µg/ml to the wells and incubated for 72 h. The number of neurons and the neurite length was measured by Cellomics.

### Statistical analysis

A two-tailed Student's t-test was performed in all experiments. All data are expressed as mean ± S.D. A *P* value of < 0.05 was considered statistically significant.

## RESULTS

### Amelioration of marmoset EAE by treatment with amino-Nogo-A Ab

The effect of an amino-Nogo-A Ab in CNS myelination was first examined in a marmoset EAE model induced by immunization with MOG34-56 in CFA<sup>21</sup>. The treatment group was administered intravenously with a humanized monoclonal amino-Nogo-A Ab at 30 mg/kg, starting one day prior to immunization and once a week thereafter, and monitored until post immunization days (p.i.d) 112 and 168. The clinical score and histopathology were compared in parallel with those of a control group where five marmosets received PBS under the same experimental conditions. As shown in Figure 1A, there was a marked reduction in EAE clinical score in the treatment group when compared to those of control marmosets (PBS or IgG1 isotype control, data not shown) ( $p < 0.01$ ), which correlated with Kaplan-Meier analysis of survival (Figure 1B). Consistent with the improvement in the clinical score was a significant reduction in demyelination (Luxol Fast Blue (LFB) staining) and axon degeneration (Bielschowsky staining) in the spinal cord of amino-Nogo-A Ab treated marmosets indicating a correlation between CNS pathology and clinical signs (Figure 1C-D).

Although the observed beneficial effects described above were accompanied with decreased infiltrating mononuclear cells by H&E staining in Ab treated group (Figure 1C), there was no evidence to suggest that amino-Nogo-A antagonism had a direct anti-inflammatory effect as shown by the lack of surface amino-Nogo-A expression in

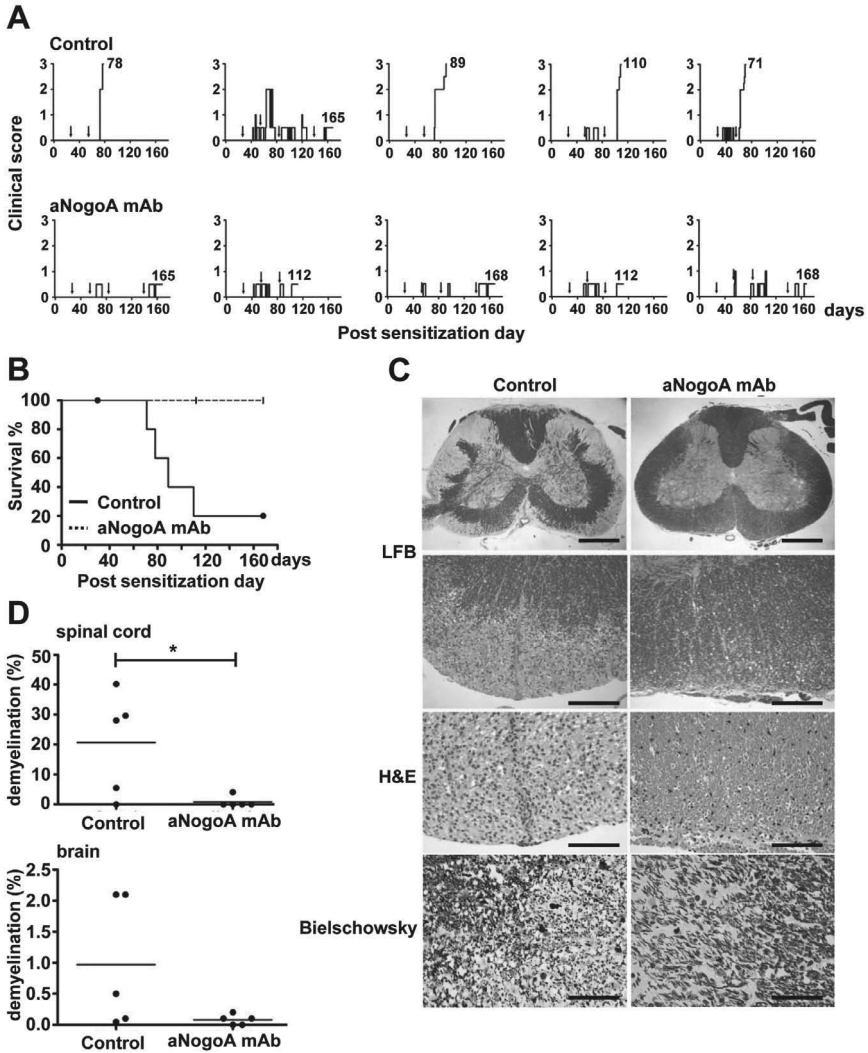


**Figure 1. Amelioration of EAE in marmosets by amino-Nogo-A antibody treatment.**

A, Individual clinical scores of EAE marmoset treated with amino-Nogo-A antibody (aNogoA mAb) and control. Animals (n=5/group) were administered intravenously with a humanized aNogoA mAb or control at 30 mg/kg, starting one day before immunization and every week thereafter and monitored until post immunization days (p.i.d) 112 and 168. B, Survival analysis in aNogoA mAb treatment and control groups. C, Representative spinal cord sections obtained from EAE marmosets analyzed for the degree of demyelination by LFB staining and axon integrity by Bielschowsky staining and infiltrating mononuclear cells by H&E staining. Scale bar, 600  $\mu$ m (LFB, upper), 200  $\mu$ m (LFB, lower), 200  $\mu$ m (H&E) and 50  $\mu$ m (Bielschowsky). (D) Percentage of demyelination areas in the white matter of spinal cord and the brain. See page 319 for a full-color representation of this figure.

mononuclear cells derived from EAE marmosets, including CD4<sup>+</sup> T-cells, B-cells, and macrophages (data not shown), and the lack of effect by amino-Nogo-A Ab treatment on T-cell reactivity to MOG, a causal activity of encephalitogenic T-cells (data not shown).

### **Reduction in non-inflammatory demyelination *in vivo* and *ex vivo* by amino-Nogo-A Ab**

To demonstrate the effect of amino-Nogo-A antagonism in myelination, we employed a non-inflammatory rodent CNS demyelination model induced by direct injection of LPC into the rat corpus callosum. As shown in Figure 2A, treatment with amino-Nogo-A Ab led to significantly reduced demyelination in corpus callosum compared to controls. Consistently, Toluidine blue staining of the lesion areas revealed a significantly decreased number of demyelinating axons (Figure 2B), which correlated with EM analysis of demyelinated axons in the affected corpus callosum (Figure 2B and 2C). At the border of the lesions, there was a significant increase in the number of preserved axons in the amino-Nogo-A Ab treated group while the number of demyelinated axons was markedly reduced (Figure 2B). EM analysis indicated that there was no difference in the total number of preserved axons between the two groups while the number of demyelinated axons in amino-Nogo-A Ab treated group was significantly reduced (Figure 2C). In both Toluidine and EM analyses, there was an increased number of small diameter axons in the treated group reminiscent perhaps of axon sprouting, which was confirmed by peripherin staining, a specific marker for axon sprouts<sup>16,17</sup> (Figure 2D).

To evaluate the role of amino-Nogo-A in myelination at the cellular level, we examined the effect of amino-Nogo-A Ab in an organotypic cerebellar slice culture system. This system has the advantage of maintaining the local CNS microenvironment and the interactions among the different neural cell types involved in demyelination and remyelination processes<sup>32</sup>. In this model, LPC treatment led to marked demyelination and, to a lesser extent, axonal injury, as shown by myelin basic protein (MBP) and neurofilament staining (Figure 3A). Addition of amino-Nogo-A Ab in the system restored the levels of MBP expression in oligodendrocytes and NF expression in axons as compared to those of isotype control (Figure 3A). The increase in areas positively co-stained for MBP and NF indicated enhanced myelination and/or remyelination upon amino-Nogo-A Ab treatment (Figure 3A). Consistent with this observation was the increased expression of both MBP and Tuj-1 (a neuronal marker) in cerebellar slice homogenates as detected by Western blot analysis (Figure 3B). Furthermore, the enzymatic activity of CNPase (2, 3-cyclic nucleotide 3-phosphodiesterase) in immature or mature oligodendrocytes was significantly enhanced by the Ab treatment (Figure 3C). Increased MBP production and remyelination by amino-Nogo-A Ab was demonstrated in LPC-induced demyelination in cerebellar slice culture where amino-Nogo-A was released as a result of myelin breakdown. This was confirmed by the detection of

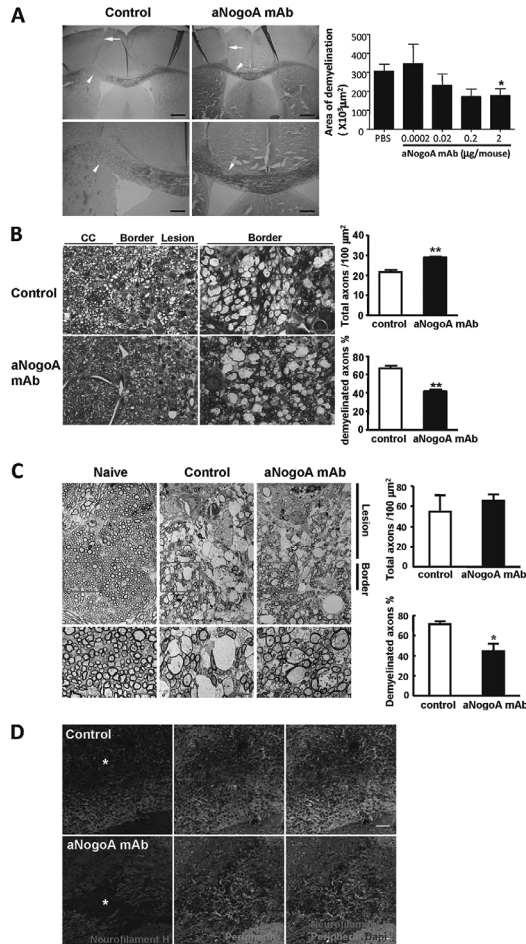


**Figure 2. Reduction of demyelination and protection of axons by the treatment of amino-Nogo-A antibody in an LPC-induced demyelination model.**

A, Area of demyelination by aNogoA mAb treatment in LPC-induced corpus callosum demyelination model. Brain samples were collected from mice 3 days after aNogoA mAb treatment or PBS control and analyzed for the degree of demyelination by LFB staining. Arrows point to the injection sites or needle tracts. Arrowheads indicate the demyelination areas. Scale bar, 500 µm (upper panels) and 200 µm (bottom panels). Bar graph represents the quantification of the area of demyelination in the corpus callosum in relation to the indicated doses of aNogoA mAb. B, Toluidine blue staining of 1 µm corpus callosum sections (left) and magnified images of the boxed border areas (right). Scale bars, 2 µm. The bar graphs represent the total number of axons and % averages of demyelinated axons from the border areas. C, Representative electromicrographs of corpus callosum sections from normal and LPC-injected mice treated with aNogoA mAb (2 µg/mouse) or control. Red asterisks denote macrophages. Boxed areas are enlarged (bottom). D, Axon sprouting in the lesion area (white asterisks) as demonstrated by peripherin staining (green) or neurofilament H (red). \*p < 0.05; \*\*p < 0.01. See page 320 for a full-color representation of this figure.

amino-Nogo-A in cerebellar slice homogenates by Western blot (Figure 3B) and by IHC staining (Supplemental Figure 2) and the direct inhibitory effect of soluble amino-Nogo-A on MBP production in cerebellar slices (Figure 3D).

Furthermore, the potential inhibitory effect of amino-Nogo-A on neurite outgrowth was assessed in an *in vitro* neurite outgrowth assay where cerebellar granule neurons (CGN) were seeded on either amino-Nogo-A or Nogo66 recombinant protein coated plate, respectively. Amino-Nogo-A Ab specifically reversed the inhibition of neurite outgrowth induced by amino-Nogo-A, but not Nogo66 (Supplemental Figure 1A and B), and partially the inhibitory effect of myelin on neurite outgrowth (Supplemental Figure 1C).

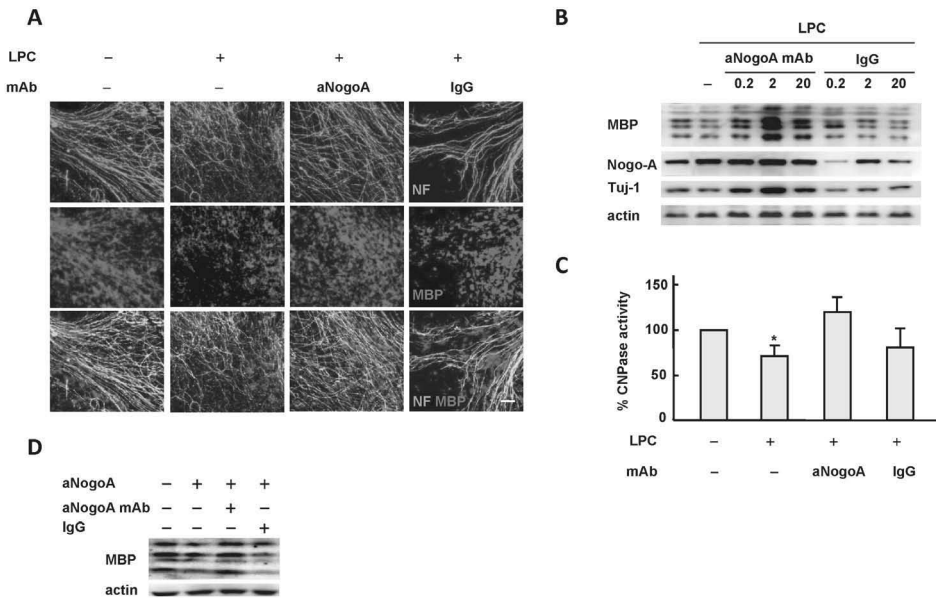


**Figure 3. Restoration of axon integrity and myelination by amino-Nogo-A antagonism in LPC-treated cerebellar slice culture.**

A, Representative confocal images of LPC-treated cerebellar slice cultured with aNogoA mAb or IgG control. Oligodendrocytes were stained with MBP antibody (red) and axons were stained with antibody directed at neurofilament (NF, green). Myelinated axons are shown by co-staining (yellow). Scale bar, 50  $\mu$ m. B, Expression of MBP, Nogo-A, and Tuj-1 in LPC-treated cerebellar slice cultured with different concentrations of aNogoA mAb or IgG control. Actin was used as a control for protein loading. C, CNPase activity in LPC-treated cerebellar slice. Homogenates prepared from LPC-treated cerebellar slice cultured with either aNogoA mAb or IgG control were analyzed in a fluorometric assay. Numbers are expressed as percentage average normalized against untreated control. D, Expression of MBP in cerebellar slice subjected to indicated treatment conditions. Actin was used as a loading control. The data are representative of three independent experiments. \* $p < 0.05$ . See page 321 for a full-color representation of this figure.

### **Effects of amino-Nogo-A and amino-Nogo-A antagonism on OPC differentiation and myelination**

To understand the role of amino-Nogo-A in myelination, we investigated its effect in differentiation, maturation, and myelination of OPC using a purified OPC culture system. The results showed that the addition of soluble amino-Nogo-A, but not Nogo66 (data not shown), resulted in a decreased number of MBP-expressing cells (Figure 4A) and a reduction in MBP expression in differentiating OPC (Figure 4B), suggesting that amino-Nogo-A directly inhibits OPC differentiation. The inhibitory effect induced by amino-Nogo-A was significantly reversed by amino-Nogo-A Ab (Figure 4A and B). To confirm the inhibitory effect of amino-Nogo-A on OPC differentiation, the expression of Nogo-A was knocked down by specific shNogo-A. Reduction of Nogo-A expression in OPC resulted in increased differentiation as evidenced by elevated MBP production (Figure 4C) as well as from the morphology of mature oligodendrocytes (data not shown).

To further assess the functional consequence of amino-Nogo-A inhibition on OPC, we examined the myelination of established DRG neurons in an OPC/DRG co-culture system as measured by MBP immunostaining. Addition of amino-Nogo-A inhibited the ability of oligodendrocytes to myelinate DRG neurons, which was abrogated by amino-Nogo-A Ab but not by control IgG (Figure 4D). Furthermore, exposure of the co-culture system to amino-Nogo-A Ab restored the area of myelinated axons to levels comparable to those of controls. These results unveiled the novel role of amino-Nogo-A in OPC differentiation, maturation, and myelination.

### **Molecular mechanism underlying the inhibition of OPC differentiation and myelination**

To gain further insights into the molecular mechanism and signaling pathways underlying the inhibition of OPC differentiation and myelination induced by amino-Nogo-A, we evaluated multiple signaling pathways that are involved in myelination, including Akt, Fyn,  $\alpha$ v or  $\beta$ 1 integrins, neuregulin, and Wnt<sup>4-8</sup>. The analyses led to the identification of Akt pathway as a critical signaling mechanism in the role of amino-Nogo-A in myelination. As shown in Figure 5A, amino-Nogo-A-mediated inhibition of MBP correlated with a decreased level of phospho-Akt (pAkt), which was reversed by the treatment with amino-Nogo-A Ab. The involvement of pAkt in this process was further confirmed using a PTEN inhibitor BvpPhen (Figure 5A and 5B) that is known to antagonize decreased levels of pAkt by suppressing PTEN catalytic activity and impeding PTEN membrane localization<sup>33</sup>. In the presence of the PTEN inhibitor, there was a dose-dependent increase in the pAkt level accompanied by a corresponding elevation in MBP (Figure 5B). Thus, the results demonstrated that pAkt was involved in amino-Nogo-A mediated inhibition of OPC differentiation, maturation and MBP production. Alternately, when PDGF was used to enhance phosphorylation of Akt, the

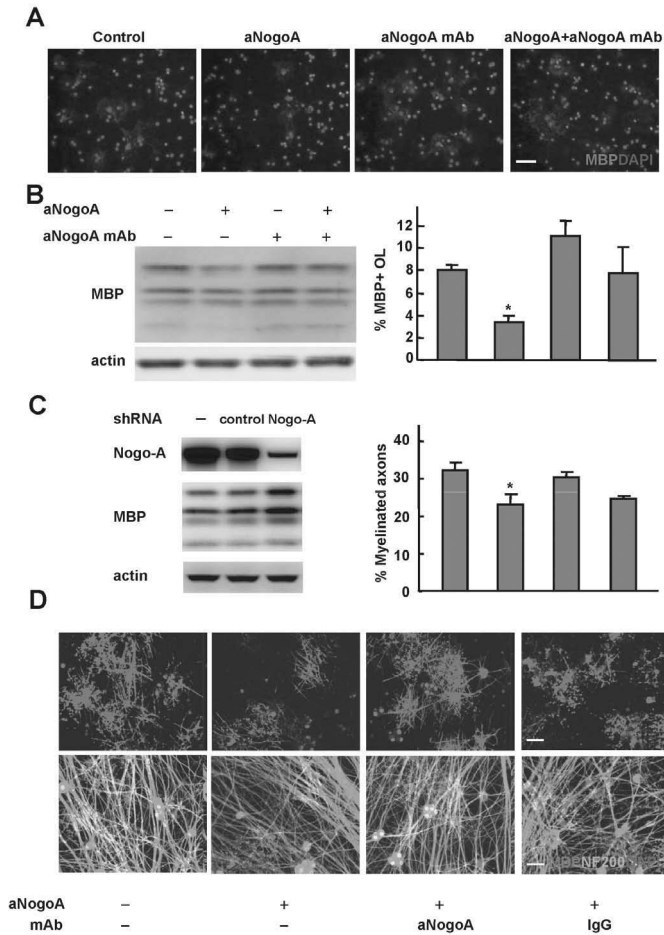


**Figure 4. Effect of amino-Nogo-A antagonism in amino-Nogo-A-mediated inhibition of OPC differentiation, maturation, and myelination.**

A-B, Inhibition of OPC differentiation by amino-Nogo-A (aNogoA). aNogoA at 4 mg/ml was added to OPC culture under differentiation condition in the presence or absence of aNogoA mAb for 4 days. The resulting OPC culture was analyzed for MBP staining (red, upper images) and the percentage of myelin producing oligodendrocytes was quantified by Cellomics (bar graph). The expression level of MBP was analyzed by Western blot. Scale bar, 50  $\mu$ m. C, Reduction in the expression of Nogo-A by shRNA through lentivirus infection. OPC were infected with lentivirus containing either shNogo-A or control shRNA. The expression of Nogo-A and MBP in mature oligodendrocytes was determined by Western blot. D, Effects of aNogoA and aNogoA mAb on OPC and DRG co-culture. aNogoA was added to OPC and DRG co-culture in the presence of aNogoA mAb or IgG control. The resulting cultures were evaluated for myelination of DRG axons by MBP (red) and NF200 (green) co-staining. Scale bar, 50  $\mu$ m. The percentage of myelinated axons was quantified in the lower panel by Cellomics. The data are representative of three independent experiments. \* $p < 0.05$ . See page 322 for a full-color representation of this figure.

inhibition of pAkt by amino-Nogo-A was reversed in the presence of amino-Nogo-A Ab (Figure 5C). Furthermore, purified OPC preparations were subjected to PCR array analysis following treatment with amino-Nogo-A in the presence or absence of amino-Nogo-A Ab. Expression levels of several genes associated with the Akt pathway were altered (data not shown) and their roles in the context of amino-Nogo-A signaling are currently under investigation. Collectively, our results suggest that the effect of amino-Nogo-A in OPC differentiation and maturation is mediated through the Akt pathway.

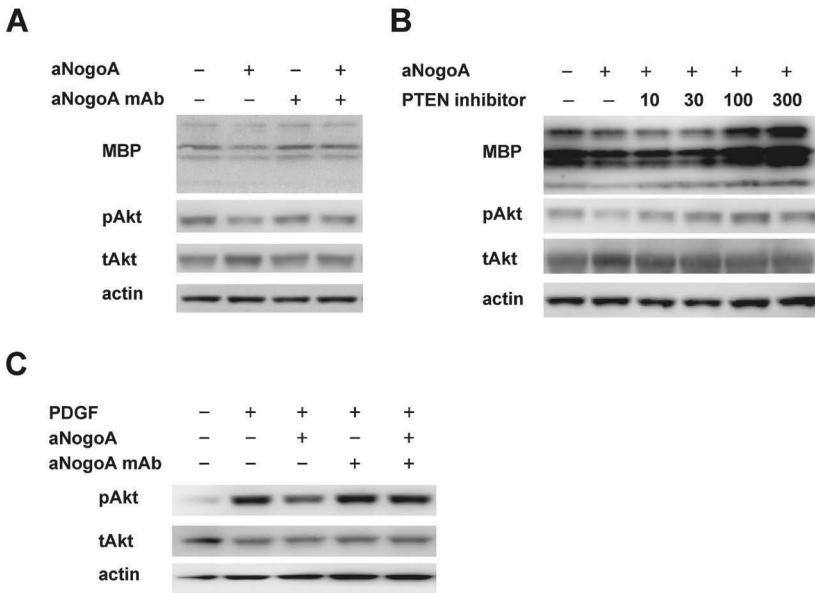


**Figure 5. The role of Akt in amino-Nogo-A-mediated inhibition of OPC differentiation and maturation.** A, aNogoA-mediated inhibition of phosphorylated-Akt (pAkt) and MBP expression in differentiating OPC. pAkt, total Akt (tAkt) and MBP levels were determined by Western blot in the presence or absence of aNogoA and/or aNogoA mAb. B, Dose-dependent effect of a PTEN inhibitor on MBP and pAkt level in the presence of aNogoA. C, Inhibition of PDGF-induced pAkt in aNogoA-treated OPC culture. Actin and total Akt were used as loading control in all immunoblot analyses. The data are representative of three independent experiments.

## DISCUSSION

Nogo-A is one of the major oligodendrocyte myelin proteins that inhibit growth cones and CNS neurite outgrowth via the Rho/Rock pathway<sup>34</sup>. It is preferentially expressed on oligodendrocytes and located at both the outer and the inner adaxonal sheath of myelin<sup>35</sup>. The inhibition of Nogo-A by gene knockout<sup>20</sup> or pharmacological agents, such as Nogo-A Ab, IN-1, NEP40, and soluble Nogo66 receptor, was shown to promote CNS axonal repair and functional recovery in a variety of CNS injury models, including rodent spinal cord injury and stroke models<sup>36-38</sup>. This study is the first demonstration indicating that amino-Nogo-A plays a critical role in myelination. We provide compelling evidence *in vitro* and in demyelinating animal models that the role of amino-Nogo-A is essential to the rate of myelination or myelin repair under pathological demyelinating conditions as amino-Nogo-A antagonism markedly altered the outcome of chemically induced or inflammation-induced demyelination in animal models. It is conceivable that accumulation of amino-Nogo-A contributes to the decreased rate of myelination or myelin repair seen in the CNS pathology in MS<sup>2,3</sup>. In MS lesions, CNS inflammatory insults lead to myelin degradation and the resulting myelin debris contain myelin proteins such as amino-Nogo-A. Our findings suggest that amino-Nogo-A present in the lesions is likely to suppress oligodendrocyte differentiation and maturation, hence affecting myelin repair. This notion is consistent with pathological characteristics of the MS lesions where OPC is abundantly present, but their ability to differentiate and repair damaged myelin is severely impaired.

The potential of amino-Nogo-A Ab as a myelin repair therapy for MS is best demonstrated by a marked reduction in demyelination in marmoset EAE model that closely resembles the human MS pathology<sup>21</sup>. The myelination effect of amino-Nogo-A Ab is specific, as an Ab for myelin associated glycoprotein (MAG) did not exhibit similar efficacy in the same marmoset EAE model (data not shown). Such therapy directly targeting myelination is novel and urgently needed to complement the immunomodulatory treatments that only address the inflammatory component of a complex pathological mechanism in MS. In this study, we also addressed the question of whether the therapeutic efficacy by amino-Nogo-A Ab was partially attributed to a potential anti-inflammatory effect of the Ab in marmoset EAE. However, our results do not support this possibility, because (a) amino-Nogo-A is not expressed on inflammatory cells, including T-cells, B-cells, and macrophages; (b) T-cell reactivity to MOG and their cytokine profile that are critical for encephalitogenicity are not altered in EAE induced marmosets treated with amino-Nogo-A Ab. Similar findings were reported in a recent study using siRNA specific for amino-Nogo-A in rodent EAE<sup>39</sup>. Furthermore, it is important to note that although the Ab is not readily permeable to the blood-brain barrier, it does accumulate in sufficient concentrations in CNS following its characteristic pharmacokinetic profile<sup>40</sup>.

There are many examples in literature where CNS-directed Ab is proven to achieve its CNS effects or clinical outcome through target engagement in both animal models and human trials<sup>40,41</sup>.

In this study, various forms of the amino-Nogo-A Ab, including the full length Ab, bivalent F(ab)<sub>2</sub>, and monovalent Fab preparations were found equally effective in neutralizing LPC-induced reduction of MBP in cerebellar slice culture systems while the Ab has no direct effect on purified OPC (data not shown). This suggests that the site of action for the Ab may be restricted to exogenous amino-Nogo-A, excluding the possibility of an alternative mechanism for amino-Nogo-AAb to interfere with membrane expressed Nogo-A with its putative receptor complex occurring at the OPC membrane surface. It is also likely that amino-Nogo-A interacts with its putative Nogo-A receptor on a neighbouring OPC. However, this notion needs to be investigated as shRNA-Nogo-A knock down leads to the increased expression of MBP, which indicates that either surface expressed amino-Nogo-A or intracellular endoplasmic reticulum-expressed Nogo-A or both, are inhibitory to OPC differentiation and myelination. The amino-Nogo-A-mediated myelination effect is specific and is not expected from Nogo66 and NgR interactions, as NgR is absent in oligodendrocytes (data not shown). Thus, the two distinct domains of Nogo-A may differentially regulate growth cone formation, axon growth, and myelination. The amino-Nogo-A-mediated myelination effect is specific and is not expected from Nogo66 and NgR interactions, as NgR is absent in oligodendrocytes (data not shown). Thus, the two distinct domains of Nogo-A may differentially regulate growth cone formation, axon growth, and myelination.

Another important finding from this study is related to signaling mechanism involved in amino-Nogo-A-mediated inhibition of myelination. A variety of signaling pathways including Akt, Fyn,  $\alpha$ v or  $\beta$ 1 integrins, neuregulin, and Wnt<sup>4-8,42</sup>, were tested in this study to identify the molecular mechanism. Only Akt phosphorylation was found to correlate with MBP expression and oligodendrocyte maturation. To date, other than amino-Nogo-A, modulation of Lingo-1 has been shown to promote myelination *in vivo*<sup>29</sup>. However, the two inhibitory proteins mediate the effect through different signaling events. In case of Lingo-1, RhoA is involved in the inhibition of OPC differentiation and myelination<sup>29</sup>. The mechanism of Lingo-1 modulation via Lingo-1 Ab is complex, as Lingo-1 is not only expressed on both neuronal and oligodendrocyte surfaces but itself represents part of the NgR/p75/Lingo-1 receptor complex. It is expected that modulation of either amino-Nogo-A or Lingo-1 triggers different signal pathways/events. The information may provide an important clue in search of a putative receptor for amino-Nogo-A.

In conclusion, amino-Nogo-A, presented either as degraded fragment from damaged myelin (Nogo-A) or as a structural domain of the Nogo-A molecule expressed on oligodendrocyte surface, negatively modulates myelination through a 'trans' interaction with a putative amino-Nogo-A receptor on OPC via the Akt signaling pathway. This newly

discovered property of amino-Nogo-A provides a novel explanation for the decreased rate of myelination or myelin repair under pathological demyelinating conditions. The evidence presented here supports the role of amino-Nogo-A antagonism as a novel therapy for MS by promoting CNS myelin repair through increased oligodendrocyte differentiation and maturation.

## ACKNOWLEDGEMENTS

We thank Jason Meng, Min Cheng, and Fenglan Wu for their excellent technical assistance. We also thank Drs Taylor Guo, Stewart Leung, Lei Fang, Yueting Zhang and Guhan Nagappan for helpful discussions and preparation of this manuscript.

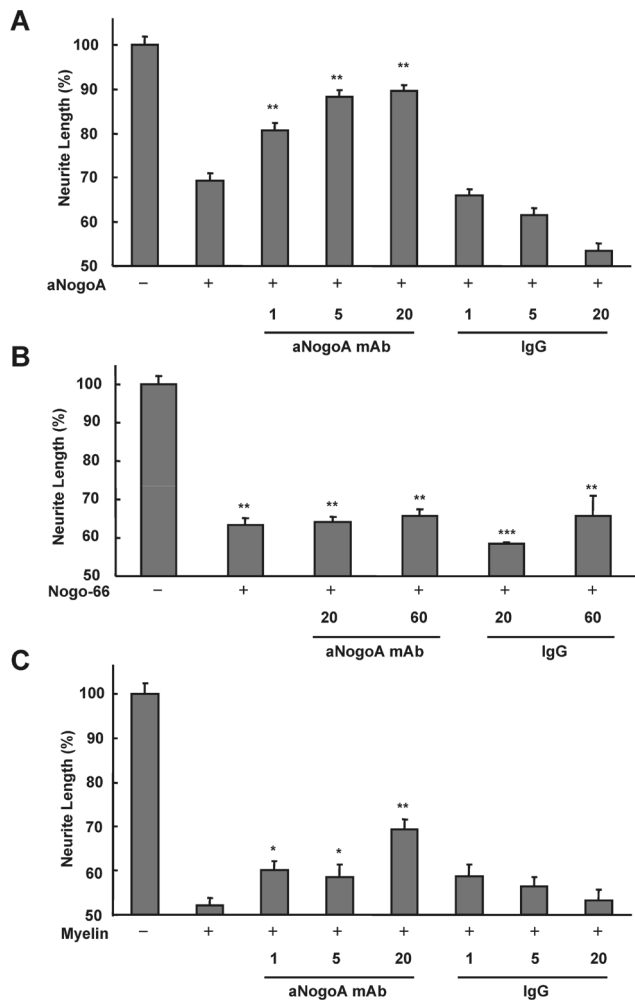
## REFERENCES

1. Kieseier BC et al. Multiple paradigm shifts in multiple sclerosis. *Curr Opin Neurol* 16:247-252 (2003)
2. Franklin RJ et al. Remyelination in the CNS: from biology to therapy. *Nat Rev Neurosci* 9:839-855 (2008)
3. Franklin RJ et al. The biology of CNS remyelination: the key to therapeutic advances. *J Neurol* 255 Suppl 1:19-25 (2008)
4. Brinkmann BG et al. Neuregulin-1/ErbB signaling serves distinct functions in myelination of the peripheral and central nervous system. *Neuron* 59:581-595 (2008)
5. Fancy SP et al. Dysregulation of the Wnt pathway inhibits timely myelination and remyelination in the mammalian CNS. *Genes Dev* 23:1571-1585 (2009)
6. Flores AI et al. Constitutively active Akt induces enhanced myelination in the CNS. *J Neurosci* 28:7174-7183 (2008)
7. Narayanan SP et al. Akt signals through the mammalian target of rapamycin pathway to regulate CNS myelination. *J Neurosci* 29:6860-6870 (2009)
8. Seiwa C et al. Restoration of FcRgamma/Fyn signaling repairs central nervous system demyelination. *J Neurosci Res* 85:954-966 (2007)
9. Caroni P et al. Two membrane protein fractions from rat central myelin with inhibitory properties for neurite growth and fibroblast spreading. *J Cell Biol* 106:1281-1288 (1988)
10. Chen MS et al. Nogo-A is a myelin-associated neurite outgrowth inhibitor and an antigen for monoclonal antibody IN-1. *Nature* 403:434-439 (2000)
11. Prinjha R et al. Inhibitor of neurite outgrowth in humans. *Nature* 403:383-384 (2000)
12. Walmsley AR et al. Targeting the Nogo-A signalling pathway to promote recovery following acute CNS injury. *Curr Pharm Des* 13:2470-2484 (2007)
13. Hu F et al. The N-terminal domain of Nogo-A inhibits cell adhesion and axonal outgrowth by an integrin-specific mechanism. *J Neurosci* 28:1262-1269 (2008)
14. Oertle T et al. Nogo-A inhibits neurite outgrowth and cell spreading with three discrete regions. *J Neurosci* 23:5393-5406 (2003)
15. Bregman BS et al. Recovery from spinal cord injury mediated by antibodies to neurite growth inhibitors. *Nature* 378:498-501 (1995)
16. Freund P et al. Anti-Nogo-A antibody treatment enhances sprouting of corticospinal axons rostral to a unilateral cervical spinal cord lesion in adult macaque monkey. *J Comp Neurol* 502:644-659 (2007)

17. Liebscher T et al. Nogo-A antibody improves regeneration and locomotion of spinal cord-injured rats. *Ann Neurol* 58:706-719 (2005)
18. Jurewicz A et al. Soluble Nogo-A, an inhibitor of axonal regeneration, as a biomarker for multiple sclerosis. *Neurology* 68:283-287 (2007)
19. Satoh J et al. Nogo-A and nogo receptor expression in demyelinating lesions of multiple sclerosis. *J Neuropathol Exp Neurol* 64:129-138 (2005)
20. Karnezis T et al. The neurite outgrowth inhibitor Nogo A is involved in autoimmune-mediated demyelination. *Nat Neurosci* 7:736-744 (2004)
21. Brok HP et al. Non-human primate models of multiple sclerosis. *Immunol Rev* 183:173-185 (2001)
22. Kap YS et al. Fast progression of recombinant human myelin/oligodendrocyte glycoprotein (MOG)-induced experimental autoimmune encephalomyelitis in marmosets is associated with the activation of MOG34-56-specific cytotoxic T cells. *J Immunol* 180:1326-1337 (2008)
23. Almagro JC et al. Humanization of antibodies. *Front Biosci* 13:1619-1633 (2008)
24. 't Hart BA et al. Histopathological characterization of magnetic resonance imaging-detectable brain white matter lesions in a primate model of multiple sclerosis: a correlative study in the experimental autoimmune encephalomyelitis model in common marmosets (*Callithrix jacchus*). *Am J Pathol* 153:649-663 (1998)
25. Aguirre A et al. A functional role for EGFR signaling in myelination and remyelination. *Nat Neurosci* 10:990-1002 (2007)
26. Stoppini L et al. A simple method for organotypic cultures of nervous tissue. *J Neurosci Methods* 37:173-182 (1991)
27. McCarthy KD et al. Preparation of separate astroglial and oligodendroglial cell cultures from rat cerebral tissue. *J Cell Biol* 85:890-902 (1980)
28. Demaison C et al. High-level transduction and gene expression in hematopoietic repopulating cells using a human immunodeficiency virus type 1-based lentiviral vector containing an internal spleen focus forming virus promoter. *Hum Gene Ther* 13:803-813 (2002)
29. Mi S et al. LINGO-1 negatively regulates myelination by oligodendrocytes. *Nat Neurosci* 8:745-751 (2005)
30. Chan MW et al. Aberrant transforming growth factor beta1 signaling and SMAD4 nuclear translocation confer epigenetic repression of ADAM19 in ovarian cancer. *Neoplasia* 10:908-919 (2008)
31. Weissbarth S et al. A sensitive fluorometric assay for 2',3'-cyclic nucleotide 3'-phosphohydrolase. *J Neurochem* 35:503-505 (1980)
32. Blakemore WF et al. Remyelination in experimental models of toxin-induced demyelination. *Curr Top Microbiol Immunol* 318:193-212 (2008)
33. Barros CS et al. Beta1 integrins are required for normal CNS myelination and promote AKT-dependent myelin outgrowth. *Development* 136:2717-2724 (2009)
34. Niederost B et al. Nogo-A and myelin-associated glycoprotein mediate neurite growth inhibition by antagonistic regulation of RhoA and Rac1. *J Neurosci* 22:10368-10376 (2002)
35. Wang X et al. Localization of Nogo-A and Nogo-66 receptor proteins at sites of axon-myelin and synaptic contact. *J Neurosci* 22:5505-5515 (2002)
36. GrandPre T et al. Nogo-66 receptor antagonist peptide promotes axonal regeneration. *Nature* 417:547-551 (2002)
37. Huber AB et al. Nogo-A, a potent inhibitor of neurite outgrowth and regeneration. *Biol Chem* 381:407-419 (2000)
38. Peng X et al. Soluble Nogo receptor down-regulates expression of neuronal Nogo-A to enhance axonal regeneration. *J Biol Chem* 285:2783-2795 (2010)
39. Yang Y et al. Silencing Nogo-A promotes functional recovery in demyelinating disease. *Ann Neurol* 67:498-507 (2010)
40. Laman JD et al. Protection of marmoset monkeys against EAE by treatment with a murine antibody blocking CD40 ( $\mu$ 5D12). *Eur J Immunol* 32:2218-2228 (2002)

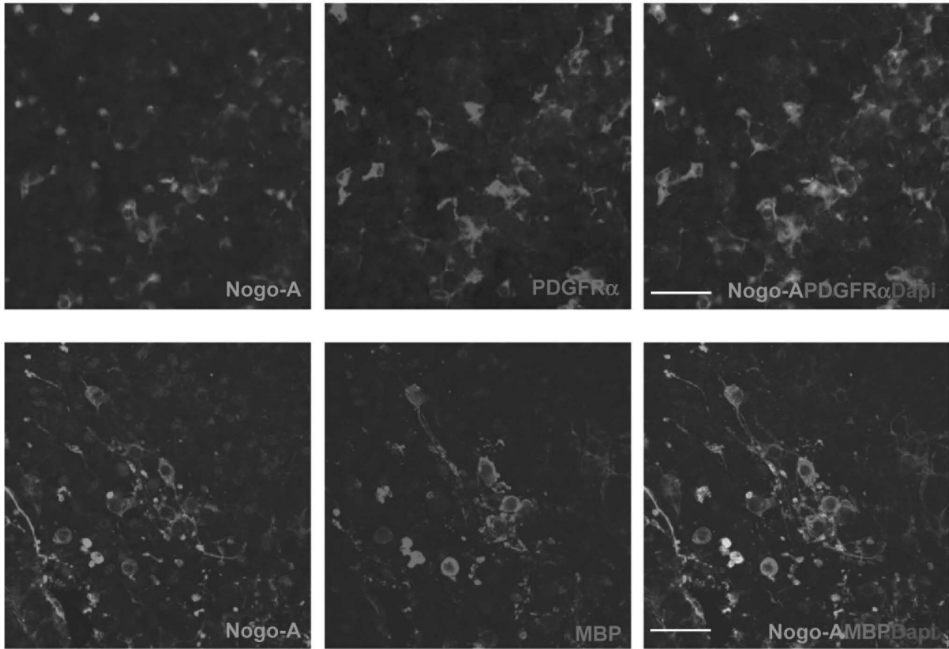
41. Tokunaga M et al. Efficacy of rituximab (anti-CD20) for refractory systemic lupus erythematosus involving the central nervous system. *Ann Rheum Dis* 66:470-475 (2007)
42. Taveggia C et al. Signals to promote myelin formation and repair. *Nat Rev Neurol* 6:276-287 (2010)

**SUPPLEMENTAL FIGURES**



**Supplemental figure 1. The effect of amino-Nogo-A and amino-Nogo-A antagonism on neurite outgrowth.**

aNogoA mAb or IgG control at the indicated concentrations was added to CGN culture in the presence of soluble aNogoA (A), soluble Nogo66 (B), or myelin (plate-coated) (C) for 72 h. Neurite outgrowth was measured by Cellomics and expressed as % of neurite length compared to untreated control. \*p < 0.05; \*\*p < 0.01. The data are representative of three independent experiments.



**Supplemental figure 2. Amino-Nogo-A expression in cerebellar slice culture.**

Cerebellar slice culture was co-stained with aNogoA mAb (green) or antibodies to PDGFRα or MBP (red). Scale bar, 20  $\mu$ m. See page 323 for a full-color representation of this figure.



# 4.5

## **Early treatment with the synthetic hCG-related tetrapeptide LQGV does not modulate experimental autoimmune encephalomyelitis in marmosets**

Yolanda S. Kap<sup>1,2,3</sup>, Nikki van Driel<sup>1</sup>, Erwin Blezer<sup>4</sup>, Robbert Benner<sup>2</sup>, Nisar A. Khan<sup>2</sup>, Jon D. Laman<sup>2,3</sup>, and Bert A. 't Hart<sup>1,2,3</sup>

<sup>1</sup>Department of Immunobiology, Biomedical Primate Research Centre, Rijswijk, The Netherlands; <sup>2</sup>Department of Immunology, Erasmus Medical Centre, Rotterdam, The Netherlands; <sup>3</sup>MS Centre ErasMS, Rotterdam, The Netherlands;

<sup>4</sup>Image Sciences Institute, University Medical Center Utrecht, Utrecht, The Netherlands



## ABSTRACT

The relapse rate of multiple sclerosis (MS) is decreased during the third trimester of pregnancy, but increased in the first three months after delivery. During the third trimester,  $\beta$ -core and presumably other fragments derived from the  $\beta$ -subunit of human chorionic gonadotropin (hCG) may be present in serum. Synthetic peptides related to the hCG  $\beta$ -subunit have remarkable modulatory effects in a broad variety of, mostly acute, inflammatory responses. In this study, we investigated whether the synthetic  $\beta$ -hCG-related tetrapeptide LQGV has modulatory potential in a more chronic inflammatory disease using a well-established experimental autoimmune encephalomyelitis (EAE) model in common marmosets. EAE was induced in marmosets by immunization with a mixture of two synthetic peptides, representing amino acids 34 to 56 and 74 to 96 from myelin oligodendrocyte glycoprotein (MOG34-56 and MOG74-96). The peptides were emulsified in incomplete Freund's adjuvant (IFA) and injected into the dorsal skin of five male marmosets. LQGV (50 mg/kg) was administered by subcutaneous injection three times per week starting two days after immunization to avoid direct interference with the immunization procedure. Treatment with LQGV did not have a consistent effect on the EAE course in this model, as observed by the clinical scores, lesion load, autoantibody levels, or T-cell responses. We conclude that the EAE course in marmosets induced by two MOG peptides in IFA is not modulated by LQGV when given three times per week at a 50 mg/kg dose.

## INTRODUCTION

Multiple sclerosis (MS) is a chronic disease characterized by inflammation, demyelination, and axonal injury in the central nervous system (CNS). MS manifests itself as a relapsing-remitting disease in about 80% of patients. The average age of onset is in the third or fourth decade of life, thus often affecting women of childbearing age<sup>1</sup>. During pregnancy, on a population basis, the relapse rate decreases with 70% in the third trimester, but increases in 30% of the women in the first three months after delivery compared to the pre-pregnancy year<sup>2</sup>. This increase correlates with the relapse-rate before and during early pregnancy<sup>2,3</sup>. The cause of the reduced relapse rate during pregnancy is unknown, but data from animal models suggests a modulatory role of pregnancy hormones, such as estradiol<sup>4</sup> or estriol<sup>5</sup>. It has been suggested that during pregnancy the adaptive immune response is skewed away from Th1 towards Th2<sup>6,7</sup>, although this hypothesis may need revision<sup>8</sup>. Pregnancy hormones may be used as treatment for MS<sup>9</sup>. Treatment of MS patients with estrogen reduced the number and volume of brain lesions, which correlated with a cytokine shift suggesting Th2 skewing<sup>10,11</sup>.

Table 1. Overview of studies with hCG-related oligopeptides.

Model	Species	Peptide (s)	Dose (mg/kg bw)	# of doses	Route	Time of administration	Duration of experiment	Result	Ref.
LPS-induced septic shock	Mouse: BALB/c	VLPALP	15	1	i.p.	2 or 24 h post LPS challenge	84 h	<ul style="list-style-type: none"> <li>Reduced mortality</li> </ul>	15
Hemorrhagic shock (HS)	Rat: Wistar	LQGV, AQQV, or LAGV	5	1	i.v.	30 min after HS induction	120 min	<ul style="list-style-type: none"> <li>Reduction in systemic and liver pro-inflammatory cytokines.</li> <li>Reduced neutrophil number</li> <li>Reduced liver damage</li> <li>LQGV most effective</li> </ul>	16
Renal ischaemia-reperfusion injury	Mouse: C57BL/6	10 peptides, e.g. LQGV and AQQV	Peptides: 5 AQQV: 0.3-30	2	i.v.	1 min before renal ischaemia and 1 min before reperfusion	72 h	<ul style="list-style-type: none"> <li>Reduced mortality</li> <li>Increased kidney function</li> <li>AQQV most effective</li> <li>AQQV:               <ul style="list-style-type: none"> <li>Reduced neutrophil influx and apoptosis in kidney</li> <li>Reduced pro-inflammatory cytokines</li> <li>Most effective: 3 and 10 mg/kg</li> <li>No effect when given after reperfusion</li> </ul> </li> <li>Increased bacterial load in spleen, liver, bone marrow, and blood</li> <li>Lower neutrophil number in blood, spleen, and peritoneal cavity</li> </ul>	17
<i>Listeria monocytogenes</i>	Mouse: C57BL/6	AQQV, LQGV, or VLPALP	50	Daily	i.p.	24 h before infection	6, 18, 48, or 72 h	<ul style="list-style-type: none"> <li>Reduced mortality</li> </ul>	18
LPS-induced septic shock	Mouse: BALB/c	7 peptides, e.g. LQGV	5	1	i.p.	2 or 24 h post LPS challenge	84 h	<ul style="list-style-type: none"> <li>Reduced mortality</li> </ul>	19
Living <i>E. coli</i> -induced septic shock	Rhesus macaque	Cocktail of AQQV, LQGV, and VLPALP	5	1	i.v.	30 min after <i>E. coli</i> infusion	8 h	<ul style="list-style-type: none"> <li>Delayed manifestation of septic shock symptoms</li> <li>Improved pathological features and haemodynamic parameters</li> <li>No change in pro-inflammatory cytokines</li> </ul>	19
Cecal ligation and puncture (CLP)	Mouse: C57BL/6	LQGV	5	2	i.v.	5 min before and 20 min after CLP procedure	21 days	<ul style="list-style-type: none"> <li>Reduced mortality</li> <li>Reduced pro-inflammatory cytokine</li> <li>Improved lung pathology</li> </ul>	Van den Berg, personal communication
Stroke	Mouse: C57BL/6	AQQV or EPPE	30 mg/ml	2	i.v.	15 min before cerebral artery occlusion and 45 min after reperfusion	24 h	<ul style="list-style-type: none"> <li>No effect on infarct volume</li> <li>No effect on cytokine or E-selectin mRNA levels</li> </ul>	Heleen den Hartog, Thesis
EAE	Marmoset	LQGV	50	3x/week	s.c.	2 days after immunization	≤162 days	<ul style="list-style-type: none"> <li>No effect on clinical symptoms, brain lesion load, or immune response</li> </ul>	This chapter

bw, body weight; LPS, lipopolysaccharide

During pregnancy, placental syncytiotrophoblasts produce the hormone human chorionic gonadotropin (hCG)<sup>12</sup>. The serum hCG level increases in the first trimester and peaks in week 10 of pregnancy, which is followed by a decline during the second and third trimester<sup>12</sup>. This pregnancy hormone is a member of the pituitary glycoprotein hormone family and consists of a common  $\alpha$ -subunit, which is shared with other members of the hormone family, and a unique  $\beta$ -subunit<sup>13</sup>. During pregnancy loop-2 of  $\beta$ -hCG is either nicked or excised. In the latter case  $\beta$ -core is the major metabolic product of hCG, which is excreted in the urine<sup>12</sup>. It has been suggested that besides  $\beta$ -core and other metabolic forms of  $\beta$ -hCG also small breakdown products of three to seven amino acids might be generated from the  $\beta$ -loop 2 sequence MTRVLQGVLPALPQ<sup>14</sup>.

Previous work has shown remarkable immunomodulatory effects of  $\beta$ -loop 2-related oligopeptides in animal models for a variety of acute inflammatory models<sup>15-19</sup>. An example of the *in vivo* potency of oligopeptides was the suppression of LPS- or *E. coli*-induced septic shock in mice and non-human primates by one (e.g. LQGV, AQGV) or a mixture of three (LQGV, AGQV, VLPALP)  $\beta$ -loop 2-related oligopeptides<sup>19</sup>. So far, AQGV and LQGV were the most promising  $\beta$ -loop 2-related oligopeptides in all models tested (Table 1).

These findings led us to investigate the effect of LQGV on experimental autoimmune encephalomyelitis (EAE), which is a chronic inflammatory animal model for MS. We have used a unique EAE model in the Neotropical primate common marmoset (*Callithrix jacchus*)<sup>20</sup>. We have previously demonstrated that the core immunopathogenic activity in this model is exerted by T-cells specific for amino acid 34 to 56 from myelin oligodendrocyte glycoprotein (MOG34-56). These T-cells express the natural killer (NK) cell marker CD56, are cytotoxic, and produce IL-17A<sup>21,22</sup>. These T-cells can be activated *in vivo* by immunization with MOG34-56 in incomplete Freund's adjuvant (IFA)<sup>22</sup>.

**Table 2. Overview of monkeys included in this study.**

PBS				LQGV			
Monkey	Sex <sup>a</sup>	Age <sup>b</sup>	Weight <sup>c</sup>	Monkey	Sex <sup>a</sup>	Age <sup>b</sup>	Weight <sup>c</sup>
M06017	M	21	352	M03148	M	48	319
M05056	M	27	388	M06011	M	20	316
M05082	M	25	393	M06005	M	21	346
M03162	M	47	352	M05045	M	17	433
M06012	M	20	370	M06023	M	20	336
Mean		28.0	371	Mean		25.2	350
S.D.		11.0	19.3	S.D.		12.8	48

<sup>a</sup> M, Male; F, Female

<sup>b</sup> Age in months of the monkeys at the start of the experiment

<sup>c</sup> Body weight of the monkeys at the start of the experiment

The aim of this study was to investigate the effect of one of the most potent  $\beta$ -hCG derived synthetic tetrapeptides, i.e. the effect of LQGV treatment on EAE induced by immunization with MOG34-56 and MOG74-96 in IFA. We have found that LQGV displayed no consistent modulatory effect on the clinical score, CNS lesion load, or cellular and humoral autoimmune parameters in the treatment regimen chosen.

## **MATERIALS AND METHODS**

### **Animals**

The common marmoset monkeys used in this study were randomly selected from the outbred colony kept at the Biomedical Primate Research Centre (Rijswijk, The Netherlands) under conventional conditions. Animals were included after a complete physical, hematological, and biochemical check-up had been performed. Animals included in the study are listed in Table 2. The control animals were shared with another experiment aiming at further validation of the IFA model<sup>22</sup>. During the study, monkeys were pair-housed in spacious cages and under intensive veterinary care. The daily diet consisted of commercial food pellets for New World monkeys (Special Diet Services, Witham, Essex, UK), supplemented with rice, raisins, peanuts, marshmallows, biscuits, and fresh fruit. Drinking water was provided ad libitum. According to the Dutch law on animal experimentation, all study protocols and experimental procedures have been reviewed and approved by the Institute's Ethics Committee.

### **EAE induction**

EAE was induced with 100  $\mu$ g MOG34-56 and 100  $\mu$ g MOG74-96 (ABC Biotechnology, London, UK and Cambridge Research Biochemicals, Cleveland, UK) emulsified in 300  $\mu$ l phosphate buffered saline (PBS) and 300  $\mu$ l IFA (Difco Laboratories, Detroit, MI). Antigen-adjuvant emulsions were prepared by gentle stirring the peptide/oil mixture at 4°C for at least 1 h. The inoculum was injected at four locations into the dorsal skin under ketamine anesthesia (40 mg/kg; Produlab Pharma, Raamsdonkveer, The Netherlands). Booster-immunizations were given every four weeks until the monkeys developed clinical score 2 (see below).

Clinical signs were scored daily by two independent observers using a previously described semi-quantitative scale<sup>23</sup>. Briefly, 0 = no clinical signs; 0.5 = apathy, loss of appetite, altered walking pattern without ataxia; 1 = lethargy, anorexia, tail paralysis, tremor; 2 = ataxia, optic disease; 2.25 = monoparesis; 2.5 = paraparesis, sensory loss; 3 = para- or hemiplegia. For ethical reasons monkeys were sacrificed before or once complete paralysis of limbs (score  $\leq$  3.0) was observed, or at the pre-determined endpoint of the study (post sensitization day (psd) 162). Body weight measurements

of conscious monkeys, which is used as a surrogate disease marker, were performed three times per week.

Monkeys selected for necropsy were first deeply sedated by intramuscular ketamin anesthesia (40 mg/kg) and subsequently euthanised by infusion of pento-barbital sodium (Euthesate; Apharmo, Duiven, The Netherlands).

### **Treatment regimen**

Synthetic LQGV (GL Biochem, Shanghai, China) with a purity of >99% (manufacturer's information) was dissolved in 10 mM PBS (pH 7.4) to a concentration of 50 mg/ml. Treatment with LQGV (50 mg/kg body weight) was started two days after immunization and repeated three times per week (psd 2, 4, 7, 9, 11, 14, 16, 18, etc). Before each administration, LQGV was dissolved freshly. Animals received 1 ml/kg body weight of 50 mg/ml LQGV subcutaneously in the flank. Control animals received 1 ml/kg body weight 10 mM PBS.

### **Blood sampling**

Venous blood was collected into heparinized vacutainers (Greiner, Sölingen, Germany) under ketamin anesthesia (40 mg/kg) every two weeks. After centrifugation plasma was collected and stored frozen at -20°C until further analysis.

At necropsy, the number of red and white blood cells was measured using a Sysmex XT-2000iV (Sysmex, Norderstedt, Germany).

### **Magnetic resonance imaging**

Post-mortem magnetic resonance imaging (MRI) was performed as described<sup>22</sup>. Briefly, brain hemispheres were fixed for two weeks in 4% buffered formalin and then transferred to PBS containing azide for equilibration purposes<sup>24</sup>. Post mortem images were obtained on a 9.4 T MRI scanner (Varian, Palo Alto, CA). Before scanning, brains were submerged in perfluoropolyether (Fomblin) to prevent unwanted susceptibility artefacts. White matter lesion load was qualitatively determined and ranged from 0 (no lesions) to 10 (complete destruction of white matter).

### **T-cell responses**

T-cell proliferation was determined as described<sup>21,22</sup>. Briefly, mononuclear cell suspensions from blood or secondary lymphoid organs were cultured for 64 h with a panel of 23-mer synthetic MOG peptides or recombinant human MOG protein (rhMOG). Proliferation was assessed by incorporation of [<sup>3</sup>H]-thymidine (0.5 µCi/well) (PerkinElmer, Boston, MA) during the last 16 h of the culture, which was measured using a matrix 9600 β-counter (Packard 9600; Packard Instrument Company, Meriden, CT). Results are expressed as the mean stimulation index (SI), which is defined as the

counts per minute (cpm) of stimulated cells divided by the cpm of unstimulated cells. SI values above 2.0 were considered to be relevant.

Phenotyping of proliferating cells was performed using CFSE vital dye dilution as described<sup>21</sup>. Briefly, CFSE labeled mononuclear cells were cultured for 7 days with MOG peptides. Cells were stained with Alexa Fluor 700-labeled anti-CD3 (BD Biosciences, CA), APC-labeled anti-CD4 (Zebra Bioscience, Enschede, The Netherlands), biotinylated anti-CD8 (Serotec, Düsseldorf, Germany), streptavidin PerCP (BD Biosciences), and PE-Cy7-labeled CD56 (BD Biosciences). Flow cytometric analysis was performed on a FACS LSRII flow cytometer using FACSDiva software 5.0 (BD Biosciences).

Supernatants of peripheral blood mononuclear cells (PBMC) or mononuclear cells from axillary lymph node (ALN) and spleen were collected after 48 h stimulation with MOG peptides. Cytokine levels were determined by ELISA, which was performed according to the manufacturers instructions for monkey tumor necrosis factor- $\alpha$  (TNF- $\alpha$ ) and monkey interferon- $\gamma$  (IFN- $\gamma$ ) (U-Cytech, Utrecht, The Netherlands) and human cross-reactive interleukin-17A (IL-17A) (eBioscience, San Diego, CA).

### Autoantibodies

Anti-MOG antibodies were determined as described<sup>22</sup>. Briefly, venous blood samples were centrifuged and plasma supernatants were collected and stored at -20°C until further analysis. Antibody binding to rhMOG or to a panel of overlapping 23-mer MOG peptides was determined using ELISA. Bound IgM was detected using alkaline phosphatase-conjugated goat-anti-monkey IgM (Rockland Immunochemicals, Gilbertsville, PA) and bound IgG Ab was detected using alkaline phosphatase-conjugated rabbit-anti-human IgG (Abcam, Cambridge, UK). The results of the antibody assays are expressed as fold increase of light absorbance at 405 nm compared to the reactivity present in sera of non-immunized marmosets.

**Table 3. Primer and probe combinations for quantitative PCR.**

Gene	Forward primer	Reverse primer	Probe
ABL	CAGAGAAGGTCTATGAACTCATGC	GGTGGATTTTCAGCAAAGGAG	GCAGTGGA
CD3	AGGCAAGAGTGTGTGAGAAGCTG	GATGCAGATGTCCACTATGACAA	GGAGGTGG
IL-17A	CCTCATTGGTGTCACTGCTG	TGCAATTCCTGCCTTCACTA	GCTGCTGA
IFN- $\gamma$	GGAGAGAGGAGGGTGACAGA	TTGGATGCTCTGGTTGTCTTTA	CAGAGCCA
TNF- $\alpha$	GGACGAGCTCTCCAAGGACT	GTCACCTCGGGATTCGAGAAG	GGCCCTGG
IL-4	CTAAACGGCTGGACAGGAA	CCTTCACAGGACAGGAGTTCA	CAGCCTGG
IL-6	CCAATCTGGATTCAATGAGGA	AACTCCAAAAGACCAGTGGTGA	GCCTGCTG
IL-10	GTTGCCTTCAGCAGAGTGAA	GCAACCCAGGTAACCCTTAAA	TGCTGGAG
IL-1 $\beta$	TGGTCCTAAACAGATGAAGTGC	GTAGTGCTGGCGGGAGAGT	GACCTGGA

### Quantitative PCR

Spleen and lymph nodes were collected aseptically and a small part was stored in RNAlater (Sigma, St. Louis, MO). RNA was isolated using RNeasy minikit (Qiagen, Hilden, Germany) and cDNA was synthesized using RevertAid First Strand cDNA Synthesis Kit (Fermentas, St. Leon-Rot, Germany) according to the manufacturers instructions. Random hexamer primers were used for cDNA synthesis. Expression levels of mRNA were determined by quantitative PCR using iTaq supermix with ROX and CFX96 Real-Time System (both from Bio-Rad, Hercules, CA). Primer and probes used are listed in table 3. Probes were obtained from the Universal Probe Library set for human (Roche, Indianapolis, In). Transcript levels were normalized against the reference gene *abelson* (ABL)<sup>25</sup>.

### Statistics

Data are presented as mean  $\pm$  sem of 5 control and 4 LQGV-treated marmosets. Statistical analysis was performed using Prism 5.0b for Mac OS X. Survival was analysed using Log-Rank test. Other data was analysed using the Mann-Whitney U test.  $p < 0.05$  was considered statistically significant.

## RESULTS

### Treatment with LQGV has no effect on clinical score

Ten marmosets were immunized with MOG34-56 and MOG74-96 in IFA and boosted with the same peptides in IFA at psd 25, 56, 84, and 133. From psd 2 onwards five animals were subcutaneously treated with LQGV at 50 mg/kg, which was repeated three times per week throughout the study. The other five animals received PBS three times per week (Table 2). All five control animals developed neurological deficit (score  $\geq 2$ ). One control animal (M06012) recovered within one week and remained devoid of neurological deficit, whereas the other four control animals were sacrificed with evident neurological disease (Figure 1A). Three of the five animals treated with LQGV developed neurological disease indistinguishable from the control animals and one animal (M05045) only developed clinical score 1 (Figure 1A). One of the five animals (M06023) of the LQGV group unexpectedly succumbed at psd 34. Post-mortem examination revealed a generalized septic process caused by unknown agents. This animal was excluded from further analyses. LQGV had no effect on disease-free survival (survival until score 2, Figure 1B) nor on survival until sacrifice with overt neurological deficit (survival until day of sacrifice with clinical score  $\geq 2$ , Figure 1C). These data demonstrate that at this dose and treatment regimen LQGV does not ameliorate nor exacerbate EAE.

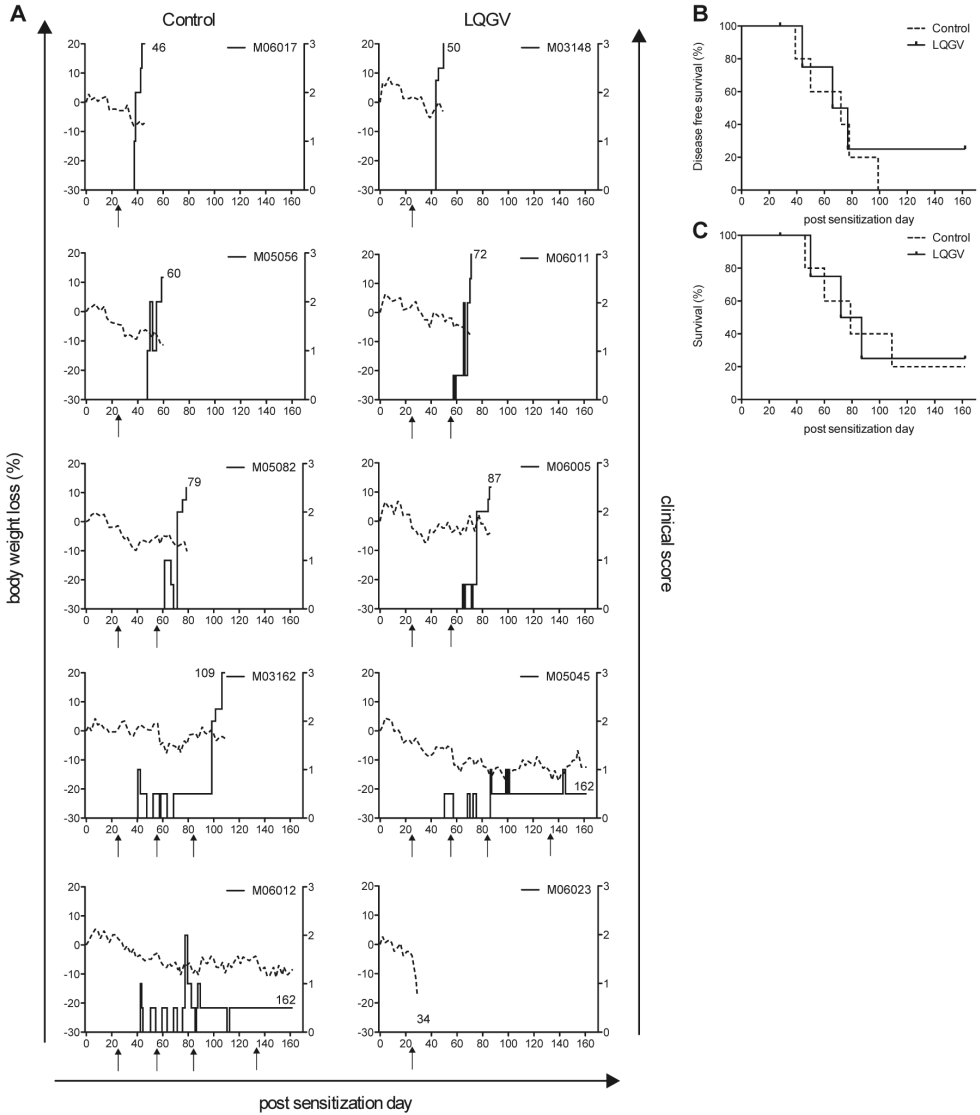


**Figure 1. LQGV does neither ameliorate nor exacerbate clinical signs of EAE.**

A, The post sensitization day is indicated on the x-axis. Animals were immunized on day zero and boosted on the days indicated with the arrows. Shown are the clinical scores of control (left row) and LQGV-treated (right row) animals. Dotted lines indicate the percentage of body weight loss compared to the day of immunization (left y-axis). Solid lines indicate the clinical score (right y-axis). Cyphers indicate the day of sacrifice. LQGV did not change the survival time until score 2 (B) or until the day of sacrifice with clinical symptoms  $\geq 2$  (C).

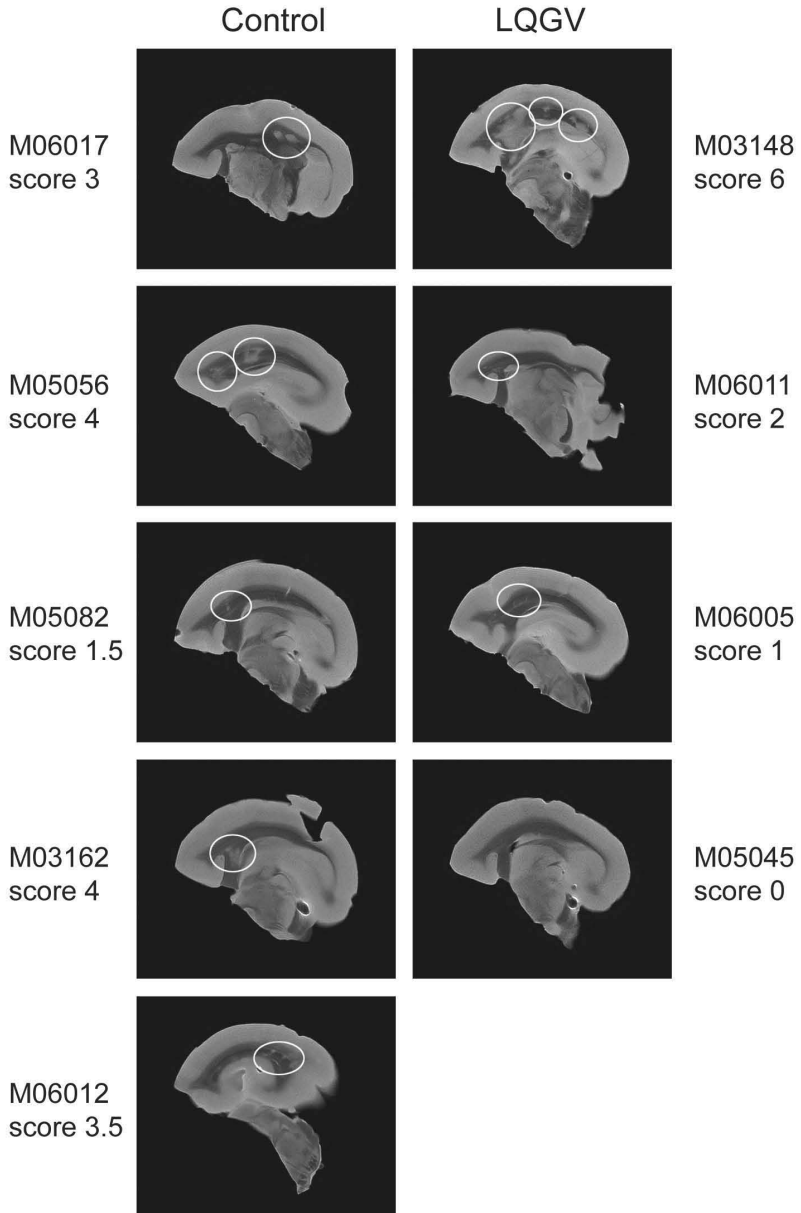


**Figure 2. White matter lesion load is comparable between control and LQGV-treated animals.** Shown is a representative brain slice of each animal. Lesion load is scored from 0 (no lesions) to 10 (complete destruction of white matter) and is indicated under each animal number.

### No change in CNS lesion load after LQGV treatment

At necropsy, one brain hemisphere was fixed in formalin for two weeks and then analysed by post-mortem MRI. T2-weighted images were used to qualify lesion load. The images did not show marked differences in lesion load between control and LQGV-treated animals (Figure 2).

### No effect of LQGV on cell numbers in blood

The number of white blood cells was determined before the start of the experiment and at necropsy. Before the immunization, all animals had comparable numbers of total white blood cells (Range:  $2.3 - 8.3 \times 10^9/l$ ), lymphocytes (Range:  $1.5 - 4.0 \times 10^9/l$ ), monocytes (Range:  $0.07 - 0.25 \times 10^9/l$ ), and neutrophils (Range:  $0.59 - 4.33 \times 10^9/l$ ). At necropsy, one control animal (M05056) showed a profound increase of monocytes and neutrophils, but not of lymphocytes. In all other control and LQGV-treated animals comparable numbers of white blood cells, lymphocytes, neutrophils, and monocytes were observed (Figure 3). These data show that LQGV has no obvious hematological effect in this animal model.

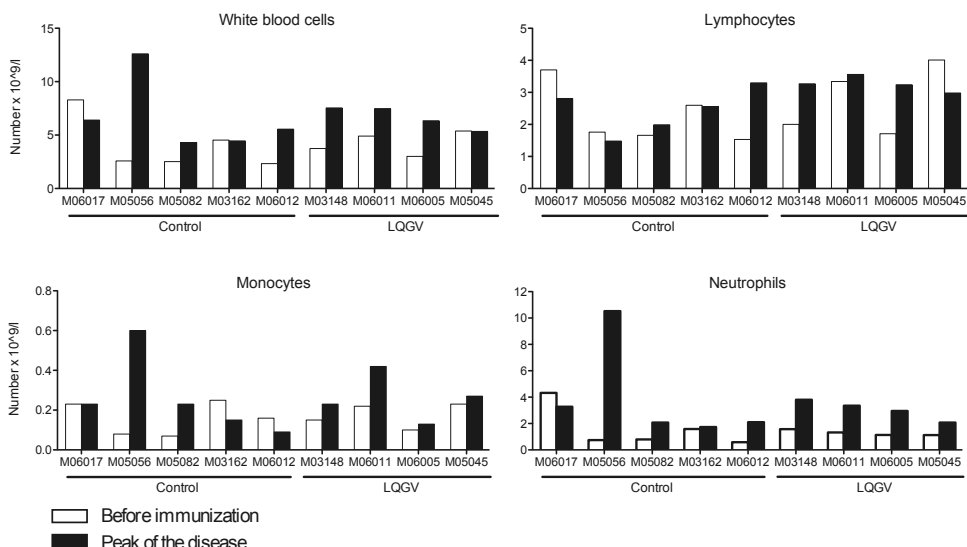


**Figure 3. LQGV treatment does not affect the white blood cell numbers during EAE.**

The number of total white blood cells, lymphocytes, monocytes, and neutrophils were counted before immunization (white bars) and at necropsy (black bars).

**No effect of LQGV on (auto)immune responses**

The effect of LQGV on humoral and cellular immune responses during EAE was investigated at the level of autoantibodies, T-cell proliferation, and cytokine production.

**Antibodies:** Plasma levels of IgM and IgG antibodies against MOG34-56, MOG74-96, and rhMOG were determined in blood samples collected throughout the study. IgM and IgG antibodies against the two immunizing MOG peptides were detected in both groups. We observed no IgM against rhMOG and only limited levels of IgG against rhMOG. Animals treated with LQGV had similar profiles of IgM and IgG antibodies as compared to control animals (Figure 4).

**T-cell proliferation:** In marmoset peripheral blood only low level proliferation against rhMOG and MOG peptides can be measured during EAE studies. Hence, we analysed T-cell proliferation only in blood and lymphoid organs collected at necropsy. Of one control animal (M05056), no proliferation data were available due to technical failure.

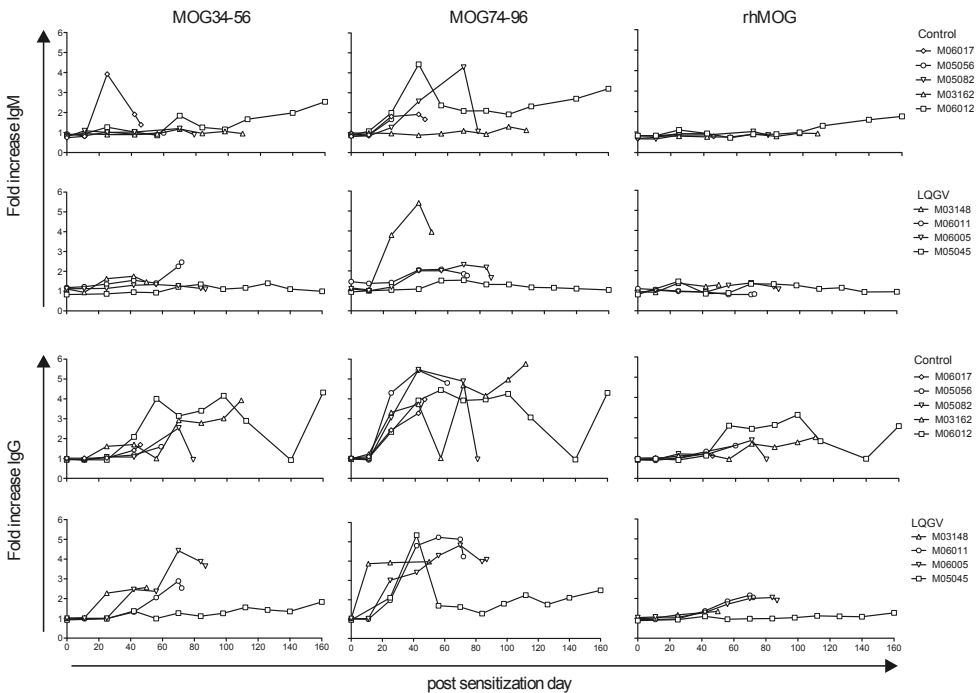


**Figure 4. All animals produced IgM or IgG in response to the immunizing MOG peptides.** IgM and IgG levels against MOG34-56, MOG74-96, and rhMOG were measured in plasma obtained every two weeks. The post sensitization day is indicated on the x-axis. IgM (two upper rows) and IgG (two lower rows) levels are shown as fold increase relative to plasma of non-immunized marmosets.

PBMC of two of the four control animals and of one of the four LQGV-treated animals proliferated in response to MOG34-56. Splenocytes of all four control animals displayed proliferation against MOG34-56 while this was detected in only two of the four LQGV-treated animals. Splenocytes of three of the four control animals proliferated against the other immunizing peptide MOG74-96, in contrast to only one LQGV-treated animal. All LQGV-treated animals and three control animals had cells that proliferated against the immunizing MOG peptides in their ALN and ILN, which drain the dorsal immunization sites. In three of the four control monkeys we observed proliferation against rhMOG in the CNS draining CLN, whereas this response was found in only one LQGV-treated monkey (Figure 5A).

The phenotype of proliferating cells in PBMC, spleen, and ALN was assessed by the CFSE dye dilution assay. Both CD4 and CD8 cells of the spleen showed a somewhat reduced proliferation towards the immunizing MOG peptides, although the number of animals analysed was limited. We observed no such difference in PBMC or ALN (Figure 5B).

**Cytokines:** To investigate whether LQGV had an effect on cytokine profiles, PBMC or mononuclear cell suspensions from spleen or ALN were cultured with rhMOG or

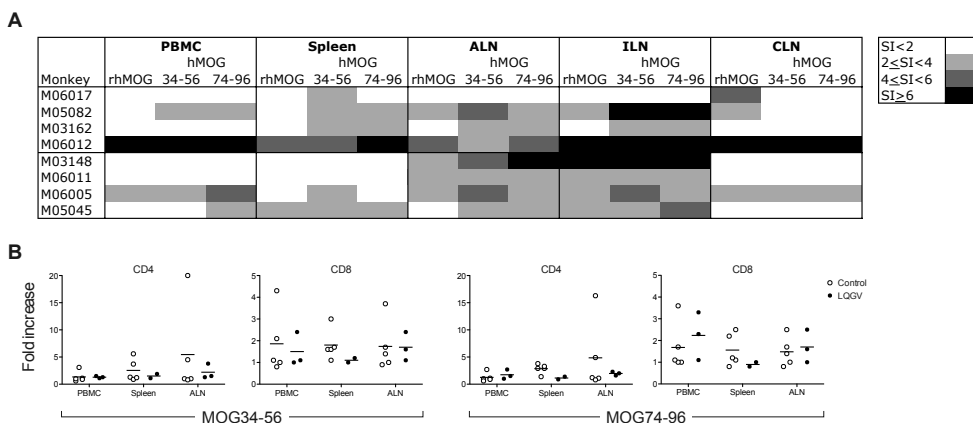


**Figure 5. *In vivo* LQGV treatment does not affect T-cell proliferation *in vitro*.**

A, T-cell proliferation at necropsy was determined by the [3H]-thymidine incorporation assay. The ranges of the stimulation index are shown in grey-scale. Upper bars, control monkeys; lower bars, LQGV-treated monkeys. B, The phenotype of proliferating cells was determined with the CFSE dye dilution assay. Mononuclear cell suspensions from blood, spleen, and ALN of some animals were stimulated with MOG34-56 or MOG74-96. The fold increase is calculated by dividing the percentage of dividing CD3<sup>+</sup>CD4<sup>+</sup> or CD3<sup>+</sup>CD8<sup>+</sup> T-cells after stimulation by the percentage of dividing cells without stimulation. ALN, axillary lymph node; CLN, cervical lymph node; ILN, inguinal lymph node; hMOG, human myelin oligodendrocyte glycoprotein.

immunizing MOG peptides for 48 h. Since the amount of supernatant and the availability of cross-reactive ELISA are limited, protein levels of only IL-17A, IFN- $\gamma$ , and TNF- $\alpha$  were analysed in the supernatant. IFN- $\gamma$  was hardly detectable, i.e. only PBMC of M06012 and splenocytes of M06017 produced detectable IFN- $\gamma$  in response to MOG34-56 (data not shown). Similar levels of TNF- $\alpha$  were detected in PBMC and spleen of both groups. Mononuclear cells derived from the ALN did not produce TNF- $\alpha$  after stimulation. The number of animals with IL-17A secreting cells in the spleen or ALN was lower in the LQGV group than in the control group. No differences were observed in PBMC (Figure 6A).

Finally, we assessed mRNA expression levels of CD3, to investigate whether the T-cell number had changed, and selected cytokines in spleen and ALN. No significant differences in the expression levels between control and LQGV-treated animals were observed, although IFN- $\gamma$ , TNF- $\alpha$ , and IL-4 tended to be increased in the ALN of LQGV-treated animals (Figure 6B).

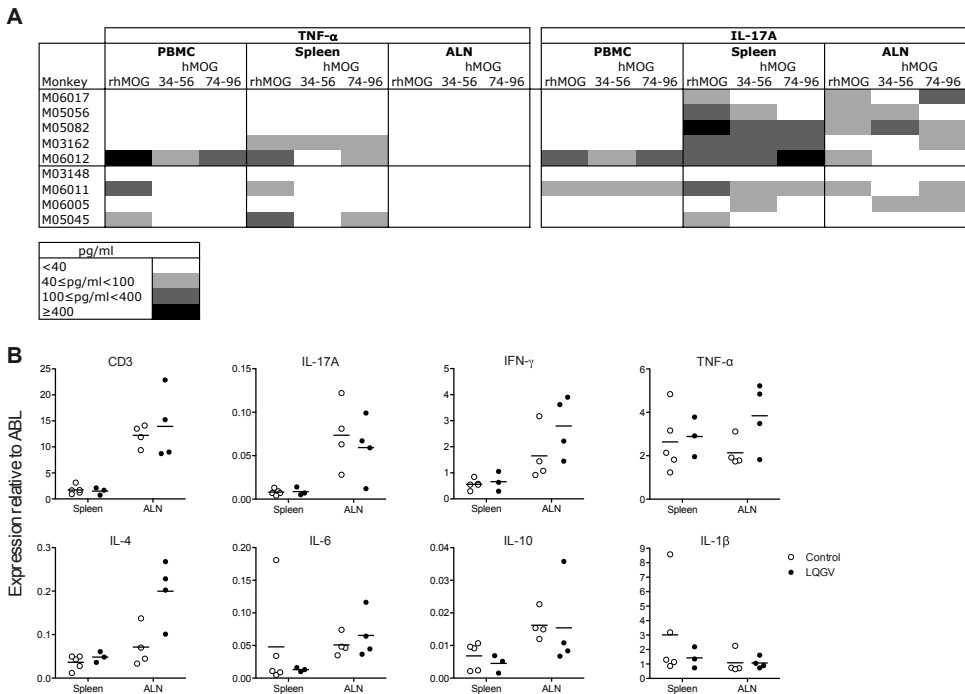


**Figure 6. LQGV does not change cytokine levels.**

A, Cytokine production (pg/ml) was determined in supernatant of cells cultured for 48 h with MOG34-56, MOG74-96, or rhMOG. Upper bars, control monkeys; lower bars, LQGV-treated monkeys. B, mRNA expression levels of CD3 and indicated cytokines in spleen and axillary lymph node (ALN) are shown relative to ABL. No RNA could be isolated from the LQGV-treated animal M03148.

**Cortisol levels**

Corticosteroids have many immunomodulatory effects that may be beneficial in MS and are widely used to accelerate MS relapse recovery<sup>26-28</sup>. Several lines of evidence suggest an influence of stress on the occurrence of relapses in MS and EAE. In addition, the hypothalamic-pituitary-adrenal axis, which is involved in cortisol production, may be disturbed in MS<sup>29</sup>. Cortisol concentrations are increased during the second and third trimester of pregnancy<sup>30</sup>.

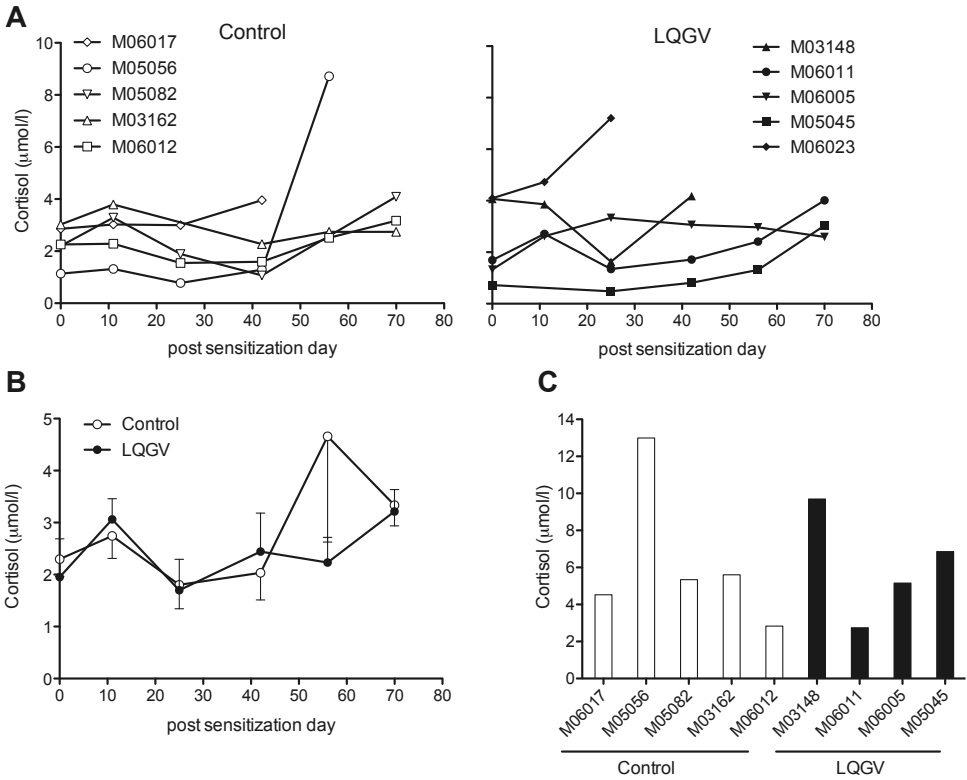


**Figure 7. LQGV does not elevate cortisol levels in plasma.**

Cortisol levels were determined in plasma every two weeks. Shown are the individual data (A) and mean  $\pm$  sem (B). It is important to note that the average cortisol levels were influenced after psd 50 by the death of some animals and the remaining number of animals. Therefore, cortisol levels are shown until psd 80 without necropsy samples. The increase in cortisol in animal M06023 may be caused by the septic process and therefore M06023 was not included in the mean cortisol levels (B). Cortisol levels at necropsy are shown in C. M06012 and M05045 were sacrificed without clinical symptoms of EAE as shown in figure 1.

In order to determine whether LQGV interferes with the cortisol production in this model, we analysed cortisol levels in plasma. During the study, analysed until psd 80, no differences were observed in cortisol level between control and LQGV-treated animals (Figure 7A-B). In the control group, one animal (M05056) had an increase in cortisol at the moment it developed clinical score 2. This animal had also the highest cortisol level at necropsy (Figure 7C). In the LQGV group one animal (M06023) had higher levels of cortisol, but this animal was sacrificed for other reasons than EAE that may have induced cortisol production. No obvious difference in cortisol levels between the two groups was observed at necropsy (Figure 7C).

## DISCUSSION

During the third trimester of pregnancy the relapse rate of MS decreases with 70%<sup>2</sup>. During the same period derivatives from the hCG  $\beta$ -core can be detected in plasma and urine<sup>12</sup>. It has been hypothesized that in this period small breakdown products might be generated from the sequence MTRVLQGVLPALPQ, which comprises the loop 2 of  $\beta$ -hCG. These small breakdown products may be three to seven amino acids long, based on preferential cleavage sites<sup>14</sup>. VLPALP was the first peptide from this sequence that was shown to be biologically active in an LPS-induced shock model in mice<sup>15</sup>. Since the reduction of the MS relapse rate and the production of hCG derivatives concur in the third trimester, we hypothesized that a causal relationship may exist. In this study, we have investigated the effect of the four amino acid peptide LQGV in the marmoset EAE model, an animal model for MS. We observed that treatment with 50 mg/kg LQGV three times per week starting two days after EAE induction had no robust effect on clinical signs, pathology, or the immune response.

Although LQGV did not significantly alter the immune parameters in the marmoset EAE model, some changes in the spleen were observed in individual animals. Proliferation was reduced in both the CD4 and CD8 T-cell compartment of the spleen. IL-17A production in response to MOG stimulation was reduced, although total IL-17A mRNA expression was not altered. During necropsy, the spleen of the LQGV-treated M03148 appeared dark brown and no leukocytes or RNA could be isolated, suggesting that the spleen did not contain viable lymphocytes. The spleen of the LQGV-treated M06011 was strongly enlarged and we were able to culture splenocytes of this animal for 135 days in standard culture medium without adding exogenous growth factors or cytokines. Most of these splenocytes expressed CD20, a B-cell marker (data not shown). A speculative interpretation was that LQGV might have suppressed immune functions engaged in the control of latent (herpes)viruses, such as the marmoset lymphocryptovirus CalHV3. In that case the CD20<sup>+</sup> cells could have been immortalized

B-cells<sup>31</sup>. However, our attempts to positively identify an EBV-related virus have failed thus far.

Although LQGV neither reduced nor exacerbated the clinical signs or pathology in the marmoset EAE model, it induced significant changes in other animal models (Table 1). LQGV reduced inflammation and organ damage in a rat hemorrhagic shock model<sup>16</sup>, and a cocktail of three peptides, among which LQGV, reduced pathology in a rhesus macaque *E. coli* induced shock model<sup>19</sup>. LQGV also increased survival in mice after LPS challenge<sup>19</sup>, renal-ischaemia-reperfusion injury in mice<sup>17</sup>, and in a low-grade cecal ligation and puncture (CLP) model in mice (J.W. van den Berg, personal communication). LQGV also enhanced the susceptibility to *Listeria monocytogenes* in mice when treatment was started prior to infection, which was associated with decreased neutrophil recruitment and increased production of pro-inflammatory cytokines<sup>18</sup>.

Why is LQGV effective in these models and not in the marmoset EAE model induced by two MOG peptides in IFA? First, EAE in marmosets is a chronic disease that can last more than 100 days, whereas all the other models are more acute disease models. The chronicity of the model has two consequences, namely the number of LQGV injections and the predominance of adaptive over innate immune responses. The average day of onset of clinical symptoms in the marmoset EAE model induced by the two MOG peptides in IFA is about 70 days. Although CNS pathology may exist earlier, there is a profound difference in the experimental time line of this EAE model with the other models in which the peptides have been tested. Clinical symptoms and pathology are present within one week after disease induction in most other models that are shown in Table 1. The only exception is the CLP study in mice that lasted 21 days. We decided to chronically treat the marmosets with LQGV, i.e. 3 times per week. This is in contrast with the other models in which the total number of injections was limited to 1 to 4. The models listed in table 1 are all dominated by innate immune responses, involving effector mechanisms of macrophages and neutrophils. Adaptive immune responses can play a role, e.g. in *L. monocytogenes* infection, but not within the time line in which the  $\beta$ -hCG-related peptides were tested<sup>18</sup>. In contrast, in the marmoset EAE model T-cells are one of the most important pathogenic cells, whereas the activation of innate antigen receptors by the inoculum is not required for the induction of the disease<sup>21,22</sup>.

Second, the concentration and dose regimen are different. Marmosets were treated subcutaneously with 50 mg/kg three times per week starting 2 days after immunization. Treatment was started two days after immunization to prevent interference with the first days of immune activation. In all the other models the treatment was started earlier (Table 1) and the LQGV was administered intravenously or intraperitoneally. In all models 5 mg/kg was given once or twice, except in the *L. monocytogenes* infection model where 50 mg/kg was administered daily during the 3 days of the experiment. The subcutaneously route in marmosets was chosen because intraperitoneal injection

is not a preferred dosing route in marmosets and intravenous injection three times per week for 160 days is causing too much discomfort. Unfortunately, we have no methods available to trace LQGV *in vivo* prohibiting *in vivo* pharmacokinetic experiments.

Third, it has not been formally demonstrated that hCG-related oligopeptides pass the blood brain barrier (BBB), which in the EAE model induced with IFA may retain its impermeability.

Recent unpublished data by van der Zee et al. (submitted for publication) show that LQGV enhances corticosterone levels about six-fold in mice up to at least 24 h after administration. This correlated with reduced pro-inflammatory immune responses. In the marmoset EAE model we did not observe an effect of LQGV on cortisol levels. However, we cannot conclude that LQGV is unable to induce cortisol in marmosets, because cortisol levels were measured in plasma three days after LQGV administration. It is therefore unclear whether LQGV induced elevated levels of cortisol within the first 24 h after injection. However, if LQGV indeed enhanced cortisol levels in marmosets, the effect of LQGV would have been more profound. Synthetic glucocorticoids can imitate the anti-inflammatory effects of cortisol and are amongst the most commonly prescribed drugs for autoimmune diseases. Glucocorticoids are also prescribed during acute relapses in MS<sup>26-28</sup>. Methylprednisolone inhibits IFN- $\gamma$  and IL-17A production in mice<sup>32</sup>. These data suggest that elevated levels of cortisol should be able to ameliorate EAE.

In conclusion, LQGV at the tested dosing regimen fails to ameliorate or exacerbate clinical signs, lesion load, and immunological parameters of EAE induced by two MOG peptides in IFA. It may be that  $\beta$ -hCG-related oligopeptides are able to inhibit EAE in marmosets when another dosing regimen is used, such as a cocktail of hCG-related peptides, administration earlier or later during the disease course, only a few injections, or chronic administration via an intravenous infusion pump. However, if the mode of immunomodulatory action of  $\beta$ -hCG-related peptides is indeed via cortisol induction and mitigation of the innate immune response, we deem it unlikely that other treatment regimens or other  $\beta$ -hCG-related peptides can ameliorate T-cell-driven EAE in marmosets.

## ACKNOWLEDGEMENTS

The authors like to thank Fred Batenburg, Mariska van Etten, and Martine Hoffmann for excellent biotechnical assistance and daily care of the monkeys, Jaco Bakker, Gerco Braskamp, and Merel Keehnen for expert veterinary care, Tom Haaksma and Dr. Ivanela Kondova for autopsy of the monkeys. The authors thank Henk van Westbroek for the artwork.

## REFERENCES

1. Compston A et al. Multiple sclerosis. *Lancet* 359:1221-1231 (2002)
2. Confavreux C et al. Rate of pregnancy-related relapse in multiple sclerosis. Pregnancy in Multiple Sclerosis Group. *N Engl J Med* 339:285-291 (1998)
3. Vukusic S et al. Pregnancy and multiple sclerosis (the PRIMs study): clinical predictors of post-partum relapse. *Brain* 127:1353-1360 (2004)
4. Bebo BF, Jr. et al. Low-dose estrogen therapy ameliorates experimental autoimmune encephalomyelitis in two different inbred mouse strains. *J Immunol* 166:2080-2089 (2001)
5. Kim S et al. Estriol ameliorates autoimmune demyelinating disease: implications for multiple sclerosis. *Neurology* 52:1230-1238 (1999)
6. Wegmann TG et al. Bidirectional cytokine interactions in the maternal-fetal relationship: is successful pregnancy a TH2 phenomenon? *Immunol Today* 14:353-356 (1993)
7. Chaouat G. Innately moving away from the Th1/Th2 paradigm in pregnancy. *Clin Exp Immunol* 131:393-395 (2003)
8. Chaouat G. The Th1/Th2 paradigm: still important in pregnancy? *Semin Immunopathol* 29:95-113 (2007)
9. Gold SM et al. Estrogen and testosterone therapies in multiple sclerosis. *Prog Brain Res* 175:239-251 (2009)
10. Sciotte NL et al. Treatment of multiple sclerosis with the pregnancy hormone estriol. *Ann Neurol* 52:421-428 (2002)
11. Soldan SS et al. Immune modulation in multiple sclerosis patients treated with the pregnancy hormone estriol. *J Immunol* 171:6267-6274 (2003)
12. Cole LA. Human chorionic gonadotropin and associated molecules. *Expert Rev Mol Diagn* 9:51-73 (2009)
13. Rao CV. An overview of the past, present, and future of nongonadal LH/hCG actions in reproductive biology and medicine. *Semin Reprod Med* 19:7-17 (2001)
14. Benner R et al. Dissection of systems, cell populations and molecules. *Scand J Immunol* 62 Suppl 1:62-66 (2005)
15. Khan NA et al. Inhibition of septic shock in mice by an oligopeptide from the beta-chain of human chorionic gonadotrophin hormone. *Hum Immunol* 63:1-7 (2002)
16. van den Berg HR et al. Synthetic oligopeptides related to the [beta]-subunit of human chorionic gonadotropin attenuate inflammation and liver damage after (trauma) hemorrhagic shock and resuscitation. *Shock* 31:285-291 (2009)
17. Khan NA et al. Amelioration of renal ischaemia-reperfusion injury by synthetic oligopeptides related to human chorionic gonadotropin. *Nephrol Dial Transplant* 24:2701-2708 (2009)
18. van der Zee M et al. Synthetic human chorionic gonadotropin-related oligopeptides impair early innate immune responses to *Listeria monocytogenes* in Mice. *J Infect Dis* 201:1072-1080 (2010)
19. Khan NA et al. Mitigation of septic shock in mice and rhesus monkeys by human chorionic gonadotrophin-related oligopeptides. *Clin Exp Immunol* 160: 466-478 (2010)
20. Kap YS et al. Experimental Autoimmune Encephalomyelitis in the Common Marmoset, a Bridge Between Rodent EAE and Multiple Sclerosis for Immunotherapy Development. *J Neuroimmune Pharmacol* 5:220-230 (2010)
21. Kap YS et al. Fast progression of recombinant human myelin/oligodendrocyte glycoprotein (MOG)-induced experimental autoimmune encephalomyelitis in marmosets is associated with the activation of MOG34-56-specific cytotoxic T cells. *J Immunol* 180:1326-1337 (2008)
22. Jagessar SA et al. Induction of progressive demyelinating autoimmune encephalomyelitis in common marmoset monkeys using MOG34-56 peptide in incomplete Freund adjuvant. *J Neuropathol Exp Neurol* 69:372-385 (2010)

23. 't Hart BA et al. Preclinical assessment of therapeutic antibodies against human CD40 and human interleukin-12/23p40 in a nonhuman primate model of multiple sclerosis. *Neurodegener Dis* 5:38-52 (2008)
24. Blezer EL et al. Quantitative MRI-pathology correlations of brain white matter lesions developing in a non-human primate model of multiple sclerosis. *NMR Biomed* 20:90-103 (2007)
25. Beillard E et al. Evaluation of candidate control genes for diagnosis and residual disease detection in leukemic patients using 'real-time' quantitative reverse-transcriptase polymerase chain reaction (RQ-PCR) - a Europe against cancer program. *Leukemia* 17:2474-2486 (2003)
26. Sellebjerg F et al. Double-blind, randomized, placebo-controlled study of oral, high-dose methylprednisolone in attacks of MS. *Neurology* 51:529-534 (1998)
27. Sloka JS et al. The mechanism of action of methylprednisolone in the treatment of multiple sclerosis. *Mult Scler* 11:425-432 (2005)
28. Tischner D et al. Glucocorticoids in the control of neuroinflammation. *Mol Cell Endocrinol* 275:62-70 (2007)
29. Heesen C et al. Stress and hypothalamic-pituitary-adrenal axis function in experimental autoimmune encephalomyelitis and multiple sclerosis. *Psychoneuroendocrinology* 32:604-618 (2007)
30. Meulenbergh PM et al. Differences between concentrations of salivary cortisol and cortisone and of free cortisol and cortisone in plasma during pregnancy and postpartum. *Clin Chem* 36:70-75 (1990)
31. Ramer JC et al. Fatal lymphoproliferative disease associated with a novel gammaherpesvirus in a captive population of common marmosets. *Comp Med* 50:59-68 (2000)
32. Mijlkovic Z et al. Methylprednisolone inhibits IFN-gamma and IL-17 expression and production by cells infiltrating central nervous system in experimental autoimmune encephalomyelitis. *J Neuroinflammation* 6:37 (2009)





**GENERAL DISCUSSION**

## PREFACE

MS lesions are composed of a multitude of cell types and mediators of the immune system. However, their exact and distinct roles in the initiation, progression, or modulation of the disease are still unknown. This lack of knowledge hampers the development of effective therapies. For more than a decade, EAE in the common marmoset has been used as a valid animal model for MS to investigate the pathogenesis. In addition, new therapies can be validated in the marmoset EAE model.

At the start of the research described in this thesis in 2006, it had been established that MOG is a crucial component of myelin for the progression of EAE in marmosets. In addition, it was already demonstrated that sensitization of marmosets against rhMOG induces EAE with a 100% disease incidence and that this high incidence mapped to the Caja-DRB1\*W1201 restricted activation of MOG24-36-specific T-cells<sup>1</sup>. In contrast to immunization with rhMOG, immunization with MOG14-36 in CFA only induced mild clinical symptoms with small perivascular infiltrates within the CNS white matter. The cause of this clinical and pathological discrepancy remained to be investigated. The research described in this thesis aimed at identifying the pathogenic mechanisms underlying EAE and MS. In addition, new therapies for MS were validated.

The main results described in this thesis are summarized in Table 1. The combination of exploratory and applied research resulted in new insights into the pathogenic mechanisms and in new possible therapy targets (Figure 1). In **chapter 3**, MOG34-

**Table 1. Advances in the marmoset EAE model.**

<b>Before 2006</b>	<b>2010 (This thesis)</b>
rhMOG induces EAE with 100% incidence	MOG34-56-specific T-cells are associated with fast disease progression in the rhMOG/CFA model
rhMOG activates MOG24-36-specific T-cells in all marmosets	MOG34-56-specific T-cells are CD4 <sup>+</sup> or CD8 <sup>+</sup> , express CD56, are cytotoxic, and produce IL-17A
Immunization with MOG14-36 induces mild EAE	Immunization with MOG34-56 induces full-blown EAE
CFA is used for disease induction	CFA can be replaced by IFA
White matter lesions in the CNS similar to MS	Grey matter lesions are also present and similar to MS
Blocking antibodies against IL-12p40 and CD40 limit EAE	Anti-IL-17A antibody has only a moderate effect on EAE onset, but antibody blocking Nogo-A and antibody depletion of CD20 <sup>+</sup> B-cells prevent EAE

56-specific T-cells were found to play an important pathogenic role in EAE. These T-cells can be activated by immunization with MOG34-56 in IFA and express CD56, are cytotoxic, and produce IL-17A. In **chapter 4**, several new therapeutic targets, such as IL-17A, CD20, and Nogo-A, were validated. These were evaluated in two different EAE models that were developed and validated in this thesis, both using CFA as adjuvant. We demonstrated that neutralization of IL-17A had no protective effect on the disease, but rather delayed the appearance of clinical signs. By contrast, the striking clinical effect of Ab that deplete CD20<sup>+</sup> B-cells or block the interaction of Nogo-A with its receptor demonstrated that B-cells and Nogo-A are major pathogenic players in the disease.

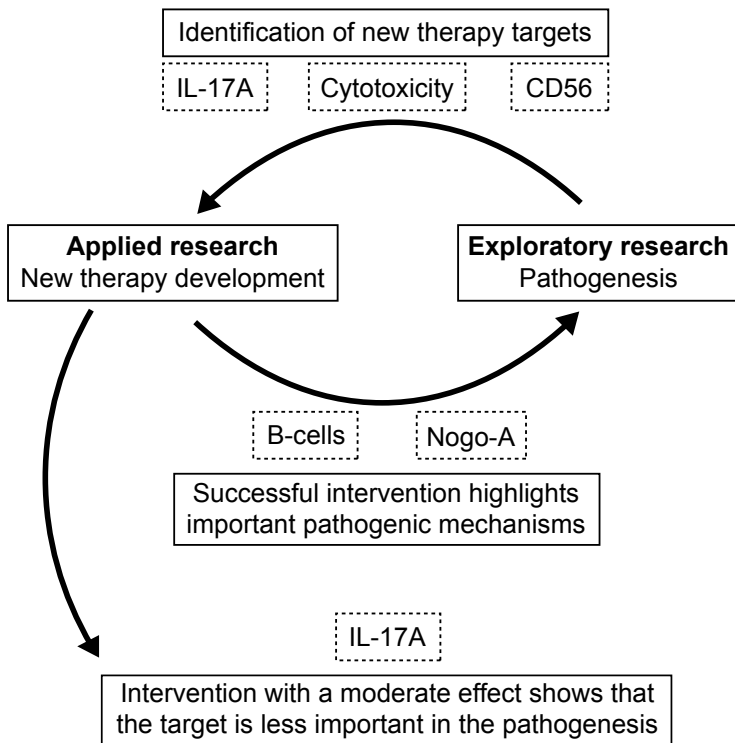


**Figure 1. Results of the research strategy.**

During the exploratory research performed in chapter 3, we showed that MOG34-56-specific T-cells are associated with EAE. These T-cells are CD56<sup>+</sup>, are cytotoxic, and produce IL-17A. Therefore, new targets for therapy may be CD56, the exocytosis of cytotoxic granules, and IL-17A. Applied research described in chapter 4 demonstrated that IL-17A is only moderately involved in the disease, whereas CD20<sup>+</sup> B-cells and Nogo-A are essential for the disease.

The induction of EAE in marmosets with a single MOG peptide in IFA without microbial ligands raises questions about the activation mechanism of T-cells and how the permeabilization of the BBB is effected. Therefore, the underlying mechanisms of the IFA model are discussed below. Next, the clinical course and immune response are compared between the three used EAE models. In addition, pathogenic mechanisms in the periphery and the CNS are discussed as well as future prospects.

## THE MECHANISMS UNDERLYING THE IFA MODEL

### CFA versus IFA

IFA is a water-in-oil emulsion composed of paraffin oil and the surfactant mannide mono-oleate. Although IFA prolongs the presence of Ag at the immunization site and enhances the uptake of Ag by dendritic cells (DC)<sup>2</sup>, the mechanisms of action of IFA are still unknown. When inactivated mycobacteria are emulsified in IFA it is called CFA. The mycobacteria provide the ligands of innate antigen receptors on APC, in particular TLR4. Engagement of TLR4 with bacterial antigens relays maturation signals to the APC resulting in the induction of co-stimulatory molecules, such as CD40 and CD80/86, and pro-inflammatory cytokines, such as IL-12 and IL-23. Previous research showed that both CD40 and IL-12/IL-23 are important in the EAE pathogenesis in the marmoset models induced with CFA<sup>3-6</sup>. IFA can be used in human vaccines, where it elicits a strong Ab response, although it is nowadays often replaced by other oil-based adjuvants<sup>7</sup>. CFA is the most frequently used adjuvant for formulation of autoantigens to induce autoimmune diseases in animals. Immunization with MOG in IFA failed to induce EAE in essentially all mouse strains<sup>8</sup>, but did induce EAE in the DA rat<sup>9</sup>. Induction of full-blown clinical EAE with widespread demyelination in CNS grey and white matter with MOG peptide in IFA has also been reported in marmosets (**Chapter 3.2**). Clearly, this new EAE model in the marmoset induced by MOG34-56 in IFA represents a major improvement for ethical, practical, and mechanistic reasons.

### IFA and the innate immune response

Although this thesis focuses mainly on the adaptive immune response, the innate immune response is also involved in MS<sup>10</sup>. In EAE, the innate immune response is activated by the mycobacteria in CFA as described above. Since IFA does not contain mycobacteria, the question raises whether the innate immune response is involved in the marmoset EAE model induced by MOG34-56/IFA.

We have demonstrated that IFA does not activate TLR- or NLR-dependent mechanisms *in vitro* (**Chapter 3.2**). Also others could not detect NLR-mediated IL-1 $\beta$  production after IFA stimulation *in vitro*<sup>11</sup> or *in vivo*<sup>12</sup>. The hCG-related oligopeptide LQGV did not

modulate EAE induced by MOG34-56+MOG74-96/IFA (**Chapter 4.5**), whereas LQGV impairs the innate immune response in mice after, for example, infection with *Listeria monocytogenes*<sup>13</sup>. This suggests that the innate immune response may not play a role in this particular IFA model. However, as also discussed in **chapter 4.5**, it is likely that other causes underlie the results of the LQGV study, such as the chosen treatment regimen. Another explanation may be that LQGV affects mainly the neutrophil compartment<sup>13,14</sup>, whereas neutrophils do not play a role in the marmoset EAE model<sup>15</sup>.

Several lines of evidence suggest that IFA can activate the innate immune response. IFA increased bacterial resistance in mice<sup>16</sup> and induced the expression of various cytokines, such as TNF- $\alpha$  and GM-CSF, suggesting that IFA can activate the innate immune system<sup>12,17</sup>. In addition, in **chapter 3.2** we demonstrate TNF- $\alpha$  production in culture supernatant and the presence of macrophages and complement deposition in WM lesions after immunization with MOG34-56/IFA.

### IFA and the APC

DC isolated from IFA-injected mice expressed MHC class II and the co-stimulatory molecules CD80, CD86, and CD40 at a low level<sup>18</sup>. This suggests that IFA does not induce DC maturation, which is needed for the activation of naive autoreactive T-cells. The addition of *M. tuberculosis* to IFA induced DC maturation *in vitro* and *in vivo*<sup>18</sup>. If non-matured DC serve as APC in the marmoset EAE model, only Ag-experienced T-cells may be activated. MOG-specific T-cells are present in the naive repertoire of marmosets<sup>19</sup>, which may have a memory phenotype. Memory T-cells are generated after, for example, a viral infection. Amino acids 986 to 993 (WLRSPFSR) from the major capsid protein UL86 of CMV and amino acid 963 to 970 (WQRTPFSV) from the major capsid protein of HHV-6 show sequence similarity with MOG39-46 (WYRPPFSR). This suggests that non-matured DC presenting MOG34-56 can activate CMV- or HHV-6-specific memory T-cells.

Alternatively, when non-matured DC are not the core APC in the marmoset EAE model, which cell type could then have that crucial function? We hypothesize that B-cells are the central APC in the MOG34-56/IFA model. Depletion of CD20<sup>+</sup> B-cells three weeks after immunization of marmosets with rhMOG/CFA significantly reduced T-cell proliferation and T-cell activation in secondary lymphoid organs (**Chapter 4.2**). This shows that B-cells can act as APC in the rhMOG/CFA model. In addition, EBV-transformed marmoset B-cell lines can be used to generate MOG34-56-specific T-cell lines *in vitro*, showing that B-cells are capable of presenting MOG34-56 to T-cells (**Chapter 3**). To investigate whether B-cells are also the APC in the MOG34-56/IFA model, the B-cell depletion protocol used in rhMOG/CFA model should be repeated in the IFA model.

### **IFA and the blood-brain barrier**

How do autoreactive T-cells that are activated in the IFA model enter the CNS? Both CFA and IFA induce BBB permeability, although CFA is the most potent one<sup>20,21</sup>. In addition, T-cells are able to enter the CNS when the BBB is not permeabilized by adjuvants, such as during immune surveillance or after adoptive transfer. Furthermore, CCR6<sup>+</sup> Th17 cells may enter the BBB via the choroid plexus by interaction with CCL20<sup>22</sup> or Th17 cells induce BBB permeabilization<sup>23,24</sup>. This suggests that CFA is not necessarily required to permeabilize the BBB and that T-cells in the IFA model are also able to enter the CNS.

### **THREE MARMOSET EAE MODELS**

Marmosets were initially immunized with human myelin emulsified in CFA in combination with two intravenous doses of heat-inactivated *Bordetella pertussis*<sup>25</sup>. To identify which myelin epitopes and which autoimmune processes are crucial for the induction and progression of EAE, the marmoset EAE model has been stepwise refined (Figure 2). This yielded three different EAE models that are induced by immunization with rhMOG/CFA, MOG34-56/CFA, or MOG34-56/IFA, respectively. These three EAE models display similar clinical signs and overall pathology, but differ with respect to the clinical course as well as the humoral and cellular autoreactivity profiles.

#### **Clinical course**

For comparison of the clinical course, we included 14 marmosets that were immunized with rhMOG/CFA (from the control groups of **chapter 4.1** and **4.2**), 16 marmosets that were immunized with MOG34-56/CFA (**Chapter 3.1** and the control group of **chapter 4.4**), and 5 marmosets that were immunized with MOG34-56/IFA (**Chapter 3.2**). Marmosets immunized with MOG34-56 plus MOG74-96 in IFA (**Chapter 3.2 and 4.5**) were not included in the analysis, because this model will not be used in the future and was only used as an intermediate refinement step from MOG34-56/CFA to MOG34-56/IFA.

The three disease induction protocols all induced a chronic progressive disease with similar clinical symptoms, such as ataxia, paresis, and paralysis. However, the progression rate to the onset of overt clinical signs (score  $\geq 2$ ) and the day of sacrifice differs between the three models (Table 2, Figure 3A). The animals immunized with rhMOG/CFA (n=14, single immunization) developed clinical score 2 with an average time of disease onset of 59 days after immunization (Table 2). In contrast to the single immunization with rhMOG/CFA, all animals immunized with MOG34-56 in either CFA or

IFA needed at least one booster immunization with MOG34-56 in IFA before developing clinical signs. All animals immunized with MOG34-56 in CFA or IFA developed score 2, except one MOG34-56/CFA-immunized animal (M02075, **chapter 3.1**). The average time to clinical score 2 was 82 days in MOG34-56/CFA-immunized animals and 69 days in MOG34-56/IFA-immunized animals (Table 2). Thus, the time to disease onset was

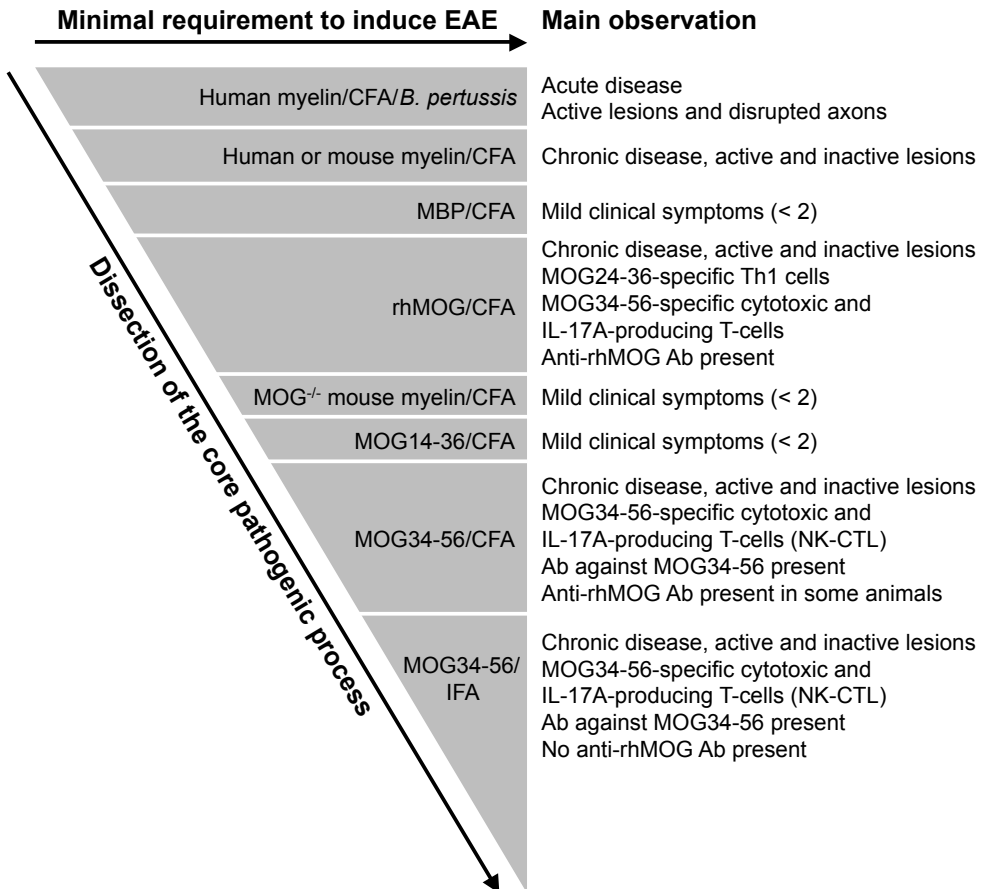


**Figure 2. Dissection of the core pathogenic process.**

EAE was originally induced in marmosets by immunization with human myelin emulsified in CFA and an injection of heat-killed *Bordetella pertussis*. The stepwise elimination of elements from the EAE induction protocol has led to a model induced by MOG34-56 emulsified in IFA. During this stepwise refinement, it became clear that MOG34-56-specific T-cells play a key pathogenic role. These T-cells are cytotoxic, express CD56, and produce IL-17A. Adapted from<sup>138</sup>.

**Table 2. Clinical course of three EAE models.**

rhMOG/CFA		MOG34-56/CFA		MOG34-56/IFA	
Score 2 <sup>a</sup>	End <sup>b</sup>	Score 2	End	Score 2	End
39	53	27	34	43	50
41	55	63	71	59	67
43	46	64	- <sup>c</sup>	71	79
46	55	68	132	79	- <sup>c</sup>
46	59	71	91	91	100
48	55	72	85		
54	60	72	86		
65	85	72	89		
66	73	73	78		
66	83	73	83		
71	78	77	91		
71	- <sup>c</sup>	80	91		
78	91	104	110		
91	111	146	151		
		164	166		
		-	- <sup>c</sup>		
59 ± 4 <sup>d</sup>	70 ± 5	82 ± 9 <sup>e</sup>	97 ± 9 <sup>e</sup>	69 ± 8	74 ± 11

<sup>a</sup> First day after immunization that score 2 was observed

<sup>b</sup> Time to the day of sacrifice with clinical score ≥ 2

<sup>c</sup> Sacrificed with clinical score ≤ 2 due to survival until pre-determined end-point

<sup>d</sup> Mean ± SEM

<sup>e</sup> Time to disease onset and time to sacrifice are significantly delayed in the MOG34-56/CFA model compared with rhMOG/CFA, see also figure 3

significantly shorter in rhMOG/CFA-immunized animals compared with the MOG34-56/CFA model, but not when compared with the MOG34-56/IFA model (Figure 3A). However, the latter experiment comprised five animals. When five animals immunized with MOG34-56/IFA of a recently performed, yet unpublished, study were included, the disease onset in the rhMOG/CFA model was also significantly earlier than in the MOG34-56/IFA model (data not shown). Immunization with MOG34-56 in CFA or IFA did not result in marked differences in time to disease onset, neither with nor without the five extra animals (Figure 3A).

In addition to the time to disease onset, the day of sacrifice was compared between the three models. Table 2 shows the day that the animals were sacrificed with a clinical score of 2 or higher. In the three models, one (rhMOG/CFA and MOG34-56/IFA) or two

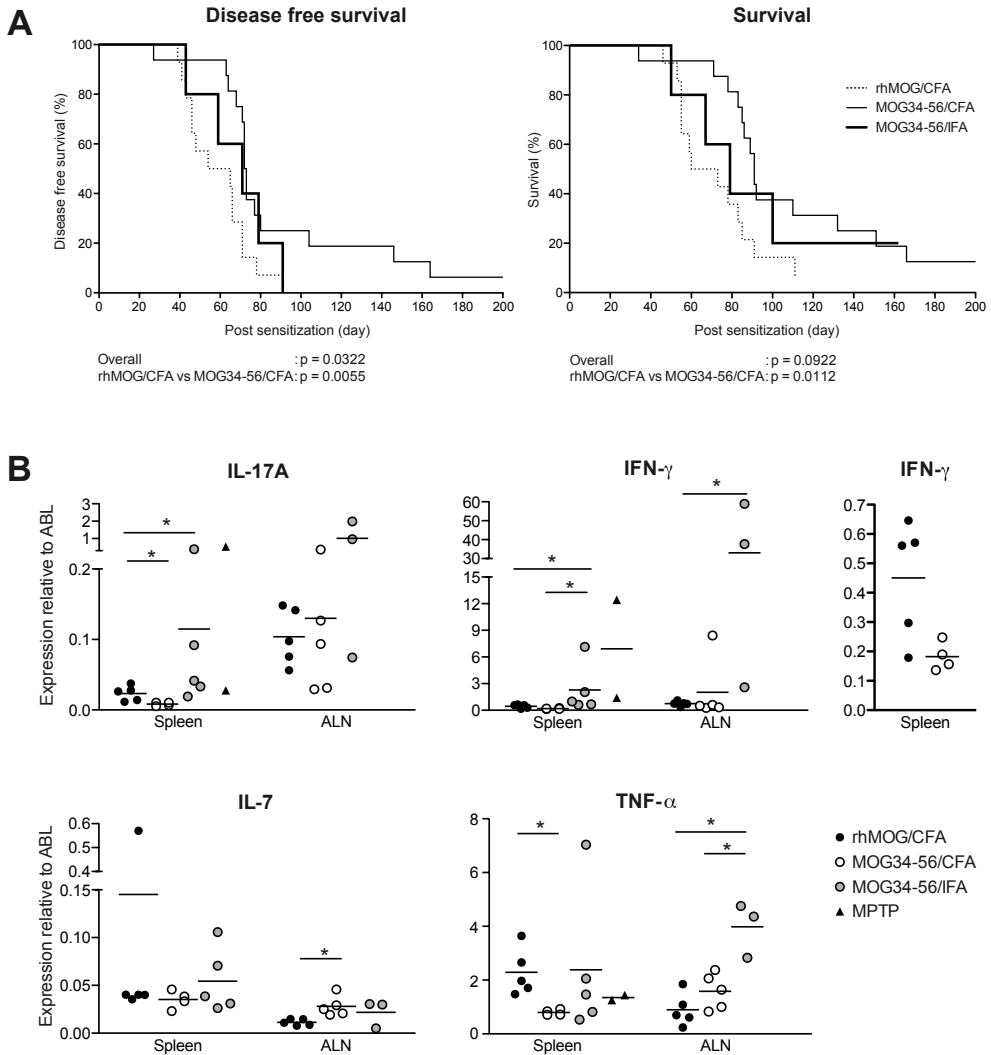


**Figure 3. Clinical course and cytokine mRNA levels in three marmoset EAE models.**

Immunization with rhMOG/CFA, MOG34-56/CFA, and MOG34-56/IFA were compared. A, Demonstrates the survival graph until clinical score 2 (left graph) and until the endpoint (right graph). Time to disease onset (clinical score 2) and time to sacrifice (with clinical score  $\geq 2$ ) is significantly delayed in the MOG34-56/CFA model compared with the rhMOG/CFA model. B, mRNA expression levels of IL-17A, IFN- $\gamma$ , IL-7, and TNF- $\alpha$  were determined by quantitative PCR in animals immunized with rhMOG/CFA, MOG34-56/CFA, or MOG34-56/IFA to induce EAE, and in two animals injected with MPTP to induce Parkinson's like disease. The right graph of IFN- $\gamma$  shows the comparison of rhMOG/CFA and MOG34-56/CFA. Statistical differences were analysed by Mann-Whitney U-test and considered significant when  $p < 0.05$  (\*).

(MOG34-56/CFA) animals were sacrificed with a clinical score lower than 2, because they survived until the pre-determined end-point of the study. The average day of sacrifice with a clinical score 2 or higher was 70, 97, and 74 days after immunization with rhMOG/CFA, MOG34-56/CFA, and MOG34-56/IFA, respectively (Table 2). The day of sacrifice was significantly earlier in the rhMOG/CFA model compared with the MOG34-56/CFA model (Figure 3A). The day of sacrifice after immunization with MOG34-56/IFA did not differ from the other two models, also not when the five animals of the unpublished study were included (data not shown).

In conclusion, immunization with rhMOG/CFA leads to a more rapid disease onset and day of sacrifice than immunization with MOG34-56/CFA. This may be caused by the involvement of autoantibodies and a broader T-cell response in the rhMOG/CFA model. In addition, the T-cell subsets activated after immunization may influence the disease course. There is no obvious difference in the clinical presentation of EAE induced with MOG34-56 in CFA or IFA. The overall pathology, such as demyelination and inflammation, does also not differ between both MOG peptide models. However, lesions should be investigated in further detail to assess whether more subtle differences may exist. Adoptive transfer of T-cells stimulated with IL-12p70 or IL-23 both induced paralysis, but with distinct cellular composition and cytokine profiles in the lesions<sup>26</sup>. If the MOG34-56/CFA model is more Th1 prone and if the MOG34-56/IFA model is more Th17 prone, the lesions in these two models may also show a different cellular composition and/or cytokine profile.

### **The anti-MOG Ab response**

The more rapid disease development in the rhMOG/CFA-immunized animals may be explained by the involvement of anti-MOG Ab. As shown and discussed in **chapter 3**, the Ab response in MOG34-56-immunized animals was mainly directed against the immunizing peptide. In about half of the MOG34-56/CFA-immunized animals, we also detected Ab binding to rhMOG, but this was not the case in MOG34-56/IFA-immunized animals. This indicates a lower capacity of Ag/IFA emulsion to induce anti-MOG Ab. This was also shown in guinea pigs, in which serum IgG concentrations increased after CFA injection, but remained low after IFA injection<sup>20</sup>.

Although deposits of IgM molecules and complement were observed in CNS lesions of MOG34-56/CFA- or MOG-34-56/IFA-immunized marmosets, it is unclear whether these contributed to lesion formation. It is possible that Ab have passively leaked into the CNS, but that they do not have a direct pathogenic role. It has been demonstrated that both CFA and IFA can affect the BBB<sup>20,21</sup>, suggesting that Ab can leak into the CNS in all three marmoset EAE models.

The results obtained in the marmoset EAE models induced with MOG34-56 suggest that anti-MOG Ab are not essential for the development of clinical signs and pathology

in marmosets. Our results are in line with results obtained in several MOG peptide induced mouse EAE models where demyelination can occur in the absence of Ab<sup>27-29</sup>. The conclusion that Ab directed against rhMOG are not essential for lesion formation in EAE does not imply that they are irrelevant. It has been well established that anti-MOG Ab can amplify demyelination under experimental conditions where demyelination is not or only marginally induced. As an example, marmosets immunized with MBP, PLP, or a chimeric MBP-PLP protein only developed demyelination when anti-MOG Ab were present<sup>30,31</sup>.

### **Anti-MOG T-cell reactivities**

Immunization with MOG34-56 in either CFA or IFA induces T-cell responses that are mainly directed against MOG34-56 and the overlapping peptide MOG24-46. This means that only one or two T-cell specificities are activated after immunization with MOG34-56. As shown in **chapter 3**, immunization with rhMOG/CFA leads to a T-cell response directed against several MOG epitopes. In chapter 3, we also demonstrated that animals with 1 or 2 anti-MOG specificities have a slower disease onset than animals with a broad anti-MOG T-cell response. This suggests that MOG34-56/CFA-immunized animals that have 1 or 2 T-cell reactivities are comparable with the slow progressors of the rhMOG/CFA model. This may contribute to the slower disease onset in MOG34-56/CFA-immunized animals.

### **The role of Th1 and Th17 cytokines**

The cytokine profile of T-cells may also partly contribute to the difference between the three EAE models. T-cells isolated from the spleen or lymph nodes of rhMOG/CFA-immunized animals that were cultured with rhMOG for 48 h secreted IL-17A and IFN- $\gamma$  (**Chapter 4.2**). In contrast, T-cells isolated from MOG34-56/IFA-immunized animals that were cultured for 48 h with MOG34-56 or rhMOG only secreted IL-17A, but no IFN- $\gamma$ . MOG34-56-induced secretion of IFN- $\gamma$  and IL-17A by T-cells isolated from MOG34-56/CFA-immunized animals will be determined in future experiments.

In addition to the MOG-induced cytokine protein data, we measured the mRNA expression levels of several cytokines in the lymphoid organs. It is important to note that these cytokine mRNA expression levels reflect the cytokine production in the whole organ and that these responses are not per se produced by MOG-specific T-cells. Although the low number of tested samples in all groups makes that data should be interpreted with caution, the results are suggestive for different mRNA levels between the three EAE models (Figure 3B).

IL-17A and TNF- $\alpha$  mRNA levels were significantly lower in the spleen, but not in the ALN, of MOG34-56/CFA-immunized animals compared with rhMOG/CFA-immunized animals. Also, the IFN- $\gamma$  mRNA level is clearly, albeit not significantly, lower in these

animals ( $p = 0.06$ ). Interestingly, IL-17A, IFN- $\gamma$ , and TNF- $\alpha$  mRNA levels were higher in MOG34-56/IFA-immunized animals compared with the other two groups. Cytokine mRNA profiles of healthy animals are not available yet. Therefore, we cannot conclude whether the cytokine levels in the IFA group are higher or normal compared with naive animals. We have compared the data with the cytokine mRNA expression levels in the spleen of two marmosets that did not receive any CFA or IFA injection, but which were subcutaneously injected with 1-methyl-4-phenyl-1,2,3,6-tetrahydropyridine (MPTP) to induce Parkinson's like-disease. The mRNA levels of IL-17A, IFN- $\gamma$ , and TNF- $\alpha$  in the spleen of MOG34-56/IFA-immunized animals were comparable with the cytokine mRNA levels in the spleen of MPTP-injected animals.

The low mRNA levels of IL-17A and IFN- $\gamma$  in the CFA models compared to the IFA model may be caused by the use of CFA, which is known to change the cellular composition of the lymphoid organs. For instance, it has been demonstrated that the spleen of rhMOG/CFA-immunized marmosets contains fewer T-cells when clinical symptoms are present<sup>32</sup>.

The mRNA level of IL-7 is highest in the spleen of the MOG34-56/IFA group and in the ALN of the MOG34-56/CFA group (Figure 3B). IL-7 is produced by nonhemopoietic stromal cells in multiple organs, such as the thymus and lymphoid organs. IL-7 is required for T-cell development and survival<sup>33,34</sup> and also acts on B-cells<sup>35</sup>. IL-7 was recently found to be essential for the survival and expansion of Th17 cells<sup>36</sup>. This suggests that the high levels of IL-7 in the spleen of the MOG34-56/IFA group may underlie the high levels of IL-17. In addition, IL-7 is involved in the survival of CD56<sup>+</sup> NK cells<sup>37</sup> and may therefore also support the survival of the CD56<sup>+</sup> MOG34-56-specific T-cells that were found to have a key pathogenic role in the marmoset EAE model. A polymorphism in the IL-7 receptor  $\alpha$  gene has been identified as a risk factor for MS<sup>38</sup> and anti-IL-7R $\alpha$  Ab is effective in mouse EAE<sup>36</sup>. In addition, we show that IL-7 mRNA levels were reduced after B-cell depletion, which may be associated with the significant effect of B-cell depletion on disease progression (**Chapter 4.2**). This suggests a pathogenic role of IL-7 in EAE and MS.

### **Concluding remarks about the three EAE models**

In conclusion, the three discussed marmoset EAE models are essentially different despite the similar clinical score and overall pathology. To further optimize and refine the marmoset EAE model, there are several promising options for future investigation. First, the development of GM lesions should be extensively investigated in all three models, because these appear to correlate well with clinical progression in MS<sup>39-41</sup>. Second, the marmoset EAE model should be further optimized by immunization with rhMOG emulsified in IFA. Predictably, this will induce EAE as MOG34-56-specific T-cells are clearly activated by immunization with rhMOG/CFA. When EAE should not

develop in marmosets immunized with rhMOG/IFA, the possibility that rhMOG contains epitopes for regulatory T-cells warrants consideration. Immunization with rhMOG/IFA may induce autoantibodies similar to the rhMOG/CFA model. Although anti-MOG Ab are not essential for the development of EAE in marmosets, this model may better reflect the pathogenesis of MS, in which autoantibodies are also present.

The question remains which model is to be preferred to test a new therapeutic compound for MS. We cannot conclude which of these three models best resembles MS, because the critical immunopathogenic mechanisms in MS are still unknown. Ideally, therapies that were or were not efficient in MS should be tested in all three EAE models to investigate which model gives similar results to MS. For example, ustekinumab, an anti-IL-12p40 Ab, was very effective in myelin/CFA- and rhMOG/CFA-induced EAE in marmosets<sup>5,6</sup>. In contrast, ustekinumab was essentially ineffective in RRMS<sup>42</sup>. It would be interesting to investigate the effect of ustekinumab in the MOG34-56/IFA model to examine whether the results are similar to MS. An example of an effective treatment in MS is B-cell depletion by an anti-CD20 Ab. B-cell depletion by an anti-CD20 Ab reduced lesion load and relapse rate in RRMS<sup>43,44</sup>. In the rhMOG/CFA marmoset EAE model, B-cell depletion was also effective (**Chapter 4.2** and **4.3**). To compare whether the MOG34-56/IFA model is similar to the rhMOG/CFA model, the B-cell depletion strategy should be repeated in the MOG34-56/IFA model. IFN- $\beta$  is another therapy that should be tested in the three marmoset EAE models. It has been shown that IFN- $\beta$  effectively inhibits EAE after adoptive transfer of Th1 cells in mice. In contrast, IFN- $\beta$  exacerbates EAE after adoptive transfer of Th17 cells. In addition, RRMS patients that are non-responders to IFN- $\beta$  treatment had elevated serum levels of IL-17F, which is produced by Th17 cells<sup>45</sup>. This suggests that IFN- $\beta$  is effective in Th1-mediated disease, but not in Th17-mediated disease. Treatment of marmosets with IFN- $\beta$  may demonstrate which EAE model is mainly Th1 or Th17 driven. If one of the three marmoset EAE models is non-responsive to IFN- $\beta$ , this model may be used to develop therapies for the IFN- $\beta$  non-responders.

## PERIPHERAL IMMUNOPATHOGENIC MECHANISMS

### MOG24-36-specific Th1 cells versus MOG34-56-specific cytotoxic T-cells

The normal repertoire of healthy marmosets contains T-cells that are specific for several MOG epitopes, mainly to MOG21-40 and MOG31-50<sup>19</sup>. Both T-cell specificities were implicated in the pathogenesis of EAE induced with rhMOG/CFA<sup>1</sup> (**Chapter 3.1**).

MOG24-36-specific T-cells are activated by APC presenting MOG24-36 via the monomorphic MHC class II allele *Caja-DRB\*W1201*, which is expressed in all marmosets despite the fact they are outbred<sup>1,46,47</sup>. MOG24-36-specific T-cells are mainly CD4<sup>+</sup> and

express IFN- $\gamma$ <sup>19</sup> suggesting they are Th1 cells. However, some MOG21-40-specific T-cell lines isolated from naive marmosets did not produce IFN- $\gamma$ <sup>19</sup>. It is unknown whether these IFN- $\gamma$  cells produce IL-17A. Therefore, we cannot conclude whether all MOG21-40-specific T-cells are Th1 and not Th17. Activation of MOG24-36-specific T-cells is not enough to induce the full spectrum of clinical symptoms and pathology as immunization with MOG14-36/CFA<sup>1</sup> or adoptive transfer of MOG21-40-specific T-cells<sup>19</sup> induced only mild clinical symptoms in marmosets. This suggests that activation of additional T-cell specificities is needed for the induction of full-blown disease.

Indeed, T-cells specific for MOG34-56 likely have a pathogenic role in the marmoset EAE model. Fast progression of the disease in marmosets immunized with rhMOG/CFA is associated with a broadened T-cell reactivity to MOG epitopes, against MOG34-56 in particular. MOG34-56-specific T-cells are CD4<sup>+</sup> or CD8<sup>+</sup>. In addition, these T-cells are cytotoxic and express the NK marker CD56, suggesting that these cells are NK-CTL (**Chapter 3.1**). However, these cells also produce IL-17A (**Chapter 3.2**). These T-cells can be activated by immunization with MOG34-56 in CFA or IFA (**Chapter 3**). Whether the MOG34-56-specific T-cells are purely Th1 or Th17 is unclear at this stage. In the marmoset IFA model, MOG34-56-specific T-cells produce IL-17A, but no IFN- $\gamma$  (**Chapter 3.2**). In contrast, two of the three MOG31-50-specific T-cell lines isolated from naive non-immunized marmosets produced IFN- $\gamma$ <sup>19</sup>.

In summary, several T-cell subsets likely contribute to the development of marmoset EAE, i.e. CD4<sup>+</sup> and CD8<sup>+</sup> T-cells, Th1 and Th17 cells, as well as MOG24-36 and MOG34-56-specific T-cells. We would like to hypothesize that after immunization MOG24-36-specific Th1-cells are activated in all animals and induce inflammation in the CNS, whereas MOG34-56-specific cytotoxic T-cells induce demyelination. The inflammation induces only mild clinical symptoms, such as altered walking pattern, whereas the activity of the MOG34-56-specific cytotoxic T-cells induces the full spectrum of clinical signs.

### **The role of IL-17A**

Until a few years ago, only two functional subsets of activated CD4<sup>+</sup> T-cells were distinguished, namely Th1 and Th2. Since then, additional subsets have been discovered, such as Th17<sup>48</sup>, Th9<sup>49</sup>, and Th22<sup>50</sup>, named after their signature cytokines. MS was initially considered a Th1 driven disease. However, with the discovery of the Th17 subset as well as that CD8<sup>+</sup> T-cells are more prevalent in MS lesions than CD4<sup>+</sup> T-cells, this became under debate (extensively reviewed in<sup>48,51</sup>). It was shown that the signature cytokine IL-17A is present in serum, CSF, and CNS of MS patients<sup>23,52-55</sup> and evidence from rodent EAE suggested also involvement of IL-17A (see below and Table 3). The activity spectrum of Th17 cells has not been completely elucidated yet. Th17 cells may play a role in the defense against extracellular pathogens<sup>56</sup>. Moreover,

Th17 cells are also considered highly pro-inflammatory and may be involved in several autoimmune diseases. Th17 cells produce among others IL-17A, IL-17F, IL-21, and IL-22<sup>56</sup>. IL-17 is a family of at least 6 members, but the effect of IL-17A in autoimmunity has been investigated in most detail. Besides CD4<sup>+</sup> T-cells, IL-17A is also produced by CD8<sup>+</sup> T-cells<sup>57</sup>, NK cells<sup>58</sup>, NKT cells<sup>59</sup>, and microglia<sup>60</sup>. IL-17 induces the production of cytokines and chemokines, especially neutrophil-attracting chemokines<sup>61,62</sup>.

By which pathways Th17 cells differentiate and expand has not been completely unraveled. These pathways differ between mice and men<sup>63</sup>. T-cells probably differentiate into Th17 cells by a cocktail of TGF- $\beta$ , IL-6, IL-1 $\beta$ , and TNF- $\alpha$ <sup>63,64</sup>. Th17 cells can expand in the gut<sup>65</sup>. IL-23 was first considered essential for the differentiation of Th17 cells, but now it is suggested to play a role in the expansion or maintenance of already differentiated Th17 cells<sup>64</sup>. IL-23 is a heterodimeric cytokine composed of a p19 and a p40 subunit that is shared with IL-12, being the most important cytokine for Th1 induction.

Many researchers have investigated the role of IL-17A in mouse EAE models using different approaches, such as knockout mice<sup>66-72</sup>, mAb treatment<sup>5,6,69,73-75</sup>, vaccination<sup>73,75,76</sup>, and adoptive transfer<sup>26,69-71,77-79</sup> (Table 3). Collectively, these studies yielded inconclusive and in part contradictory results. This suggests that the pathogenic function of autoreactive Th1 and Th17 cells in EAE and MS is highly complex and differs between individual animals or humans. Treatment with anti-IL-17A Ab in the rhMOG/CFA marmoset model, starting one day before immunization, caused only a modest delay of the disease onset without a marked effect on pathology and immune response. This is consistent with anti-IL-17A Ab treatments in mouse EAE models in which incidence and maximum score was only reduced 50% and not 100% (Table 3). These findings argue against a prominent role of IL-17A in the induction phase of EAE in rhMOG/CFA-immunized marmosets (**Chapter 4.1**).

That anti-IL-17A Ab did not prevent the development of EAE in marmosets can be explained in several ways. First, the pathogenic role of Th17 cells may not be (exclusively) mediated by the signature cytokine IL-17A. It has been shown that both Th1 and Th17 cells can induce EAE after adoptive transfer<sup>26,79</sup>. Second, neutralization of IL-17A may have no beneficial effect on the cytotoxicity of MOG34-56-specific T-cells, which is dependent on granule exocytosis as shown in **chapter 3.2**. This suggests that MOG34-56-specific T-cells activated by rhMOG/CFA retain their cytotoxic activity and thus the ability to induce pathology and thereby clinical signs. Third, EAE induced by CFA may not be the appropriate model to test the efficacy of anti-IL-17A Ab treatment, since both Th1 and Th17 cells are activated in this model. We have shown that MOG34-56-specific T-cells activated by immunization with MOG34-56 in IFA produce IL-17A, but no IFN- $\gamma$ . This suggests that the anti-IL-17A Ab may be more effective in the MOG34-56/IFA model. Which of the three marmoset EAE models is the best representative for MS is so far unclear. MS patients that are non-responders to IFN- $\beta$  treatment have elevated

**Table 3. IL-17 manipulation in EAE models.**

<b>IL-17A essential for EAE induction?</b>					
<b>Species</b>	<b>EAE induction</b>	<b>Transgenic</b>	<b>Yes (+) No (-) Maybe (-/+)</b>	<b>Remarks</b>	<b>Ref.</b>
Mouse: C57BL/6	MOG34-56/ CFA+PTX	IL-23p19 <sup>-/-</sup>	+	Resistant to EAE; IL-23 not needed for T-cells to cross BBB	68,69,71
		IL-12/23p40 <sup>-/-</sup>	+	Resistant to EAE	66-68
		IL-12p35 <sup>-/-</sup>	+	Susceptible to EAE; IL-23, but not IL-12, is essential for EAE	66-68
		IL-17 <sup>-/-</sup>	-/+	Suppression of EAE; 91% incidence with clinical score 2 (Wt 100%, score 3)	70,72
		Overexpression of IL-17A	-	No change in EAE	72
<b>Species</b>	<b>EAE induction</b>	<b>mAb treatment</b>			
Mouse: SJL	PLP139-151/ CFA	Anti-IL-17A Ab (day 7)	-/+	Partial protection of EAE; 3/5 mice with clinical score 2 (5/5 control score 4)	69
	PLP139-151/ CFA+PTX	Anti-IL-17A Ab (day -1, 6)	-/+	Partial protection of EAE; clinical score 1 (control 2) No change in CNS inflammation	74
	PLP139-151/ CFA	Anti-IL-17A Ab (2x/week from day 0)	+	EAE prevented in 8/10 mice; 2/10 mice score 0.5	75
Mouse: C57BL/6	MOG34-56/ CFA	Anti-IL-17A Ab (day 6, 10, 14)	-/+	EAE score reduced from 2 to 1	73
Marmoset	rhMOG/CFA	Anti-IL-17A Ab (weekly, from day -1)	-	Time of onset delayed, but not significant	This thesis
Mouse: SJL	PLP139-151/ CFA+PTX	Anti-IL-12p40 (day -1, 6)	+	Partial amelioration of EAE; 21 % incidence with clinical score 1; IL-12 or IL-23 needed for EAE	74
		Anti-IL-23p19 Ab (day -1, 6)	+	Prevention of EAE; 8% incidence with score 0.3; IL-23 needed for EAE induction	
Marmoset	Myelin/CFA	Anti-IL-12p40 (day 14-86, weekly)	+	Prevention of EAE; 1/5 animals score 2.5; IL-12 or IL-23 needed for EAE	5
	rhMOG/CFA	Anti-IL-12p40 (when MRI lesions present)	-/+	Time to score 2 delayed	6

Species	EAE induction	Vaccination			
Mouse: C57BL/6	MOG34-56/ CFA+PTX	IL-17-VLP (before EAE induction)	-/+	Partial protection against EAE; 30% incidence with score 1.2 (control 2.4)	<sup>76</sup>
		IL-17-receptor-Fc fusion protein (after onset clinical signs)	-/+	Partial protection of EAE; 0.5 reduction in clinical scores for a few days	<sup>73</sup>
Mouse: SJL	PLP139-151/ CFA	IL-17A-OVA (before EAE induction)	+	Prevention of EAE	<sup>75</sup>
<b>Adoptive transfer</b>					
Donor	Recipient				
MOG-specific lymphocytes from MOG35-55/CFA/PTX-immunized Wt C57BL/6	p40 <sup>-/-</sup> C57BL/6 +PTX		-/+	EAE severity decreased; 40% incidence with score 2.4 (control 3); IL-12 or IL-23 is essential in effector phase of EAE	<sup>77</sup>
CD4 <sup>+</sup> T-cells from MOG35-55/CFA-immunized IL-17 <sup>-/-</sup> C57BL/6	Wt C57BL/6		+	MOG specific T-cells from IL-17A <sup>-/-</sup> mice cannot efficiently induce EAE	<sup>70</sup>
MOG-specific CD4 <sup>+</sup> T-cells from MOG35-55/CFA/PTX-immunized Wt C57BL/6	p19 <sup>-/-</sup> C57BL/6 p35 <sup>-/-</sup> C57BL/6 p19/p35 <sup>-/-</sup> C57BL/6		-	Similar to Wt recipient; IL-23 is not required during effector phase of EAE	<sup>71</sup>
MOG-specific CD4 <sup>+</sup> T-cells from MOG35-55/CFA/PTX-immunized p19 <sup>-/-</sup> C57BL/6	Wt C57BL/6		-/+	EAE severity reduced; 100% incidence; score 2 instead of 4; IL-23 plays a role in induction phase	
PLP-specific CD4 <sup>+</sup> T-cells from PLP139-151-immunized SJL, primed with IL-23 or IL-12	Wt SJL		+	Th1 and Th17 both enter CNS; Th17 induce clinical signs	<sup>69</sup>
PLP-specific CD4 <sup>+</sup> T-cells from PLP139-151/IFA primed SJL, IL-12p70 or IL-23 polarized	Wt SJL		+	Both Th1 and Th17 induce EAE, but using distinct effector mechanism	<sup>26</sup>
MOG-specific lymphocytes from MOG35-55/CFA-immunized Wt C57BL/6 mice, polarized to Th17 or Th1	Wt C57BL/6		-/+	Th17 cells only enter the CNS when Th1 cells are present	<sup>78</sup>
MOG-specific CD4 <sup>+</sup> T-cells from naive 2D2 mice polarized to Th1 or Th2	Wt C57BL/6		-/+	Th17 can induce EAE, but with very late onset	<sup>79</sup>

PTX, pertussis toxin

serum levels of IL-17F, suggesting that Th17 cells dominate in these patients<sup>45</sup>. This may indicate that the MS population exists of different subgroups of patients in which the disease is driven by different immune-mediated mechanisms. Therefore, MS patients that are non-responders to IFN- $\beta$  might be responders to anti-IL-17A therapy.

Instead of targeting single cytokines, such as IL-17A, it may be more efficient to functionally eliminate Th1 and Th17 cells more upstream during the induction. Mice lacking the p40 subunit are resistant to EAE<sup>66-68</sup> and treatment of mice or marmosets with anti-IL-12p40 prevented or ameliorated EAE<sup>5,6,74</sup>. This suggests that IL-12p40 is a promising target for therapy in MS. Unfortunately, treatment of RRMS with the same anti-IL-12p40 mAb that was tested in marmosets, known as ustekinumab, did not reduce the number of gadolinium enhancing lesions<sup>42</sup>. Several explanations for this failure were suggested, such as suboptimal patient selection, since the patients were not in the early phase of the disease, and the inability of ustekinumab to cross the BBB<sup>42,80,81</sup>. Another explanation for the failure of ustekinumab may be that Th17 cells are pathogenic, but that their induction is not affected by neutralization of IL-23 by ustekinumab. IL-23 is probably more involved in the maintenance, and not the induction of Th17 cells in humans<sup>64</sup>. The possibility that neutralization of IL-12/IL-23p40 by ustekinumab prevents the development of Th1 cells only, and not of Th17 cells needs consideration. Furthermore, if ustekinumab is able to prevent the development of Th1 and Th17, the cytotoxic T-cells are still present. This thesis provides evidence that CD4<sup>+</sup>CD56<sup>+</sup> or CD8<sup>+</sup>CD56<sup>+</sup> cytotoxic T-cells contribute to the disease. This explains why ustekinumab is effective in the marmoset EAE model induced with CFA, which is probably Th1 prone, and not in MS, which may be more dominated by cytotoxic T-cells. This should be further investigated in the MOG34-56/IFA model in which Th1 cells are less dominant.

### **The role of B-cells in secondary lymphoid organs**

Treatment of RRMS patients with the CD20<sup>+</sup> B-cell depleting Ab rituximab reduced the number of gadolinium-enhancing lesions and the number of relapses<sup>43,44</sup>. However, the underlying mechanism is unclear, since total IgG levels were not altered after B-cell depletion. This suggests that B-cells have additional functions in the MS pathogenesis besides Ab-production.

We investigated the role of B-cells in the pathogenesis of EAE in rhMOG/CFA-immunized marmosets. Depletion of B-cells by anti-CD20 Ab, starting 21 days after immunization, prevented the development of clinical signs (**Chapter 4.2**). As an underlying mechanism we demonstrated that B-cell depletion halts the progressive production of anti-MOG IgG. In addition, we found evidence that B-cells may act as APC in secondary lymphoid organs. B-cell depletion led to reduced overall and MOG-induced T-cell proliferation and cytokine production in spleen and lymph nodes. We did

not observe a reduced proliferation in PBMC, neither MOG-specific, nor in response to the mitogen ConA. This contrasts with the effect on PBMC activation in MS patients that were treated with the CD20<sup>+</sup> B-cell depleting Ab rituximab. Overall T-cell proliferation and the production of IL-17A and IFN- $\gamma$  were reduced<sup>82</sup>. MOG-specific T-cell proliferation was not tested in the MS clinical trials, probably because the MOG-specific responses in PBMC are too low and secondary lymphoid organs are only exceptionally available. Our data together with the data obtained from MS patients suggest that B-cells are involved in the activation of T-cells in the periphery.

B-cell depletion does not only affect its APC function, but may also interrupt other mechanisms. A mechanism that also fits with our results is proposed by Lund and Randall<sup>83</sup>. They propose that effector T-cells and effector B-cells interact with each other in a feedforward loop. This leads to the expansion of both subsets. During autoimmunity this Ag-driven feedforward loop may not be susceptible to suppression by regulatory T-cells or regulatory B-cells. B-cell depletion leads to the interruption of the feedforward loop and consequently T-cell activity and pro-inflammatory cytokine levels reduce. This favors the generation of regulatory T-cells. The B-cells that repopulate likely are regulatory B-cells<sup>83</sup>. The suggested tolerance or regulatory environment that occurs after B-cell depletion is in line with the higher level of IL-10 in the spleen and axillary lymph node of B-cell depleted marmosets (**Chapter 4.2**). Currently, the phenotype of regulatory T-cells and regulatory B-cells is unknown in marmosets. Therefore, these subsets cannot be investigated in B-cell depleted marmosets.

## IMMUNOPATHOGENIC MECHANISMS WITHIN THE CNS

### Cytotoxicity of MOG34-56-specific T-cells

MOG34-56-specific cytotoxic T-cells express CD56 (**Chapter 3**), which is neural cell adhesion molecule. CD56 is a transmembrane glycoprotein of the immunoglobulin family and is expressed on cells of the CNS, such as neurons and glial cells<sup>84-86</sup>. In addition, CD56 is expressed on NK cells, several T-cell subsets, NKT-cells, and NK-CTL<sup>85,87-89</sup>. Expression of CD56 was also observed on T-cells specific for MBP in MS patients and healthy controls<sup>90,91</sup>.

Although CD56 is expressed on cytotoxic T-cells in marmosets, it is unknown whether CD56 in marmosets has the same cellular distribution and function as in humans. Mouse NK cells do not express the murine equivalent of CD56<sup>92</sup>. Also in the rhesus macaque, an Old World monkey, CD56 is not expressed on NK cells<sup>93</sup>. However, others have demonstrated CD56 expression on CD3<sup>-</sup> and CD3<sup>+</sup> cells in PBMC of rhesus macaques<sup>94,95</sup>. This suggests that a CD56<sup>+</sup> T-cell subset similar to marmosets is present

in rhesus macaques. Similar to our results, another group also demonstrated CD56 expression on CD4<sup>+</sup> and CD8<sup>+</sup> T-cells of marmosets<sup>96</sup>.

The expression of clinical EAE in marmosets is associated with the activation of MOG34-56-specific CD56<sup>+</sup> T-cells. We hypothesize that these T-cells induce demyelination via a specific cytotoxic attack on the myelin-forming oligodendrocytes. The question remains how they exert their cytotoxic activity. Below four possible mechanisms are discussed.

- MHC class II restricted: The cytolytic activity of MBP-specific CD4<sup>+</sup> T-cells isolated from MS patients and healthy donors is HLA class II restricted<sup>97,98</sup>. The MHC restriction of MOG34-56-specific T-cells isolated from marmosets has not been tested yet. Although MHC class II restricted killing of MHC class II expressing target cells, i.e. EBV-transformed B-cell lines, was detected *in vitro*<sup>97,98</sup>, it is less likely that this is the mechanism of demyelination *in vivo*. Oligodendrocytes do not express MHC class II molecules, neither in active MS lesions<sup>99</sup>, nor after stimulation with IFN- $\gamma$ <sup>100</sup>.
- MHC class Ia restricted: MBP-specific CD8<sup>+</sup> cytotoxic T-cells isolated from MS patients and healthy donors can induce cytolysis of human oligodendrocytes in a HLA-A2 dependent manner<sup>101</sup>. Human oligodendrocytes express low level HLA class I molecules *in vitro*, which can be enhanced by IFN- $\gamma$ <sup>100,101</sup>. However, marmosets lack the equivalents of the classical MHC class I molecules of humans, i.e. MHC-A, -B, or -C<sup>102</sup>. Therefore, it is difficult to envisage that marmoset oligodendrocytes are killed by MOG34-56-specific T-cells in a MHC class Ia restricted manner.
- MHC class Ib restricted: The marmoset genome encodes the equivalents of two human non-classical MHC class I genes that are also expressed in the CNS, i.e. Caja-G and Caja-E<sup>103</sup>. NK-CTL kill CMV-infected target cells in an MHC-E restricted manner<sup>88,104-107</sup>. To conclude that the MOG34-56-specific killing is MHC-E restricted in marmosets, it should be investigated whether the EBV-transformed B-cells used for the *in vitro* cytotoxicity assays express Caja-E. Next, it should be tested whether this interaction can be blocked with an anti-MHC-E Ab. In addition, the expression of MHC-E on oligodendrocytes in healthy and MS brains should be investigated.
- MHC-independent, CD56 dependent: The lysis of several tumor cell lines by MBP-specific CD4<sup>+</sup>CD56<sup>+</sup> T-cells depends on CD56 homophilic interaction<sup>90</sup>. Human oligodendrocytes express CD56 and can be lysed by MBP-specific CD4<sup>+</sup>CD56<sup>+</sup> T-cells via an MHC-independent, but CD56 dependent mechanism<sup>91</sup>. This may explain the cytotoxicity in marmosets, since CD56 is expressed by EBV-transformed marmoset B-cell lines (data not shown), which are used as target cells in the cytotoxicity assays.

To summarize, it is unlikely that MOG34-56-specific T-cells exert their cytotoxicity in marmosets via classical MHC class Ia or class II, since these are not expressed

on marmoset oligodendrocytes. Although further investigations are needed, the most plausible mechanism of MOG34-56-specific cytotoxicity to oligodendrocytes in marmosets is via Caja-E.

### The role of B-cells

B-cells can be detected in the CNS of MS patients<sup>108,109</sup> and in marmoset EAE brains (Figure 2 in **Chapter 4.3**). B-cells may have at least three different roles in the CNS of MS patients and in EAE, namely autoantibody production, Ag presentation, and modulation of local immune responses via cytokines. It has been well demonstrated that Ab against MOG can enhance demyelination and myelin phagocytosis *in vitro*<sup>110,111</sup> and *in vivo*<sup>30,31,112-114</sup>. However, in the MOG34-56/IFA model demyelination occurs in the absence of MOG-binding Ab, suggesting that Ab against MOG are not essential for EAE induction in marmosets (**Chapter 3.2**).

No T-cells were detected in the CNS after B-cell depletion, in contrast to the animals of the placebo group (**Chapter 4.3**). One explanation is that T-cells did not migrate into the CNS, because they were not activated in the periphery. Another explanation may be that B-cells attract T-cells to the CNS.

B-cell depletion not only prevents the development of WM lesions, but also the development of GM lesions (**Chapter 4.3**). GM lesions contain only a minimal number of lymphocytes, low level of complement deposition, and an intact BBB, suggesting that inflammation is less prominent in these lesions<sup>115-117</sup>. How does B-cell depletion then prevent the development of grey matter lesions? B-cells are present in the meninges of MS brains<sup>118</sup>. The number of lymphocytes in the meninges does not correlate with the percentage of cortical demyelination<sup>118</sup>. However, B-cells in the meninges produce cytokines or chemokines, which may lead to microglia activation in the cortex. Depletion of meningeal B-cells by anti-CD20 Ab treatment may reduce microglia activation in the cortex.

### The role of Nogo-A

Treatment with anti-Nogo-A Ab in the MOG34-56/CFA model, started one day before immunization, effectively prevented clinical symptoms and abrogated pathology. Nogo-A binds to its receptor (NgR) expressed on neurons and thereby it inhibits neurite outgrowth<sup>119,120</sup>. The novel finding published in **chapter 4.4** is that the reverse signal from the binding of an yet unidentified receptor to Nogo-A abrogates demyelination and seems to promote remyelination. We hypothesize the role of Nogo-A in MS as follows. In non-injured CNS, the interaction of Nogo-A with its receptors prevents axonal sprouting and myelination (Figure 4A). In MS lesions, Nogo-A is still present in the remaining myelin and in the debris resulting from demyelination. Thus, the locally available Nogo-A may still prevent axonal outgrowth and remyelination (Figure 4B). Intervening into the two-way signaling between Nogo-A and Nogo-A receptor has a dual effect, removing

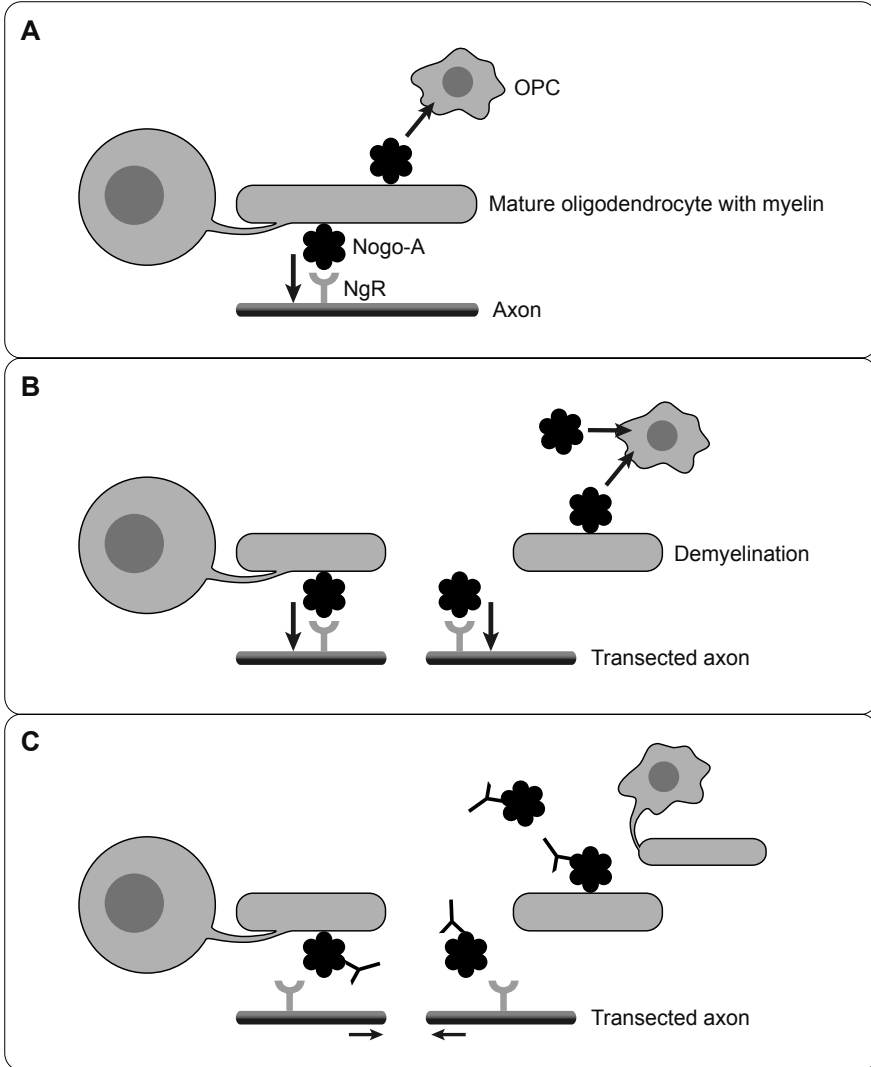


**Figure 4. The role of Nogo-A in remyelination.**

Nogo-A is expressed by oligodendrocytes and binds to the Nogo-A receptor (NgR) on axons. Nogo-A is also able to inhibit differentiation of oligodendrocyte precursor cells (OPC). In A and B the inhibitory signals are indicated with the black arrows. Shown is the situation in a healthy brain (A), in MS (B), and after treatment with the mAb against Nogo-A (C). In a healthy situation, Nogo-A prevents ongoing axonal sprouting and myelination. In MS lesions, Nogo-A is still present in the remaining myelin, but may be also released as a soluble compound upon demyelination and tissue damage. Nogo-A is still able to bind to NgR and prevents axonal outgrowth and remyelination. Anti-Nogo-AAb treatment blocks the interaction between Nogo-A and its receptor. Axons and OPC lose the inhibitory signal and axonal outgrowth (black arrows) and remyelination is promoted.

the block on axonal outgrowth and axon remyelination (Figure 4C). This indicates that Nogo-A is a good target for MS therapy, acting as a two-edged sword, preventing axonal injury on the one hand and promoting remyelination on the other.

Not only neurons express NgR, but also macrophages<sup>121</sup> and B-cells (Figure 5). Macrophages express NgR1<sup>121</sup>, which is a receptor for Nogo-A and other inhibitory proteins such as MAG. CD20<sup>+</sup> B-cells, which were isolated from a MOG34-56/CFA-immunized marmoset, express NgR2, but not NgR1. NgR2 mainly binds to MAG and not to Nogo-A<sup>122</sup>. EBV-transformed marmoset B-cell lines express both receptors. The percentage of NgR expressing cells is higher in EBV-transformed B-cells compared with CD20<sup>+</sup> B-cells isolated from blood or lymphoid organs (Figure 5). This suggests that EBV-transformed B-cells, but not normal B-cells, can bind Nogo-A in myelin. NgR is also a receptor for B lymphocyte stimulator (BLYS), which is indispensable for B-cell development. Binding of BLYS to NgR on neurons inhibited neurite outgrowth<sup>123</sup>. BLYS binds to several known receptors on B-cells, such as BLYS receptor 3 and TACI<sup>124</sup>, but it may also bind to NgR on B-cells. The role of NgR expression on, mainly EBV-transformed, B-cells in the pathogenesis of EAE and MS remains to be investigated.

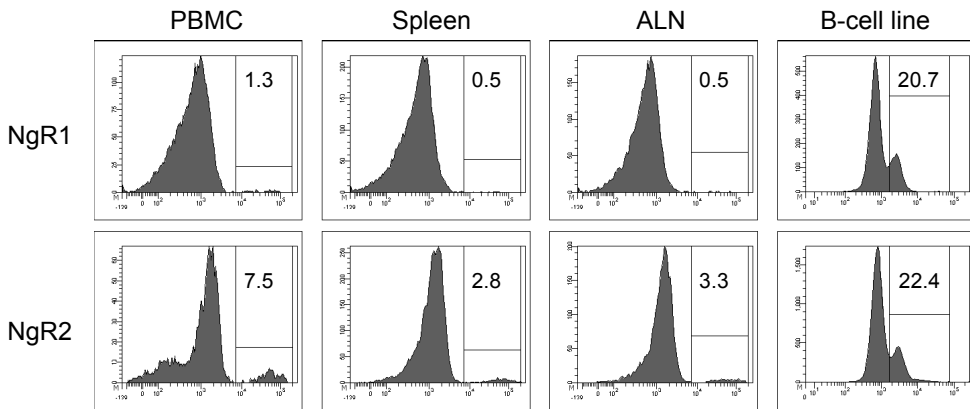


**Figure 5. The expression of Nogo-A receptor on CD20<sup>+</sup> B-cells.**

The expression of Nogo-A receptors (NgR) was analysed by flow cytometry of PBMC, mononuclear cells isolated from spleen and axillary lymph node (ALN), and EBV-transformed marmoset B-cell lines. NgR1 is a receptor for Nogo-A and other inhibitory proteins. NgR2 mainly binds to MAG and not to Nogo-A. Shown is the expression of NgR1 and NgR2 on CD20<sup>+</sup> gated cells. CD3<sup>+</sup> cells were uniformly negative for both NgR1 and NgR2 (data not shown). CD20<sup>+</sup> B-cells isolated from PBMC or lymphoid organs do not express NgR1 and only a small percentage express NgR2. This suggests that these B-cells cannot bind to Nogo-A. In contrast, a large percentage of CD20<sup>+</sup> EBV-transformed marmoset B-cell lines express NgR1 and NgR2. This suggests that EBV-transformed B-cells can bind to Nogo-A.

## OUTSTANDING QUESTIONS

### **Are MOG34-56-specific T-cells able to induce demyelination?**

This thesis demonstrates that MOG34-56-specific T-cells are cytotoxic against EBV-transformed B-cell lines that present MOG34-56 *in vitro*. The question remains whether these T-cells are capable of inducing demyelination or killing of oligodendrocytes. One way to address this would be adoptive transfer. However, creation of MOG34-56-specific T-cell lines on a large scale for adoptive transfer remains a major challenge, since these T-cells kill the autologous MOG34-56 pulsed B-cell lines that are used as APC. As an alternative we plan to investigate this in a three-dimensional spheroid culture system, which will be set-up with newborn marmoset brains similar to rodent brain spheroids<sup>125,126</sup>. In this system, oligodendrocytes produce myelin and therefore demyelination or oligodendrocyte death induced by T-cells can be investigated. In addition, this system can be used to investigate the pathogenic role of anti-MOG Ab.

### **How can the activity of MOG34-56-specific T-cells be inhibited?**

The anti-CD52 Ab alemtuzumab<sup>127</sup> and the anti-CD25 Ab daclizumab<sup>128</sup> inhibit T-cell activity in MS. However, these therapies also target other T-cells that are not involved in MS. Therefore, targeting the specific activity of MOG34-56-specific T-cells may be a better option.

This thesis demonstrates that MOG34-56-specific T-cells are cytotoxic. Inhibition of exocytosis of cytotoxic granules by concanamycin A prevented the cytolytic activity of MOG34-56-specific T-cells *in vitro* (**Chapter 3.2**). Inhibition of exocytosis of cytotoxic granules may prevent cytolysis *in vivo*. However, this is not an option for therapy, because exocytosis of cytotoxic granules is crucial for the anti-viral defense. Inhibition of exocytosis may thus lead to viral reactivation or new viral infections.

Although CD56 is a marker of the MOG34-56-specific T-cells, CD56 itself cannot be used as a target for therapy. Anti-CD56 Ab did not prevent lysis of tumor cell lines by MBP-specific CD4<sup>+</sup>CD56<sup>+</sup> T-cells<sup>90</sup>. In addition, many other cell types express CD56, such as NK cells. CD3<sup>+</sup>CD56<sup>+</sup> NK-cell frequencies are reduced in RRMS compared to healthy controls<sup>129</sup> and increased after treatment with IFN- $\beta$  and daclizumab<sup>130,131</sup>. It is suggested that NK cells have a regulatory function in MS<sup>132</sup> and these should not be inhibited or depleted by an anti-CD56 therapy.

MOG34-56-specific T-cells produce IL-17A. Treatment of marmosets with anti-IL-17A Ab was not effective in the rhMOG/CFA model, in which both Th1 and Th17 cells are activated. Before concluding whether IL-17A is essential for the disease or not, it should be tested whether neutralization of IL-17A is effective in the MOG34-56/IFA model.

Based on our current knowledge we think that the best therapy to inhibit both the cytotoxicity and IL-17A production by MOG34-56-specific T-cells is to prevent that these T-cells are activated. We have shown that depletion of B-cells by an anti-CD20 Ab reduced the proliferation and cytokine production by MOG-specific T-cells. This prevented the development of clinical signs and profoundly reduced pathology (**Chapter 4.2** and **4.3**). Therefore, this may be the preferred therapy to inhibit the activity of MOG34-56-specific T-cells.

### **Which new developments can optimize *in vivo* parameters?**

The clinico-radiological paradox describes the discrepancy between the clinical status and brain WM lesion load in MS<sup>133,134</sup>. In marmosets, the clinical scores do also not correlate very well with the brain WM lesion load. This paradox can be overcome by improving the clinical as well as the radiological parameters.

The clinical scoring system used for the research in this thesis was mainly focused on motor defects, such as ataxia and paralysis. Before these symptoms appear, changes in walking pattern and behavior are observed. However, it is difficult to translate these changes into a clinical score, because they are not as obvious as, for example, ataxia. A way to measure the first changes in activity is telemetry. For example, an implanted transponder that measures the total activity during the day as well as the night may show a reduction in activity before other clinical symptoms appear.

It has been suggested that clinical symptoms in MS better correlate with GM lesions than with WM lesions. Therefore, GM lesions should be followed in marmosets by longitudinal *in vivo* MRI, after which the correlation with clinical symptoms can be investigated.

### **Will there be a role for the intestinal flora in the pathogenesis?**

It has been reported that Th17 cells expand in the lamina propria of the small intestine and colon of mice<sup>65,135</sup>. In addition, a special microflora is required for the differentiation of Th17 cells<sup>65</sup>. This raises the question whether alteration of the microflora by antibiotics may prevent EAE. Indeed, treatment of C57BL/6 and SJL mice with oral antibiotics reduced the IL-17A production and reduced the clinical score of EAE<sup>136</sup>. Future investigations are warranted to unravel the role of the microbial flora in the intestine of humans, among others in relation to the IL-17A production and the clinical symptoms. Marmosets are conventionally housed, which means that their microbial flora is more closely related to humans than specific pathogen free mice. Therefore, the marmoset may be a suitable model to investigate whether the intestinal flora is involved in the pathogenesis of EAE and MS.

A new method has been developed to screen the bacterial composition in the intestinal tract by genomic sequencing of faecal samples. This technique can differentiate

between healthy individuals and patients with ulcerative colitis or Crohn's disease<sup>137</sup>. This technique may be used to compare MS patients with healthy controls as well as to analyse differences between fast and slow progressors in the marmoset EAE model.

## REFERENCES

1. Brok HP et al. Myelin/oligodendrocyte glycoprotein-induced autoimmune encephalomyelitis in common marmosets: the encephalitogenic T cell epitope pMOG24-36 is presented by a monomorphic MHC class II molecule. *J Immunol* 165:1093-1101 (2000)
2. Billiau A et al. Modes of action of Freund's adjuvants in experimental models of autoimmune diseases. *J Leukoc Biol* 70:849-860 (2001)
3. Boon L et al. Prevention of experimental autoimmune encephalomyelitis in the common marmoset (*Callithrix jacchus*) using a chimeric antagonist monoclonal antibody against human CD40 is associated with altered B cell responses. *J Immunol* 167:2942-2949 (2001)
4. Laman JD et al. Protection of marmoset monkeys against EAE by treatment with a murine antibody blocking CD40 ( $\mu$ 5D12). *Eur J Immunol* 32:2218-2228 (2002)
5. Brok HP et al. Prevention of experimental autoimmune encephalomyelitis in common marmosets using an anti-IL-12p40 monoclonal antibody. *J Immunol* 169:6554-6563 (2002)
6. 't Hart BA et al. Suppression of ongoing disease in a nonhuman primate model of multiple sclerosis by a human-anti-human IL-12p40 antibody. *J Immunol* 175:4761-4768 (2005)
7. Chang JC et al. Adjuvant activity of incomplete Freund's adjuvant. *Adv Drug Deliv Rev* 32:173-186 (1998)
8. Visser L et al. Proinflammatory bacterial peptidoglycan as a cofactor for the development of central nervous system autoimmune disease. *J Immunol* 174:808-816 (2005)
9. Lorentzen JC et al. Protracted, relapsing and demyelinating experimental autoimmune encephalomyelitis in DA rats immunized with syngeneic spinal cord and incomplete Freund's adjuvant. *J Neuroimmunol* 63:193-205 (1995)
10. Sospedra M et al. Immunology of multiple sclerosis. *Annu Rev Immunol* 23:683-747 (2005)
11. Eisenbarth SC et al. Crucial role for the Nalp3 inflammasome in the immunostimulatory properties of aluminium adjuvants. *Nature* 453:1122-1126 (2008)
12. Rothel JS et al. Antibody and cytokine responses in efferent lymph following vaccination with different adjuvants. *Vet Immunol Immunopathol* 63:167-183 (1998)
13. van der Zee M et al. Synthetic human chorionic gonadotropin-related oligopeptides impair early innate immune responses to *Listeria monocytogenes* in mice. *J Infect Dis* 201:1072-1080 (2010)
14. van den Berg HR et al. Synthetic oligopeptides related to the  $\beta$ -subunit of human chorionic gonadotropin attenuate inflammation and liver damage after (trauma) hemorrhagic shock and resuscitation. *Shock* 31:285-291 (2009)
15. 't Hart BA et al. Histopathological characterization of magnetic resonance imaging-detectable brain white matter lesions in a primate model of multiple sclerosis: a correlative study in the experimental autoimmune encephalomyelitis model in common marmosets (*Callithrix jacchus*). *Am J Pathol* 153:649-663 (1998)
16. Castro AP et al. Adjuvant treatment increases the resistance to *Mycobacterium avium* infection of mycobacteria-susceptible BALB/c mice. *Clin Exp Immunol* 92:466-472 (1993)
17. Mussener A et al. TNF- $\alpha$  dominates cytokine mRNA expression in lymphoid tissues of rats developing collagen- and oil-induced arthritis. *Scand J Immunol* 42:128-134 (1995)
18. Kai H et al. Critical role of M. tuberculosis for dendritic cell maturation to induce collagen-induced arthritis in H-2b background of C57BL/6 mice. *Immunology* 118:233-239 (2006)
19. Villoslada P et al. Frequency, heterogeneity and encephalitogenicity of T cells specific for myelin oligodendrocyte glycoprotein in naive outbred primates. *Eur J Immunol* 31:2942-2950 (2001)

20. Reiber H et al. The effect of Freund's adjuvants on blood-cerebrospinal fluid barrier permeability. *J Neurol Sci* 63:55-61 (1984)
21. Rabchevsky AG et al. Peripheral injections of Freund's adjuvant in mice provoke leakage of serum proteins through the blood-brain barrier without inducing reactive gliosis. *Brain Res* 832:84-96 (1999)
22. Reboldi A et al. C-C chemokine receptor 6-regulated entry of TH-17 cells into the CNS through the choroid plexus is required for the initiation of EAE. *Nat Immunol* 10:514-523 (2009)
23. Kebir H et al. Human TH17 lymphocytes promote blood-brain barrier disruption and central nervous system inflammation. *Nat Med* 13:1173-1175 (2007)
24. Huppert J et al. Cellular mechanisms of IL-17-induced blood-brain barrier disruption. *Faseb J* 24:1023-1034 (2010)
25. Massacesi L et al. Active and passively induced experimental autoimmune encephalomyelitis in common marmosets: a new model for multiple sclerosis. *Ann Neurol* 37:519-530 (1995)
26. Kroenke MA et al. IL-12- and IL-23-modulated T cells induce distinct types of EAE based on histology, CNS chemokine profile, and response to cytokine inhibition. *J Exp Med* 205:1535-1541 (2008)
27. Hjelmsstrom P et al. B-cell-deficient mice develop experimental allergic encephalomyelitis with demyelination after myelin oligodendrocyte glycoprotein sensitization. *J Immunol* 161:4480-4483 (1998)
28. Cross AH et al. T cells are the main cell type expressing B7-1 and B7-2 in the central nervous system during acute, relapsing and chronic experimental autoimmune encephalomyelitis. *Eur J Immunol* 29:3140-3147 (1999)
29. Sekiguchi Y et al. Antibodies to myelin oligodendrocyte glycoprotein are not involved in the severity of chronic non-relapsing experimental autoimmune encephalomyelitis. *Immunol Lett* 122:145-149 (2009)
30. McFarland HI et al. Determinant spreading associated with demyelination in a nonhuman primate model of multiple sclerosis. *J Immunol* 162:2384-2390 (1999)
31. Genain CP et al. Antibody facilitation of multiple sclerosis-like lesions in a nonhuman primate. *J Clin Invest* 96:2966-2974 (1995)
32. de Vos AF et al. Severe T-cell depletion from the PALS leads to altered spleen composition in common marmosets with experimental autoimmune encephalomyelitis (EAE). *J Neuroimmunol* 161:29-39 (2005)
33. Fry TJ et al. The many faces of IL-7: from lymphopoiesis to peripheral T cell maintenance. *J Immunol* 174:6571-6576 (2005)
34. Jacobs SR et al. IL-7 Is Essential for Homeostatic Control of T Cell Metabolism In Vivo. *J Immunol* 184:3461-3469 (2010)
35. Goodwin RG et al. Human interleukin 7: molecular cloning and growth factor activity on human and murine B-lineage cells. *Proc Natl Acad Sci USA* 86:302-306 (1989)
36. Liu X et al. Crucial role of interleukin-7 in T helper type 17 survival and expansion in autoimmune disease. *Nat Med* 16:191-197 (2010)
37. Michaud A et al. IL-7 enhances survival of human CD56bright NK cells. *J Immunother* 33:382-390 (2010)
38. Hafler DA et al. Risk alleles for multiple sclerosis identified by a genome-wide study. *N Engl J Med* 357:851-862 (2007)
39. Vrenken H et al. Altered diffusion tensor in multiple sclerosis normal-appearing brain tissue: cortical diffusion changes seem related to clinical deterioration. *J Magn Reson Imaging* 23:628-636 (2006)
40. Kutzelnigg A et al. Cortical lesions and brain atrophy in MS. *J Neurol Sci* 233:55-59 (2005)
41. Geurts JJ et al. Grey matter pathology in multiple sclerosis. *Lancet Neurol* 7:841-851 (2008)
42. Segal BM et al. Repeated subcutaneous injections of IL12/23 p40 neutralising antibody, ustekinumab, in patients with relapsing-remitting multiple sclerosis: a phase II, double-blind, placebo-controlled, randomised, dose-ranging study. *Lancet Neurol* 7:796-804 (2008)

43. Hauser SL et al. B-cell depletion with rituximab in relapsing-remitting multiple sclerosis. *N Engl J Med* 358:676-688 (2008)
44. Bar-Or A et al. Rituximab in relapsing-remitting multiple sclerosis: a 72-week, open-label, phase I trial. *Ann Neurol* 63:395-400 (2008)
45. Axtell RC et al. T helper type 1 and 17 cells determine efficacy of interferon-beta in multiple sclerosis and experimental encephalomyelitis. *Nat Med* 16:406-412 (2010)
46. Antunes SG et al. The common marmoset: a new world primate species with limited Mhc class II variability. *Proc Natl Acad Sci USA* 95:11745-11750 (1998)
47. Doxiadis GG et al. Reactivation by exon shuffling of a conserved HLA-DR3-like pseudogene segment in a New World primate species. *Proc Natl Acad Sci USA* 103:5864-5868 (2006)
48. Steinman L. A brief history of T(H)17, the first major revision in the T(H)1/T(H)2 hypothesis of T cell-mediated tissue damage. *Nat Med* 13:139-145 (2007)
49. Wong MT et al. Regulation of human Th9 differentiation by type I interferons and IL-21. *Immunol Cell Biol* (2010)
50. Eyerich S et al. Th22 cells represent a distinct human T cell subset involved in epidermal immunity and remodeling. *J Clin Invest* 119:3573-3585 (2009)
51. Friese MA et al. Pathogenic CD8(+) T cells in multiple sclerosis. *Ann Neurol* 66:132-141 (2009)
52. Matuszewski D et al. Interleukin-17 mRNA expression in blood and CSF mononuclear cells is augmented in multiple sclerosis. *Mult Scler* 5:101-104 (1999)
53. Lock C et al. Gene-microarray analysis of multiple sclerosis lesions yields new targets validated in autoimmune encephalomyelitis. *Nat Med* 8:500-508 (2002)
54. Ifergan I et al. The blood-brain barrier induces differentiation of migrating monocytes into Th17-polarizing dendritic cells. *Brain* 131:785-799 (2008)
55. Tzartos JS et al. Interleukin-17 production in central nervous system-infiltrating T cells and glial cells is associated with active disease in multiple sclerosis. *Am J Pathol* 172:146-155 (2008)
56. Bettelli E et al. Th17: the third member of the effector T cell trilogy. *Curr Opin Immunol* 19:652-657 (2007)
57. Ciric B et al. IL-23 drives pathogenic IL-17-producing CD8+ T cells. *J Immunol* 182:5296-5305 (2009)
58. Passos ST et al. IL-6 promotes NK cell production of IL-17 during toxoplasmosis. *J Immunol* 184:1776-1783 (2010)
59. Rachitskaya AV et al. Cutting Edge: NKT Cells Constitutively Express IL-23 Receptor and ROR $\gamma$  and Rapidly Produce IL-17 upon Receptor Ligation in an IL-6-Independent Fashion. *J Immunol* 180:5167-5171 (2008)
60. Kawanokuchi J et al. Production and functions of IL-17 in microglia. *J Neuroimmunol* 194:54-61 (2008)
61. Kolls JK et al. Interleukin-17 family members and inflammation. *Immunity* 21:467-476 (2004)
62. Pelletier M et al. Evidence for a cross-talk between human neutrophils and Th17 cells. *Blood* 115:335-343 (2010)
63. de Jong E et al. Translational mini-review series on Th17 cells: development of mouse and human T helper 17 cells. *Clin Exp Immunol* 159:148-158 (2010)
64. Veldhoen M et al. TGF $\beta$  in the context of an inflammatory cytokine milieu supports de novo differentiation of IL-17-producing T cells. *Immunity* 24:179-189 (2006)
65. Ivanov II et al. Specific microbiota direct the differentiation of IL-17-producing T-helper cells in the mucosa of the small intestine. *Cell Host Microbe* 4:337-349 (2008)
66. Becher B et al. Experimental autoimmune encephalitis and inflammation in the absence of interleukin-12. *J Clin Invest* 110:493-497 (2002)
67. Gran B et al. IL-12p35-deficient mice are susceptible to experimental autoimmune encephalomyelitis: evidence for redundancy in the IL-12 system in the induction of central nervous system autoimmune demyelination. *J Immunol* 169:7104-7110 (2002)
68. Cua DJ et al. Interleukin-23 rather than interleukin-12 is the critical cytokine for autoimmune inflammation of the brain. *Nature* 421:744-748 (2003)

69. Langrish CL et al. IL-23 drives a pathogenic T cell population that induces autoimmune inflammation. *J Exp Med* 201:233-240 (2005)
70. Komiyama Y et al. IL-17 plays an important role in the development of experimental autoimmune encephalomyelitis. *J Immunol* 177:566-573 (2006)
71. Thakker P et al. IL-23 Is Critical in the Induction but Not in the Effector Phase of Experimental Autoimmune Encephalomyelitis. *J Immunol* 178:2589-2598 (2007)
72. Haak S et al. IL-17A and IL-17F do not contribute vitally to autoimmune neuro-inflammation in mice. *J Clin Invest* 119:61-69 (2009)
73. Hofstetter HH et al. Therapeutic efficacy of IL-17 neutralization in murine experimental autoimmune encephalomyelitis. *Cell Immunol* 237:123-130 (2005)
74. Chen Y et al. Anti-IL-23 therapy inhibits multiple inflammatory pathways and ameliorates autoimmune encephalomyelitis. *J Clin Invest* 116:1317-1326 (2006)
75. Uyttenhove C et al. Development of an anti-IL-17A auto-vaccine that prevents experimental autoimmune encephalomyelitis. *Eur J Immunol* 36:2868-2874 (2006)
76. Rohn TA et al. Vaccination against IL-17 suppresses autoimmune arthritis and encephalomyelitis. *Eur J Immunol* 36:2857-2867 (2006)
77. Becher B et al. IL-23 produced by CNS-resident cells controls T cell encephalitogenicity during the effector phase of experimental autoimmune encephalomyelitis. *J Clin Invest* 112:1186-1191 (2003)
78. O'Connor RA et al. Cutting edge: Th1 cells facilitate the entry of Th17 cells to the central nervous system during experimental autoimmune encephalomyelitis. *J Immunol* 181:3750-3754 (2008)
79. Jager A et al. Th1, Th17, and Th9 effector cells induce experimental autoimmune encephalomyelitis with different pathological phenotypes. *J Immunol* 183:7169-7177 (2009)
80. Longbrake EE et al. Why did IL-12/IL-23 antibody therapy fail in multiple sclerosis? *Expert Rev Neurother* 9:319-321 (2009)
81. Steinman L. Mixed results with modulation of T(H)-17 cells in human autoimmune diseases. *Nat Immunol* 11:41-44 (2010)
82. Bar-Or A et al. Abnormal B-cell cytokine responses a trigger of T-cell-mediated disease in MS? *Ann Neurol* 67:452-461 (2010)
83. Lund FE et al. Effector and regulatory B cells: modulators of CD4(+) T cell immunity. *Nat Rev Immunol* 10:236-247 (2010)
84. Lanier LL et al. The relationship of CD16 (Leu-11) and Leu-19 (NKH-1) antigen expression on human peripheral blood NK cells and cytotoxic T lymphocytes. *J Immunol* 136:4480-4486 (1986)
85. Lanier LL et al. Identity of Leu-19 (CD56) leukocyte differentiation antigen and neural cell adhesion molecule. *J Exp Med* 169:2233-2238 (1989)
86. Shapiro L et al. Adhesion molecules in the nervous system: structural insights into function and diversity. *Annu Rev Neurosci* 30:451-474 (2007)
87. Mendes R et al. Flow cytometric visualisation of cytokine production by CD3-CD56+ NK cells and CD3+CD56+ NK-T cells in whole blood. *Cytometry* 39:72-78 (2000)
88. Mazzarino P et al. Identification of effector-memory CMV-specific T lymphocytes that kill CMV-infected target cells in an HLA-E-restricted fashion. *Eur J Immunol* 35:3240-3247 (2005)
89. Poli A et al. CD56bright natural killer (NK) cells: an important NK cell subset. *Immunology* 126:458-465 (2009)
90. Vergelli M et al. A novel population of CD4+CD56+ myelin-reactive T cells lyses target cells expressing CD56/neural cell adhesion molecule. *J Immunol* 157:679-688 (1996)
91. Antel JP et al. Non-MHC-restricted cell-mediated lysis of human oligodendrocytes in vitro: relation with CD56 expression. *J Immunol* 160:1606-1611 (1998)
92. Hayakawa Y et al. Functional subsets of mouse natural killer cells. *Immunol Rev* 214:47-55 (2006)
93. Carter DL et al. CD56 identifies monocytes and not natural killer cells in rhesus macaques. *Cytometry* 37:41-50 (1999)

94. Slukvin, Il et al. Phenotypic and functional characterization of rhesus monkey decidual lymphocytes: rhesus decidual large granular lymphocytes express CD56 and have cytolytic activity. *J Reprod Immunol* 50:57-79 (2001)
95. Gansuud B et al. Phenotypic and functional characterization of long-term cultured rhesus macaque spleen-derived NKT cells. *J Immunol* 171:2904-2911 (2003)
96. Foerster M et al. Comparative study on age-dependent development of surface receptors on peripheral blood lymphocytes in children and young nonhuman primates (marmosets). *Life Sci* 60:773-785 (1997)
97. Weber WE et al. Human myelin basic protein-specific cytolytic T lymphocyte clones are functionally restricted by HLA class II gene products. *Cell Immunol* 120:145-153 (1989)
98. Martin R et al. Fine specificity and HLA restriction of myelin basic protein-specific cytotoxic T cell lines from multiple sclerosis patients and healthy individuals. *J Immunol* 145:540-548 (1990)
99. Lee SC et al. Multiple sclerosis: oligodendrocytes in active lesions do not express class II major histocompatibility complex molecules. *J Neuroimmunol* 25:261-266 (1989)
100. Hirayama M et al. Induction of human leukocyte antigen-A,B,C and -DR on cultured human oligodendrocytes and astrocytes by human gamma-interferon. *Neurosci Lett* 72:369-374 (1986)
101. Jurewicz A et al. MHC class I-restricted lysis of human oligodendrocytes by myelin basic protein peptide-specific CD8 T lymphocytes. *J Immunol* 160:3056-3059 (1998)
102. Cadavid LF et al. Evolutionary instability of the major histocompatibility complex class I loci in New World primates. *Proc Natl Acad Sci USA* 94:14536-14541 (1997)
103. Rolleke U et al. Differential expression of major histocompatibility complex class I molecules in the brain of a New World monkey, the common marmoset (*Callithrix jacchus*). *J Neuroimmunol* 176:39-50 (2006)
104. Pietra G et al. The analysis of the natural killer-like activity of human cytolytic T lymphocytes revealed HLA-E as a novel target for TCR alpha/beta-mediated recognition. *Eur J Immunol* 31:3687-3693 (2001)
105. Pietra G et al. Comparative analysis of NK- or NK-CTL-mediated lysis of immature or mature autologous dendritic cells. *Eur J Immunol* 33:3427-3432 (2003)
106. Moretta L et al. NK-CTLs, a novel HLA-E-restricted T-cell subset. *Trends Immunol* 24:136-143 (2003)
107. Romagnani C et al. HLA-E-restricted recognition of human cytomegalovirus by a subset of cytolytic T lymphocytes. *Hum Immunol* 65:437-445 (2004)
108. Serafini B et al. Detection of ectopic B-cell follicles with germinal centers in the meninges of patients with secondary progressive multiple sclerosis. *Brain Pathol* 14:164-174 (2004)
109. Willis SN et al. Epstein-Barr virus infection is not a characteristic feature of multiple sclerosis brain. *Brain* 132:3318-3328 (2009)
110. Kerlero de Rosbo N et al. Demyelination induced in aggregating brain cell cultures by a monoclonal antibody against myelin/oligodendrocyte glycoprotein. *J Neurochem* 55:583-587 (1990)
111. Van der Goes A et al. The role of anti-myelin (auto)-antibodies in the phagocytosis of myelin by macrophages. *J Neuroimmunol* 101:61-67 (1999)
112. Morris-Downes MM et al. Pathological and regulatory effects of anti-myelin antibodies in experimental allergic encephalomyelitis in mice. *J Neuroimmunol* 125:114-124 (2002)
113. Schluesener HJ et al. A monoclonal antibody against a myelin oligodendrocyte glycoprotein induces relapses and demyelination in central nervous system autoimmune disease. *J Immunol* 139:4016-4021 (1987)
114. Linington C et al. Augmentation of demyelination in rat acute allergic encephalomyelitis by circulating mouse monoclonal antibodies directed against a myelin/oligodendrocyte glycoprotein. *Am J Pathol* 130:443-454 (1988)
115. Bö L et al. Intracortical multiple sclerosis lesions are not associated with increased lymphocyte infiltration. *Mult Scler* 9:323-331 (2003)
116. Brink BP et al. The pathology of multiple sclerosis is location-dependent: no significant complement activation is detected in purely cortical lesions. *J Neuropathol Exp Neurol* 64:147-155 (2005)

117. van Horssen J et al. The blood-brain barrier in cortical multiple sclerosis lesions. *J Neuropathol Exp Neurol* 66:321-328 (2007)
118. Kooi EJ et al. Meningeal inflammation is not associated with cortical demyelination in chronic multiple sclerosis. *J Neuropathol Exp Neurol* 68:1021-1028 (2009)
119. Chen MS et al. Nogo-A is a myelin-associated neurite outgrowth inhibitor and an antigen for monoclonal antibody IN-1. *Nature* 403:434-439 (2000)
120. Prinjha R et al. Inhibitor of neurite outgrowth in humans. *Nature* 403:383-384 (2000)
121. Fry EJ et al. A role for Nogo receptor in macrophage clearance from injured peripheral nerve. *Neuron* 53:649-662 (2007)
122. Giger RJ et al. Mechanisms of CNS myelin inhibition: evidence for distinct and neuronal cell type specific receptor systems. *Restor Neurol Neurosci* 26:97-115 (2008)
123. Zhang L et al. Identification of BLYS (B lymphocyte stimulator), a non-myelin-associated protein, as a functional ligand for Nogo-66 receptor. *J Neurosci* 29:6348-6352 (2009)
124. Cancro MP. The BLYS family of ligands and receptors: an archetype for niche-specific homeostatic regulation. *Immunol Rev* 202:237-249 (2004)
125. Teunissen CE et al. Whole brain spheroid cultures as a model to study the development of nitric oxide synthase-guanylate cyclase signal transduction. *Brain Res Dev Brain Res* 125:99-115 (2000)
126. Vereyken EJ et al. An in vitro model for de- and remyelination using lysophosphatidyl choline in rodent whole brain spheroid cultures. *Glia* 57:1326-1340 (2009)
127. Coles AJ et al. Alemtuzumab vs. interferon beta-1a in early multiple sclerosis. *N Engl J Med* 359:1786-1801 (2008)
128. Ali EN et al. Daclizumab in treatment of multiple sclerosis patients. *Mult Scler* 15:272-274 (2009)
129. De Jager PL et al. Cytometric profiling in multiple sclerosis uncovers patient population structure and a reduction of CD8low cells. *Brain* 131:1701-1711 (2008)
130. Vandenbark AA et al. Interferon-beta-1a treatment increases CD56bright natural killer cells and CD4+CD25+ Foxp3 expression in subjects with multiple sclerosis. *J Neuroimmunol* 215:125-128 (2009)
131. Wynn D et al. Daclizumab in active relapsing multiple sclerosis (CHOICE study): a phase 2, randomised, double-blind, placebo-controlled, add-on trial with interferon beta. *Lancet Neurol* 9:381-390 (2010)
132. Takahashi K et al. The regulatory role of natural killer cells in multiple sclerosis. *Brain* 127:1917-1927 (2004)
133. Barkhof F. MRI in multiple sclerosis: correlation with expanded disability status scale (EDSS). *Mult Scler* 5:283-286 (1999)
134. Barkhof F. The clinico-radiological paradox in multiple sclerosis revisited. *Curr Opin Neurol* 15:239-245 (2002)
135. Niess JH et al. Commensal gut flora drives the expansion of proinflammatory CD4 T cells in the colonic lamina propria under normal and inflammatory conditions. *J Immunol* 180:559-568 (2008)
136. Ochoa-Reparaz J et al. Role of gut commensal microflora in the development of experimental autoimmune encephalomyelitis. *J Immunol* 183:6041-6050 (2009)
137. Qin J et al. A human gut microbial gene catalogue established by metagenomic sequencing. *Nature* 464:59-65 (2010)
138. 't Hart BA et al. Multiple sclerosis - a response-to-damage model. *Trends Mol Med* 15:235-244 (2009)



A large, stylized grey number '6' is centered on the page. The number has a thick stroke and a decorative flourish at the top right. Inside the number, the words 'SUMMARY' and 'SAMENVATTING' are printed in a bold, black, sans-serif font.

**SUMMARY**  
**SAMENVATTING**

## SUMMARY

Multiple sclerosis (MS) is a chronic disease characterized by inflammation, demyelination, and axonal injury in the white and grey matter of the central nervous system (CNS). To date, the immunopathogenic mechanisms causing MS are still unknown and a therapy to arrest the progressive accumulation of neurological deficits is still lacking. Therefore, the aim of this thesis was to investigate the pathogenic mechanisms underlying MS as a basis for the development of new therapies.

The investigation of immunopathogenic mechanisms and the efficacy of new therapies benefits from an animal model that approximates MS in its clinical and pathological manifestation. Common marmosets are genetically, immunologically, and anatomically closely related to humans. The animal model for MS, experimental autoimmune encephalomyelitis (EAE), can be induced in marmosets. At the start of the research described in this thesis, EAE could be induced in 100% of the marmosets from an outbred colony by immunization with myelin or recombinant human myelin oligodendrocyte glycoprotein (rhMOG) in complete Freund's adjuvant (CFA). To identify the core pathogenic mechanisms, the marmoset model was refined to the minimal requirements for EAE induction. In addition, we used the marmoset model to validate pathogenic concepts by the efficacy analysis of several new therapies for MS.

Studies in experimental animal models rely on the availability of cross-reactive reagents and techniques, such as flow cytometry and immunohistochemistry. A large panel of anti-human antibodies that can be used to phenotype marmoset cells with flow cytometry is available. However, detailed *in situ* examination of lymphoid tissue was often hampered by the lack of cross-reactive antibodies. In **chapter 2**, we have investigated the cross-reactivity of a selection of anti-human antibodies against lymphoid tissue of non-human primates, including the marmoset. Of the 116 monoclonal antibodies tested, 69 antibodies (60%) were cross-reactive with marmoset spleen or lymph node tissue.

In previous marmoset EAE experiments, immunization with rhMOG/CFA induced a 100% disease incidence with a heterogeneous disease onset. The disease heterogeneity seems to be inherent to the outbred nature of the marmoset colony from which animals were recruited. The immunopathogenic mechanisms underlying this heterogeneity were investigated in **chapter 3.1**. We have found that fast disease progression is associated with a broadened T-cell response against a panel of 23-mer MOG peptides. The prevalent T-cell response in the fast progressor monkeys was directed against MOG34-56 and MOG74-96. MOG35-55 peptide was already known as an important epitope for disease induction in rodents. It was therefore not surprising that immunization of marmosets with MOG34-56 formulated in CFA led to a chronic disease. In this model, we have identified MOG34-56-specific T-cells

as major players in the disease. These T-cells have characteristics of natural killer cells and cytotoxic T-cells suggesting they are natural killer-cytotoxic T-lymphocytes (NK-CTL).

Immunization with MOG74-96 in CFA only induced mild symptoms and pathology. However, when these animals were given a single boost with MOG34-56 in incomplete Freund's adjuvant (IFA), neurological deficit as well as profound CNS lesion formation was observed. This led us to hypothesize that EAE in marmosets could also be induced with only MOG34-56 in IFA. In **chapter 3.2**, we demonstrated that MOG34-56 in IFA induced a chronic disease in marmosets with similar clinical symptoms and pathology as in the rhMOG/CFA and MOG34-56/CFA marmoset models. In this model, we identified that the MOG34-56-specific T-cells also produce IL-17A. This model induced without the use of CFA is a major refinement for ethical, practical, and mechanistic reasons.

Whether IL-17A production by MOG34-56-specific T-cells is indeed essential for the disease development was investigated in **chapter 4.1**. IL-17A was neutralized by weekly administration of two doses of anti-IL-17A antibody in the rhMOG/CFA model. Treatment with the anti-IL-17A antibody did not prevent the development of clinical signs and pathology, although the disease onset was slightly delayed. The treatment affected the number of IL-17A producing cells in lymphoid organs, but not in the brain. This suggests that IL-17A does not have a major pathogenic role in the induction phase of the disease in the chosen EAE model, but may rather play a role in the disease progression.

The CD20<sup>+</sup> B-cell depleting antibody rituximab is a promising treatment for MS, because clinical deterioration is prevented and lesion formation in the brain white matter is attenuated. The pathogenic mechanisms targeted by the antibody in MS are still unknown. We have therefore investigated the effect of late B-cell depletion with a novel anti-CD20 antibody (HuMab 7D8), i.e. well after (21 days) T-cell and B-cell priming and clonal expansion, on the immune system and CNS pathology in the marmoset EAE model induced by rhMOG in CFA. In **chapter 4.2**, we demonstrated that B-cells may act as antigen presenting cells in the EAE model, since T-cell proliferation and cytokine production were significantly reduced in lymphoid organs of B-cell depleted animals. In addition, B-cell depletion prevented demyelination and inflammation in brain white and grey matter as well as in spinal cord and optic nerve, as shown in **chapter 4.3**. These data underline an important pathogenic role of B-cells in the peripheral activation of T-cells and the induction of widespread CNS pathology.

Instead of interfering with the immune response, promotion of (re)myelination and neuronal outgrowth are also promising therapy targets. To investigate this, MOG34-56/CFA-immunized marmosets were treated with a monoclonal antibody against the myelin-associated neurite outgrowth inhibitor Nogo-A. In **chapter 4.4**, we demonstrated that anti-Nogo-A antibody abrogates the development of clinical signs and pathology.

In addition, we show that Nogo-A is not only a neurite outgrowth inhibitor, but that Nogo-A is also involved in the myelination process and the differentiation of oligodendrocyte precursor cells. This supports the promise that Nogo-A is a good therapeutic target for MS and other demyelinating diseases.

MS relapse rate decreases during pregnancy, especially during the third trimester. In this phase of pregnancy, fragments derived from the  $\beta$ -subunit of the pregnancy hormone human chorionic gonadotropin (hCG) can be detected in serum and urine. Previous studies in rodent and non-human primate models of immune-mediated inflammatory disease showed that synthetic oligopeptides related to the hCG  $\beta$ -subunit have modulatory effects in acute, inflammatory responses. We have investigated whether the hCG-related tetrapeptide LQGV has modulatory potential in a more chronic inflammatory disease, namely EAE in marmosets. In **chapter 4.5**, we reported that the tested dose and treatment regimen of LQGV had no effect on clinical signs, pathology, or the immune response in marmosets immunized with MOG34-56 and MOG74-96 in IFA.

In conclusion, the studies collectively support the interpretation that the major pathogenic immune response is mediated by MOG34-56-specific T-cells, which display a unique combination of cytotoxicity and IL-17A production. These T-cells can be activated *in vivo* by immunization with MOG34-56 in IFA, showing that in contrast to the generally held dogma, microbial ligands in the adjuvant are not required for their activation. In addition, we have shown that anti-IL-17A antibody and LQGV are not effective in the marmoset models tested, although both treatments may be effective in other EAE marmoset models. Furthermore, B-cell depletion and targeting Nogo-A are promising treatments for MS. The improved and refined marmoset EAE model will be useful to further dissect the pathogenesis and to validate new therapies for MS.

## SAMENVATTING

Multipele sclerose (MS) is een chronische aandoening die zich kenmerkt door ontsteking, demyelinisatie, en schade aan de zenuwcellen in de witte en grijze stof van de hersenen en het ruggenmerg. Demyelinisatie wordt mogelijk veroorzaakt doordat cellen van het immuunsysteem, zoals macrofagen en T-cellen, zich richten tegen de myeline laag om zenuwcellen. De exacte pathogenese, oftewel de oorzaak en de ontwikkeling, van MS is nog niet bekend. Tevens is er nog geen medicijn om de progressieve voortgang van de ziekte te stoppen. Dit proefschrift beschrijft onderzoek dat gedaan is naar de pathogenese van MS en een aantal nieuwe geneesmiddelen die zijn getest op hun effectiviteit.

Om onderzoek te kunnen doen naar de pathogenese en het effect van nieuwe geneesmiddelen is een diermodel nodig. Dit diermodel moet zo sterk mogelijk lijken op MS in het klinische verloop en in de ontwikkeling van de lesies in de hersenen en het ruggenmerg. De marmoset, ook wel bekend als de penseelaap, is grotendeels vergelijkbaar met de mens op het genetische, immunologische, en anatomische vlak. Het diermodel voor MS is experimentele autoimmuun encefalomyelitis (EAE). Voordat het onderzoek beschreven in dit proefschrift werd begonnen, was al bekend dat EAE geïnduceerd kon worden in marmosets. EAE werd geïnduceerd door immunisatie met de recombinante versie van humaan myeline oligodendrocyt glycoproteïne (rhMOG) in compleet Freund's adjuvant (CFA). MOG is één van de eiwitten die aanwezig zijn in de myelineschede om zenuwcellen en waartegen een deel van de immunrespons in MS is gericht. CFA is een adjuvant dat er onder andere voor zorgt dat er een langdurige afgifte ontstaat van rhMOG op de immunisatie plek. Hierdoor wordt het immuunsysteem langdurig geactiveerd door rhMOG. CFA bevat ook geïnactiveerde mycobacteriën waardoor het immuunsysteem nog extra geactiveerd wordt.

Eén van de onderzoeksvragen richtte zich op het vinden van de minimale benodigdheden om EAE te induceren. Door de verfijning van het immunisatieprotocol is er meer bekend geworden over de minimale benodigdheden voor de inductie van EAE. Hierdoor is er ook meer bekend geworden over de pathogenese. Verder is het marmoset EAE model gebruikt als preklinisch model om de effectiviteit van nieuwe geneesmiddelen te onderzoeken.

Om studies in experimentele (dier)modellen te kunnen uitvoeren zijn kruisreactieve reagentia nodig, onder andere voor analyse met flow cytometrie en immunohistochemie. Om marmoset cellen te kleuren voor flow cytometrie was al een groot panel van anti-humane antistoffen beschikbaar die kruisreageren met marmoset cellen. Het onderzoek van lymfoïde organen met immunohistochemie werd nog beperkt doordat de kruisreactiviteit van anti-humane antistoffen niet bekend was. In **hoofdstuk 2** is de kruisreactiviteit getest van een selectie anti-humane antistoffen op lymfoïde weefsel

van zes niet-humane primaten, inclusief de marmoset. Van de 116 geteste antistoffen waren er 69 (60%) kruisreactief met marmoset weefsel.

Uit eerdere marmoset EAE experimenten was al bekend dat immunisatie met rhMOG in CFA klinische symptomen induceert in alle marmosets. De dag dat de eerste klinische symptomen zich openbaarden was echter wel verschillend tussen de dieren. Deze heterogeniteit wordt veroorzaakt doordat de marmosets genetisch verschillend zijn van elkaar, in tegenstelling tot ingeteelde knaagdier stammen die ook voor EAE worden gebruikt. Welke immuunresponsen verantwoordelijk zijn voor de heterogeniteit in marmosets was nog niet bekend en is onderzocht in **hoofdstuk 3.1**. Het blijkt dat dieren die relatief kort na immunisatie symptomen ontwikkelen, een brede T-cel respons hebben die gericht is tegen meerdere epitopen van MOG. De meest voorkomende T-cel responsen waren gericht tegen het peptide 34 tot en met 56 van MOG (MOG34-56) en MOG74-96. Het was al bekend dat MOG34-56 belangrijk is voor de inductie van EAE in knaagdieren. Ook in marmosets leidt immunisatie met MOG34-56 in CFA tot een chronisch ziektebeeld. T-cellen die specifiek reageren op MOG34-56 blijken een belangrijke rol te spelen in het marmoset EAE model. Deze T-cellen hebben bepaalde kenmerken die zowel overeenkomen met natural killer cellen als cytotoxische T-cellen en behoren daarom mogelijk tot de natural killer-cytotoxische T-lymfocyt populatie (NK-CTL).

Immunisatie van marmosets met MOG74-96 in CFA leidt tot milde klinische symptomen en pathologie. Deze dieren ontwikkelen dezelfde klinische symptomen en pathologie als dieren die zijn geïmmuniseerd met MOG34-56 in CFA als zij éénmaal worden geboost met MOG34-56 in incompleet Freund's adjuvant (IFA). In tegenstelling tot CFA bevat IFA geen bacteriële antigenen, waardoor het immuunsysteem op een andere manier wordt geactiveerd. Onze hypothese was dat CFA niet noodzakelijk is voor de inductie van EAE en dat MOG34-56 in IFA voldoende is. In **hoofdstuk 3.2** hebben we aangetoond dat immunisatie van marmosets met MOG34-56 in IFA leidt tot een chronische ziekte met gelijke klinische symptomen en pathologie als in de rhMOG in CFA en MOG34-56 in CFA modellen. In dit model worden dezelfde MOG34-56-specifieke T-cellen geactiveerd en deze maken tevens IL-17A. Dit model zonder CFA is een aanzienlijke verfijning in ethisch, praktisch en conceptueel opzicht.

Om te onderzoeken of de productie van IL-17A door MOG34-56-specifieke T-cellen essentieel is voor de ziekte, hebben we in het rhMOG in CFA model IL-17A geneutraliseerd door wekelijks te behandelen met twee verschillende concentraties van een antistof tegen IL-17A. In **hoofdstuk 4.1** laten we zien dat behandeling met dit antistof de ontwikkeling van klinische symptomen en pathologie niet kon voorkomen, maar dat het wel langer duurde voordat de behandelde dieren ziek werden vergeleken met de controle dieren. Na de behandeling was het aantal IL-17A producerende cellen veranderd in de lymfoïde organen, maar niet in de hersenen. Dit onderzoek suggereert

dat IL-17A geen essentiële rol speelt in de inductie fase van dit model, maar mogelijk speelt het wel een rol bij de regulatie van de progressie van de ziekte.

Het verwijderen van CD20<sup>+</sup> B-cellen is een veelbelovende behandeling voor MS. Het anti-CD20-antistof rituximab verminderde de klinische achteruitgang en de ontwikkeling van lesies in de witte stof van de hersenen van mensen met MS. Het mechanisme dat ten grondslag ligt aan dit effect is onbekend. Wij hebben het effect van B-cel depletie op het immuunsysteem en de pathologie onderzocht. Drie weken na immunisatie met rhMOG in CFA, wanneer de T-cel respons in gang is, werden de B-cellen verwijderd door wekelijkse behandeling met een nieuw anti-CD20 antistof (HuMab 7D8). In **hoofdstuk 4.2** laten we zien dat B-cellen mogelijk werken als antigeen presenterende cel in het marmoset EAE model. In de behandelde dieren was de deling en cytokine productie van T-cellen in lymfoïde organen verminderd vergeleken met de niet behandelde dieren. In **hoofdstuk 4.3** laten we zien dat het verwijderen van B-cellen leidt tot minder demyelinisatie en ontsteking in de witte en grijze stof van de hersenen, in het ruggenmerg en de oogzenuw. Deze resultaten tonen aan dat B-cellen mogelijk een pathogene rol spelen door de activatie van autoreactieve T-cellen en de inductie van de pathologie.

In plaats van het onderdrukken van de immuunrespons, is het stimuleren van nieuwe myeline aanmaak en de uitgroei van zenuwcellen een andere therapeutische strategie. Om dit te onderzoeken zijn marmosets geïmmuniseerd met MOG34-56 in CFA en wekelijks behandeld met een antistof tegen Nogo-A. Nogo-A is aanwezig in myeline en remt de uitgroei van zenuwcellen. In **hoofdstuk 4.4** is aangetoond dat een anti-Nogo-A antistof de ontwikkeling van klinische symptomen en pathologie remt. Nogo-A blijkt ook betrokken bij de aanmaak van myeline en de ontwikkeling van de myeline-producerende oligodendrocyten. Een anti-Nogo-A antistof kan dus potentieel een goede therapie zijn voor MS en andere ziekten waarin afbraak van myeline plaatsvindt.

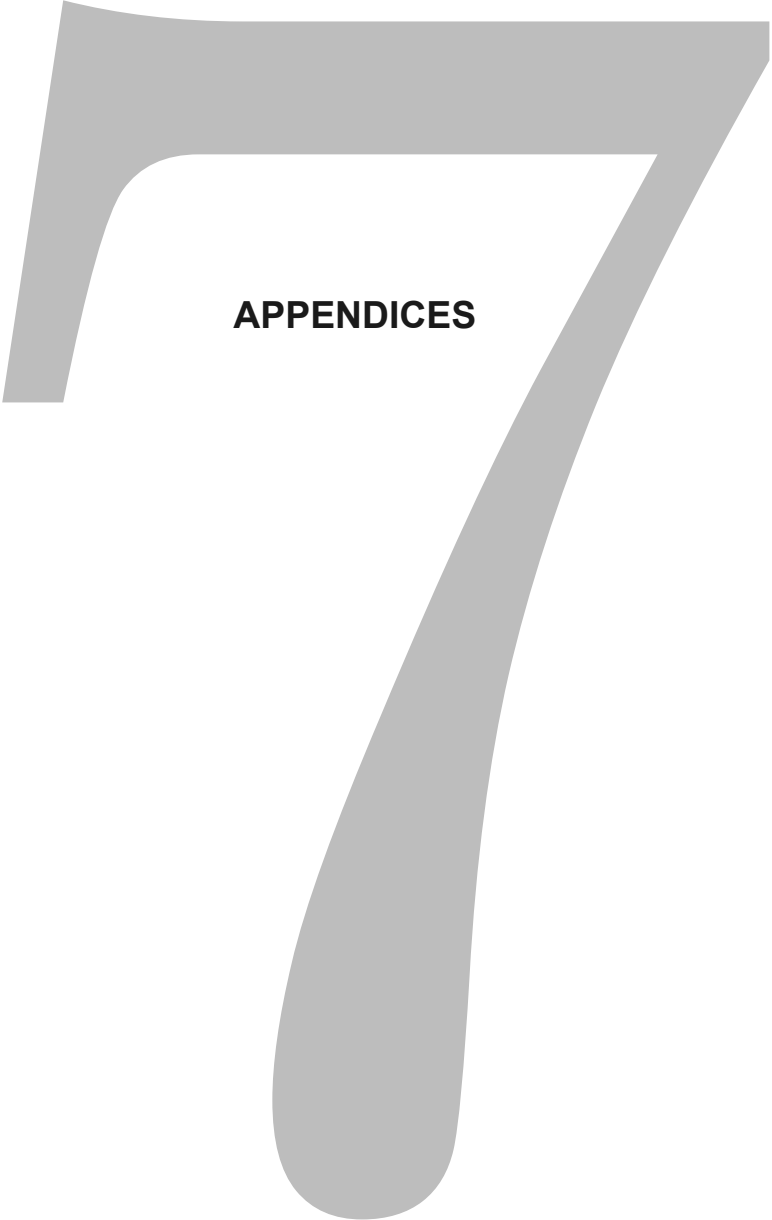
Het aantal MS-aanvallen neemt af tijdens zwangerschap en dan met name tijdens het derde trimester. In deze fase zijn fragmenten van de  $\beta$ -subunit van het zwangerschapshormoon humaan choriongonadotropine (hCG) aanwezig in serum en urine. In eerdere studies is aangetoond dat hCG-gerelateerde peptiden, zoals LQGV, een acute immuunrespons kunnen moduleren. Het effect van het hCG-gerelateerde peptide LQGV op een chronische immuunrespons is onderzocht in het marmoset EAE model. Marmosets werden geïmmuniseerd met MOG34-56 en MOG74-96 in IFA en drie keer per week behandeld met LQGV. Uit **hoofdstuk 4.5** blijkt dat LQGV in de geteste dosis en behandelingsregime geen effect heeft op klinische symptomen, pathologie of de immuunrespons in marmosets geïmmuniseerd met MOG34-56 en MOG74-96 in IFA.

Deze studies verschaffen evidentie dat MOG34-56-specifieke T-cellen een belangrijke rol spelen in de pathogenese van EAE en mogelijk ook in MS. Deze T-cellen hebben

de unieke combinatie van cytotoxiciteit en IL-17A productie en kunnen geactiveerd worden door immunisatie met MOG34-56 in IFA. Dit laat zien dat, in tegenstelling tot het algemene dogma, microbiële liganden in het adjuvant niet noodzakelijk zijn voor de activatie van deze T-cellen. Tevens hebben we aangetoond dat een anti-IL-17A antistof en LQGV niet effectief zijn in de geteste marmoset EAE modellen. B-cel depletie en een anti-Nogo-A antistof zijn wel veelbelovende behandelmethode voor MS. Het verbeterde en verfijnde marmoset EAE model zal in de toekomst bijdragen aan verdere ontrafeling van de pathogenese en tevens meer gebruikt worden voor de preklinische validatie van nieuwe geneesmiddelen.





A large, stylized, light gray number '7' is centered on the page. The number has a thick, rounded top bar and a long, curved stem that tapers towards the bottom. The word 'APPENDICES' is printed in a bold, black, sans-serif font, centered within the upper portion of the '7'.

**APPENDICES**

## ABBREVIATIONS

(m)Ab	(monoclonal) antibody
Ag	antigen
ALN	axillary lymph node
APC	antigen presenting cell
BBB	blood-brain barrier
B-LCL	B-lymphoblastoid cells
BLyS	B lymphocyte stimulator
Caja	<i>Callithrix jacchus</i>
CD	cluster of differentiation
CFA	complete Freund's adjuvant
CFSE	carboxyfluorescein diacetate succinimidyl ester
CLN	cervical lymph node
CMV	cytomegalovirus
CNS	central nervous system
cpm	counts per minute
CSF	cerebrospinal fluid
DC	dendritic cell
DTI	diffusion tensor imaging
EAE	experimental autoimmune encephalomyelitis
EBV	Epstein-Barr virus
GM	grey matter
HHV	human herpesvirus
HIV	human immunodeficiency virus
HLA	human leukocyte antigen
IFA	incomplete Freund's adjuvant
IFN	interferon
Ig	immunoglobulin
IL	interleukin
ILN	inguinal lymph node
LPC	lysophosphatidylcholine
MAG	myelin associated glycoprotein
MBP	myelin basic protein
MHC	major histocompatibility complex
MNC	mononuclear cell suspension
MOG	myelin oligodendrocyte glycoprotein
MRI	magnetic resonance imaging
MS	multiple sclerosis

MTR	magnetization transfer ratio
NAWM/NAGM	normal appearing white/grey matter
NgR	Nogo-receptor
NHP	non-human primate(s)
NK-CTL	natural killer-cytotoxic T lymphocyte
NLR	Nodlike receptor
OPC	oligodendrocyte glycoprotein
PBMC	peripheral blood mononuclear cells
PLP	proteolipid protein
PML	progressive multifocal leukoencephalopathy
PPMS	primary progressive MS
PRMS	progressive relapsing MS
psd	post sensitization day
rh	recombinant human
ROI	region of interest
RRMS	relapsing-remitting MS
SI	stimulation index
SPMS	secondary progressive MS
T1W/T2W	T1- or T2-weighted
TCL	T-cell line
TCR	T-cell receptor
TLR	Toll-like receptor
TNF	tumor necrosis factor
Th	T helper
WM	white matter

## DANKWOORD

Na het schrijven van de belangrijkste onderdelen voor dit boekje, is het nu tijd voor het meest gelezen onderdeel, het dankwoord. Omdat er geen ruimte is om iedereen hier persoonlijk te noemen, wil ik allereerst iedereen bedanken die op enige wijze heeft bijgedragen aan mijn proefschrift.

Bert, bedankt voor je enthousiasme, je positiviteit, je ideeën, en je verklaringen als er weer eens een experiment anders verliep dan ik hoopte. Wat ik vooral heb gewaardeerd, is de vrijheid die jij je promovendi geeft, waardoor ik veelal mijn eigen gang kon gaan. Zoals je weet, moest ik in het begin erg wennen aan de combinatie van fundamentele wetenschap en de toegepaste wetenschap, in mijn project het testen van nieuwe geneesmiddelen. Dankzij jou zie ik in hoeveel beide onderdelen aan elkaar toevoegen. Ik ben dan ook heel erg blij met dit eindresultaat. Ook als post-doc ben ik van plan om het maximale uit deze combinatie te halen.

Jon, vier jaar lang was je actief betrokken bij mijn promotie. Jij was altijd bereid om naar het BPRC te komen voor een bespreking, en ik was altijd welkom om experimenten op te zetten op de afdeling Immunologie. Als er iets nagekeken moest worden kreeg ik dat zeer snel van je terug, met nuttig commentaar. Jij hebt mij geleerd om kritisch te kijken naar mijn experimenten en manuscripten. Bedankt voor dit alles. Hopelijk kunnen we onze samenwerking nog vele jaren doorzetten.

Professor Benner, beste Rob, bedankt dat u mij de mogelijkheid heeft gegeven om mijn promotieonderzoek uit te voeren op het BPRC en voor het feit dat ik twee keer op werkbezoek mocht naar Oklahoma. Ik kijk met heel veel plezier terug op deze tijd.

Nikki, zonder jouw hulp was dit boekje zeker de helft dunner geworden. Ik hoop dat we nog heel veel jaren mogen samenwerken. Ik ben blij dat jij mijn paranimf wilt zijn. Anwar, in het begin hebben wij even samengewerkt als promovendus en analist. Jij wilde liever je eigen onderzoek doen en besloot om ook promotieonderzoek te gaan doen. Veel succes met het afronden volgend jaar! Elia, bedankt voor de gezellige jaren en dat ik altijd even mijn verhaal bij je kon doen. Ik vind het heel fijn dat jij naast mij wilt staan als paranimf. Céline, vooral in de maanden dat we 'buurvrouwen in 139' waren, hebben we het erg gezellig gehad en veel aio-frustraties gedeeld. De laatste tijd moesten we af en toe even een korte koffiepauze inlassen om ons aio-leed te delen. Heel veel succes met de laatste loodjes! Krista en Ruth, bedankt voor al jullie hulp en goede tips die een beginnende promovendus altijd wel kan gebruiken. 'Schiedam-meiden', bedankt voor alle heerlijke en gezellige etentjes en alle keren dat ik met jullie mee mocht rijden als we weer een labuitje hadden of als de treinen niet reden. Alle andere collega's van Immunobiologie, CG&R, en Alternatieven, bedankt voor de gezellige tijd. Niels en Sam, bedankt voor alle keren dat jullie geduldig antwoord gaven als ik weer eens een vraag had over de FACS. Herbert, bedankt voor

het opzetten van het model; jouw boekje heeft vier jaar lang binnen handbereik op mijn bureau gelegen.

Zonder de statistiek van Ed en de mooie figuren van Henk was dit boekje niet tot stand gekomen, heel erg bedankt voor jullie hulp! Ook wil ik iedereen van de ASD bedanken, en een paar mensen in het bijzonder. Jaco, Fred, Mariska, Martine en Annelies, heel erg bedankt voor jullie toewijding en goede zorg voor de dieren. Zonder jullie zou ik mijn werk niet kunnen doen. Ook Ivanela, Tom, Jan, en Willem, bedankt!

Natuurlijk zijn er ook veel mensen buiten het BPRC die ik wil bedanken. Marjan, dankzij jouw hulp en tips zitten er een aantal mooie immunohistochemie figuren in mijn boekje, bedankt! Hopelijk vind je het goed als ik je de komende jaren ook om tips blijf vragen. Wendy, Geertje, Erna en Marcia, bedankt voor jullie ondersteunende hulp en het verzorgen van de lay-out, samen met Wendy Schoneveld. Erwin en Jan, elk artikel bevat toch minstens één figuur of tabel met jullie resultaten. Zonder jullie zouden mijn artikelen een stuk minder interessant zijn geworden. Dear Doug, Marilyn, and Jennifer, although the Listeria paper is not a part of this thesis, I want to thank you for the wonderful time.

Lieve papa, mama en Erik, bedankt voor jullie onvoorwaardelijke steun en liefde. Ik weet dat jullie trots op mij zijn, ik ben ook heel trots op jullie. Ik hou van jullie. Lieve familie, vrienden en mijn liefste vriendinnetje Nicole, bedankt voor jullie gezelligheid, interesse in mijn werk, en begrip als ik het weer eens te druk had om iets af te spreken.

Lieve Marten, het valt niet mee om tegelijkertijd te promoveren en allebei gestrest te zijn op dezelfde momenten. Gelukkig is het nu helemaal klaar! Bedankt voor je geduld als ik mijn frustraties thuis liep te uiten en bedankt voor alle keren dat jij mij gemotiveerd hebt. Onze twee bezoeken aan Oklahoma zal ik nooit meer vergeten, wat hebben we het daar leuk gehad. Ik hou van jou!

Yolanda

## **CURRICULUM VITAE**

Yolanda Kap was born on October 12th 1980 in Amstelveen, the Netherlands. She completed secondary school at the Hermann Wesselink College in Amstelveen in 1999. She proceeded to study zoology at Higher Laboratory Education (HLO), the first year in Amsterdam and three years in Utrecht. During this study, she did her internship at the Netherlands Brain Institute in Amsterdam, investigating the influence of the central nervous system on abdominal organs during the metabolic syndrome under the supervision of Prof. Dr. R.M. Buijs and Dr. F. Kreier. In 2003, she obtained her degree Bachelor of Applied Science.

From 2003 to 2005, she studied Biomedical Sciences at the Free University in Amsterdam. She did her first internship at the Department of Molecular Cell Biology and Immunology of the VUMC in Amsterdam, investigating the expression of tight junction proteins in multiple sclerosis under the supervision of Dr. J. van Horsen and Dr. H.E. de Vries. During her second internship she investigated novel targets of the endoplasmic reticulum stress response in Alzheimer's disease under supervision of Dr. W. Scheper at the Department of Neurogenetics of the AMC in Amsterdam. In 2005, she obtained her Master's degree.

In November 2005, Yolanda started this PhD project at the Department of Immunology of the Erasmus MC and the Department of Immunobiology of the BPRC under supervision of Prof. Dr. J.D. Laman, Prof. Dr. R. Benner, and Dr. B.A. 't Hart. During her PhD, she went to Oklahoma for a total of 3 months to participate in a research project investigating the effect of hCG-related oligopeptides on the innate immune response to *Listeria monocytogenes* infection under the supervision of Dr. D.A. Drevets.

Since May 2010, she works as a postdoc at the Department of Immunobiology of the BPRC to continue her work in the marmoset EAE model.

## PHD PORTFOLIO

### PhD training

#### *General academic skills*

Introduction to data-analysis (NIHES <sup>1</sup> )	2006
Classical methods for data-analysis (NIHES)	2008
Academic writing in English for PhD students	2008
Management for PhD students and postdocs (NIBI <sup>2</sup> )	2008

#### *Research skills*

Laboratory animal science (Article 9)	2001
Basic radiation protection 5B	2003
Biomedical research techniques (MolMed <sup>3</sup> )	2006

#### *In-depth courses*

Inflammatory mechanisms in neurodegenerative diseases (MolMed)	2006
Molecular immunology (MolMed)	2006
7 <sup>th</sup> European School of Neuroimmunology, Oxford, UK	2007
8 <sup>th</sup> European School of Neuroimmunology, Fort Worth, TX	2008

#### *Didactic skills*

Teach-the-Teacher (Desiderius school)	2008
---------------------------------------	------

#### *Seminars and workshops*

Nieuwe ontwikkelingen in de medische immunologie, Rotterdam (Nov 23)	2005
10 <sup>th</sup> Molecular Medicine Day (Feb 1)	2006
Dept. Immunology, Erasmus MC, Rotterdam:	
Immunity, macrophages, and the nervous system (Nov 22)	2005
Pattern recognition and innate immunity (Feb 2)	2006
Brain-body immune debate (Feb 2)	2009

#### *(Inter)national conferences*

Dutch MS Research meeting, Amsterdam (Nov 24-25)	2005
Annual meeting NVVI <sup>4</sup> , Lunteren (Mar 23-24)	2006
European marmoset research group meeting, Milan, Italy (Sep 27-29)	2006
Dutch MS Research meeting, Rotterdam (Nov 16-17)	2006
Annual meeting NVVI, Noordwijkerhout (Dec 7-8)	2006
Annual meeting NVVI, Noordwijkerhout (Dec 20-21)	2007

Annual meeting NVVI, Lunteren (Apr 3-4)	2008
9 <sup>th</sup> International Congress of Neuroimmunology, Fort Worth, TX (Oct 27-30)	2008
Annual meeting NVVI, Lunteren (Apr 2-3)	2009
Dutch MS Research meeting, Groningen (Nov 12-13)	2009
Annual meeting NVVI, Noordwijkerhout (Dec 17-18)	2009
9 <sup>th</sup> International Conference on New Trends in Immunosuppression and Immunotherapy, Geneva, Switzerland (Feb 4-6)	2010
From genes to pathogenesis of MS, organized by COST-Neurinfnet, Lofoten, Norway (Aug 15-19)	2010
<i>Poster presentation</i>	
Fast progression of rhMOG-induced EAE in marmosets is associated with the activation of anti-MOG34-56 cytotoxic T-cells (Annual meeting NVVI)	2007
Discrepant oxyradical production by phagocytes from marmoset and rhesus monkeys with differential encephalitis pathology (9 <sup>th</sup> International Congress of Neuroimmunology)	2008
Discrepant oxyradical production by phagocytes from marmoset and rhesus monkeys with differential encephalitis pathology (Annual meeting NVVI)	2009
A non-human primate model for multiple sclerosis without the use of complete Freund's adjuvant (9 <sup>th</sup> International Conference on New Trends in Immunosuppression and Immunotherapy)	2010
<i>Oral presentation</i>	
MOG34-56 induces EAE in the common marmoset (Dutch MS Research meeting)	2006
Anti-Nogo-A antibody prevents MOG34-56-induced EAE in marmosets (BPRC retreat)	2008
Depletion of B-cells prevents EAE in marmosets (BPRC retreat)	2009
Discrepant oxyradical production by phagocytes from marmoset and rhesus monkeys with differential encephalitis pathology (Dutch MS Research meeting)	2009
Experimental autoimmune encephalomyelitis in the marmoset: pre-clinical model for MS (United Europeans for development of Pharmacogenomics in MS)	2010
EAE in the common marmoset, a tool for translational research in MS (From genes to pathogenesis of MS, organized by COST-Neurinfnet)	2010

**Teaching activities**

Immunology practicals for 2nd year medical students 2006-2010

**Other**

Two working visits of 6 weeks to Oklahoma University, Oklahoma City, OK 2007/2008

Translation of articles for [www.MSweb.nl](http://www.MSweb.nl) (a website for people with MS) 2006-2010

<sup>1</sup> Netherlands Institute for Health Sciences

<sup>2</sup> Netherlands Institute for Bioscience

<sup>3</sup> Postgraduate school Molecular Medicine

<sup>4</sup> Nederlandse Vereniging voor Immunologie/Dutch Society for Immunology

## LIST OF PUBLICATIONS

**Kap YS**, Bauer J, van Driel N, Parren PWHI, Bleeker WK, Laman JD, Craigen JL, Blezer E, 't Hart BA. Late CD20<sup>+</sup> B-cell depletion attenuates demyelination in the CNS white and grey matter of EAE-affected marmoset monkeys. *Manuscript in preparation*

Li YY\*, Wang R\*, **Kap YS\***, Zhang Y, Liu A, Zhao Y, Song M, Zhang L, Lu Z, Prinjha RK, Xu Y, Xu J, van Driel N, Blezer E, Bauer J, Cleveland M, Wurthner JU, Faulkner JD, Lee D, Lu H, 't Hart BA, Zhang J. Role of amino-Nogo-A antagonism in oligodendrocyte differentiation and myelination in experimental demyelinating diseases. *Submitted for publication*

\* share first authorship

**Kap YS**, Jagessar SA, van Driel N, Blezer E, Bauer J, van Meurs M, Smith P, Laman JD, 't Hart BA. Effects of early IL-17A neutralization on disease induction in a primate model of experimental autoimmune encephalomyelitis. *J Neuroimmune Pharmacol (in press)*

**Kap YS**, van Driel N, Blezer E, Parren PWHI, Bleeker WK, Laman JD, Craigen JL, 't Hart BA. Late B-cell depletion with a human anti-human CD20 IgG1 $\kappa$  mAb halts the development of experimental autoimmune encephalomyelitis in marmosets. *J Immunol (in press)*

Jagessar SA\*, **Kap YS\***, Heijmans N, van Driel N, van Straalen L, Bajramovic JJ, Brok HPM, Blezer ELA, Bauer J, Laman JD, 't Hart BA. Induction of progressive demyelinating autoimmune encephalomyelitis in common marmoset monkeys using MOG34-56 peptide in incomplete Freund adjuvant. *J Neuropathol Exp Neurol* 2010, 69:372-385

\* share first authorship

van der Zee M, Dik WA, **Kap YS**, Dillon MJ, Benner R, Leenen PJM, Khan NA, Drevets DA. Synthetic human chorionic gonadotropin-related oligopeptides impair early innate immune responses to *Listeria monocytogenes* in mice. *J Infect Dis* 2010, 201:1072-1080

**Kap YS**, Laman JD, 't Hart BA. Experimental autoimmune encephalomyelitis in the common marmoset, a bridge between rodent EAE and multiple sclerosis for immunotherapy development. *J Neuroimmune Pharmacol* 2010, 5:220-230

**Kap YS**, van Meurs M, van Driel N, Koopman G, Melief MJ, Brok HPM, Laman JD, 't Hart BA. A monoclonal antibody selection for immunohistochemical examination of lymphoid tissues from non-human primates. *J Histochem Cytochem* 2009, 57:1159-1167

**Kap YS\***, Smith P\*, Jagessar SA\*, Remarque E, Blezer E, Strijkers G, Laman JD, Hintzen, RQ, Bauer J, Brok HPM, 't Hart BA. Fast progression of recombinant human myelin/oligodendrocyte glycoprotein (MOG)-induced experimental autoimmune encephalomyelitis in marmosets is associated with the activation of MOG34-56-specific cytotoxic T-cells. *J Immunol* 2008, 180:1326-1337

\* share first authorship

't Hart BA, Jagessar SA, **Kap YS**, and Brok HPM. Preclinical models of multiple sclerosis in non-human primates. *Expert Rev Clin Immunol* 2007, 3:749-761

't Hart BA, **Kap YS**, Jagessar SA, Amor S, Brok HPM. Neuroimmunology research in non-human primates. Book chapter in: Neuroimmunology Research Perspectives, Johansson LM, Nova Science Publishers, Hauppauge, NY, 2007

Brok HP, Boven L, van Meurs M, Kerlero de Rosbo N, Celebi-Paul L, **Kap YS**, Jagessar A, Hintzen RQ, Keir G, Bajramovic J, Ben-Nun A, Bauer J, Laman JD, Amor S, 't Hart BA. The human CMV-UL86 peptide 981-1003 shares a crossreactive T-cell epitope with the encephalitogenic MOG peptide 34-56, but lacks the capacity to induce EAE in rhesus monkeys. *J Neuroimmunol* 2007, 182:135-152

**Kap YS**, Hoozemans JJ, Bodewes AJ, Zwart R, Meijer OC, Baas F, Scheper W. Pin1 levels are down-regulated during ER stress in human neuroblastoma cells. *Neurogenetics* 2007, 8:21-27

Kreier F, **Kap YS**, Mettenleiter TC, van Heijningen C, van der Vliet J, Kalsbeek A, Sauerwein HP, Fliers E, Romijn JA, Buijs RM. Tracing from fat tissue, liver, and pancreas: a neuroanatomical framework for the role of the brain in type 2 diabetes. *Endocrinology* 2006, 147:1140-1147



## COLOR FIGURES

### Chapter 1

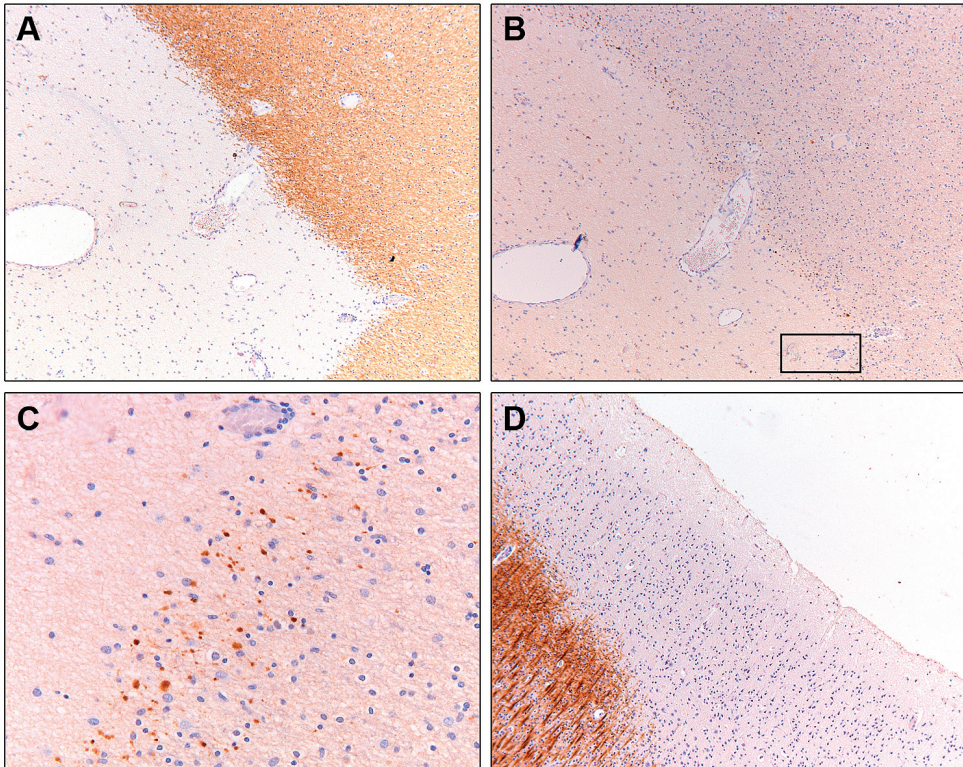
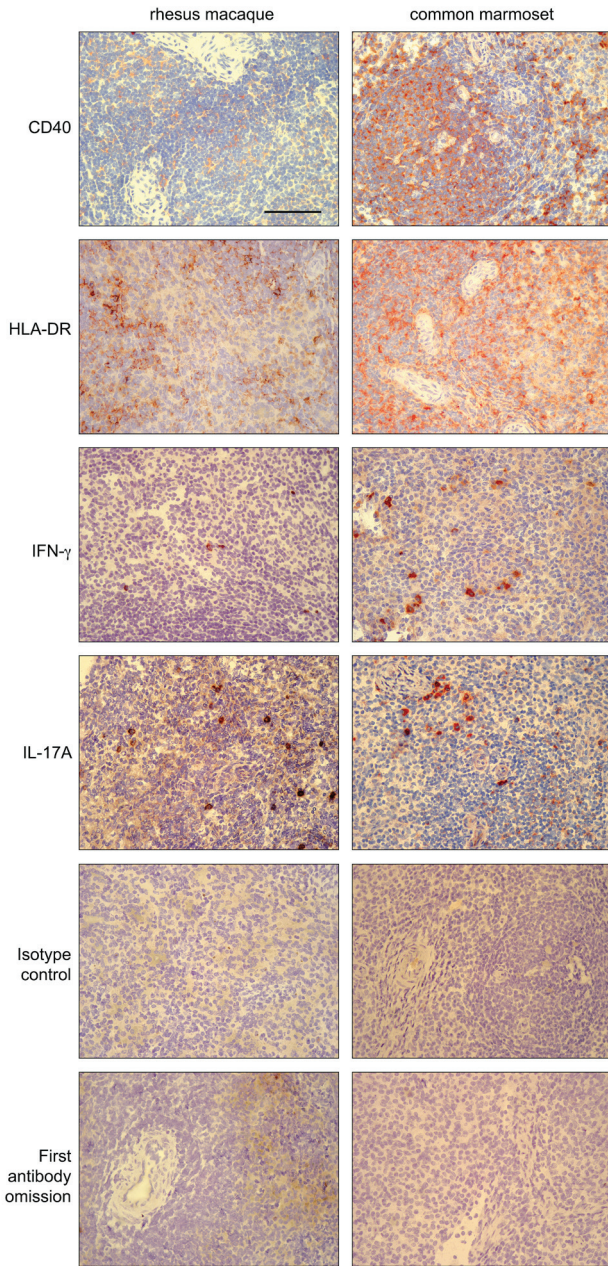


**Figure 3. Pathology of MS.**

A, A staining for proteolipid protein (PLP) shows the demyelinated hypocellular center of a chronic active lesion in the white matter of a MS brain (original magnification x50). B, At the rim of the lesion, where myelin is phagocytosed by macrophages, axonal transections are visualized by a staining for the amyloid precursor protein (original magnification x50). Axonal transections at the rim of the lesion in the square are enlarged in C (original magnification x100). D, A PLP staining of the grey matter shows a subpial lesion (original magnification x50). Photographs are kindly provided by E.-J. Kooi and Dr. J. Geurts (Department of Pathology, VU University Medical Center, Amsterdam, The Netherlands).

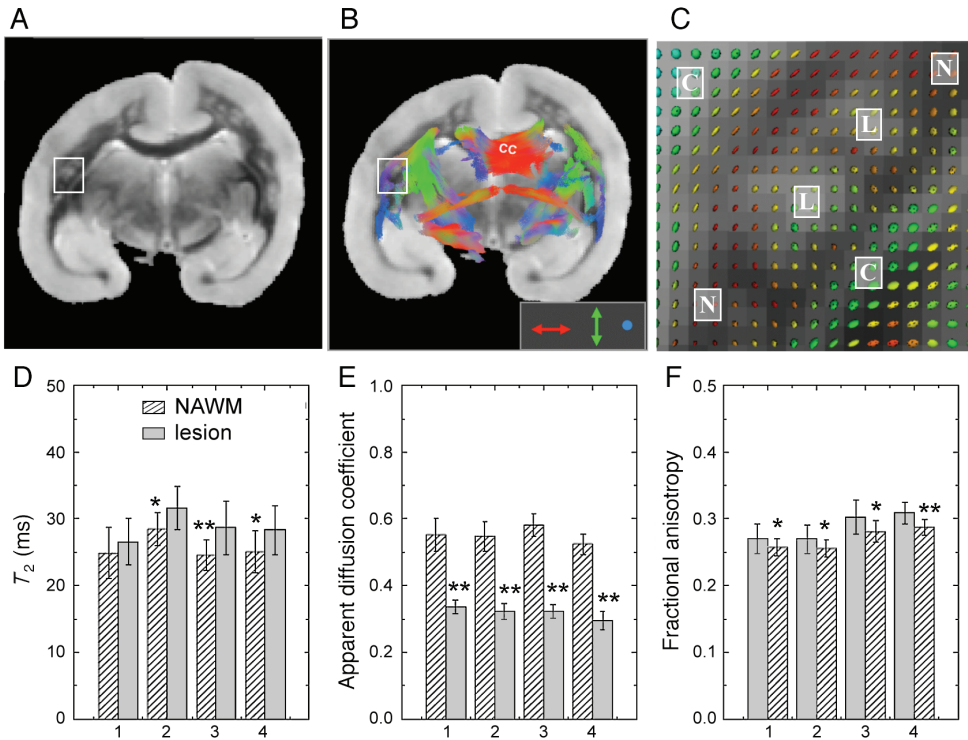


Chapter 2.1

**Figure 1. Representative selection of cross-reactive monoclonal antibodies on spleen cryosections of rhesus macaque and common marmoset.**

Spleen sections were stained for CD40, HLA-DR, IFN- $\gamma$ , and IL-17A. Controls included isotype control and first antibody omission. Bar = 100  $\mu$ m.

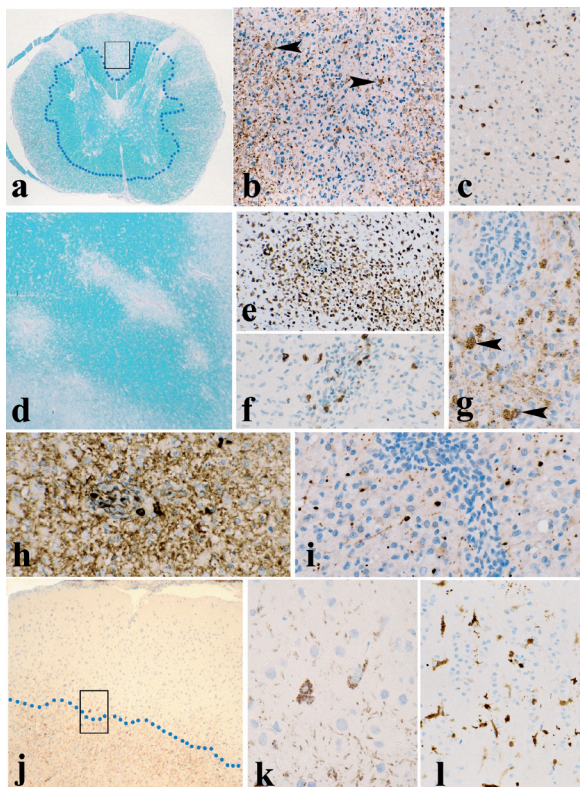
## Chapter 3.1



**Figure 4. Diffusion tensor imaging of MOG34-56-induced brain lesions.**

The disruption of the normally restricted orientation (anisotropic) of water diffusion in white matter was used as an indirect MRI measure of tissue destruction in formalin-fixed brains. Brains from the four MOG34-56-immunized monkeys in experiment 1 (see Table 1) were used for this analysis. A tomographic section of the brain of monkey M0167 is depicted as a representative example. A, High contrast T2W images were made to visualize hyperintense structural abnormalities. B, The (disturbance of) fiber direction within the white matter is visualized with the standard color codes (red, left ==> right; blue, superior ==> inferior; green, anterior ==> posterior). C, The ellipsoid representation of fiber orientation within a lesion-rich area (white square) shows a round shape in the cortical (C) and lesion (L) area whereas these are more unidirectional in the compact white matter. D-F, Mean values of the total lesion (grey bars) and white matter (hatched bars) area of four monkeys (M0131, M0167, M0178, and M0182) are shown. The depicted quantitative parameters are as follows: 1) the mean of all voxels for  $T_2$  relaxation times (D), which is higher in the lesions than in the NAWM due to increased water content; 2) the degree of fractional anisotropy (E), which is decreased due to destruction of compact myelin; and 3) and the apparent diffusion coefficient (F), which is slightly higher in lesions than in NAWM. Data are mean  $\pm$  SD. \*  $P < 0.05$ , \*\*  $P < 0.001$ .

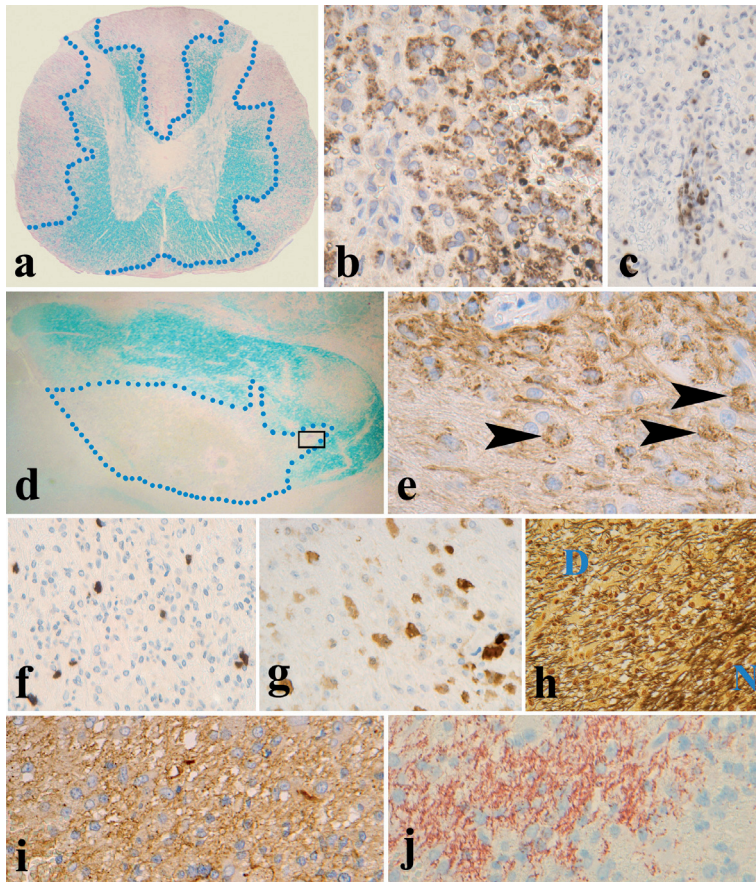
## Chapter 3.1



**Figure 5. MOG34-56 induces inflammation and demyelination in the CNS.**

A, Luxol fast blue staining (original magnification x23) reveals that in this cross-section of spinal cord > 50% of the white matter has been demyelinated (blue line, border with normal white matter) and is remyelinating. Magnified views of the rectangle are shown in B and C. B, CNPase staining (original magnification x160) confirms demyelination and remyelination. Arrowheads point at oligodendrocyte cell bodies in the lesion centre. C, CD3 staining (original magnification x160) shows the presence of T lymphocytes in this area. D, Luxol fast blue staining (original magnification x38) indicates the presence of demyelinating lesions in the corpus callosum. E, MRP-14 positive macrophages are present in these lesions (E, original magnification x99) together with CD3 positive T lymphocytes (F, original magnification x200). G, PLP staining (original magnification x310) reveals PLP degradation products in macrophages (arrowheads). H, IgM staining (original magnification x290) shows plasma cells and Ig deposition on myelin. I, Axonal injury (axonal spheroids) in these white matter lesions is visualized by amyloid precursor protein staining (original magnification x275). In addition to spinal cord and brain white matter lesions, prominent cortical demyelination is also present. J, PLP staining (original magnification x50) reveals subpial demyelination. The meningeal lining is at the upper part of the figure, the blue lining marks the border of the demyelinated cortex, and a magnified view of the area inside the rectangle is shown in K. K, The area inside the rectangle in J (original magnification x990) in which microglial cells with uptake of PLP-positive myelin degradation products can be found. L, These activated microglial cells (original magnification x185) also stain positively with MRP-14, being an early activation marker of macrophages.

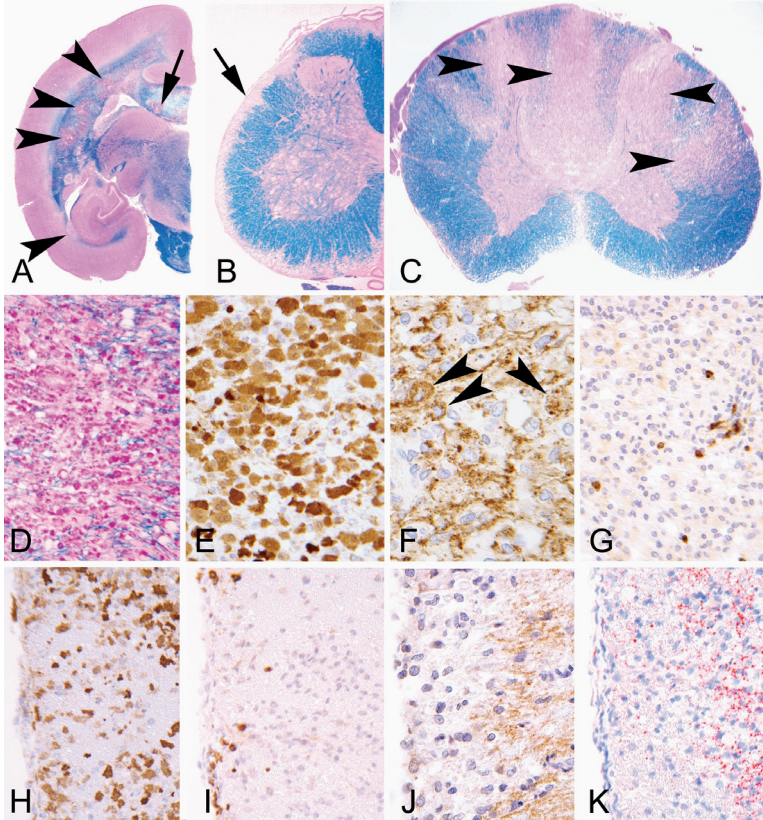
## Chapter 3.1



**Figure 7. Pathology of MOG34-56-boosted EAE in MOG74-96-immunized monkeys.**

Pathology present in the spinal cord of monkey M03033 is shown in A-C; pathology in the optic tract is shown in D-J. A, Staining for luxol fast blue (original magnification x20) reveals demyelinated areas (bordered by blue dotted line) in the spinal cord white matter. B, Late active demyelination (original magnification x350) is shown by the presence of PLP-positive degradation products in macrophages. C, Besides demyelination, inflammation of the lesions is characterized by the presence of CD3<sup>+</sup> lymphocytes (original magnification x150). D, Luxol fast blue staining (original magnification x45) shows large demyelinated lesions (borders indicated by dotted line) in the optic tract. Magnified views of the rectangular area are shown in E-J. E, Staining for PLP (original magnification x350) reveals the presence of PLP degradation products in macrophages (arrowheads). F, The optic tract lesions contained CD3<sup>+</sup> lymphocytes (original magnification x150). G, Single macrophages are stained positively for MRP-14 (original magnification x150). H, A bielschowsky stain for axons (original magnification x150) shows a reduced density of axonal fibers in the demyelinated area (D) compared to the surrounding NAWM (N). I, Staining for IgM (original magnification x300) and complement C9 (J, original magnification x300) shows deposition in the demyelinated areas.

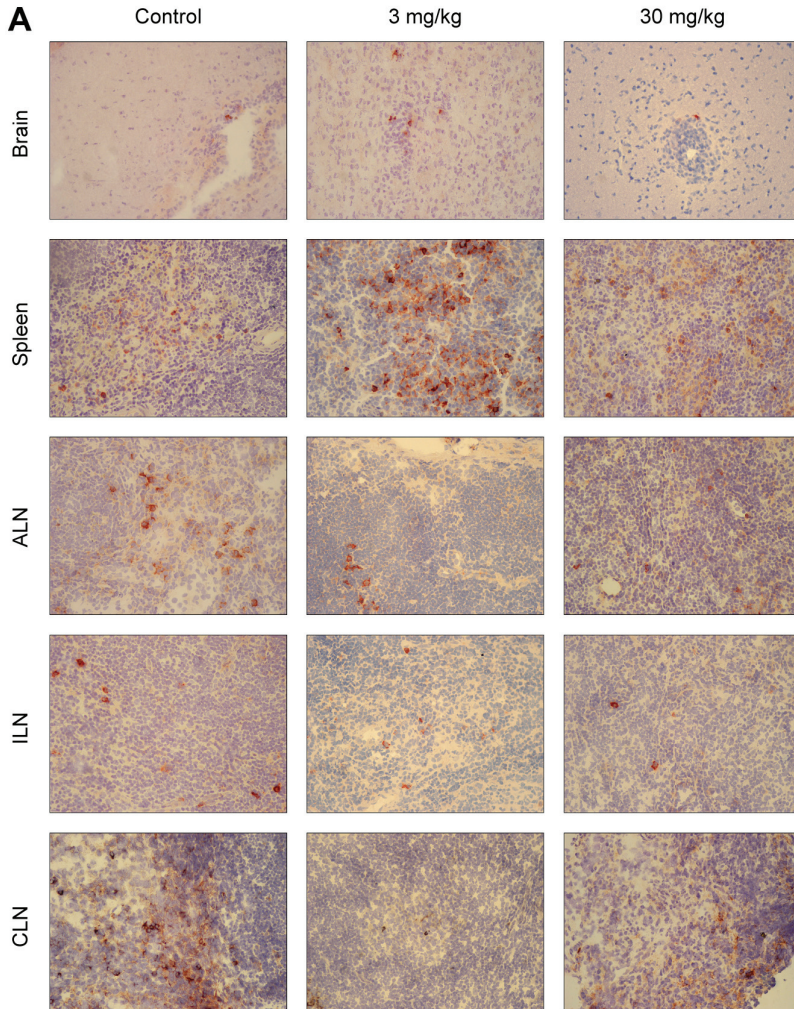
Chapter 3.2



**Figure 4. MOG34-56 in IFA induces demyelination and inflammation in brain and spinal cord.**

Hyperintense white matter areas that were detected in T2-weighted images were analyzed with histology and immunohistochemistry. Brain of M05047 (A, D-G) and spinal cord of 9847 (B,C, H-K) are shown as representatives. A, Luxol fast blue-Periodic acid-Schiff (LFB-PAS) staining (original magnification x4) shows multiple large demyelinating lesions (arrowheads). The lesion in the corpus callosum (arrow) is enlarged in figures D-G. B, Subpial demyelination in spinal cord demonstrated with LFB-PAS (original magnification x25). The arrow indicates the area enlarged in H-K. C, Multiple large focal lesions are also seen in the spinal cord (arrowheads; original magnification x25). D, Enlargement of the area indicated with arrow in panel A. LFB-PAS (original magnification x125) staining shows late active demyelination and the presence of PAS-positive macrophages. E, Macrophage immunostaining using the macrophage marker MRP14 (original magnification x400). F, Immunostaining for myelin PLP (original magnification x500) shows macrophages containing phagocytosed PLP positive fragments (arrowheads). G, Immunostaining for CD3 (original magnification x200) shows that the lesions contain few T-cells. H-K, (original magnification x200) H, Subpial spinal cord area immunostained for MRP14 shows the presence of macrophages. I, CD3 immunostaining shows some meningeal T lymphocytes. J, K, Staining for immunoglobulin (J) reveals deposition in a pattern that overlaps with that of complement factor C9neo (K).

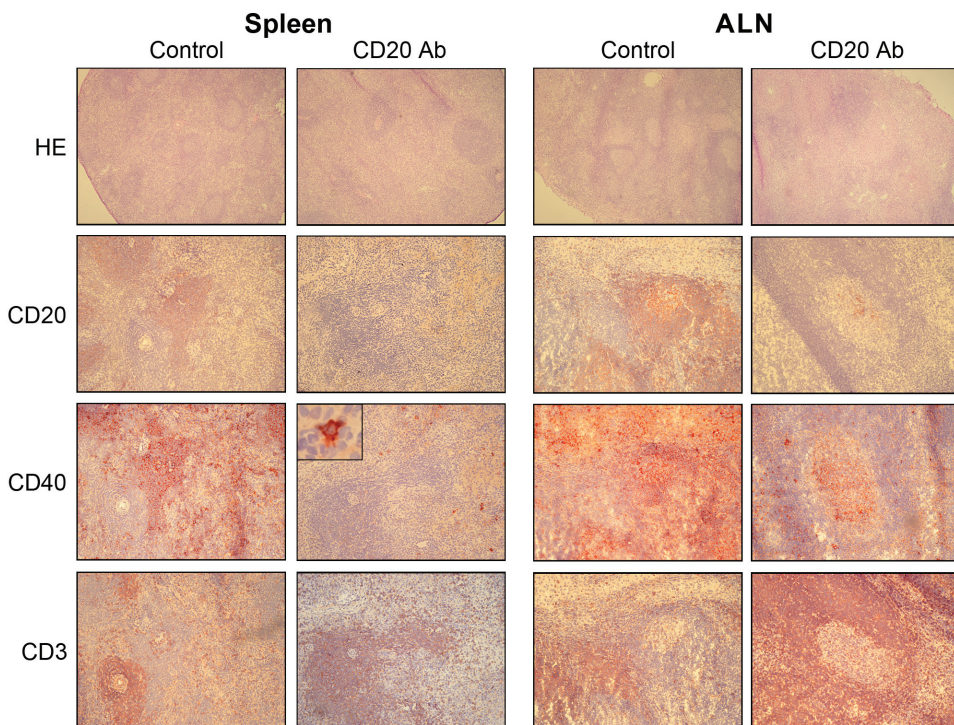
## Chapter 4.1



**Figure 4. Differential expression of IL-17A in the brain and lymphoid organs.**

IL-17A expression was detected by immunohistochemistry. Panel A (original magnification x200) shows representative examples of each group for brain, spleen, and axillary (ALN), inguinal (ILN), and cervical (CLN) lymph nodes.

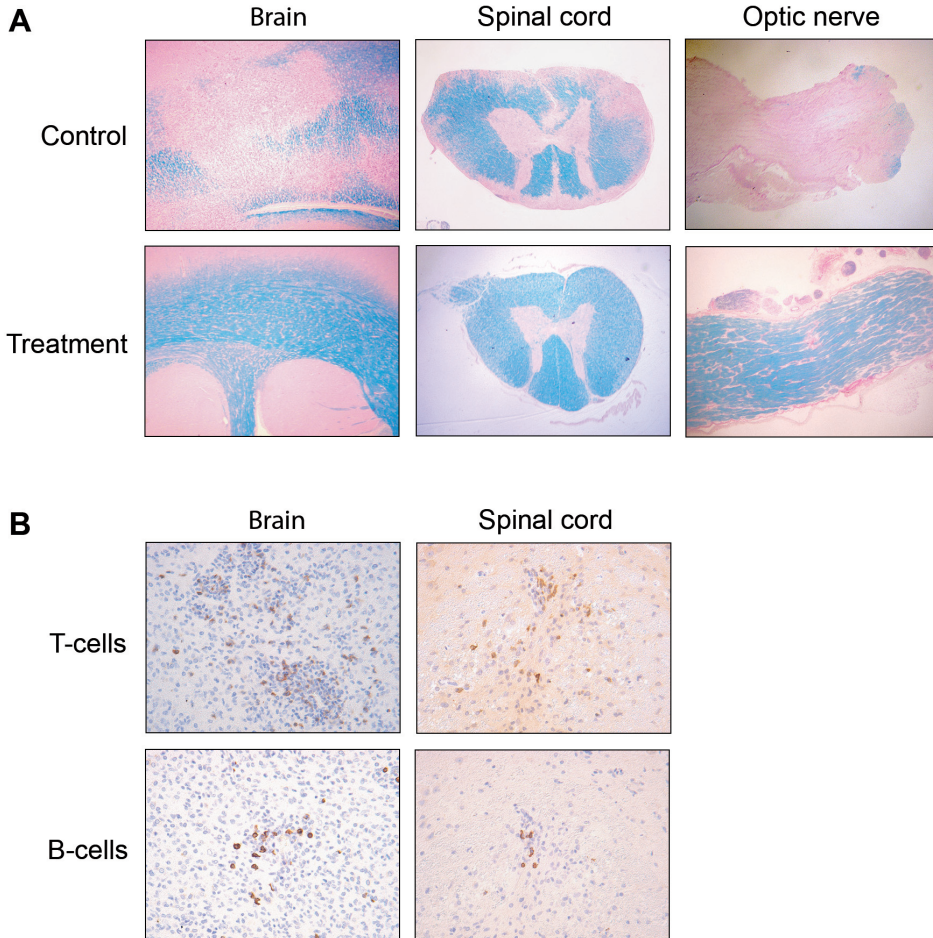
## Chapter 4.2



**Figure 9. Histological analysis of T-cell and B-cell areas in the spleen and ALN of B-cell depleted and control monkeys.**

Shown are representative examples of HE (original magnification x40), CD20 (original magnification x100), CD40 (original magnification x100), and CD3 (original magnification x100) staining on spleen (two left columns) and ALN (two right columns). The HE staining shows that the overall histology of the spleen and ALN was not changed by B-cell depletion. Spleen: The CD20 staining of the control animal shows a clearly demarcated B-cell area in the white pulp, which is also CD40<sup>+</sup>. CD40<sup>+</sup> cells are also present in the red pulp. The CD3 staining of the white pulp shows the CD3<sup>+</sup> T-cell area. In the B-cell depleted spleen no CD20<sup>+</sup> cells are present. A few CD40<sup>+</sup> cells are present, but these morphologically resemble follicular dendritic cells or macrophages (insert). The white pulp of the B-cell depleted animal seems to consist completely of T-cells. ALN: The ALN of the control animal contains a clearly demarcated CD20<sup>+</sup> area, which stains also CD40<sup>+</sup>. CD40<sup>+</sup> cells are also observed in the medulla. CD3<sup>+</sup> cells are confined to the T-cell areas of the cortex. In the ALN of B-cell depleted animals, the B-cell area is hypocellular with a few CD20<sup>+</sup> and CD40<sup>+</sup> cells, but the latter do not have the morphology of B-cells. The number of T-cells seems to be increased in the cortex of the ALN of B-cell depleted animals.

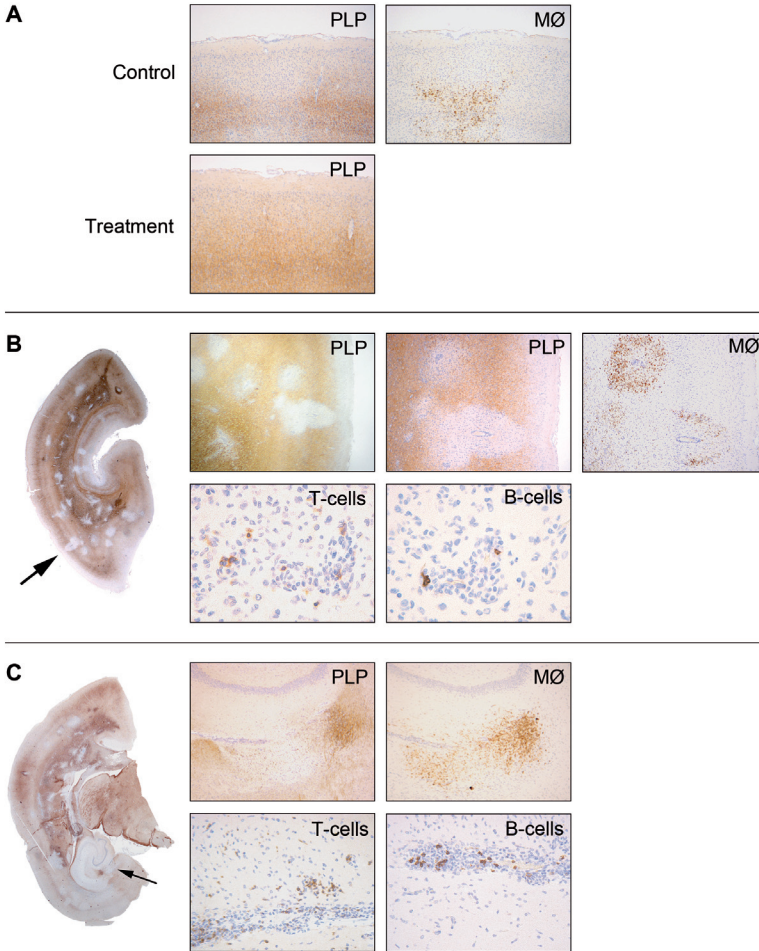
## Chapter 4.3



**Figure 2. Reduced demyelination and inflammation in the white matter after B-cell depletion.**

A, Luxol fast blue staining for myelin shows demyelination in the brain (original magnification x50), spinal cord (original magnification x25), and optic nerve (original magnification x25) of a representative control animal (upper panel). The lower panel shows the intact myelin pattern in brain, spinal cord, and optic nerve of treated animals. B, T-cells (upper panel) and B-cells (lower panel) were observed in brain and spinal cord lesions of control animals, but not in treated animals (original magnification x200).

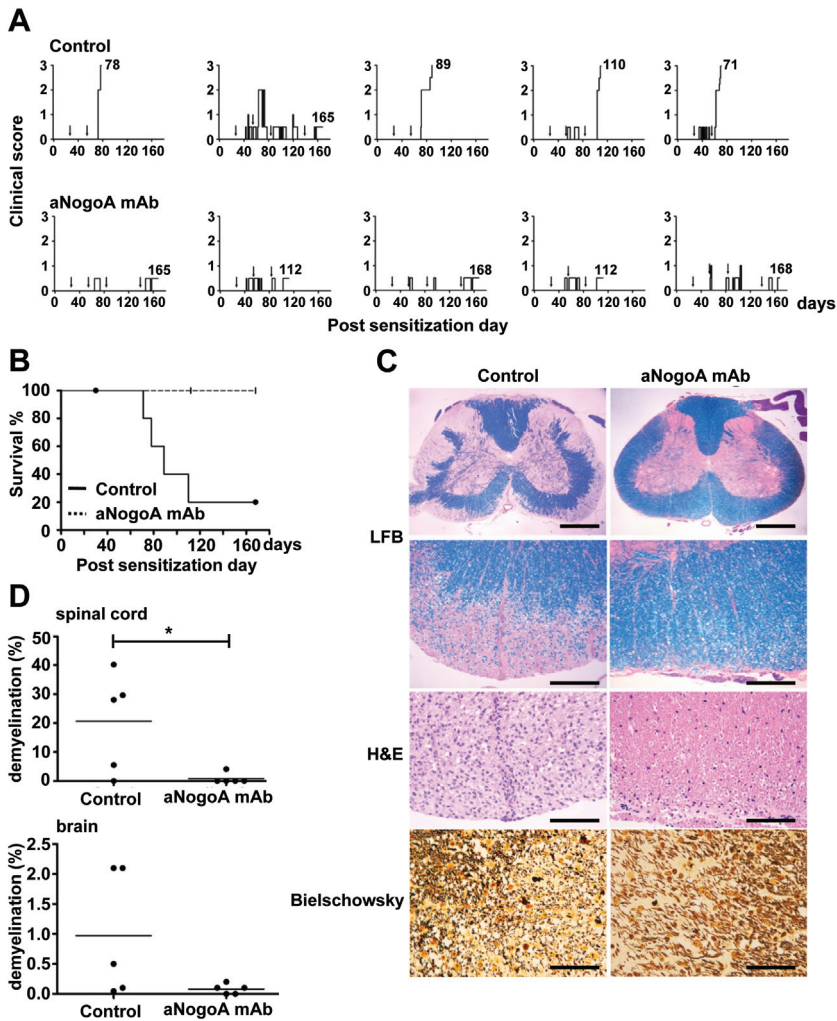
Chapter 4.3



**Figure 3. B-cell depletion prevents the development of grey matter lesions.**

A, stainings for proteolipid protein and MRP14<sup>+</sup> macrophages show a large demyelinated lesion in cortical grey matter of a control animal (upper panel). No grey matter demyelination was observed in CD20<sup>+</sup> B-cell depleted animals (lower panel) (original magnification x500). B, Left hemisphere of a control animal is immunostained for PLP. The arrow points to a group of lesions that are depicted in the five smaller photographs. The first two photographs show the grey matter lesions in a PLP staining (original magnification x25 and x50). MRP14<sup>+</sup> staining shows an active lesion (upper lesion) with many (recently infiltrated) macrophages and an inactive lesion with macrophages only at the rim of the lesion (lower lesion). T-cells and B-cells were present in these lesions (original magnification x400). C shows a lesion in the hippocampus (arrow). Demyelination is shown by PLP staining. MRP14<sup>+</sup> macrophages, T-cells and B-cells were present in this lesion.

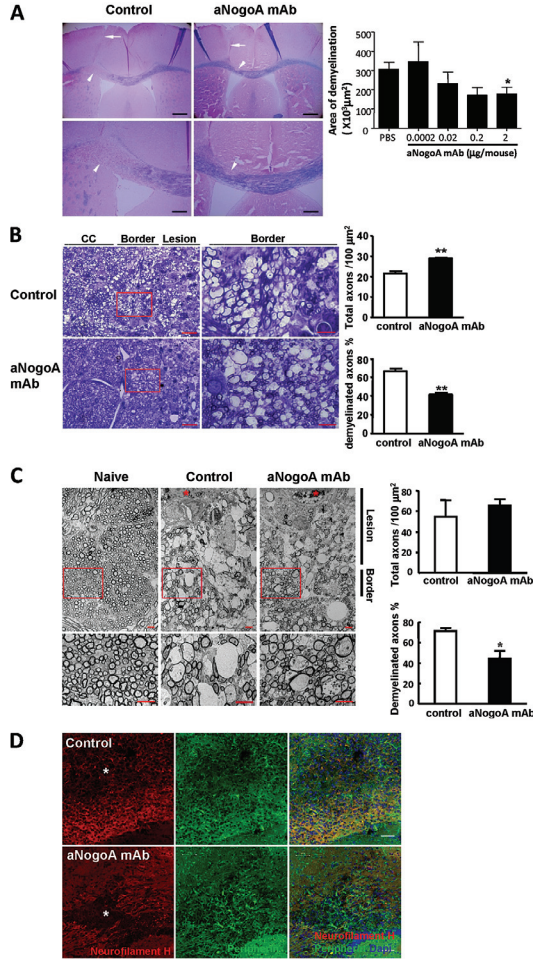
Chapter 4.4



**Figure 1. Amelioration of EAE in marmosets by amino-Nogo-A antibody treatment.**

A, Individual clinical scores of EAE marmoset treated with amino-Nogo-A antibody (aNogoA mAb) and control. Animals (n=5/group) were administered intravenously with a humanized aNogoA mAb or control at 30 mg/kg, starting one day before immunization and every week thereafter and monitored until post immunization days (p.i.d) 112 and 168. B, Survival analysis in aNogoA mAb treatment and control groups. C, Representative spinal cord sections obtained from EAE marmosets analyzed for the degree of demyelination by LFB staining and axon integrity by Bielschowsky staining and infiltrating mononuclear cells by H&E staining. Scale bar, 600  $\mu$ m (LFB, upper), 200  $\mu$ m (LFB, lower), 200  $\mu$ m (H&E) and 50  $\mu$ m (Bielschowsky). (D) Percentage of demyelination areas in the white matter of spinal cord and the brain and the brain.

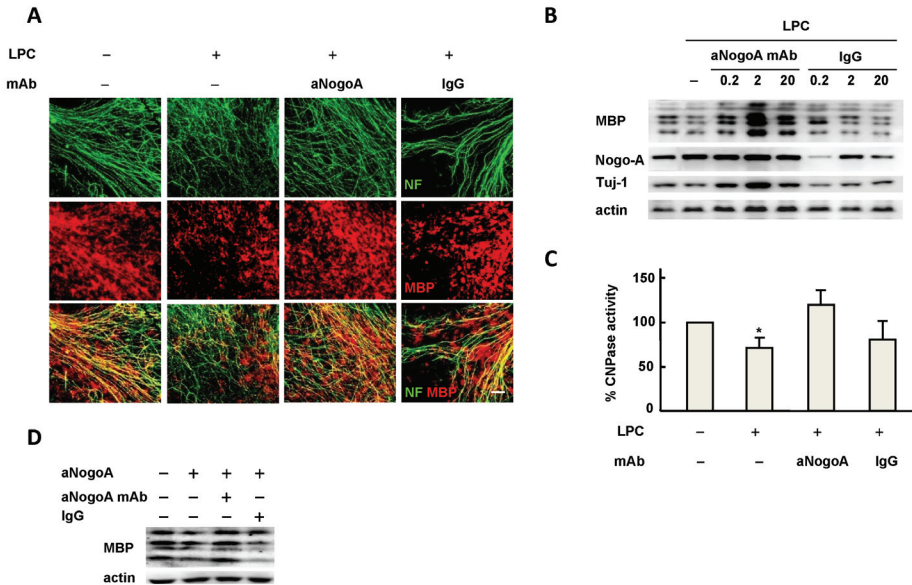
Chapter 4.4



**Figure 2. Reduction of demyelination and protection of axons by the treatment of amino-Nogo-A antibody in an LPC-induced demyelination model.**

A, Area of demyelination by aNogoA mAb treatment in LPC-induced corpus callosum demyelination model. Brain samples were collected from mice 3 days after aNogoA mAb treatment or PBS control and analyzed for the degree of demyelination by LFB staining. Arrows point to the injection sites or needle tracts. Arrowheads indicate the demyelination areas. Scale bar, 500 µm (upper panels) and 200 µm (bottom panels). Bar graph represents the quantification of the area of demyelination in the corpus callosum in relation to the indicated doses of aNogoA mAb. B, Toluidine blue staining of 1 µm corpus callosum sections (left) and magnified images of the boxed border areas (right). Scale bars, 2 µm. The bar graphs represent the total number of axons and % averages of demyelinated axons from the border areas. C, Representative electromicrographs of corpus callosum sections from normal and LPC-injected mice treated with aNogoA mAb (2 µg/mouse) or control. Red asterisks denote macrophages. Boxed areas are enlarged (bottom). D, Axon sprouting in the lesion area (white asterisks) as demonstrated by peripherin staining (green) or neurofilament H (red). \*p < 0.05; \*\*p < 0.01.

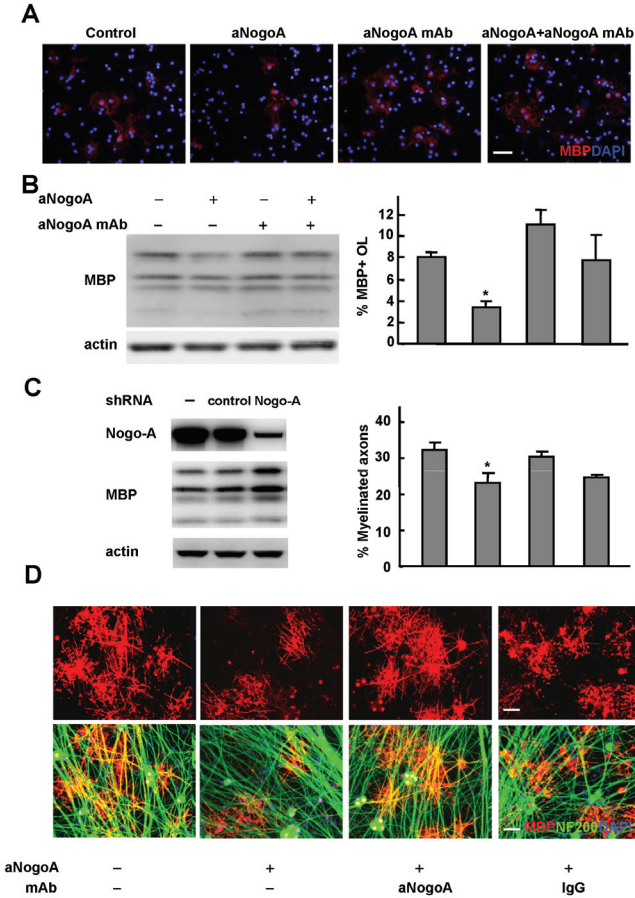
Chapter 4.4



**Figure 3. Restoration of axon integrity and myelination by amino-Nogo-A antagonism in LPC-treated cerebellar slice culture.**

A, Representative confocal images of LPC-treated cerebellar slice cultured with aNogoA mAb or IgG control. Oligodendrocytes were stained with MBP antibody (red) and axons were stained with antibody directed at neurofilament (NF, green). Myelinated axons are shown by co-staining (yellow). Scale bar, 50  $\mu$ m. B, Expression of MBP, Nogo-A, and Tuj-1 in LPC-treated cerebellar slice cultured with different concentrations of aNogoA mAb or IgG control. Actin was used as a control for protein loading. C, CNPase activity in LPC-treated cerebellar slice. Homogenates prepared from LPC-treated cerebellar slice cultured with either aNogoA mAb or IgG control were analyzed in a fluorometric assay. Numbers are expressed as percentage average normalized against untreated control. D, Expression of MBP in cerebellar slice subjected to indicated treatment conditions. Actin was used as a loading control. The data are representative of three independent experiments. \* $p < 0.05$ .

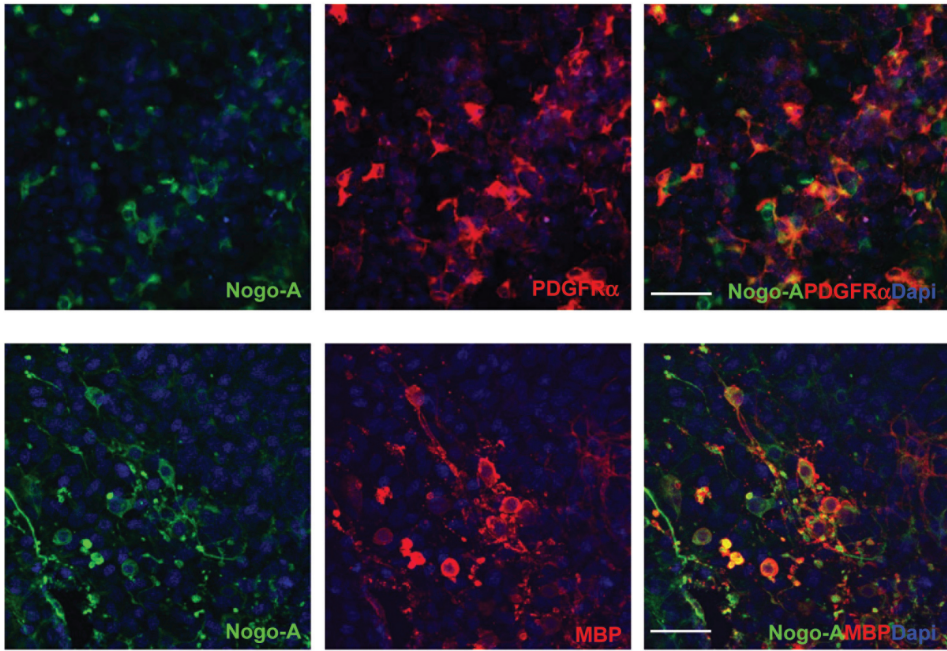
Chapter 4.4



**Figure 4. Effect of amino-Nogo-A antagonism in amino-Nogo-A-mediated inhibition of OPC differentiation, maturation, and myelination.**

A-B, Inhibition of OPC differentiation by amino-Nogo-A (aNogoA). aNogoA at 4 mg/ml was added to OPC culture under differentiation condition in the presence or absence of aNogoA mAb for 4 days. The resulting OPC culture was analyzed for MBP staining (red, upper images) and the percentage of myelin producing oligodendrocytes was quantified by Cellomics (bar graph). The expression level of MBP was analyzed by Western blot. Scale bar, 50  $\mu$ m. C, Reduction in the expression of Nogo-A by shRNA through lentivirus infection. OPC were infected with lentivirus containing either shNogo-A or control shRNA. The expression of Nogo-A and MBP in mature oligodendrocytes was determined by Western blot. D, Effects of aNogoA and aNogoA mAb on OPC and DRG co-culture. aNogoA was added to OPC and DRG co-culture in the presence of aNogoA mAb or IgG control. The resulting cultures were evaluated for myelination of DRG axons by MBP (red) and NF200 (green) co-staining. Scale bar, 50  $\mu$ m. The percentage of myelinated axons was quantified in the lower panel by Cellomics. The data are representative of three independent experiments. \* $p < 0.05$ .

## Chapter 4.4

**Supplemental figure 2. Amino-Nogo-A expression in cerebellar slice culture.**

Cerebellar slice culture was co-stained with aNogoA mAb (green) or antibodies to PDGFR $\alpha$  or MBP (red). Scale bar, 20  $\mu$ m.

